ABSTRACT

HOPKINS, ZACHARY RYAN. Granular Activated Carbon Adsorption of Per- and Polyfluoroalkyl Substances - from Scale-Up to Factors Affecting Performance. (Under the direction of Dr. Detlef Knappe).

Per- and polyfluoroalkyl substances (PFAS) are widely detected in drinking water. Because of their adverse health effects, PFAS are a concern for drinking water providers and consumers. Water professionals require information about the PFAS removal effectiveness of readily deployable treatment technologies. Granular activated carbon (GAC) adsorption, the focus of this dissertation, is one such treatment option.

Overarching research aims were to 1) develop a scale-up approach to predict PFAS removal by field-scale GAC adsorbers from rapid small-scale column tests (RSSCTs) and 2) investigate factors controlling PFAS adsorption by GAC. Specific objectives for the second aim were to quantify the effects of the following factors on PFAS removal: 1) physicochemical properties of PFAS, 2) GAC properties, 3) dissolved organic matter (DOM), and 4) empty bed contact time (EBCT).

To develop a scale-up approach, PFAS breakthrough data were collected for constant diffusivity RSSCT (CD-RSSCT), proportional diffusivity (PD-RSSCT), and pilot-scale designs using matching GACs and water matrices. Neither CD-RSSCT nor PD-RSSCT breakthrough data could directly predict PFAS breakthrough at the field-scale. CD-RSSCT data yielded PFAS adsorption capacities that closely matched pilot-scale adsorption capacities. Therefore, CD-RSSCT data were used to develop a scale-up approach involving the pore surface diffusion model to scale adsorption kinetics. Results obtained for 22 PFAS, 7 GACs, and water matrices ranging from groundwater to coagulated surface water to treated wastewater suggest that intraparticle PFAS flux increases with GAC particle size raised to the power 0.25.

PFAS characteristics influencing adsorbability included chain length, incorporation of ether oxygen linkages, and branching. PFAS adsorbability increased with increasing chain length irrespective of subclass. Incorporation of one or more ether oxygen linkages did not affect adsorbability when comparing linear perfluoroalkyl ether carboxylic acids (PFECAs) and perfluoroalkyl carboxylic acids (PFCAs) of equivalent chain length. However, branched monoether PFECAs broke through earlier than PFCAs of equivalent chain length suggesting branching reduces adsorbability.

Four GACs were evaluated to determine the effect of GAC characteristics on PFAS removal. Adsorbability for the majority of PFAS followed the trend of reagglomerated subbituminous coal-based > enhanced coconut shell-based > lignite-based GAC. Correlations between PFAS adsorbability and pore volume suggested PFAS adsorption is controlled by the volume of micropores in the pore width range from 8-20 Å. A correlation between PFAS molecular diameter and mean pore diameter suggested PFAS preferentially adsorb in mean pore diameters about twice their molecular diameter (R^2=0.732).

GAC influent containing DOM concentrations ranging from <0.5 to 2.3 mg L^{-1} were used to evaluate the effect of DOM on PFAS removal. GAC use rates increased by a factor of ~10 for the majority of PFAS when the DOM concentration in the GAC influent increased from <0.5 to 2.3 mg L^{-1}. For short-chain PFAS, GAC use rate increased by a factor of ~6 over the same DOM range.

Data collected for both pilot-scale GAC adsorbers and RSSCTs demonstrated that increasing EBCT from 10 to 20 min decreased GAC use rates by a factor of ~2 for the majority of PFAS when a 90% removal criterion was applied. To explain the EBCT effect, Biot and Stanton numbers, indicators of mass transfer processes controlling adsorption, were calculated

for a wide range of RSSCT and pilot-scale scenarios. Results highlighted that longer EBCTs are beneficial for contaminants with relatively slow adsorption kinetics, as is the case for many PFAS.

Key contributions of this research were the development of a validated approach to scale up RSSCT data and the quantification of factors that control GAC use rates for PFAS removal. The information supports the design of GAC adsorbers and provides GAC manufacturers with information for the development of effective GAC for PFAS removal.

Granular Activated Carbon Adsorption of Per- and Polyfluoroalkyl Substances - from Scale-Up to Factors Affecting Performance

by
Zachary Ryan Hopkins

A dissertation submitted to the Graduate Faculty of
North Carolina State University
in partial fulfillment of the
requirements for the degree of
Doctor of Philosophy

Civil Engineering

Raleigh, North Carolina

2021

APPROVED BY:

_____	_____
Detlef Knappe Committee Chair	Joel Ducoste
_____	_____
Douglas Call	Owen Duckworth

_____
Mark Strynar
External Member

DEDICATION

To my family and friends who have been there for me through thick and thin. I can't put into words the many thanks for the noticed and unnoticed support during this long journey.

Success is not final,

failure is not fatal:

it is the courage to continue that counts.

-Winston S. Churchill

BIOGRAPHY

Zack Hopkins was born in Rockville, Maryland where he grew up and found his passion for protecting the environment. He received his bachelor's degree in chemical engineering and master's degree in civil and environmental engineering from the University of Maryland, Baltimore County. Afterwards he moved south to continue growing as a researcher investigating environmentally relevant contaminants. In the Fall of 2014 he joined North Carolina State University to pursue his doctoral studies under the direction of Detlef R.U. Knappe.

ACKNOWLEDGMENTS

I'll try to keep this short and sweet. I would like to start by thanking again family and friends for the endless support over the years. Without the constant support I would not have made it this far. When times were tough y'all held the light. Big or small the support kept me going. I would also like to thank my advisor Detlef Knappe for all the support over the last 7 years and providing a space not just for me but all the lab members to grow. To all my committee members, I thank you all for being a part of this project no matter how small it was.

I want to also thank all the current and past lab members. Thanks for all the moments talking through research ideas and making the lab an enjoyable place to be even when times were tough. The bonding and growing has allowed all of us to succeed.

This research was mainly funded by the Water Research Foundation Project No. 4913 and so I would like to thank them for supporting this work. I would also like to thank the Cape Fear Public Water Utility staff for support in running pilots and helping to collect the endless 55 gallon drums of water.

I would also like to thank the support from the communities affected by this horrible class of chemicals. Without the help to collect field samples and highlight this environmental issue none of this work is possible. We will never stop fighting to protect communities against these harmful chemicals.

Table of Contents

LIST OF TABLES vii
LIST OF FIGURES ix
CHAPTER 1 INTRODUCTION AND OBJECTIVES 1
1.1 Motivation 1
1.2 Research objectives 2
CHAPTER 2 PER- AND POLYFLUOROALKYL SUBSTANCES: FOREVER CHEMICALS 4
2.1 Per- and polyfluoroalkyl substances 4
2.2 Emission pathways into drinking water sources 16
2.3 Environmental occurrence of PFAS 17
2.4 Health impacts associated with PFAS 20
2.5 Regulations and guidance 22
2.6 Water treatment 27
2.7 Adsorptive treatment 32
CHAPTER 3 MATERIALS AND METHODS 46
3.1 Materials 46
3.2 Methods 50
CHAPTER 4 DEVELOPMENT OF SCALE-UP APPROACH TO SCALE RSSCT TO FIELD-SCALE 61
4.1 Introduction 61
4.2 Materials and methods 64
4.3 Results and discussion 68
4.4 Conclusions 88
CHAPTER 5 FACTORS INFLUENCING GAC REMOVAL OF PFAS 89
5.1 Introduction 89
5.2 Materials and methods 92
5.3 Results and discussion 98
5.4 Conclusions 128
CHAPTER 6 CONCLUSIONS AND FUTURE RESEARCH 130
6.1 Hypothesis conclusions 130
6.2 Future research 134
REFERENCES 135
APPENDICES 158
Appendix A Analytical method 159

Appendix B Scale-up of RSSCT plots 162
Appendix C Factors effecting PFAS removal 189

LIST OF TABLES

Table 2.1: Classes of per- and polyfluoroalkyl substances (adapted from Wang 2017 and Bell et al. 2019). 5
Table 2.2: Byproducts of the fluorochemical manufacturing process. 10
Table 2.3: Occurrence of PFAS in environmental water matrices. 18
Table 2.4: Example regulatory standards (existing or proposed) for PFAS in drinking water. ... 23
Table 2.5: Example regulatory guidelines (existing or proposed) for PFAS in drinking water. .. 24
Table 2.6: Comparison of testing adsorptive removal performance. 40
Table 2.7: Dimensionless parameters relating full-scale and RSSCT designs. 42
Table 2.8: RSSCT design equations. 43

Table 3.1: Water quality parameters for RSSCT and Pilot tests in surface water and groundwater. 46
Table 3.2: Average PFAS concentrations for RSSCT and pilot tests in surface water and groundwater. 48
Table 3.3: GAC types and characteristics for RSSCT and field-scale tests. 49
Table 3.4: Mass spectrometer ion source parameters. 51
Table 3.5: Design specifications for pilot-scale GAC adsorber and RSSCTs in source waters A and C. 56
Table 3.6: Design specifications for RSSCTs conducted in source water A. 57
Table 3.7: Design specifications for pilot-scale GAC adsorber and RSSCTs tested in source water B. 58
Table 3.9: AdDesignS^{TM} Pore Surface Diffusion Model input parameters. 60

Table 4.1: Different intraparticle diffusion cases for RSSCTs. 79
Table 4.2: Determination of scaled adsorption kinetics from scaled NTIF case. 80

Table A.1: PFAS analyte acronyms, precursor and product ion m/z values, fragmentor and collision energies, and capillary voltages – (1) quantitation ion, (2) confirmation ion (note: only one transition is available for PFBA and PFPeA). 160

Table B.1: AdDesignS inputs for Freundlich adsorption capacity and kinetic parameters for best fit PSDMs for field-scale and CD-RSSCT, TOC =2.3 mgL^{-1}. Carbon: Carbon A, EBCT = 10 and 20 min..... 167

Table B.2: AdDesignS inputs for Freundlich adsorption capacity and kinetic parameters for best fit PSDMs for field-scale and CD-RSSCT, TOC =2.3 mgL^{-1}. Carbon: Carbon B and Carbon D, EBCT = 10. 168

Table B.3: AdDesignS inputs for Freundlich adsorption capacity and kinetic parameters for best fit PSDMs for field-scale and PD-RSSCT, TOC =2.3 mgL^{-1}. Carbon: Carbon A and Carbon D, EBCT = 10. 169

Table B.4: AdDesignS inputs for Freundlich adsorption capacity and kinetic parameters for best fit PSDMs for field-scale and CD-RSSCT, TOC <0.5 mgL^{-1}. Carbon: Carbon A, EBCT = 10. 170

Table B.5: Overview of PFAS for each scaling case compared to field-scale bed volumes to 10% breakthrough. 173

Table B.6: Overview of PFAS for each scaling case compared to field-scale bed volumes to 20% breakthrough. 173

Table B.7: Overview of PFAS for each scaling case compared to field-scale bed volumes to 50% breakthrough. 173

Table B.8: AdDesignS inputs for Freundlich adsorption capacity and kinetic parameters for field-scale and scaled CD-RSSCT, Carbon: Carbon A, EBCT: 10 minutes, TOC =2.3 mgL^{-1}. 174

Table B.9: AdDesignS inputs for Freundlich adsorption capacity and kinetic parameters for field-scale and scaled CD-RSSCT, Carbon: Carbon A, EBCT: 20 minutes, TOC =2.3 mgL^{-1}. 174

Table B.10: AdDesignS inputs for Freundlich adsorption capacity and kinetic parameters for field-scale and scaled CD-RSSCT, Carbon: Carbon B, EBCT: 10 minutes, TOC =2.3 mgL^{-1} 175

Table B.11: AdDesignS inputs for Freundlich adsorption capacity and kinetic parameters for field-scale and scaled CD-RSSCT, Carbon: Carbon C, EBCT: 10 minutes, TOC =2.3 mgL^{-1} 175

Table B.12: AdDesignS inputs for Freundlich adsorption capacity and kinetic parameters for field-scale and scaled CD-RSSCT, Carbon: Carbon A, EBCT: 10 minutes, TOC <0.5 mgL^{-1} 176

Table B.13: AdDesignS inputs for Freundlich adsorption capacity and kinetic parameters to compare RSSCT particle size effect, Carbon: Carbon A, EBCT: 10 minutes. TOC = 1.3 mgL^{-1} 185

LIST OF FIGURES

Figure 2.1: Examples of a A) perfluoroalkyl substance: perfluorooctanesulfonate (PFOS) and a B) polyfluoroalkyl substance: 6:2 fluorotelomer sulfonate (6:2FTS). 5

Figure 2.2: Examples of replacement PFAS for phased out PFOS and PFOA. (Sheng et al. 2018). 9

Figure 2.3: Comparison of HFPO-DA and GenX structures, as well as the common anionic form in water (Hopkins et al. 2018). 15

Figure 2.4: Emission pathways of PFAS from fluorochemical manufacturer, adapted from Davis et al. 2006. 16

Figure 2.5: Fingerprints of surface waters collected in the vicinity of fluorochemical plant. 17

Figure 2.6: Removal of per- and polyfluoroalkyl ether acids (PFEA) by conventional and advanced treatment options at a drinking water treatment plant in the Cape Fear River basin. 29

Figure 2.7: Leaching of PFAS from GAC following source control. Finished water represents blended effluent from three contactors. Service lives: 4,170, 11,900, and 19,000 bed volumes; Empty bed contact time: 14 minutes. 31

Figure 2.8: Adsorption and desorption phenomena as shown by a contaminant breakthrough curve for GAC. 34

Figure 2.9: Breakthrough of PFEA in full-scale GAC contactor, Reactivated F300, EBCT = 14 minutes. 35

Figure 2.10: a) Legacy PFAS and b) PFEA breakthrough in pilot-scale GAC adsorbers. Reagglomerated subbituminous coal-based carbon (Carbon A), EBCT=10 minutes. 36

Figure 3.1: Experimental set-up for constant diffusivity RSSCT. The influent is pumped with an HPLC pump (1). Influent sampling port (3). Each column is filled with designed mass of carbon (3). Treated water is sampled for PFAS and TOC analysis post treatment from a sampling port (4). 54

Figure 4.1: Comparison of bed volumes to 10, 20, and 50% breakthrough for PD-RSSCT at 100x200 and 200x2300 mesh sizes in TOC = 1.3 mgL^{-1} coagulated surface water post biofiltration and for CD-RSSCT at 200x230 and 230x325 mesh sizes in TOC = 1.5 mgL^{-1} coagulated surface water. Shaded region indicate 20% deviation from perfect agreement (1:1 dashed line) between the two RSSCT designs. Carbon: A, Simulated EBCT: 10 minutes. Design specifications in Section 3.2.4. 69

Figure 4.2: Breakthrough curves for PFAS in coagulated/settled surface water (TOC =2.3 mgL^{-1}) for field-scale, CD-RSSCT, and PD-RSSCT. Carbon: Carbon A, Simulated EBCT = 10 minutes. 72

Figure 4.3: Breakthrough curves for PFAS in coagulated/settled surface water (TOC =2.3 mgL^{-1}) for field-scale, CD-RSSCT, and PD-RSSCT. Carbon: Carbon B, Simulated EBCT = 10 minutes. 73

Figure 4.4: Breakthrough curves for PFAS in coagulated/settled surface water (TOC =2.3 mgL^{-1}) for field-scale, CD-RSSCT, and PD-RSSCT. Carbon: Carbon C, Simulated EBCT = 10 minutes. 74

Figure 4.5: Breakthrough curves for PFAS in coagulated/settled surface water (TOC =2.3 mgL^{-1}) for field-scale, CD-RSSCT, and PD-RSSCT. Carbon: Carbon A, Simulated EBCT = 20 minutes. 75

Figure 4.6: Direct comparison of CD-RSSCT (red) and PD-RSSCT (green) data and PSDMs to pilot-scale (blue) breakthrough for PFHxS in coagulate/settled surface water (TOC = 2.3 mg L^{-1}), Carbon: Carbon A, simulated EBCT= 10 minutes. The symbols represent experimental or pilot data; the lines represent best fit PSDM for each data set; the shaded region 20% variance from best fit PSDM. 76

Figure 4.7: Comparison of Freundlich adsorption capacity parameters for CD-RSSCT and PD-RSSCT to field-scale..... 77

Figure 4.8: Comparison of bed volumes to 10% breakthrough for field-scale and scaled CD-RSSCT. Dashed line represents 1:1 line for pilot breakthrough to 10%. Shaded region around dashed line represents 20% variance for bed volumes to 10% breakthrough for field-scale. 81

Figure 4.9: Prediction of field-scale breakthrough for PSDMs using scaled kinetics assuming X=0.25. Carbon: Carbon A, TOC=2.3 mgL^{-1}, EBCT=10 minutes. 83

Figure 4.10: Comparison of bed volumes to 10% breakthrough for scaled CD-RSSCT PSDM and field-scale. A) Validation for wastewater-impacted groundwater with TOC=1.6 mgL^{-1}, B) Validation for groundwater with TOC<0.5mgL^{-1}, EBCT: 10 minutes, Pilot data represented by black squares with +/-20% variance, Scaled CD-RSSCT for X=0.0 (blue diamond), X=0.25 (orange triangle) X=0.5 (green x), and X=1.0 (red circle) with +/-20% variance. 85

Figure 4.11: Direct comparison of RSSCT designed using equation 2 for X=0.25 (orange) and field-scale (black) data sets in coagulate/settled surface water (TOC = 2.3 mg L^{-1}), Carbon: Carbon A, simulated EBCT= 10 minutes. 87

Figure 5.1: Breakthrough curves for different classes of PFAS. Carbon: Carbon A, EBCT=10 minutes, TOC= 2.3 mgL^{-1}. 99

Figure 5.2: Effect of molar volume on bed volumes to 10% breakthrough. TOC = 2.3 mgL^{-1}; A) Carbon A, EBCT = 10 minutes, B) Carbon A, EBCT = 20 minutes, C) Carbon B, EBCT = 10 minutes, D) Carbon C, EBCT = 10 minutes, E) Carbon D, EBCT = 10 minutes. 100

Figure 5.3: Effect of chain length on bed volumes to 10% breakthrough. TOC = 2.3 mgL^{-1}; A) Carbon A, EBCT = 10 minutes, B) Carbon A, EBCT = 20 minutes, C) Carbon B, EBCT = 10 minutes, D) Carbon C, EBCT = 10 minutes, E) Carbon D, EBCT = 10 minutes. 101

Figure 5.4: Effect of branching on PFAS breakthrough. A) PMPA vs PFPeA, B) PEPA vs PFHxA, C) GenX vs PFHpA. Carbon: Carbon A, EBCT = 10 minutes, TOC = 2.3 mgL^{-1}. 104

Figure 5.5: Effect of incorporation of ether oxygen linkage on PFAS breakthrough. No ether oxygen linkage (Solid line), Ether oxygen linkage (dashed line). A) PFBA vs PFMOAA, B) PFHxA vs PFO2HxA, C) PFOA vs PFO3OA. Carbon: Carbon A, EBCT = 10 minutes, TOC = 2.3 mgL^{-1}. 106

Figure 5.6: Effect of carbon selection on bed volumes to 10% breakthrough with Carbon A used as a basis for comparison. Carbon: A (Black), B (Red), C (Green), D (Orange); EBCT= 10minutes; TOC=2.3 mg L^{-1}. 108

Figure 5.7: Comparison of pore size distributions of GACs tested. Carbon A (black circles), Carbon B (red squares), Carbon C (green diamonds), and Carbon D (yellow triangles). 109

Figure 5.8: Relationships between bed volumes to 10% breakthrough and pore volumes in the secondary micropore range in coagulated/settled surface water. Carbon A (black circle), Carbon B (red square), Carbon D (yellow triangle). 111

Figure 5.9: Correlation between molecular diameter of PFAS and preferred mean pore diameter for adsorption based on results from Figure 5.8 and Figure C.9 and C.13. For data collected from adsorption in coagulated surface water, TOC = 2.3 mgL^{-1}. 112

Figure 5.10: Correlation for collision cross-sections and mean pore diameter with relationships for PFAS with estimated collision cross-section for [M-H-CO2] (Top) and [M-H] (bottom). Based on results for preferred adsorption of PFAS in mean pore diameter in Figure 5.8 and Figure C.9-C13. TOC = 2.3 mgL^{-1} and EBCT=10 minutes. 114

Figure 5.11: Effect of carbon selection on bed volumes to 10% breakthrough. Carbon: Carbon A (Black), Carbon C (Green); EBCT= 10minutes; TOC=1.3 mg L^{-1}. 115

Figure 5.12: Comparison of GAC use rates calculated for individual PFAS removed by four different carbons. Carbon A (black circles), Carbon B (red squares), Carbon C (green diamonds), and Carbon D (yellow triangles). EBCT = 10 minutes, TOC = 2.3 mgL^{-1}. 117

Figure 5.13: Comparison of breakthrough curves for individual PFAS in RSSCT designed for EBCTs of 0.056 (Red squares and dashed line) and 0.112 (Green circles and dotted line) minutes. Shaded region represents +/- 20% variance of PSDM line. Carbon: Carbon A, TOC = 2.3 mgL^{-1}. 119

Figure 5.14: Comparison of breakthrough curves for individual PFAS in RSSCT designed for EBCTs of 10 (Red squares and dashed line) and 20 (Green circles and dotted line) minutes. Shaded region represents +/- 20% variance of PSDM line. Carbon: Carbon A, TOC = 2.3 mgL^{-1}. 120

Figure 5.15: Effect of empty bed contact time on bed volumes to 10% breakthrough. Carbon: A; TOC =2.3 mg L^{-1}. 122

Figure 5.16: Effect of empty bed contact time on bed volumes to 20% breakthrough. Carbon: A; TOC =2.3 mg L^{-1}. 122

Figure 5.17: Determination of constant pattern mass transfer zone formation in RSSCTs and pilot adsorbers. Source water A and B was tested with Carbon A, EBCT = 10 and 20 minutes, TOC = 2.3 mgL^{-1}; Fountain RSSCTs Carbon: F400; SCWA water was tested for F830S GAC, EBCT = 5 and 11 minutes, TOC = 0.81 mgL^{-1} (Knappe et al. 2017); Part et al. (2020) Carbon: F400, EBCT = 5, 10, 20 minutes, TOC = 0.78 mgL^{-1} 124

Figure 5.18: Effect of background organic matter concentration on breakthrough to 10%. Carbon: Carbon A, TOCs: <0.5 mgL^{-1} (green), 1.3 mgL^{-1} (red), 2.3 mgL^{-1} (black). 125

Figure 5.19: Effect of background organic matter concentration on breakthrough to 10%. Carbon: Carbon C, TOCs: <0.5 mgL^{-1} (green), 1.3 mgL^{-1} (red), 2.3 mgL^{-1} (black). 126

Figure 5.20: Comparison of GAC use rates for individual compounds in three different TOC waters. Carbon: Carbon A; EBCT = 10 minutes. 127

Figure B.1: Comparison of simulated breakthrough curves using pore surface diffusion model for two constant diffusivity column designs. The black lines represent breakthrough for a RSSCT designed under perfect similitude and the green dashed lines represent breakthrough for a RSSCT designed under reduced hydraulic loading condition. 162

Figure B.2: Direct comparison of CD-RSSCT (red), PD-RSSCT (green), and pilot-scale (blue) breakthrough for PFAS in coagulate/settled surface water (TOC = 2.3 mg L-1), Carbon: Carbon A, simulated EBCT= 10 minutes. The symbols represent experimental or pilot data; the lines represent best fit PSDM for each data set; the shaded region 20% variance from best fit PSDM. 163

Figure B.3: Direct comparison of CD-RSSCT (red), PD-RSSCT (green), and pilot-scale (blue) breakthrough for PFAS in coagulate/settled surface water (TOC = 2.3 mg L-1), Carbon: Carbon C, simulated EBCT= 10 minutes. The symbols represent experimental or pilot data; the lines represent best fit PSDM for each data set; the shaded region 20% variance from best fit PSDM. 164

Figure B.4: Direct comparison of CD-RSSCT (red) and pilot-scale (blue) breakthrough for PFAS in coagulate/settled surface water (TOC = 2.3 mg L-1), Carbon: Carbon B, simulated EBCT= 10 minutes. The symbols represent experimental or pilot data; the lines represent best fit PSDM for each data set; the shaded region 20% variance from best fit PSDM. 165

Figure B.5: Direct comparison of CD-RSSCT (red) and pilot-scale (blue) breakthrough for PFAS in coagulate/settled surface water (TOC = 2.3 mg L-1), Carbon: Carbon A, simulated EBCT= 20 minutes. The symbols represent experimental or pilot data; the lines represent best fit PSDM for each data set; the shaded region 20% variance from best fit PSDM..... 166

Figure B.6: Comparison of bed volumes to 20% breakthrough for field-scale and scaled CD-RSSCT. Dashed line represents 1:1 line for pilot breakthrough to 10%. Shaded region around dashed line represents 20% variance bed volumes to 10% breakthrough for pilot-scale..... 171

Figure B.7: Comparison of bed volumes to 50% breakthrough for field-scale and scaled CD-RSSCT. Dashed line represents 1:1 line for pilot breakthrough to 10%. Shaded region around dashed line represents 20% variance bed volumes to 10% breakthrough for pilot-scale..... 172

Figure B. 8: Comparison of bed volumes to 10% breakthrough for scaled CD-RSSCT PSDM and field-scale. Carbon: Carbon A, EBCT: 10 minutes, Pilot data represented by black squares with +/-20% variance, Scaled CD-RSSCT for X=0.0 (blue diamond), X=0.25 (orange triangle) X=0.5 (green x), X=1.0 (red circle) with +/-20% variance..... 177

Figure B.9: Comparison of bed volumes to 20% breakthrough for scaled CD-RSSCT PSDM and field-scale. Carbon: Carbon A, EBCT: 10 minutes, Pilot data represented by black squares with +/-20% variance, Scaled CD-RSSCT for X=0.0 (blue diamond), X=0.25 (orange triangle) X=0.5 (green x), X=1.0 (red circle) with +/-20% variance..... 177

Figure B.10: Comparison of bed volumes to 50% breakthrough for scaled CD-RSSCT PSDM and field-scale. Carbon: Carbon A, EBCT: 10 minutes, Pilot data represented by black squares with +/-20% variance, Scaled CD-RSSCT for X=0.0 (blue diamond), X=0.25 (orange triangle) X=0.5 (green x), X=1.0 (red circle) with +/-20% variance..... 178

Figure B.11: Comparison of bed volumes to 10% breakthrough for scaled CD-RSSCT PSDM and field-scale. Carbon: Carbon A, EBCT: 20 minutes, Pilot data represented by black squares with +/-20% variance, Scaled CD-RSSCT for X=0.0 (blue diamond), X=0.25 (orange triangle) X=0.5 (green x), X=1.0 (red circle) with +/-20% variance..... 179

Figure B.12: Comparison of bed volumes to 20% breakthrough for scaled CD-RSSCT PSDM and field-scale. Carbon: Carbon A, EBCT: 20 minutes, Pilot data represented by black squares with +/-20% variance, Scaled CD-RSSCT for X=0.0 (blue diamond), X=0.25 (orange triangle) X=0.5 (green x), X=1.0 (red circle) with +/-20% variance..... 179

Figure B.13: Comparison of bed volumes to 50% breakthrough for scaled CD-RSSCT PSDM and field-scale. Carbon: Carbon A, EBCT: 20 minutes, Pilot data represented by black squares with +/-20% variance, Scaled CD-RSSCT for X=0.0 (blue diamond), X=0.25 (orange triangle) X=0.5 (green x), X=1.0 (red circle) with +/-20% variance. 180

Figure B. 14: Comparison of bed volumes to 10% breakthrough for scaled CD-RSSCT PSDM and field-scale. Carbon:Carbon B, EBCT: 10 minutes, Pilot data represented by black squares with +/-20% variance, Scaled CD-RSSCT for X=0.0 (blue diamond), X=0.25 (orange triangle) X=0.5 (green x), X=1.0 (red circle) with +/-20% variance. 181

Figure B.15: Comparison of bed volumes to 20% breakthrough for scaled CD-RSSCT PSDM and field-scale. Carbon:Carbon B, EBCT: 10 minutes, Pilot data represented by black squares with +/-20% variance, Scaled CD-RSSCT for X=0.0 (blue diamond), X=0.25 (orange triangle) X=0.5 (green x), X=1.0 (red circle) with +/-20% variance. 181

Figure B.16: Comparison of bed volumes to 50% breakthrough for scaled CD-RSSCT PSDM and field-scale. Carbon:Carbon B, EBCT: 10 minutes, Pilot data represented by black squares with +/-20% variance, Scaled CD-RSSCT for X=0.0 (blue diamond), X=0.25 (orange triangle) X=0.5 (green x), X=1.0 (red circle) with +/-20% variance. 182

Figure B.17: Comparison of bed volumes to 10% breakthrough for scaled CD-RSSCT PSDM and field-scale. Carbon Carbon C, EBCT: 10 minutes, Pilot data represented by black squares with +/-20% variance, Scaled CD-RSSCT for X=0.0 (blue diamond), X=0.25 (orange triangle) X=0.5 (green x), X=1.0 (red circle) with +/-20% variance. 183

Figure B.18: Comparison of bed volumes to 20% breakthrough for scaled CD-RSSCT PSDM and field-scale. Carbon Carbon C, EBCT: 10 minutes, Pilot data represented by black squares with +/-20% variance, Scaled CD-RSSCT for X=0.0 (blue diamond), X=0.25 (orange triangle) X=0.5 (green x), X=1.0 (red circle) with +/-20% variance. 183

Figure B.19: Comparison of bed volumes to 50% breakthrough for scaled CD-RSSCT PSDM and field-scale. Carbon Carbon C, EBCT: 10 minutes, Pilot data represented by black squares with +/-20% variance, Scaled CD-RSSCT for X=0.0 (blue diamond), X=0.25 (orange triangle) X=0.5 (green x), X=1.0 (red circle) with +/-20% variance. 184

Figure B.20: Prediction of field-scale breakthrough for PSDMs using scaled kinetics assuming X=0.25. Carbon: Carbon A, TOC=2.3 mgL-1, EBCT=20 minutes. 186

Figure B.21: Prediction of field-scale breakthrough for PSDMs using scaled kinetics assuming X=0.25. Carbon: Carbon B, TOC=2.3 mgL-1, EBCT=10 minutes. 187

Figure B.22: Prediction of field-scale breakthrough for PSDMs using scaled kinetics assuming X=0.25. Carbon: Carbon C, TOC=2.3 mgL-1, EBCT=10 minutes. 188

Figure C.1: Breakthrough curves for different classes of PFAS. Carbon: Carbon A, EBCT=20 minutes, TOC= 2.3 mgL^{-1}. 189

Figure C.2: Breakthrough curves for different classes of PFAS. Carbon: Carbon B, EBCT=10 minutes, TOC= 2.3 mgL^{-1}. 190

Figure C.3: Breakthrough curves for different classes of PFAS. Carbon: Carbon C, EBCT=10 minutes, TOC= 2.3 mgL^{-1}. 191

Figure C.4: Breakthrough curves for different classes of PFAS. Carbon: Carbon D, EBCT=10 minutes, TOC= 2.3 mgL^{-1}. 192

Figure C.5: Effect of molar volume on bed volumes to 20% breakthrough. TOC = 2.3 mgL^{-1}; A) Carbon A, EBCT = 10 minutes, B) Carbon A, EBCT = 20 minutes, C) Carbon B, EBCT = 10 minutes, D) Carbon C, EBCT = 10 minutes, E) Carbon D, EBCT = 10 minutes.... 193

Figure C.6: Effect of molar volume on bed volumes to 50% breakthrough. TOC = 2.3 mgL^{-1}; A) Carbon A, EBCT = 10 minutes, B) Carbon A, EBCT = 20 minutes, C) Carbon B, EBCT = 10 minutes, D) Carbon C, EBCT = 10 minutes, E) Carbon D, EBCT = 10 minutes.... 194

Figure C.7: Effect of chain length on bed volumes to 20% breakthrough. TOC = 2.3 mgL^{-1}; A) Carbon A, EBCT = 10 minutes, B) Carbon A, EBCT = 20 minutes, C) Carbon B, EBCT = 10 minutes, D) Carbon C, EBCT = 10 minutes, E) Carbon D, EBCT = 10 minutes.... 195

Figure C.8: Effect of chain length on bed volumes to 50% breakthrough. TOC = 2.3 mgL^{-1}; A) Carbon A, EBCT = 10 minutes, B) Carbon A, EBCT = 20 minutes, C) Carbon B, EBCT = 10 minutes, D) Carbon C, EBCT = 10 minutes, E) Carbon D, EBCT = 10 minutes.... 196

Figure C.9: Effect of branching on PFAS breakthrough. A) PMPA vs PFPeA, B) PEPA vs PFHxA, C) GenX vs PFHpA. Carbon: Carbon A, EBCT = 20 minutes, TOC = 2.3 mgL^{-1}. 197

Figure C.10: Effect of branching on PFAS breakthrough. A) PMPA vs PFPeA, B) PEPA vs PFHxA, C) GenX vs PFHpA. Carbon: Carbon B, EBCT = 10 minutes, TOC = 2.3 mgL^{-1}. 198

Figure C.11: Effect of branching on PFAS breakthrough. A) PMPA vs PFPeA, B) PEPA vs PFHxA, C) GenX vs PFHpA. Carbon: Carbon C, EBCT = 10 minutes, TOC = 2.3 mgL^{-1}. 199

Figure C.12: Effect of branching on PFAS breakthrough. A) PMPA vs PFPeA, B) PEPA vs PFHxA, C) GenX vs PFHpA. Carbon: Carbon D, EBCT = 10 minutes, TOC = 2.3 mgL^{-1}. 200

Figure C.13: Effect of branching on PFAS breakthrough. A) PMPA vs PFPeA, B) PEPA vs PFHxA, C) GenX vs PFHpA. Carbon: Carbon A, EBCT = 10 minutes, TOC = 1.3 mgL^{-1}. 201

Figure C.14: Effect of branching on PFAS breakthrough. A) PMPA vs PFPeA, B) PEPA vs PFHxA, C) GenX vs PFHpA. Carbon: Carbon C, EBCT = 10 minutes, TOC = 1.3 mgL^{-1}. 202

Figure C.15: Effect of branching on PFAS breakthrough. A) PMPA vs PFPeA, B) PEPA vs PFHxA, C) GenX vs PFHpA. Carbon: Carbon A, EBCT = 10 minutes, TOC < 0.5 mgL^{-1}. 203

Figure C.16: Effect of branching on PFAS breakthrough. A) PMPA vs PFPeA, B) PEPA vs PFHxA, C) GenX vs PFHpA. Carbon: Carbon C, EBCT = 10 minutes, TOC < 0.5 mgL^{-1}. 204

Figure C.17: Effect of incorporation of ether oxygen linkage on PFAS breakthrough. No ether oxygen linkage (Solid line), Ether oxygen linkage (dashed line). A) PFBA vs PFMOAA, B) PFHxA vs PFO2HxA, C) PFOA vs PFO3OA. Carbon: Carbon A, EBCT = 20 minutes, TOC = 2.3 mgL^{-1}. 205

Figure C.18: Effect of incorporation of ether oxygen linkage on PFAS breakthrough. No ether oxygen linkage (Solid line), Ether oxygen linkage (dashed line). A) PFBA vs PFMOAA, B) PFHxA vs PFO2HxA, C) PFOA vs PFO3OA. Carbon: Carbon B, EBCT = 10 minutes, TOC = 2.3 mgL^{-1}..... 206

Figure C.19: Effect of incorporation of ether oxygen linkage on PFAS breakthrough. No ether oxygen linkage (Solid line), Ether oxygen linkage (dashed line). A) PFBA vs PFMOAA, B) PFHxA vs PFO2HxA, C) PFOA vs PFO3OA. Carbon: Carbon C, EBCT = 10 minutes, TOC = 2.3 mgL^{-1}..... 207

Figure C.20: Effect of incorporation of ether oxygen linkage on PFAS breakthrough. No ether oxygen linkage (Solid line), Ether oxygen linkage (dashed line). A) PFBA vs PFMOAA, B) PFHxA vs PFO2HxA, C) PFOA vs PFO3OA. Carbon: Carbon D, EBCT = 10 minutes, TOC = 2.3 mgL^{-1}. 208

Figure C.21: Effect of incorporation of ether oxygen linkage on PFAS breakthrough. No ether oxygen linkage (Solid line), Ether oxygen linkage (dashed line). A) PFBA vs PFMOAA, B) PFHxA vs PFO2HxA, C) PFOA vs PFO3OA. Carbon: Carbon A, EBCT = 10 minutes, TOC = 1.3 mgL^{-1}. 209

Figure C.22: Effect of incorporation of ether oxygen linkage on PFAS breakthrough. No ether oxygen linkage (Solid line), Ether oxygen linkage (dashed line). A) PFBA vs PFMOAA, B) PFHxA vs PFO2HxA, C) PFOA vs PFO3OA. Carbon: Carbon C, EBCT = 10 minutes, TOC = 1.3 mgL^{-1}..... 210

Figure C.23: Effect of incorporation of ether oxygen linkage on PFAS breakthrough. No ether oxygen linkage (Solid line), Ether oxygen linkage (dashed line). A) PFBA vs PFMOAA, B) PFHxA vs PFO2HxA, C) PFOA vs PFO3OA. Carbon: Carbon A, EBCT = 10 minutes, TOC < 0.5 mgL^{-1}. 211

Figure C.24: Effect of incorporation of ether oxygen linkage on PFAS breakthrough. No ether oxygen linkage (Solid line), Ether oxygen linkage (dashed line). A) PFBA vs PFMOAA, B) PFHxA vs PFO2HxA, C) PFOA vs PFO3OA. Carbon: Carbon C, EBCT = 10 minutes, TOC < 0.5 mgL^{-1}..... 212

Figure C.25: Relationships between bed volumes to 10% breakthrough and pore volumes in the secondary micropore range in coagulated/settled surface water. Carbon A (black circle), Carbon B (red square), Carbon D (yellow triangle). 213

Figure C.26: Relationships between bed volumes to 10% breakthrough and pore volumes in the secondary micropore range in coagulated/settled surface water. Carbon A (black circle), Carbon B (red square), Carbon D (yellow triangle). 214

Figure C.27: Relationships between bed volumes to 10% breakthrough and pore volumes in the secondary micropore range in coagulated/settled surface water. Carbon A (black circle), Carbon B (red square), Carbon D (yellow triangle). 215

Figure C.28: Relationships between bed volumes to 10% breakthrough and pore volumes in the secondary micropore range in coagulated/settled surface water. Carbon A (black circle), Carbon B (red square), Carbon D (yellow triangle). 216

Figure C.29: Relationships between bed volumes to 10% breakthrough and pore volumes in the secondary micropore range in coagulated/settled surface water. Carbon A (black circle), Carbon B (red square), Carbon D (yellow triangle). 217

CHAPTER 1 INTRODUCTION AND OBJECTIVES

1.1 Motivation

Per- and polyfluoroalkyl substances (PFAS) are a broad class of emerging contaminants that impact surface water and groundwater resources globally (Wang et al. 2017; Hopkins et al. 2018; Hu et la. 2016; Gebbink et al. 2017; Banzhaf et al. 2017; Crone et al. 2019; Andrews et al. 2020; Kabore et al. 2018; Kolpin et al. 2021). PFAS exhibit a wide range of physicochemical properties that have made them ideal for use in a variety of manufacturing processes and consumer products. Through water and air emissions at manufacturing sites and use of products containing PFAS, these chemicals have ended up in the environment. Many PFAS are persistent in the environment and are difficult to remove from drinking water sources. As a result of their persistent, bioaccumulative, and toxic nature, the U.S. EPA has proposed studying the occurrence of 29 PFAS in drinking water under the fifth unregulated contaminant monitoring rule (UCMR5) (U.S. EPA 2021). PFAS exhibit a wide range of adverse health effects, which has created concern for their detection in treated drinking water. As a result, government agencies are setting maximum contaminant levels (MCLs) or health advisory levels that are driving the need to understand the effectiveness of water treatment approaches for PFAS removal (ITRC 2020, ECHA 2021).

Previous research has demonstrated that many conventional and advanced treatment approaches do not effectively remove PFAS (Hopkins et al. 2018; Crone et al. 2018). Many water purveyors are evaluating the performance of granular activated carbon (GAC) for the removal of PFAS. GAC adsorption is effective for removal of a wide range of micropollutants detected in drinking water sources. However, assessing performance of GAC at the field-scale for the wide range of PFAS potentially present in drinking water sources is time intensive and

costly. Rapid small-scale column tests (RSSCTs) were developed to reduce cost and time for assessing removal of micropollutants by GAC in a laboratory setting (Crittenden et al.1986; Crittenden et al. 1987). RSSCTs can be designed assuming intraparticle diffusivity of micropollutants scales either constantly or proportionally with GAC particle size, which gave rise to the constant diffusivity (CD) and proportional diffusivity (PD) RSSCT designs. To date no effective scale-up approach has been developed to predict field-scale removal of PFAS by RSSCTs. Additionally, there is limited knowledge about factors controlling the removal of short- and long-chain perfluoroalkyl acids and novel PFAS, such as per- and polyfluoroalkyl ether acids by GAC. Information is needed to understand how PFAS properties, GAC characteristics, GAC adsorber design, and background water quality parameters affect PFAS removal by GAC.

1.2 Research objectives

1.2.1 Overall research goals

The overall goals of this research were to (1) develop a scale-up approach to predict PFAS removal in field-scale GAC contactors from rapid small-scale column tests (RSSCTs) and (2) evaluate factors that control PFAS adsorption by GAC.

1.2.2 Specific objectives

The following objectives were pursued to achieve the above goals:

1. Evaluate the suitability of RSSCT design approaches (e.g., constant diffusivity, proportional diffusivity) for predicting PFAS removal in field-scale GAC adsorbers.
2. Develop a scale-up procedure to predict PFAS removal from RSSCT data.
3. Elucidate physical and chemical properties of PFAS that control adsorbability to GAC.
4. Identify GAC properties that yield enhanced PFAS removal.

5. Assess the effect of dissolved organic matter (DOM) on PFAS removal.
6. Determine the effect of empty bed contact time on PFAS removal.

1.2.3 Hypotheses

The following hypotheses were tested in this work.

1. Based on previous research conducted with neutral organic contaminants, the PD-RSSCT design will effectively predict PFAS adsorption kinetics in field-scale GAC contactors, but adsorption capacity will be overpredicted by PD-RSSCTs.
2. PFAS adsorbability increases with increasing chain length, while incorporation of ether oxygen groups and branching of PFAS will translate into decreased adsorbability.
3. Based on results of prior research for the adsorption of natural organic matter (NOM) and the similarity of size and charge between PFAS and NOM, GAC with substantial pore volume in the secondary micropores (8 Å< d_p < 20 Å) and small mesopores will be most effective for PFAS removal.
4. Higher concentrations of DOM will increase carbon use rates for PFAS removal because of increased direct adsorption competition, pore blockage, and electrostatic repulsion.
5. Increasing empty bed contact time (EBCT) from 10 to 20 minutes will decrease GAC use rates for a treatment goal of >90% PFAS removal because the longer EBCT promotes the development of a shorter mass transfer zone within the adsorber bed.

CHAPTER 2 PER- AND POLYFLUOROALKYL SUBSTANCES: FOREVER CHEMICALS

2.1 Per- and polyfluoroalkyl substances

Per- and polyfluoroalkyl substances (PFAS) are a class of xenobiotic chemicals receiving extensive public and research attention because they are ubiquitous in the environment and widely detected in the blood of people around the world (Glassmeyer et al. 2017; OLEM 2019; Hu et al. 2016; Xiao et al. 2017; Braun et al. 2016; Barry et al. 2013; Hopkins et al. 2018; Cousins et al. 2019; Yao et al. 2020; Yao et al. 2021; US EPA 2021). PFAS are of concern because they are persistent and some are associated with adverse environmental and human health effects (Conley et al. 2019; Conley et al. 2021; Lohmann et al. 2020; Woodlief et al. 2021; Chen et al. 2021; De Silva et al. 2020; Fenton et al. 2021). To date, several thousand PFAS have been used in industrial and consumer applications. PFAS consist of both polymeric and non-polymeric forms. The non-polymeric forms are of greater concern to the public and environmental regulators currently because polymers use non-polymeric PFAS to manufacture. For example, perfluorooctanoic acid (PFOA) and hexafluoroproplyene oxide-dimer acid (HFPO-DA) are used as polymer processing aids (PPAs) in the production of polymers, including polytetrafluoroethylene (PTFE). These non-polymeric processing aids have been released into the environment and can represent a long-term source of PFAS. (Jarnberg et al. 2006; Xiao et al. 2017) The non-polymeric PFAS can be split into two classes (1) perfluoroalkyl substances (e.g., perfluorooctanesulfonate), in which all carbon-hydrogen bonds have been replaced with carbon-fluorine bonds, and (2) polyfluoroalkyl substances (e.g. 6:2 fluorotelomer sulfonate) that are not fully fluorinated (Figure 2.1). Within these two major classes there are a variety of subgroups

(Table 2.1). (Ristscher et al. 2018; OECD 2018; Wang et al. 2017; OECD 2013; Kwiatkowski et al. 2020)

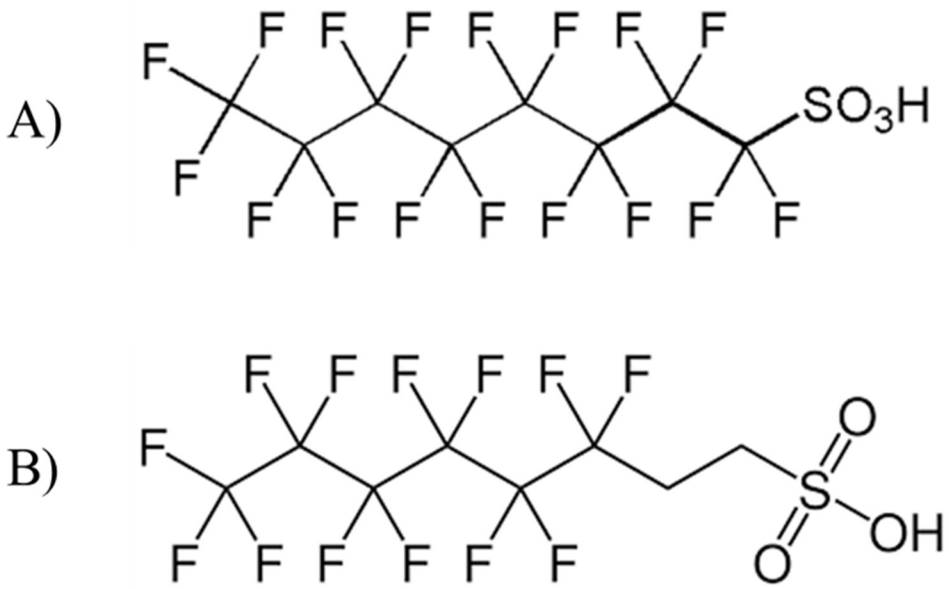

Figure 2.1: Examples of a A) perfluoroalkyl substance: perfluorooctanesulfonate (PFOS) and a B) polyfluoroalkyl substance: 6:2 fluorotelomer sulfonate (6:2FTS).

Table 2.1: Classes of per- and polyfluoroalkyl substances (adapted from Wang 2017 and Bell et al. 2019).

Class of PFAS	Examples
Perfluorocarboxylic acids (PFCA) (C_nF_{2n+1}-COOH)	Perfluorobutanoic acid (PFBA, n=4)
	Perfluorohexanoic acid (PFHxA, n-6)
	Perfluorooctanoic acid (PFOA, n=8)
	Perfluorononanoic acid (PFNA, n=9)
---	---
Perfluorosulfonic acids (PFSA) (C_nF_{2n+1}-SO_3H)	Perfluorobutanesulfonate (PFBS, n=4)
	Perfluorohexanesulfonate (PFHxS, n=6)
	Perfluorooctanesulfonate (PFOS, n=8)

Table 2.1: (continued).

Perfluoroalkyl phosphonic acids (PFPA) (C_nF_{2n+1}-PO_3H_2)	Perfluorohexanephosphonic acid (PFHxPA, n=6) Perfluorooctanephosphonic acid (PFOPA, n=8)
---	---
Perfluoroalkyl phosphinic acids (PFPiA) (C_nF_{2n+1}-PO_2H-C_mF_{2m+1})	C4/C4 PFPiA (n,m=4) C6/C6 PFPiA (n,m=6) C6/C6 PFPiA (n,m=8)
---	---
Perfluoroalkyl ether carboxylic acids (PFECA)	Hexafluoropropylene oxide-dimer acid (HFPO-DA, GenX) 4,8-Dioxa-3H-perfluorononanoic acid (ADONA)
---	---
Perfluoroalkyl ether sulfonic acids (PFESA)	6:2 Chlorinated perfluoroalkyl ether sulfonate (6:2 Cl-PFESA, F-53B)
---	---
Perfluoroalkyl sulfonamide substances (C_nF_{2n+1}-SO_2-R)	Perfluorooctanesulfonamide (FOSA, n=8, R=NH_2) N-Methylperfluorooctanesulfonamide (MeFOSA, n=8, R=$N(CH_3)H$) N-Methylperfluorooctanesulfonamidoethanol (MeFOSE, n=8, R=$N(CH3)C_2H_4OH$)

Table 2.1: (continued).

	6:2 fluorotelomer sulfonate (6:2 FTS, n=6, $R=SO_3H$)
Fluorotelomer-based substances (C_nF_{2n+1}-C_2H_4-R)	4:2 Fluorotelomer alcohol (4:2 FTOH, n=4, R=OH)
	6:2 Fluorotelomer phosphate diester (6:2 diPAP, n=6, $R=(C_6F_{13}C_2H_4O)_2$-PO_2H)

Fluoropolymers	Polyvinylidene fluoride (PVDF)
	Polytetrafluoroethylene (PTFE)

Perfluoropolyethers (PFPEs)	Fluorinated polymers with a backbone of ether-linked carbon atoms

Structurally these PFAS are all either fully fluorinated or contain C-F bonds replaced with non-fluorinated C-H bonds (OECD 2013; Buck et al. 2011) The C-F bond gives PFAS unique physicochemical properties. The combination of a hydrophobic and lipophobic fluorinated chain as a tail and a hydrophilic functional group (e.g., carboxylic acid, sulfonic acid, sulfonamide) as the head produces a chemical that is biologically, thermally, and chemically stable. For this reason, PFAS are ideal for use in a variety of industrial and consumer applications. Examples include stain repellents, non-stick cookware, lubricants, food packaging coatings, cosmetics, and fire-fighting foams. (Ritscher et al. 2018; OECD 2018; Wang et al. 2017; OECD 2013; Buck et al. 2011) As a result of the consumer and industrial application of PFAS these chemicals have become widely detected in the environment (Herzke et al. 2012; De

Silva et al. 2021; Yao et al. 2021; Muir et al. 2021) The persistence of PFAS has resulted in numerous detections in water sources used as intakes for drinking water treatment plants. The detection of PFAS in finished drinking water has sparked public concern because of their toxicity and persistence. Evidence from epidemiological studies suggest there is a probable link between exposure to PFAS and adverse health effects including high cholesterol, ulcerative colitis, thyroid disease, testicular cancer, kidney cancer, and pregnancy induced hypertension. (C8 Science Panel 2017; Fei et al. 2007; Melzer et al. 2010; Steeland et al. 2009; Fenton et al. 2021)

The persistent, bioaccumulative, and toxic nature of PFAS resulted in a 2006 global stewardship program involving fluorochemical manufactures. The companies were asked to "commit to reducing PFOA and related chemicals from facility emissions and in product content by 95% no later than 2010 and to work toward eliminating PFOA from emissions and in product content no later than 2015". (U.S. EPA 2015) The phasing out of production and use of long-chain PFAS in the United States has resulted in fluorochemical manufacturers shifting production to shorter-chain PFAS (e.g. perfluoro carboxylic acids with chain length ≤ 6) and fluorinated alternatives (e.g. per- and polyfluoroalkyl ether acids). For example, GenX, which contains an ether oxygen linkage in place of a $-CF_2$ group, is used as a replacement for ammonium perfluorooctanonate in the production of fluoropolymers (e.g. polytetrafluoroethylene). Other examples of replacement PFAS are shown in Figure 2.2.

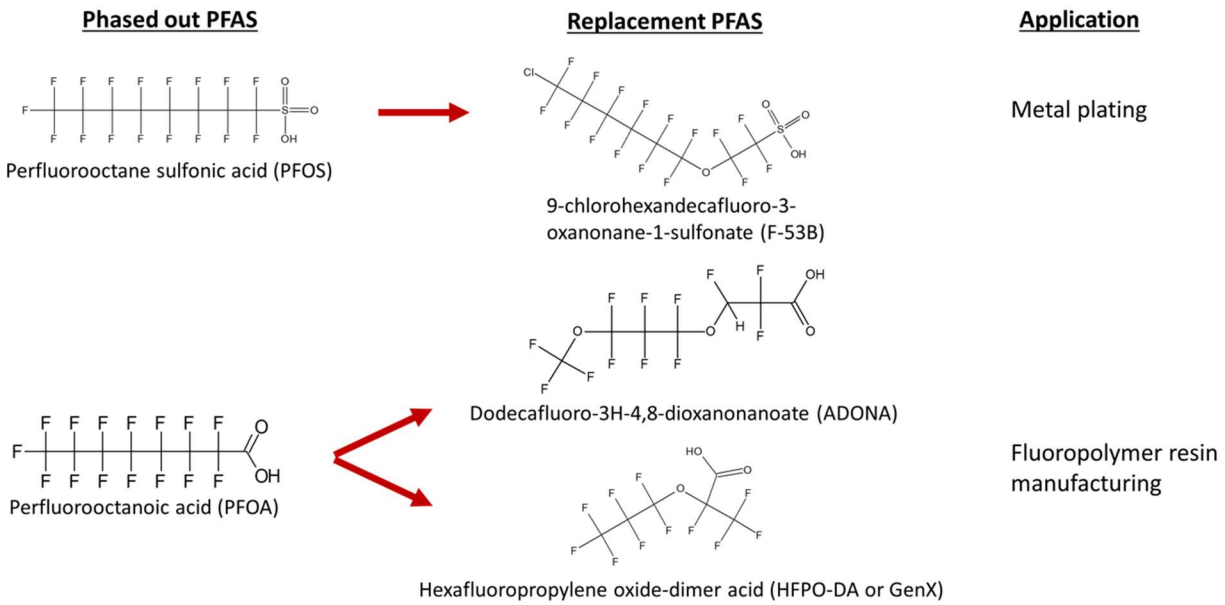

Figure 2.2: Examples of replacement PFAS for phased out PFOS and PFOA. (Sheng et al. 2018).

The production of fluoropolymer and perfluoropolyether results in numerous byproducts. For example, Strynar et al. 2015 and Hopkins et al. 2018 showed the occurrence of byproducts of fluorochemical manufacturing in surface water in North Carolina (Table 2.2). McCord et al. (2020) showed in water near a New Jersey industrial complex the occurrence of novel chloro-perfluoro-polyether carboxylates being used in fluoropolymer production.

Table 2.2: Byproducts of the fluorochemical manufacturing process.

Compound	CAS (hyperlinked to US EPA Chemicals Dashboard)[a]	Structure
	Linear ether carboxylic acid	
Perfluoro-2-methoxyacetic acid (PFMOAA)	674-13-5	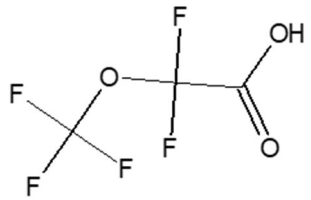
Perfluoro-3,5-dioxahexanoci acid (PFO2HxA)	39492-88-1	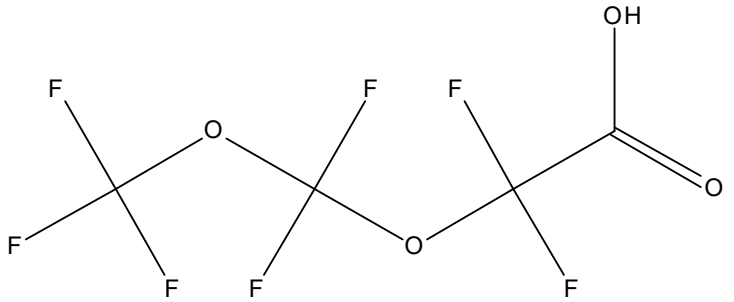
Perfluoro-3,5,7-trioxaoctanoic acid (PFO3OA)	39492-89-2	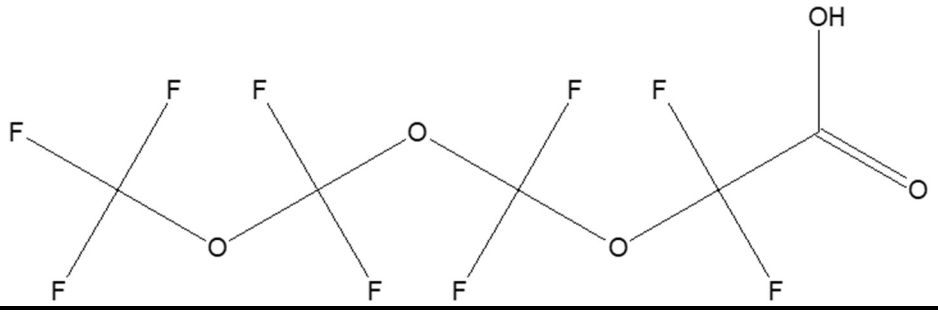

Table 2.2: (continued).

Perfluoro-3,5,7,9-tetradecanoic acid (PFO4DA)	39492-90-5	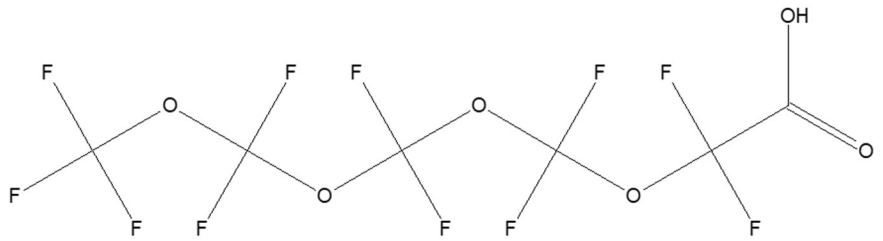
Perfluoro-3,5,7,9,11-pentadodecanoic acid (PFO5DoA)	39492-91-6	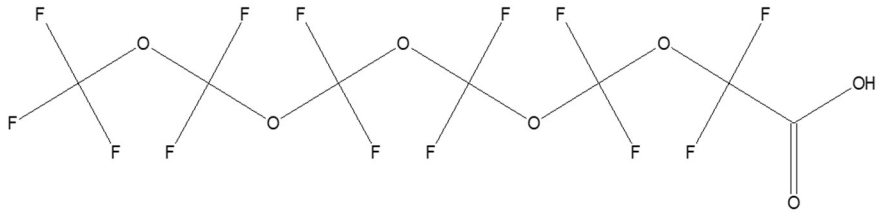
Branched ether carboxylic acid		
Perfluoro-2-methoxypropoanoic acid (PMPA)	13140-29-9	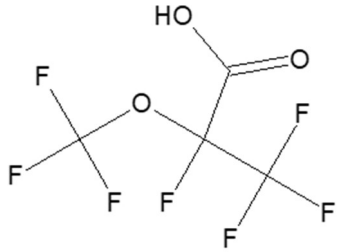

Table 2.2: (continued).

Perfluoro-2-ethoxypropanoic acid (PEPA)	267239-61-2	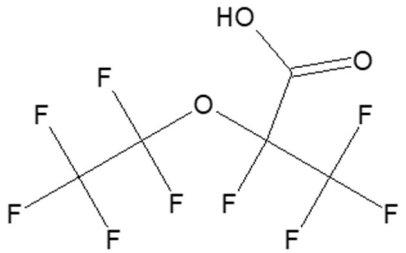
Perfluoro-2-propoxypropanoic acid (HFPO-DA or GenX)	13252-13-6	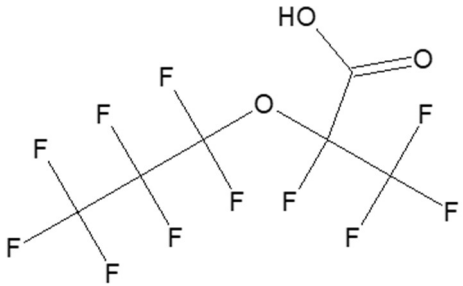
2,2,3,3-Tetrafluoro-3-{[1,1,1,2,3,3-hexafluoro-3-(1,2,2,2-tetrafluoroethoxy)propan-2-yl]oxy} propanoic acid (Hydro-Eve)	773804-62-9	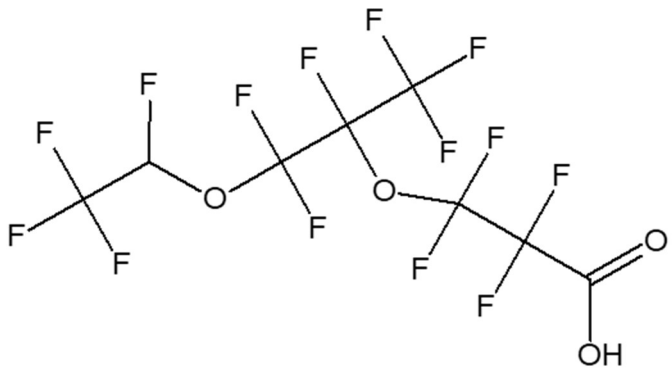

Table 2.2: (continued).

	Linear ether sulfonic acid	
1,1,2,2-Tetrafluoro-2-(1,2,2,2-tetrafluoroethoxy)ethanes ulfonic acid (NVHOS)	801209-99-4	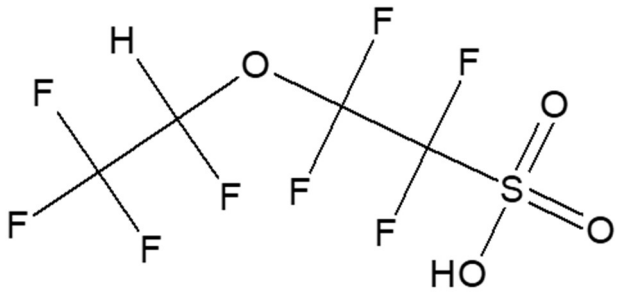
	Branched ether sulfonic acid	
Perfluoro-3,6-dioxa-4-methyl-7-octene-1-sulfonic acid (Nafion by-product 1)	29311-67-9	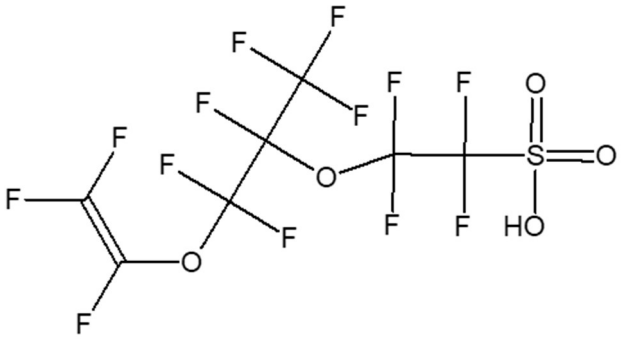

Table 2.2: (continued).

Perfluoro-2-{[perfluoro-3-(perfluoroethoxy)-2-propanyl]oxy}ethanesulfonic acid (Nafion by-product 2)	749836-20-2	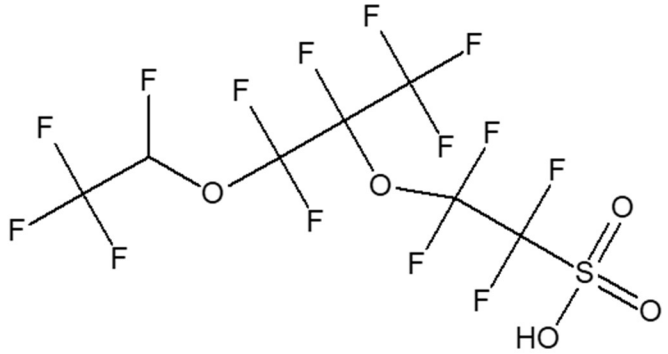
		Diprotic ether acid
Nafion by-product 4	NOCAS_893414	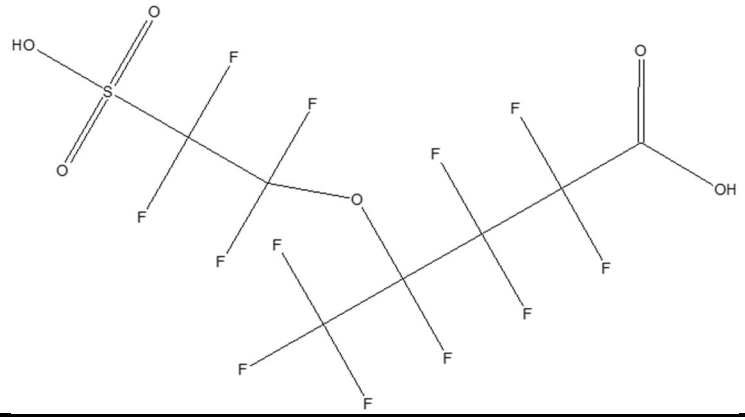

[a] denotes CAS numbers from https://comptox.epa.gov/dashboard

Terminology for these replacement and byproduct PFAS is challenging as a number of different terms have been used by manufacturers and regulators. For example, the processing aid in the production of fluoropolymeric compounds, GenX can also be referred to using the name hexafluoropropylene oxide-dimer acids (HFPO-DA). However, from a water quality and treatment perspective, GenX and HFPO-DA discharges lead to the same anionic species that would have to be removed from water (Figure 2.3)

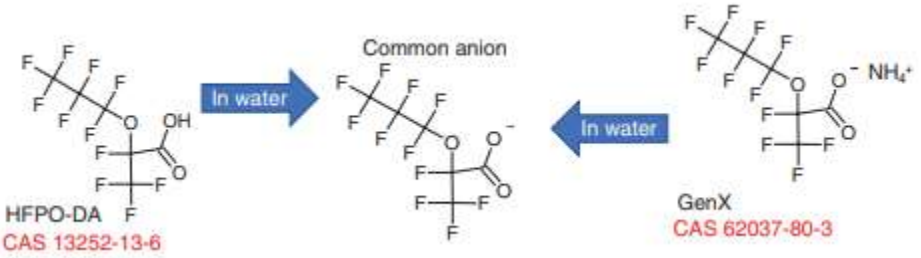

Figure 2.3: Comparison of HFPO-DA and GenX structures, as well as the common anionic form in water (Hopkins et al. 2018).

For regulators, the extensive byproduct nomenclature coupled with the fact that previously the U.S. EPA stipulated manufacturers were not required to capture byproducts produces a challenging situation for knowing exactly what PFAS are present in the environment. Additionally, regulators have required fluorochemical manufactures to demonstrate replacement chemicals are less bioaccumulative and toxic than PFOA and other long-chain PFAS, this does not include byproducts of fluorochemical manufacturing. (U.S. EPA 2017) As a result, when these byproducts are detected limited information is available publicly and from peer-reviewed studies for regulators to conclude the risk of adverse health effects. The limited knowledge on byproducts and replacement chemicals hinders regulatory agencies from properly evaluating approaches for mitigating PFAS discharges.

2.2 Emission pathways into drinking water sources

PFAS emissions can be attributed to a variety of sources including fire training facilities, landfills, wastewater treatment plants, biosolids land application, manufacturing of derivative products, and direct fluorochemical manufacturing. (Hopkins et al. 2018; Sun et al. 2016; Guelfo et al. 2018; Brendel et al. 2018; Davis et al. 2007; Hu et al. 2016; Lindstrom et al. 2011) Each of these sources potentially provides a pathway for PFAS to enter drinking water sources. Due to the physiochemical characteristics of PFAS, they can persist in the environment leading to long-term contamination of water resources. Therefore, assessing PFAS emission pathways is important to preventing new and continued contamination of drinking water sources (Figure 2.4).

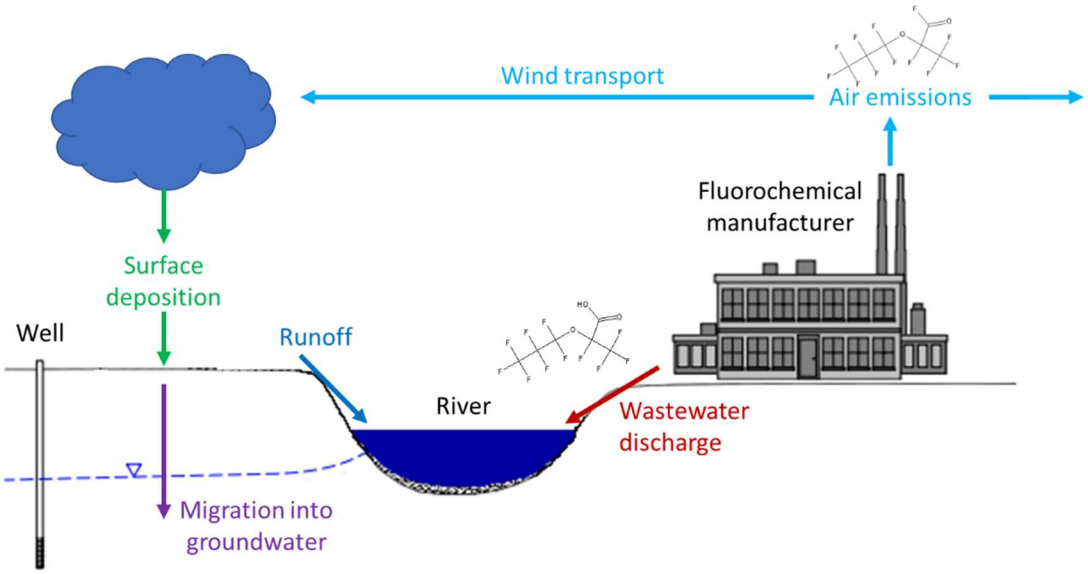

Figure 2.4: Emission pathways of PFAS from fluorochemical manufacturer, adapted from Davis et al. 2006.

As analytical techniques have advanced, the frequency of PFAS detection in the environment has increased. (Sun et al. 2016; Strynar et al. 2015; McCord et al. 2019; Gebbink et al. 2017; Anderson et al. 2016; Murakami et al. 2008; Boone et al. 2019; Wang et al. 2014; McCord et al. 2020) These methods have improved identification of PFAS sources and helped to

evaluate the extent of contamination to the environment and drinking water sources. For example, samples collected from surface waters near a fluorochemical manufacturer (Figure 2.5) demonstrate that the emission pathway can dictate the composition of PFAS detected in a specific environmental sample. (Hopkins et al. 2018)

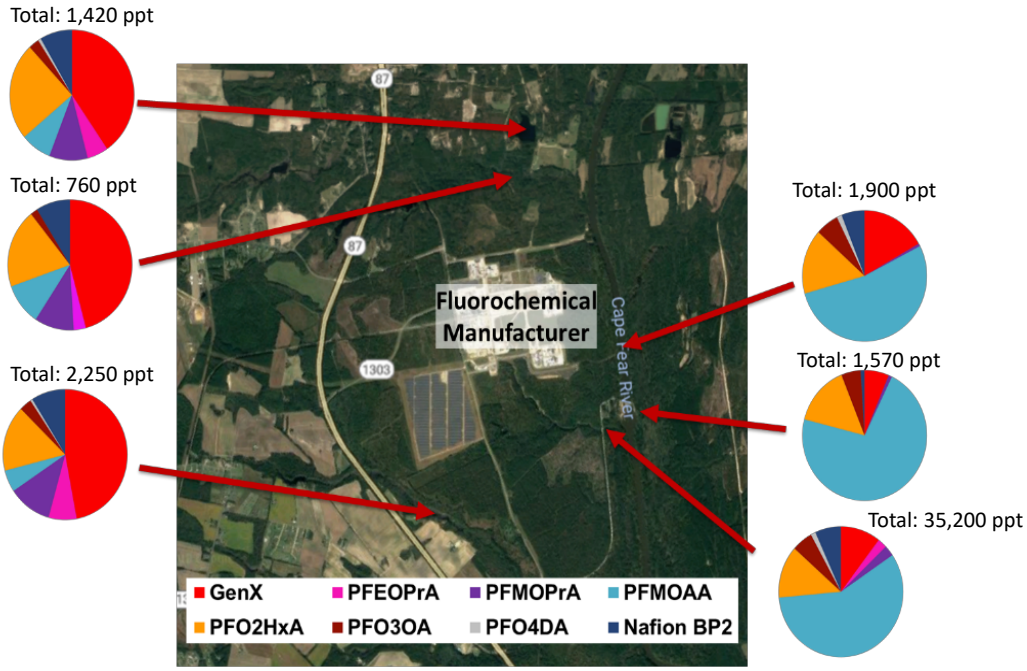

Figure 2.5: Fingerprints of surface waters collected in the vicinity of fluorochemical plant.

Fingerprinting of samples illustrates just how different the composition of PFAS contamination can be depending on the source of emissions (e.g., air emissions or wastewater discharge). Approaches including sample fingerprinting will potentially help to identify new PFAS sources in the future.

2.3 Environmental occurrence of PFAS

PFAS have been widely detected in surface water, groundwater, and finished drinking water. Results from a selection of studies related to such occurrences are summarized in Table 2.3.

Table 2.3: Occurrence of PFAS in environmental water matrices.

Location	PFHxA (ng/L)	PFOA (ng/L)	PFNA (ng/L)	PFHxS (ng/L)	PFOS (ng/L)	GenX (ng/L)	Ref
Drinking water							
USA (18 DWTP)	0.52-62	<5.0-57	<0.5-55	<0.25-5.6	<0.25-15	-	Appleman et al. 2013
USA (29 DWTP)	0.09-60	0.72-105	0.09-38	0.04-21	0.13-37	-	Boone et al. 2019
Netherlands (6 DWTP)	<0.1-5.3	<0.3-11	0.02-0.43	0.02-0.43	<0.03-0.41	<0.2-11	Gebbink et al. 2017
USA (7 DWTP)	<1.0-23	<5.0-30	<1.0-9.7	<1.0-12	<1.0-57	-	Quinones et al. 2009
USA (3 DWTP)	<10-318	<10-137	<10-38	<10-193	<10-346	<10-4560	Sun et al. 2016
Ruhr region, Germany	<2-56	<2-519	-	-	<2-22	-	Exner et al. 2006
Osaka, Japan	-	6.5-48	-	-	<0.5-3.7	-	Takagi et al. 2011
Queensland, Australia	<0.18-5.5	<0.18-9.7	-	<0.18-14.4	<0.18-15.6	-	Thompson et al. 2011

Table 2.3: (continued).

Surface water							
Netherlands (18 rivers)	4.0-6.4	2.8-12	0.49-1.0	1.5-2.2	2.7-7.1	<0.2-812	Gebbink et al. 2017
Germany (Rhine River)	2.2-6.8	4.4-8.9	0.09-0.76	1.0-4.4	<0.03-3.4	<0.47-108	Heydebreck et al. 2015
Global rivers (12 rivers)	0.1-198	0.15-53	0.05-5.7	0.09-1434	0.09-30	0.18-144	Pan et al. 2018
Ruhr region, Germany	<2-3040	<2-33900	-	-	<2-5900	-	Skutlarek et al. 2006
Cape Fear River Basin, NC	<1-23	<1-287	<1-194	<1-35.1	<1-132	-	Nakayama et al. 2007
Groundwater							
Osaka, Japan (22 wells)	9.7-970	45-74	2.2-44	-	-	-	Shiwaku et al. 2016
New Jersey	ND-36	ND-57	ND-96	ND-10	ND-12	-	NJDEP 2014
USA (10 USAF sites)*	0.006-340	0.009-220	0.022-10	0.01-910	0.019-9700	-	Anderson et al. 2016

*Concentrations for U.S. Air Force sites are reported in µg/L

2.4 Health impacts associated with PFAS

Toxicological research on PFAS has focused primarily on PFOA and PFOS. Though their production and use have been halted by manufacturers under the 2006 stewardship program (U.S. EPA 2015), environmental concentrations of these PFAS remain a concern. Persistence of PFAS in the environment and the human body is directly related to the dual lipophilic and hydrophobic nature of these chemicals. Elimination from the human body can vary widely among PFAS. For example, PFBS with 4 carbons can be eliminated from the human body in approximately 1 month, while PFOA and PFOS require 3.8 and 5.4 years, respectively. (Betts et al. 2007) Kotlarz et al. (2020) also demonstrated after 6 months levels of significant decreased for PFECA/PFESA. As a result, the continued investigation of PFAS toxicity is warranted as they will remain persistent in the environment and humans (Fenton et al. 2021).

Evidence collected through experimental animal models and human exposure demonstrate that PFOA, PFOS, and other carboxylic and sulfonic acid PFAS are toxic to multiple systems in animals and humans. Evidence for PFOA toxicity is sufficient enough to have the compound classified as a possible carcinogen to humans by the International Agency for Research on Cancer. (IARC 2016) While the U.S. National Toxicology Program has classified both PFOA and PFOS as “presumed to be immune hazards to humans”. (U.S. NTP 2016) Additional research has also demonstrated adverse health effects for exposure to PFOA and PFOS to include but not limited to high cholesterol, thyroid function, infertility, lowered immune response, liver cancer, and birth defects. (U.S. NTP 2016; Grandjean et al. 2012; Saikat et al. 2013; U.S. EPA 2017; Mastrantonio et al. 2017; He et al. 2018; Fenton et al. 2021)

The long-chain legacy PFAS only represent a small fraction of the estimated several thousand currently used or produced. Following the global phasing out of PFOA and PFOS,

manufacturers began to use and manufacture (1) short-chain PFAS and (2) fluorinated alternatives (e.g., GenX, ADONA, F53-B). (Hopkins et al. 2018; Ritscher et al. 2018; Strynar et al. 2015; Boone et al. 2019; Renner 2006; McCord et al. 2020) The phase out is apparent with the decrease in blood serum levels of PFOS in pregnant and nursing women in Sweden, though there has been an increase in PFBS and PFHxS levels since 2004. (Glynn et al. 2012)

The shift in fluorochemical manufacturing presents a broader issue as represented by the emission of byproducts from these manufacturing processes (Table 2.2). For the majority of these byproducts, there are insufficient peer-reviewed studies to conclude whether these fluorochemical byproducts represent a risk for adverse health effects. (Wang et al. 2015; Hoppin et al. 2019; Shi et al. 2015; Guo et al. 2019; Woodlief et al. 2021) For byproducts that have been studied, the results suggest multi-system toxicity. For example, exposure to GenX for Sprague-Dawley Rats demonstrated in male rats higher maternal liver weights, and lower maternal serum thyroid hormone and lipid profiles. These exposure results, though they required higher oral doses, produced similar outcomes to prior toxicity evaluations on PFAS, including PFOA and PFOS. (Conley et al. 2019) In another study, Richards et al. (2018) showed that environmentally relevant concentrations of GenX inhibited the P-glycoprotein (P-gp) transport activity and expression in rat brain capillaries for both males and females. This finding is significant due to the role of P-gp for exporting drugs out of cells. GenX is not the only byproduct shown to cause adverse health effects. For example, Wang et al. (2016) demonstrated in addition to GenX the tetramer form demonstrated hepatic effects greater than GenX. Additionally, Guo et al. (2019) demonstrated that PFO4DA caused hepatoxicity in male mice, though to a lesser degree at a dose of 10 mg/kg/d, and induced a urea cycle disorder. Long-chain fluoroethers, including PFO4DA

and PFO5DoDA, demonstrated adverse effects to hepatic stress signals, and glucose and lipid metabolism in male mice (Chen et al. 2021).

Globally there has been a scientific call to address the "extraordinary persistence, human and environmental exposure to PFAS". (Ritscher et al. 2018; Blum et al. 2015; Ng et al. 2021) There is clear evidence that further research needs to be conducted to better understand adverse health effects of these chemicals and identify levels at which these effects occur. Particularly, this clear gap in toxicity data for the majority of these byproducts (Table 2.2) hinders regulatory agencies from effectively providing guidance to protect environmental and human health. To reduce the risk associated with these chemicals, there is an urgent need to overcome the current insufficiency in peer-reviewed toxicity data for PFAS.

2.5 Regulations and guidance

The water soluble nature of many PFAS and continued detection in drinking water makes the consumption of drinking water an important exposure route. (Post et al. 2017; Pachkowski et al. 2019; Post 2021) As a result, measures have been established by different entities over the last decade to improve the protection of environmental and human health. (U.S. EPA 2018; NH DES 2019; NJ DEP 2019; ATSDR 2021; VT DHS 2019; NC DHHS 2019; MN DHS 2019; ECHA 2021) For example, extensive work has been conducted by the New Jersey Department of Environmental Protection for "the development of health-protective and scientifically sound guidelines for PFAAs in drinking water". (Post et al. 2017) In recent years at both the federal and state-level values for health advisory levels, minimum contaminant levels, and reference doses have been established to provide protection to human health from exposure to PFAS (Table 2.4 and Table 2.5)

Table 2.4: Example regulatory standards (existing or proposed) for PFAS in drinking water.

State or Country	Concentration (ng/L)
European Commission	Proposed standards:
	Individual PFAS = 100
	Total PFAS = 500
New Jersey	Health-based maximum contaminant level:
	PFOA = 14
	PFNA = 13
	PFOS = 13
New Hampshire	Proposed MCL
	PFOA = 12
	PFNA = 11
	PFHxS = 18
	PFOS = 15
	∑ PFOA + PFOS = 70

*Table 2.4: (*continued).

Michigan	Proposed Drinking water standards
	PFHxA = 400,000
	PFOA = 8
	PFNA = 6
	PFBS = 420
	PFHxS = 51
	PFOS = 16
	GenX = 370

Table 2.5: Example regulatory guidelines (existing or proposed) for PFAS in drinking water.

Agency/Country/State	Concentration (ppt) or Dose (mg/kg/day)
Agency for Toxic Substances and Disease	Intermediate oral MRL dose:
Registry (ATSDR)	PFOA = $3x10^{-6}$ mg/kg/day
	PFNA = $3x10^{-6}$ mg/kg/day
	PFHxS = $2x10^{-5}$ mg/kg/day
	PFOS = $2x10^{-6}$ mg/kg/day
U.S. EPA	**Chronic provisional reference dose:**
	PFBS = 0.0003 mg/kg/day
	GenX = 0.000003 mg/kg/day
	Health advisory level
	∑(PFOA + PFOS) = 70 ppt

Table 2.5: (continued).

Alaska	**Recommended alternate water supply:**
	∑(PFOA + PFOS) = 70 ppt
	Groundwater cleanup level:
	PFOA = 400 ppt
	PFOS = 400ppt
California	**Notification level:**
	PFOA =5.1 ppt
	FPOS = 6.5 ppt
	Response level:
	∑(PFOA + PFOS) = 70 ppt
Minnesota	**Health-based values for groundwater**
	and drinking water:
	PFBA = 7,000
	PFOA = 35
	PFBS = 2,000
	PFHxS = 27 ppt recommended
	PFOS = 27
Nevada	**Basic comparison level:**
	PFOA = 667 ppt
	PFOS = 667 ppt
	PFBS = 667,000 ppt

Table 2.5: (continued).

North Carolina	**Groundwater protective level:** PFOA = 290 ppt **Health Advisory:** ∑(PFOA + PFOS) = 70 ppt **Health goal:** GenX = 140 ppt
Texas	**Groundwater protective concentration:** PFOA = 290 ppt PFOS = 560 ppt PFNA = 290 ppt PFHxS = 93 ppt PFBS = 34,000 ppt PFBA = 71,000 ppt PFHxA = 93 ppt PFHpA = 560 ppt PFPeA = 93 ppt PFOSA = 290 ppt PFDA = 290 ppt PFDoA = 290 ppt
Connecticut	**Drinking water action level:** ∑(PFOA+PFOS+PFHpA+PFNA+PFHxS) = 70 ppt

Table 2.5: (continued).

Massachusetts	**Drinking water action level:** ∑(PFOA+PFOS+PFHpA+PFNA+PFHxS) = 70 ppt
Vermont	**Drinking water action level:** ∑(PFOA+PFOS+PFHpA+PFNA+PFHxS) = 20 ppt

These guidelines are being updated by states and federal agencies as more toxicity studies have become publicly available. These levels have been derived in a manner consistent with how the U.S. EPA derived the health advisory level for PFOA and PFOS. Often, the vast majority of PFAS do not have associated health advisory levels due to the limited toxicological data available. This hinders regulatory agencies from providing appropriate guidelines to protect environmental and human health.

Improved peer-reviewed occurrence and toxicity data for PFAS will help to develop new guidelines for PFAS present in the environment. These guidelines will also help water purveyors make decisions when evaluating treatment processes for removal of PFAS from source waters.

2.6 Water treatment

The outstanding strength of the carbon-fluorine bond is the key characteristic that makes PFAS so persistent in the environment resulting in wide spread contamination of drinking water sources. Treatment trains vary among drinking water treatment plants with different conventional and advanced treatment processes used to achieve treatment goals. However, the occurrence of PFAS in source waters has challenged many treatment plants to remove PFAS using many

conventional (e.g., coagulation, flocculation, sedimentation) and advanced treatment processes (e.g., ozonation, UV). As a result, drinking water providers are exploring additional treatment options including adsorption by GAC and anion exchange resins, and membrane filtration processes to remove PFAS.

2.6.1 Conventional treatment

Various studies have demonstrated treatment of PFAS by coagulation, flocculation, sedimentation, and filtration are ineffective for the removal of PFAS. (Boone et al. 2019; Appleman et al. 2013; Quinones et al. 2009; Vecitis et al. 2009; Hopkins et al. 2018) For example, Boone et al. (2019) demonstrated in 29 drinking water treatment plants conventional treatment processes were ineffective for removal of PFAS with the overall composition and concentration of PFAS similar between raw and finished water. Additionally, work conducted by Hopkins et al. (2018) demonstrated similar results for conventional treatment processes in the lower Cape Fear River basin of North Carolina. Peak area counts for PFAS (Table 2.2) emitted from a fluorochemical manufacturer were similar from raw water through to tap water (Figure 2.6).

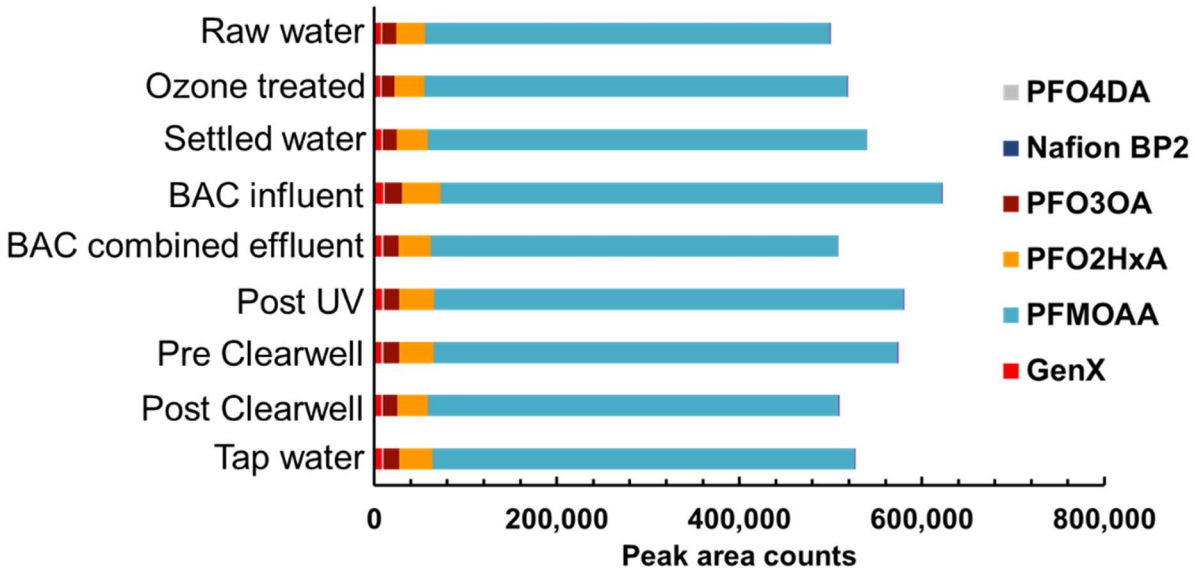

Figure 2.6: Removal of per- and polyfluoroalkyl ether acids (PFEA) by conventional and advanced treatment options at a drinking water treatment plant in the Cape Fear River basin.

In Figure 2.6 no significant reduction in PFAS is demonstrated from raw water to tap water by conventional and advanced treatment processes. The reduction across the biologically activated carbon (BAC) filter is expected to be a result of dilution from the mixing of filter effluents. These results demonstrate the need for more advanced or tailored processes to remove PFAS in drinking water sources.

2.6.2 Oxidative processes

The fluorine atom is extremely electronegative, which makes it thermodynamically unfavorable to oxidize PFAS. Therefore, such processes as chlorination/chloramination, ozonation, and advanced oxidation processes (AOPs) are ineffective for removal of these compounds (Figure 2.6). (Hopkins et al. 2018; Sun et al. 2016; Gebbink et al. 2017; Vecitis et al. 2009) Additionally, oxidative processes can lead to the formation of commonly monitored PFAS. For example, if precursor compounds are present in the water prior to oxidation, following oxidation terminal products may form including PFOS and PFOA. (Rahman et al.

2014; Houtz et al. 2012) The shift from long-chain PFAS to fluorinated alternatives, including PFEA and short-chain PFAS, has not led to changes in the persistence of these compounds. For example, Sun et al. (2016) and Hopkins et al. (2018) both demonstrated ozone and AOPs did not measurably oxidize fluoroethers detected in a NC drinking water source (Figure 2.6). Zhang et al. (2019) demonstrated that several fluoroethers (e.g., ADONA, Nafion Byproduct 2, NVHOS, HydroEve) could be oxidized to unknown terminal products. Some more intensive oxidative processes have been shown to be effective for PFAS, including photocatalytic oxidation, photochemical oxidation, photochemical reduction, persulfate radical treatment, thermally induced reduction, and sonochemical pyrolysis. (Lazerte et al. 1953; Hori et al. 2005; Moriwaki et al. 2005; Yamamoto et al. 2007; Bruton et al. 2017; Lu et al. 2020) However, from a cost-effectiveness standpoint, these technologies are currently not feasible for drinking water treatment.

2.6.3 Biological processes

Biofiltration and microbial treatment to enhance PFAS removal have been demonstrated to be mostly ineffective for PFAS removal. Under acidic pH and iron rich conditions the Faemmox process was demonstrated to degrade PFOS and PFOA (Huang and Jaffe 2019). These conditions would not be expected to exist in drinking water treatment. Though Figure 2.6 shows a reduction in PFAS response across the BAC contactors, this reduction can be explained by dilution from the combining of contactor effluents. In many cases, biofilters and other granular activated carbon (GAC) filters become ineffective for PFAS removal or even release PFAS into treated water. For example, following reduction of PFAS in source water, due to source control,

there was an increase in finished water concentrations compared to source water concentrations for a GAC contactor that had been loaded with PFAS for several months (Figure 2.7).

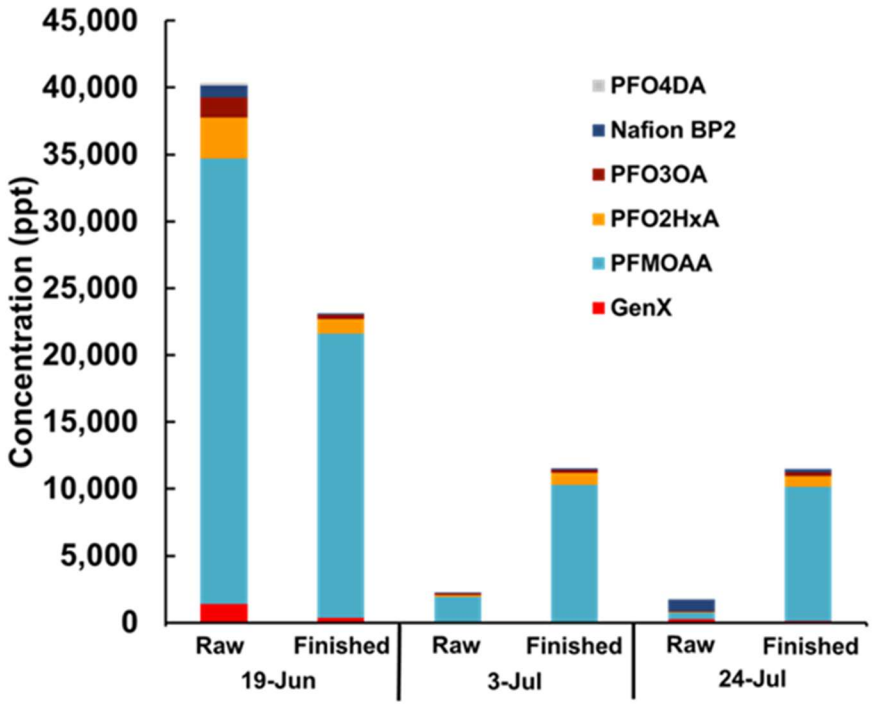

Figure 2.7: Leaching of PFAS from GAC following source control. Finished water represents blended effluent from three contactors. Service lives: 4,170, 11,900, and 19,000 bed volumes; Empty bed contact time: 14 minutes.

2.6.4 Additional advanced treatment processes

In addition to the processes discussed in the previous sections, there are more advanced processes being considered for PFAS removal including membranes and destructive technologies (Kucharzyk et al. 2017; Murray et al. 2019). Average rejection rates for PFAS by a virgin membrane were 99.3% and following induced fouling the rejection dropped to 95.3%. (Steinle et al. 2008) A question for membranes and reverse-osmosis systems is the management of the concentrate stream. Currently these streams would just return to the wastewater treatment plant and be reemitted to source waters due to the ineffective removal of PFAS by wastewater treatment plant processes. However, if small volume/high concentration streams can be collected

then next-generation technologies may be effective in remediating these waste streams. For example, destructive-based technologies (e.g., AOP/ARP and eBean irradiation) may become feasible for these smaller volume waste streams. (Stratton et al. 2017; Wang et al. 2016)

2.7 Adsorptive treatment

While conventional water treatment processes and some advanced options have been demonstrated to be ineffective or not feasible for PFAS removal, treatment processes employing adsorbent materials (e.g., powdered activated carbon, granular activated carbon) have been shown to effectively remove micropollutants in a drinking water treatment context. (Gebbink et al. 2017; Appleman et al. 2013; Quinones et al. 2009; Vecitis et al. 2009; Ternes et al. 2002; Rossner et al. 2009; Corwin et al. 2012; Summers et al. 2011; Reinert et al. 2013) Granular activated carbon (GAC) is effective for removal of contaminants of emerging concern (CECs) because of the large internal surface area, which provides a surface for physical adsorption of CECs through nonspecific van der Waals forces. (Crittenden et al. 2012)

2.7.1 Removal of PFAS by activated carbon

Both powdered activated carbon (PAC) and GAC have been shown to be effective for the removal of a wide range of PFAS. (Sun et al. 2016; Hansen et al. 2010; Dudley et al. 2012; Piai et al. 2019; Zhi et al. 2015; Park et al. 2020) Previous results demonstrate adsorption trends among PFAS including (1) adsorbability increases with increasing carbon chain length and (2) the acidic head group affects adsorbability, sulfonic acid>carboxylic acid. (Hansen et al. 2010; Dudley et al. 2012; Arevalo et al. 2014; Park et al. 2020) However, Dudley et al. 2015 suggested that PAC is not a feasible treatment option when a high percentage of removal is required (e.g.

90%), in which case very high carbon doses are required. If lower removal percentages are required (e.g. 50%), then PAC could be feasible for the removal of longer-chain PFAS, such as PFOA, PFNA, perfluorodecanoic acid (PFDA), PFHxS, and PFOS. While adsorptive removal of shorter-chain PFAS (e.g., PFBA, PFPeA, and PFBS) required PAC doses that were practically too high for drinking water treatment. Sun et al. (2016) evaluated the adsorption of PFAS emitted from a fluorochemical manufacturer. For example, 30% removal of GenX was achieved at a PAC dose of 60 mg/L, while at a similar dose 80% PFOA and >95% PFOS were achieved. Treatment of the short-chain PFEA (e.g. PMPA and PEPA) by PAC showed <20% removal, even when 100 mg/L PAC was dosed. (Sun et al. 2016) The results suggest use of PAC is not feasible treatment option for waters contaminated by replacement fluorochemicals including short-chain PFAS and PFEA.

In addition to PAC, GAC has been previously evaluated as a treatment option for the removal of PFAS from contaminated waters. (Hansen et al. 2010; Senevirathna et al. 2010; Carter et al. 2010; Park et al. 2020; Rodowa et al. 2020; Belkouteb et al. 2020; Franke et al. 2019) Park et al. (2020) and Rodowa et al. (2020) both demonstrated how physicochemical properties of PFAS (e.g., chain length, functional head group) affect removal of traditionally studied PFCA and PFSA in groundwater. Park et al. (2020) also studied PFAS removal by four bituminous coal-based carbon using RSSCTs. While these studies provide information about removal efficiency of traditionally PFCA and PFSA, there are still several knowledge gaps yet to be fully explained. A few additional factors to be considered by drinking water providers if GAC is to be considered a (cost)effective treatment option include 1) how chemical and physical characteristics of short-chain PFAS and fluorinated alternatives affect removal efficiency, 2) how source water characteristics influence treatment goals (e.g. 50%, 75%, or 90% removal), and 3)

how GAC type affects removal (e.g. coal-based vs. coconut based vs. lignite). Greater understanding of these knowledge gaps will allow drinking water providers to better manage PFAS contamination in source water and potentially describe the initial removal, rapid breakthrough, and desorption of PFAS from GAC treatment systems (Figure 2.8)

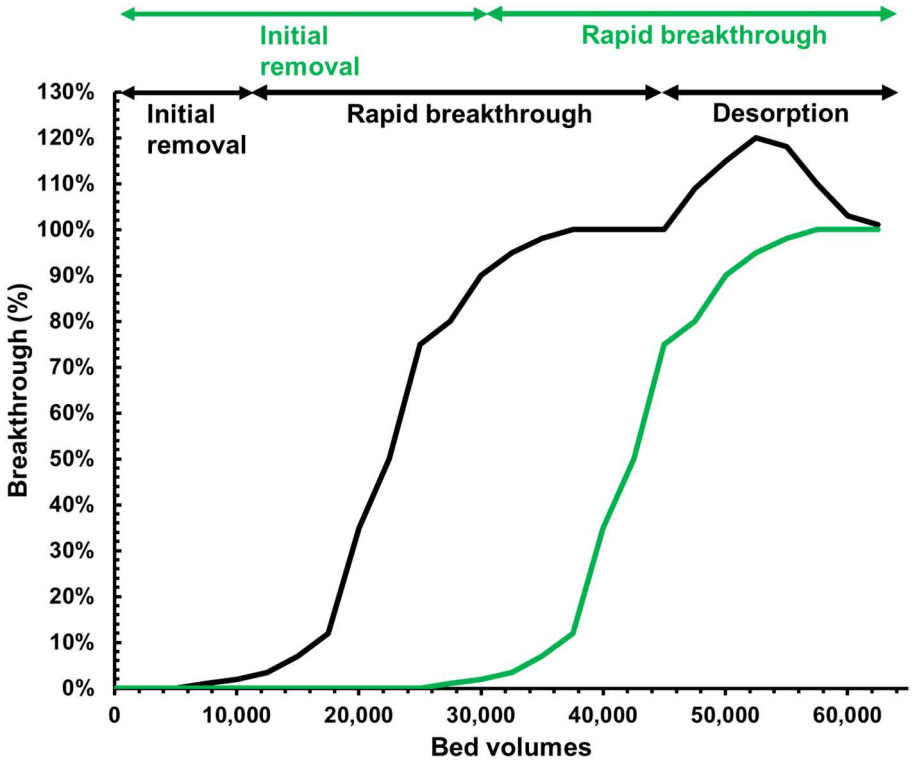

Figure 2.8: Adsorption and desorption phenomena as shown by a contaminant breakthrough curve for GAC.

Understanding how source water conditions, empty bed contact time, or adsorbent selection affect breakthrough of contaminants would allow for better predicting GAC service life. For example, selection of an adsorbent with a higher adsorption capacity could result in obtaining >90% removal for an additional 20,000 to 30,000 bed volumes (green breakthrough curve, Figure 2.8). If short-chain PFAS or PFEA are targets for removal from source water, then an increase GAC performance from breakthrough at ~15,000 to ~35,000 bed volumes could

potentially increase the feasibility of GAC as a treatment option. Only a few studies to date have demonstrated the removal of PFEA using GAC. (Hopkins et al. 2018; CFPUA 2017) For example, Hopkins et al. (2018) showed for a GAC contactor being loaded with PFEA contaminated source water, that a regenerated subbituminous coal-based carbon could remove these contaminants for a few thousand bed volumes (Figure 2.9).

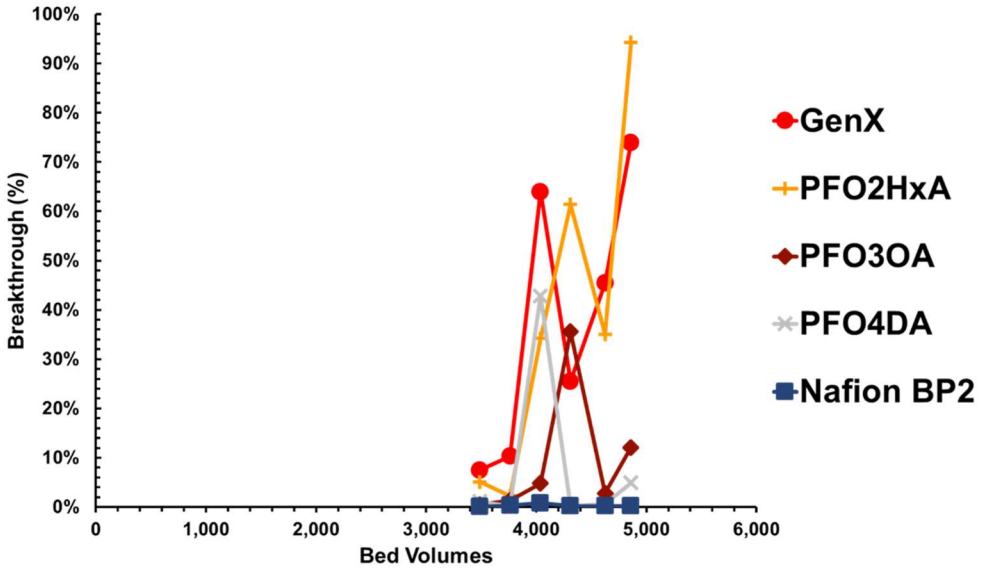

Figure 2.9: Breakthrough of PFEA in full-scale GAC contactor, Reactivated F300, EBCT = 14 minutes.

Figure 2.9 demonstrates that GenX reached 7% and 74% breakthrough after approximately 3,500d and 5,000 bed volumes of treated water, respectively. PFO2HxA is shown to break through at a similar bed volume as GenX while for PFO3OA and PFO4DA breakthrough occurred at slightly longer bed volumes. Nafion byproduct 2 removal efficiency by GAC can be expected for at least 5,000 bed volumes (Figure 2.9). Additional data collected at an earlier port on the adsorber, corresponding to a shorter EBCT, demonstrated that Nafion byproduct 2 breaks through at 10,000 to 15,000 bed volumes.

Similarly, a pilot-scale study conducted in similar source water demonstrated rapid breakthrough of short-chain PFAS and fluorinated alternatives (Figure 2.10). (CPFUA 2017)

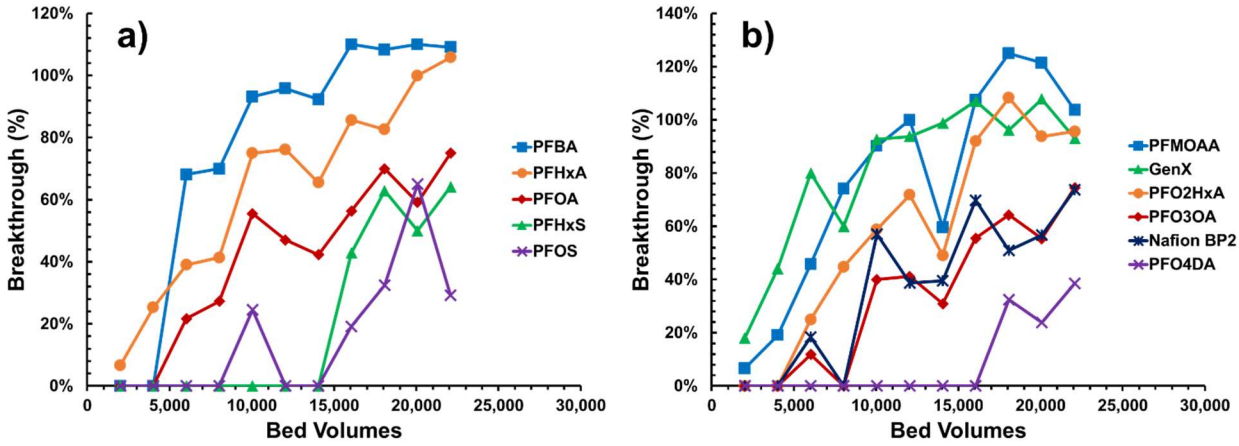

Figure 2.10: a) Legacy PFAS and b) PFEA breakthrough in pilot-scale GAC adsorbers. Reagglomerated subbituminous coal-based carbon (Carbon A), EBCT=10 minutes.

Comparing Figure 2.9 and Figure 2.10b, similar breakthrough trends are exhibited by both the pilot-scale and full-scale, respectively. Both the full-scale (Figure 2.9) and pilot-scale (Figure 2.10b) illustrate that GAC can only remove GenX from a moderate TOC coagulated and filtered surface water for short period of time. Figure 2.10b shows early breakthrough of short-chain PFEA (e.g. 3,000-8,000 bed volumes). While for the longer-chain PFEA breakthrough occurs after 8,000 bed volumes (e.g., PFO3OA, PFO4DA, and Nafion Byproduct 2). One difference between the pilot and full-scale data is that breakthrough of PFAS is slightly more spread out. This could potentially be due either a difference in the two reagglomerated subbituminous coal-based carbons or a difference in background water quality characteristics during the GAC contactors service life. Further research is required to better understand how performance varies among different adsorbents and background water matrices. This will be further discussed in Chapter 5.

2.7.2 Effect of carbon type

Selection of an effective GAC for removal of PFAS is important to minimizing carbon use rates. Activated carbons are produced from a variety of organic feedstocks, including wood, coconut shell, bituminous coal, and lignite. The feedstock is pyrolyzed and subsequently activated changing the pore structure, surface area, and surface chemistry of the feedstock. The internal pore structure provides a large surface area allowing for potentially effective removal of micropollutants in water treatment. The GAC produced is highly porous with an internal surface area typically in the range of 800-1500 m^2/g. (Bansal et al. 1988) The distribution of pore size directly affects the compounds which can adsorb and the kinetics of adsorption. (Summers et al. 2011) The IUPAC classifies pores into 3 main categories: micropores (<2nm), mesopores (2-50nm), and macropores (>50nm). (Zhang et al. 2007; Moore 2003) Generally, coconut-based carbons exhibit a larger portion of micropores, while a bituminous coal-based carbon might exhibit a more desirable distribution of all pore types. (Zhang et al. 2007) GAC used in water treatment exhibits a heterogeneous pore structure containing a mix of the four pore types. The pore size distribution is one of the most important characteristics affecting GAC performance. There are two ways in which adsorption of a contaminant can be affected (1) size exclusion and (2) strength of adsorbate-adsorbent interaction. Size exclusion will limit the adsorption of a contaminant to a pore equal to or larger than the contaminant. Adsorption in these pores of equal size can be hindered when background natural organic matter (NOM) is present because of pore blockage. This reduces access to pore volume in smaller pore size ranges, which reduces the adsorption capacity of a carbon. The strength of the adsorbate-adsorbent interaction influences adsorption of micropollutants. Typically, the strength of the interaction increases with decreasing pore size because once the pore width is less than half the adsorbate diameter the adsorption

potential between the walls overlaps.. While it is important to determine how PFAS adsorption varies among different GAC, there is equal importance to understand the effect of background NOM on GAC performance.

2.7.3 Effect of water matrix

GAC has been demonstrated to be effective for a variety of micropollutants, GAC is a non-selective media. (Summers et al. 2014; Corwin et al. 2010; Inyang et al. 2017; McCleaf et al. 2017) Due to the non-selective nature of GAC, removal of micropollutants in source waters containing NOM is potentially difficult due to competition for adsorption sites. The mixture of compounds, including background organic matter, reduces the number of available adsorption sites either through direct competition for adsorption sites or pore blockage. (Li et al. 2002; Carter et al. 1992; Pelekani et al. 1999) Competition among these organic constituents is also heavily dependent on the nature of the background NOM and concentration. Background NOM consists of humic and non-humic substances, wastewater derived organic matter and synthetic organic compounds.

Previous work has demonstrated that NOM can inhibit the adsorption of micropollutants through competition for adsorption sites and pore blockage. (Li et al. 2003; Kennedy et al. 2013) As a result, NOM reduces both adsorption capacity and kinetics of micropollutants. (Li et al. 2002; Kennedy et al. 2013; Sontheimer et al. 1988) Operation of adsorbers in a continuous manner allows for preloading of NOM onto GAC. Preloading is when the NOM mass transfer zone moves through the bed faster than the target compound(s), which results loading of adsorption sites deeper in the GAC bed before the micropollutant mass transfer zone reaches the same point. The preloading of NOM will will decrease time to breakthrough of the

micropollutant and increase GAC use rates. (Matsui et al. 2002; Schideman et al. 2007) Therefore it is important to understand how different concentrations and types of background organic matter affect the adsorptive removal of short-chain PFAS and fluorinated alternatives.

2.7.4 Rapid small-scale column test design and operation

Design of bench-scale rapid small-scale column test (RSSCT) is important for collecting data at the bench-scale that can be scaled to predict full-scale treatment systems. Additionally, the final design will help to understand factors affecting adsorptive removal discussed in sections 2.7.2 and 2.7.3.

To assess these factors affecting adsorptive removal of PFAS, research is required to determine an approach for conducting this work. Ideally, work should be conducted at the scale that the treatment process will be operated. However, the operation of pilot and full-scale methods are costly and time consuming to obtain performance data. As a result, an approach to reduce the time and cost of obtaining removal performance has been created called the rapid small-scale column test. (Crittenden et al. 1986; Crittenden et al. 1987; Crittenden et al. 1991; Summers et al. 1995) Pros and cons for why the RSSCT design should be considered compared to pilot testing are provided in Table 2.6.

Table 2.6: Comparison of testing adsorptive removal performance.

Approach	Advantages	Disadvantages
Pilot-scale tests	1) Very accurate at predicting full-scale performance 2) Employs the same carbon size as full-scale reducing organic matter issues	1) Time required to conduct these can be lengthy 2) Expensive and must be conducted onsite
RSSCTs	1) Can predict GAC performance accurately 2) Requires less water for testing, which allows for testing offsite (e.g, in a central laboratory) 3) Reduced run time and cost to run	1) Don't accurately reflect adsorption capacity due to reduction in background organic matter fouling 2) Beneficial effects of biodegradation not captured 3) Site specific and can only be compared to similar influent conditions

Advantages of the RSSCT design make the approach desirable for assessing the performance of GAC for removing micropollutants. The RSSCT approach also allows for simultaneously studying a variety of factors affecting removal of PFAS (e.g., empty bed contact time, GAC type, water matrix). However, to scale RSSCT results to full-scale limitations including the difference in adsorption capacity need to be overcome.

The RSSCT was, originally proposed by Crittenden et al. (1986) to evaluate GAC performance at the bench-scale. The bench-scale approach is based on mass transfer models that provide the basis for scaling full-scale adsorbers to bench-scale. To maintain perfect similitude between the full-scale and RSSCT, Crittenden et al. (1986, 1987) required that dimensionless parameters in Table 2.7 be kept constant.

Table 2.7: Dimensionless parameters relating full-scale and RSSCT designs.

Parameter	Equation
Pore solute distribution parameter	$D_g = \frac{\varepsilon_p(1-\varepsilon)}{\varepsilon}$
Pore diffusion modulus	$Ed_p = \frac{4D_pD_gL\varepsilon}{d_p^2 v_f}$
Surface diffusion modulus	$Ed_s = \frac{4D_sC_FL\varepsilon}{d_p^2 v_f}$
Peclet number	$Pe = \frac{Lv_f}{\varepsilon D_z}$
Stanton number	$St = \frac{2k_fL(1-\varepsilon)}{d_p v_f}$

Variables used to calculate parameters in Table 2.7 are the intraparticle porosity (εp), bed porosity (ε), pore diffusion coefficient (Dp), fluid residence time in packed bed (t), particle diameter (dp), surface diffusivity (Ds), capacity factor (C_F), bed length (L), fluid velocity (v_f), dispersion coefficient (Dx), and film mass transfer coefficient (k_f).

Since the RSSCT utilizes a smaller GAC particle size than full-scale adsorbers, several equations were developed to relate the large-scale design to the bench-scale columns (Crittenden et al. 1986,Crittenden et al. 1987). These equations are presented in Table 2.8. Large column and small column parameters are denoted by subscripts of LC and SC, respectively.

Table 2.8: RSSCT design equations.

Parameter	Equation
Scaling factor (SF)	$SF = \left(\frac{d_{p,LC}}{d_{p,SC}}\right)$
Diffusion coefficients (D)	$D_{SC} = (SF)^{-X} D_{LC}$
Empty bed contact time (EBCT)	$EBCT_{SC} = (SF)^{X-2} EBCT_{LC}$
Design factor (DF)	$DF = \frac{EBCT_{SC}}{EBCT_{LC}} = (SF)^{X-2}$

These design equations (Table 2.8) in conjunction with the dimensionless parameters (Table 2.7) allow for keeping perfect similitude between the large column and bench-scale. Application of equations in Table 2.8 can be used to determine how intraparticle diffusivity controls adsorption kinetics. For example, the assumption could be made that intraparticle diffusivity scales independently of particle size or decreases linearly with particle size when designing a RSSCT. The assumption of intraparticle diffusivity being independent of particle size is commonly used. This design is referred to as the constant diffusivity design, where the proportionality factor (X) is zero in the design equations (Table 2.8). (Crittenden et al. 1991; Summers et al. 2014) The CD-RSSCT design has been used for determining GAC selection and estimating GAC service life because these experiments can be conducted in a relatively short period of time (<1 month). Bench-scale experiments also use the proportional diffusivity design (PD-RSSCT). The PD-RSSCT assumes that intraparticle diffusivity decreases linearly with particle size by applying a proportionality factor of X=1.0 to the design equations (Table 2.8). (Crittenden et al. 1987). The PD-RSSCT has been used to simulate background NOM adsorption and micropollutant removal in the presence of background NOM. (Corwin et al. 2010) However,

the PD-RSSCT design requires large bed depths, which results in higher head loss and larger water requirements. (Crittenden et al. 1987) As a result, the similitude between the large column and small column designs is not maintained. To reduce the bed depth and hydraulic loading rate a minimum Reynolds number was introduced (Equation 2.1).

$$Re_{SC,min} = \frac{500}{S_c} \qquad \textit{Equation 2.1}$$

Where S_c is the Schmidt number. Typically, the minimum Reynolds number ranges from 0.023 to 0.13 for organic chemicals and background organic matter. This value is also dependent on the target compound. Using the minimum Reynolds number, the hydraulic loading rate for the PD-RSSCT can be calculated (Equation 2.2).

$$\frac{v_{f,SC}}{v_{f,LC}} = \left[\frac{d_{p,LC}}{d_{p,SC}}\right]\left[\frac{Re_{SC,min}}{Re_{LC}}\right] \qquad \textit{Equation 2.2}$$

In Equation 2.2, v_f represents the hydraulic loading rate and d_p represents the GAC particle diameter. The PD-RSSCT approach has not been as widely used as the CD-RSSCT because the time required for completion is longer (~3 months).

As stated previously, the similarity between the large column and RSSCT design is not required for the successful design of the small-scale column. As long as the mass transfer is mostly due to internal mass transfer the equations in Table 2.8 can still apply. The CD-RSSCT has also been demonstrated to be effective at estimating GAC performance for micropollutant removal in natural waters when perfect similitude is not maintained (Knappe et al. 1997). The minimum Reynolds number approach is applied to maintain conditions under which external mass transfer and dispersion do not become dominant. The main advantage of this CD-RSSCT is that it permits the rapid completion of the experiments in less than one week. The CD- and PD-RSSCT can also be conducted with differing GAC aprticle size in order to determine whether intraparticle diffusivity varies with particle size at the bench-scale. For example, the use of a

200x230 U.S. mesh size particle compared to a 100x200 U.S. mesh size particle reduces operation time to treat ~100,000 bed volumes by ~1-2 months.

To date, the question as to which RSSCT design is best determining GAC performance for removal of short-chain and fluorinated alternatives has not been addressed. This research will determine what RSSCT design is best for describing field-scale PFAS breakthrough and develop a scale-up approach to describe breakthrough using the bench-scale design.

CHAPTER 3 MATERIALS AND METHODS

3.1 Materials

3.1.1 Waters

There are three different water sources used in this research (A, B, C). Specific water quality parameters, including total organic carbon (TOC) and ultraviolet absorbance at 254nm (UV254), for waters collected from sources A, B, and C are presented in Table 3.1.

Table 3.1: Water quality parameters for RSSCT and Pilot tests in surface water and groundwater.

	Water A				Water B		Water C	
Source	**Surface water**				**Wastewater-impacted Groundwater**		**Groundwater**	
Parameters	**RSSCT**			**Pilot**	**RSSCT**	**Pilot**	**RSSCT**	**Pilot**
TOC (mg L^{-1})	1.3	1.5	2.3	2.3	1.6	1.3	<0.5	<0.5
UV254	0.073	0.138	0.209	--	--	--	0.04	--

Waters collected from source water A was either settled coagulated surface water (TOC = 1.5 or 2.3 mgL^{-1}) or settled coagulated surface water after biofiltration (TOC = 1.3 mgL^{-1}). Source A waters were collected in 55 gallon high-density polyethylene (HDPE) barrels. PFAS and TOC samples were collected upon arrival and prior to experiments to confirm PFAS and TOC concentrations. TOC was analyzed using a Shimadzu TOC analyzer (Model TOC-VCSN, Shimadzu Scientific, Columbia, MD). PFAS were analyzed using Agilent liquid chromatography triple quadrupole mass spectrometer (Agilent Technologies, Santa Clara, CA) in accordance with a method developed in our lab (Section 3.2.1).

Water collected from source B was a wastewater-impacted groundwater. All of the primary data in this thesis concerning Water B as provided by Orange County Water Distract

(OCWD). Water collected from source water B was a groundwater. Source B water was collected in 5 gallon HDPE carboys.

Source water C was a groundwater collected in 5 gallon HDPE containers. Similar to source water A, water C was characterized by PFAS and TOC analysis upon receiving and prior to experiments.

3.1.2 Adsorbates

Across all bench-scale and pilot-scale tests, a total of 22 environmentally relevant PFAS were studied in this dissertation. The average influent concentrations of PFAS selected for this work are listed in Table 3.2. PFAS concentrations for pilot-scale studies were native concentrations. For bench-scale experiments, additional PFAS were dosed into the influent to achieve concentrations that were 1) environmentally relevant, 2) above minimum reporting limits, and 3) able to measure the onset of breakthrough at an effluent concentration corresponding to approximately 10% of the influent concentration. For waters used at bench-scale, influent samples collected at minimum at the beginning and end of experiments to estimate influent concentrations. All the PFAS used for spiking influent water were sourced from Synquest Laboratories Inc. (Alachua, FL) and The Chemours Company (Wilmington, DE).

Table 3.2: Average PFAS concentrations for RSSCT and pilot tests in surface water and groundwater.

PFAS	Concentration (ng/L)					
	Coagulated surface water		Wastewater-impacted Groundwater		Groundwater	
	Pilot	RSSCT	Pilot	RSSCT	Pilot	RSSCT
Perfluorocarboxylic acids (PFCAs)						
Perfluorobutanoic acid (PFBA)	10	109	--	--	9	129
Perfluoropentanoic acid (PFPeA)	21	112	--	--	13	133
Perfluorohexanoic acid (PFHxA)	23	119	2.8	--	19	129
Perfluoroheptanoic acid (PFHpA)	16	106	--	--	10	106
Perfluorooctanoic acid (PFOA)	11	98	16	15	33	143
Perfluorononanoic acid (PFNA)	--	106	2.2	--	44	157
Perfluorodecanoic acid (PFDA)	--	121	3.1	--	--	136
Perfluorosulfonic acids						
Perfluorobutane sulfonate (PFBS)	3	118	14	--	--	129
perfluorohexane sulfonate (PFHxS)	5	119	11	--	2	98
perfluorooctane sulfonate (PFOS)	12	131	23	--	6	139
Fluorotelomer sulfonic acid						
6:2 fluorotelomer sulfonic acid (6:2 FTS)	--	89	--	--	--	114
Perfluoroalkylether carboxylic acids						
Perfluoro-2-methoxyacetic acid (PFMOAA)	1452	158	--	--	--	85
Perfluoro-2-methoxypropanoic acid (PMPA)	--	111	--	--	--	107
Perfluoro-2-ethoxypropanoic acid (PEPA)	--	100	--	--	--	91
Perfluoro-2-propoxypropanoic acid (GenX)	19	94	--	--	--	132
Perfluoro-3,5-dioxahexanoic acid (PFO2HxA)	116	119	--	--	--	94
Perfluoro-3,5,7-trioxaoctanoic acid (PFO3OA)	52	107	--	--	--	112
Perfluoro-3,5,7,9-tetraoxadecanoic acid (PFO4DA)	24	97	--	--	--	96
Perfluoro-3,5,7,9,11-pentaoxadodecanoic acid (PFO5DoA)	--	97	--	--	--	98
2,2,3,3-Tetrafluoro-3-{[1,1,1,2,3,3-hexafluoro-3-(1,2,2,2-tetrafluoroethoxy)propan-2-yl]oxy}propanoic acid (HydroEve Acid)	--	96	--	--	--	97
Polyfluoroether sulfonic acids						
1,1,2,2-tetrafluoro-2-(1,2,2,2-tetrafluoro-ethoxy)ethane sulfonic acid (NVHOS)	--	93	--	--	--	106
Perfluoro-2-{[perfluoro-3-(perfluoroethoxy)-2-propanyl]oxy}ethanesulfonic acid (Nafion by-product 2)	33	99	--	--	--	103

3.1.3 Adsorbents

For Chapter 4, all GAC tested at the bench-scale were selected based on GAC tested at the pilot-scale. The GAC studied included 4 coal-based carbons (Carbons A, B, E, and G), one coconut shell-based carbon (Carbon D), and one lignite-based carbon (Carbon F). In Chapter 5, GAC tested at bench-scale included two coal-based carbons (Carbons A and B), one coconut

shell-based carbon (Carbon C), and one lignite-based carbon (Carbon D). Information about GAC is provided in Table 3.3.

Table 3.3: GAC types and characteristics for RSSCT and field-scale tests.

GAC	Base material	U.S. mesh Size		Apparent (bed) density (g/cm³)	Pore volume (cm³/g)		
		Pilot	RSSCT		Primary micropore (<8 Å)	Secondary micropore (8-20 Å)	Mesopore (20-50 Å)
A	Reagglomerated subbituminous coal	12x40	200x230[a] 100x140[b]	0.54	0.1389	0.1532	0.0403
B	Reagglomerated subbituminous coal	12x40	200x230[a]	0.50	0.1210	0.1838	0.0628
C	coconut shell	12x30	200x230[a]	0.41	0.1770	0.3199	0.1114
D	Lignite	8x30	200x230[a]	0.38	0.0975	0.0756	0.0974
E	Reagglomerated subbituminous coal	12x40	100x140[b]	0.62	---	---	---
F	Lignite	10x30	80x120[b]	0.39	---	---	---
G	Low density coal	12x40	100x140[b]	0.50	---	---	---

[a] mesh size used for Source water A and Water C RSSCTs and Pilots
[b] mesh size used for Source B RSSCTs and Pilots

3.1.4 Rapid small-scale column tests

All materials in the RSSCTs were either polypropylene (PP) or stainless steel (SS). Tubing was either 0.318 cm ID PP tubing (Thermo Fisher Scientific Inc., Walktham, MA), 0.476 cm ID PP tubing (Thermo Fisher Scientific Inc., Walktham, MA), or 0.4cm ID SS tubing. Water was fed to the RSSCTs through polyetheretherketone (PEEK) tubing using a Shimadzu LC pump (Model LC-20AT, Shimadzu Scientific, Columbia, MD) from either a 55 gal HDPE barrel or 5 gal HDPE carboy. All valves and fittings were sourced from Swagelok (Solon, OH).

3.2 Methods

3.2.1 Analytical methods

Analysis of PFAS shown in Table 3.2 were conducted by high performance liquid chromatography (1260 series, Agilent) and tandem mass spectrometry (Ultivo, Agilent) at North Carolina State University. A large volume direct injection method was developed for analysis of PFAS samples. Advantages of this method include rapid analysis and minimal sample preparation, compared to traditional solid-phase extraction methods. Samples for experiments were collected in 15 mL polypropylene falcon tubes. From the falcon tube a 1,620 µL aliquot of sample was transferred into an LC vial and spiked with 180 µL of internal standard. The total 1,800 µL volume allowed for two complete injections at 800 µL each at high and low temperature mass spectrometer settings to maximize response for the targeted PFAS.

A 800-µL aliquot of each sample, calibration standard, and quality control sample was injected into the LC system that was equipped with a 900 µL sample loop. Analytes were chromatographically separated using a Zorbax RR Eclipse Plus C18 column (4.6 x 50 mm, 3.5 µm; Agilent). Conditions were as follows: eluent flow rate: 0.7 mL/min; column temperature: 50°C; mobile phase A: ammonium acetate buffer (5 mM) in water, and mobile phased B: methanol; gradient: 0-18 min linear from 90:10 A/B to 5:95 A/B, 18-22 min constant 5:95 A/B; followed by a 6 min post-analysis time for equilibration.

PFAS were detected using electrospray ionization in negative polarity mode and multiple reaction monitoring. Ion source parameters are provided in Table 3.4. For quantification of PFAS containing a carboxylic acid moiety, low-temperature settings were used. For quantification of PFAS with a sulfonic acid moiety, high-temperature settings were used.

Table 3.4: Mass spectrometer ion source parameters.

Parameter	Low Temperature	High Temperature
Drying gas temperature (°C)	100	230
Drying gas flow rate (L/min)	13	13
Sheath gas temperature (°C)	250	350
Sheath gas flow rate (L/min)	12	12
Nebulizer pressure (psi)	20	15

Data acquisition and processing were performed using Agilent MassHunter Quantitative Analysis Version B.09.00. A list of target analytes and internal standards used for quantitation is provided in Appendix A, Table A.1. With the exception of PFBA, PFPeA, PFMOAA, and PMPA each analyte has a pair of precursor-product ion transitions for quantitation and confirmation, respectively. Quantitation was conducted using an isotope dilution approach, i.e., the ratio of the peak area of the analyte to the peak area of the internal standard was used to develop standard curves and determine analyte concentrations. If a mass-labeled analog of the analyte was not available, a structurally similar mass-labeled internal standard with a similar retention time was used for quantitation (Table A.1).

3.2.2 Preparing micropollutant stocks

PFAS stock solutions were prepared from either 1) commercially available neat standards or 2) standards provided by The Chemours Company. For neat standards purchased from Synquest, stock solutions were prepared in 95:5 (v/v%) methanol: 2.5M sodium hydroxide at 10,000 ng μL^{-1}. Stock solutions from The Chemours Company were received in water at approximately 1,000 ng μL^{-1}.

3.2.3 Granular activated carbon preparation

For field-scale testing the as-received carbon was used. The GAC used for the RSSCTs was wet milled with a mortar and pestle and then wet sieved to separate and collect the targeted particle size. The GAC particle size targeted for experiments were 100x200, 200x230, and 230x325 U.S. Standard Mesh fraction. Eight-inch diameter brass sieves were used (McMaster-Carr, Cleveland, OH). The following protocol was used when preparing carbon for RSSCTs.

1) Approximately fifteen grams of carbon was weighted out and placed in a ceramic mortar.
2) A small amount of water was added to the mortar to wet mill the carbon.
3) Periodically, the carbon was transferred to the top-most sieve (e.g., 200 U.S. Standard Mesh), which stacked on top of another sieve (e.g., 230 U.S. Standard Mesh).
4) The sieves were then shaken with deionized water running over the carbon to rinse crushed carbon through to the bottom sieve.
5) The remaining carbon in the top sieve was then transferred back to the mortar for additional wet-milling.
6) The wet-milling process, steps 3-5, was repeated until no carbon was visible in the stop sieve.
7) Once completed the carbon remaining on the bottom sieve was transferred to an a clean dish for drying
8) The carbon was placed in a 105°C oven to dry for several days.
9) Following the drying process, the GAC was placed in a desiccator for storage.
10) Prior to an experiment, the GAC was dried again in a 105°C oven for 24 hours.

11) After cooling in a desiccator the required amount of GAC for a particular RSSCT was weighted out and placed in a separate beaker.
12) Deionized water was added to the beaker to wet the carbon and degassed under vacuum for 24 hours to remove trapped air bubbles.

3.2.4 Rapid small-scale column tests

RSSCTs were designed according either the proportional diffusivity (PD) or constant diffusivity (CD) design approach (Crittenden et al. 1991, Summers et al. 1995, Kennedy et al. 2015). The RSSCTs were designed to simulate field-scale empty bed contact times (EBCTs) of 10 and 20 minutes. Design of individual RSSCTs was conducted according to previously developed design Equations 3.1 and 3.2,

$$\left[\frac{EBCT_{RSSCT}}{EBCT_{field-scale}}\right] = \left[\frac{d_{RSSCT}}{d_{field-scale}}\right]^{2-X} \qquad \textit{Equation 3.1}$$

$$HLR_{RSSCT} = HLR_{field-scal}\left(\frac{d_{field-scale}}{d_{RSSCT}}\right)\left(\frac{Re_{RSSCT,min}}{Re_{field-scale}}\right) \qquad \textit{Equation 3.2}$$

where d represents the diameter of the GAC particle, HLR is the hydraulic loading rate, and Re is the Reynolds number for a fixed-bed adsorber with GAC. These relationships were developed from equating dimensionless parameters in the pore and surface diffusion model between field-scale and bench-scale columns (Crittenden et al.. 1986; Crittenden et al. 1987; Crittenden et al. 1989). Figure 3.1 shows the set-up of a CD-RSSCT.

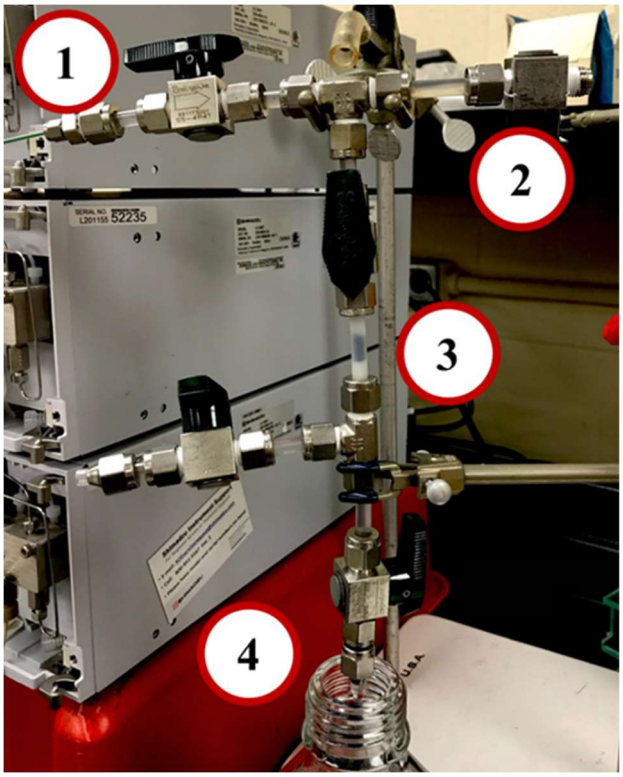

Figure 3.1: Experimental set-up for constant diffusivity RSSCT. The influent is pumped with an HPLC pump (1). Influent sampling port (3). Each column is filled with designed mass of carbon (3). Treated water is sampled for PFAS and TOC analysis post treatment from a sampling port (4).

The RSSCT column for PD-RSSCTs was made out of polypropylene tubing. The CD-RSSCTs were initially made out of a stainless-steel guard column. However, a combination of high cost and lack of visual observation of the GAC bed during testing led to designing CD-RSSCTs with polypropylene tubing. The wetted and degassed GAC was loaded into the column using a glass Pasteur pipette with a ~2cm glass wool base, which provides support for the GAC. Once the column was filled deionized water was flowed through the column for 24 hours at the design flow rate to allow the column to settle. The influent line was switched to either a 5 gal carboy or 55 gal drum of spiked water (Table 3.1) prior to experiments depending on water requirements. Prior to the start of an RSSCT spiked water was collected as an initial influent sample. Additional influent samples were then taken from a well-mixed carboy or drum at middle and end of the experiment. Over the course of the RSSCT run, effluent samples were

collected from the bottom port 4 (Figure 3.1) for TOC/UV254 and PFAS analysis. For example, samples were taken approximately every ~500 bed volumes for the first ~4,000 to ~5,000 bed volumes treated, then every ~5,000 bed volumes from ~5,000 to ~50,000 bed volumes treated, and finally every ~10,000 bed volumes from ~50,000 to 120,000 bed volumes treated. The sampling intervals allowed for description of PFAS breakthrough. The operating parameters for each conducted are provided in Tables 3.5-3.7.

Table 3.5: Design specifications for pilot-scale GAC adsorber and RSSCTs in source waters A and C.

Parameter		Carbon A									Carbon B		Carbon C			Carbon D
		Pilot			PD-RSSCT-PP	CD-RSSCT-SS	CD-RSSCT-PP[d]	CD-RSSCT-PP	XD-RSSCT-PP[f]	CD-RSSCT-PP	Pilot	CD-RSSCT-PP[d]	Pilot	PD-RSSCT-PP	CD-RSSCT-SS	CD-RSSCT-SS
Water TOC (mg L^{-1})		2.3	2.3	<0.5	2.3	2.3	2.3	2.3	2.2	<0.5	2.3	2.3	2.3	2.3	2.3	2.3
(Simulated) EBCT (min)		9.4 (10.0)	18.7 (20.0)	12.4 (10.0)	0.769 (9.5)[a] (11.9)[b] (10.3)[c]	0.056 (9.6)[a] (13.5)[b] (10.1)[c]	0.057 (8.4)[a] (13.0)[b] (9.7)[c]	0.112 (17.1)[a] (26.8)[b] (20.1)[c]	0.107 (8.9)[a] (13.1)[b] (10.2)[c]	0.055 (8.3)[a] (13.0)[b] (9.8)[c]	10.1 (10.0)	0.056 (8.5)[a] (13.2)[b] (9.9)[c]	9.6 (10.0)	0.636 (9.3)[a] (10.6)[b] (9.8)[c]	0.043 (9.2)[a] (11.9)[b] (10.1)[c]	0.0286 (8.6)[a] (13.2)[b] (10.0)[c]
GAC particle size (mm)	Geometric mean[a]	0.85	0.85	0.85	0.069	0.069	0.069	0.069	0.069	0.069	0.85	0.069	1.01	0.069	0.069	0.069
	Arithmetic mean[b]	1.06	1.06	1.06	0.069	0.069	0.069	0.069	0.069	0.069	1.06	0.069	1.15	0.069	0.069	0.069
	Log-mean[c]	0.92	0.92	0.92	0.069	0.069	0.069	0.069	0.069	0.069	0.92	0.069	1.06	0.069	0.069	0.069
Media US Standard mesh size		12x40	12x40	12x40	200x230	200x230	200x230	200x230	200x230	200x230	12x40	200x230	12x30	200x230	200x230	200x230
Bed diameter (mm)		102	102	50.8	4.76	4.00	3.18	3.18	3.18	3.18	102	3.18	102	4.76	4.00	3.18
Bed length (cm)		119	237	182.9	8.8	1.0	0.95	2.0	1.9	0.95	122	0.975	126	7.1	1.0	0.5
Hydraulic loading rate (m/hr)		7.6	7.6	8.9	6.9	10.7	10.5	10.7	10.6	10.4	7.3	10.5	7.9	6.7	14.0	10.5
GAC mass (g)		5195	10390	2002	0.808	0.0672	0.0427	0.0853	0.0815	0.0427	4952	0.0395	4172	0.533	0.0514	0.0154
Re-Sc[e]		5403-9814	5403-9814	6312-11465	417-758	647-1175	639-1160	650-1180	645-1170	634-1151	5167-9385	639-1162	6426-11672	407-739	859-1561	650-1180
Biot number[e]		93-111	93-111	99-119	33-37	38-44	38-44	38-44	38-44	38-43	91-09	38-44	100-120	32-37	42-49	38-44

[a] GAC particle size estimated using geometric mean and simulated RSSCT EBCT calculated using pilot-scale geometric mean GAC particle size;
[b] GAC particle size estimated using arithmetic mean and simulated RSSCT EBCT calculated using pilot-scale arithmetic mean GAC particle size;
[c] GAC particle size estimated using log-mean and simulated RSSCT EBCT calculated using pilot-scale log-mean GAC particle size;
[d] CD-RSSCT parameters are average of two RSSCTs
[e] Re-Sc and Bi values calculated using log-mean GAC particle size
[f] RSSCT designed assuming proportionality factor of X=0.25
SS denotes stainless steel column; PP denotes polypropylene column

Table 3.6: Design specifications for RSSCTs conducted in source water A.

Parameter		Carbon A			
		PD-RSSCT-PP	PD-RSSCT-PP	CD-RSSCT-PP	CD-RSSCT-PP
Water TOC (mg L^{-1})		1.3	1.3	1.5	1.5
(Simulated) EBCT (min)		1.20 (10.2)[a]	0.748 (10.0)[a]	1.20 (10.1)[a]	1.20 (10.0)[a]
GAC particle size (mm)	Geometric mean	0.106	0.069	0.069	0.053
	Arithmetic mean	0.113	0.069	0.069	0.053
	Log-mean[a]	0.108	0.069	0.069	0.053
Media US Standard mesh size		100x200	200x230	200x230	230x325
Bed diameter (mm)		4.76	4.76	3.18	3.18
Bed length (cm)		13.5	8.8	1.0	0.6
Hydraulic loading rate (m/hr)		6.8	7.1	10.6	10.6
GAC mass (g)		1.29	0.846	0.0427	0.0258
Re-Sc[b]		647-1175	429-779	650-1180	503-913
Biot number[b]		38-44	33-38	38-44	35-40

[a] GAC particle size estimated using log-mean and simulated RSSCT EBCT calculated using pilot-scale log-mean GAC particle size;
[b] Re-Sc and Bi values calculated using log-mean GAC particle size;
PP denotes polypropylene column

Table 3.7: Design specifications for pilot-scale GAC adsorber and RSSCTs tested in source water B.

Parameter		Carbon A		Carbon E		Carbon F		Carbon G	
		Pilot	CD-RSSCT	Pilot	CD-RSSCT	Pilot	CD-RSSCT	Pilot	CD-RSSCT
Water TOC (mg L^{-1})		1.3	1.6	1.3	1.6	1.3	1.6	1.3	1.6
(Simulated) EBCT[a] (min)		10.1 (10.0)	0.228 (10.3)[a] (16.0)[b] (12.0)[c]	10.1 (10.0)	0.228 (10.3)[a] (16.0)[b] (12.0)[c]	10.1 (10.0)	0.19 (10.2)[a] (14.4)[b] (11.3)[c]	10.1 (10.0)	0.228 (10.3)[a] (16.0)[b] (12.0)[c]
GAC particle size (mm)	Geometric mean[a]	0.85	0.126	0.85	0.126	1.10	0.150	0.85	0.126
	Arithmetic mean[b]	1.06	0.128	1.06	0.128	1.30	0.153	1.06	0.128
	Log-mean[c]	0.92	0.127	0.92	0.127	1.16	0.151	0.92	0.127
Media US Standard mesh size		12x40	100x140	12x40	100x140	10x30	80x120	12x40	100x140
Bed diameter (mm)		77.2	7	77.2	7	77.2	7	77.2	7
Bed length (cm)		132	3.4	132	3.4	132	2.3	132	3.4
Hydraulic loading rate (m/hr)		7.88	7.95	7.88	7.95	7.88	6.70	7.88	7.95
GAC mass (g)		3344	0.55	3840	0.69	2353	0.34	3066	0.53
Re-Sc[b]		7192-10175	1143-1617	7192-10175	1143-1617	9093-12865	1147-1622	7192-10175	1143-1617
Biot number		102-112	45-50	203-226	45-50	113-125	45-50	102-112	45-50

[a] GAC particle size estimated using geometric mean and simulated RSSCT EBCT calculated using pilot-scale geometric mean GAC particle size;
[b] GAC particle size estimated using arithmetic mean and simulated RSSCT EBCT calculated using pilot-scale arithmetic mean GAC particle size;
[c] GAC particle size estimated using log-mean and simulated RSSCT EBCT calculated using pilot-scale log-mean GAC particle size;
[d] Re-Sc and Bi values calculated using log-mean GAC particle size

3.2.4 Pore surface diffusion modeling

Diffusion of micropollutants can occur via both pore and surface diffusion within GAC particles. Therefore, modeling of breakthrough should account for both pore and surface diffusion when describing field-scale and RSSCTs. The Pore Surface Diffusion Model (PDSM) in AdDesignS^{TM} is a finite element model that has been previously used to describe micropollutant breakthrough. (Summers et al. 2014) The PDSM model requires input parameters including adsorbate properties, adsorbent properties, kinetic parameters, and equilibrium parameters. A list of input parameters for the PDSM model is shown in Appendix B Tables B.1-B.3.

To obtain 1) a good description of breakthrough curves and 2) critical information for scale-up method development, Freundlich adsorption capacity (K) and adsorption kinetics parameters, including tortuosity (τ) and surface-pore diffusion flux ratio (SPDFR), were user varied. The Freundlich 1/n value was set equal to a value of 1 (Corwin et al. 2010). The collected best fit K, τ, and SPDFR values for RSSCTs were used to develop a scale-up approach to field-scale and predict PFAS breakthrough (Chapter 4 and Chapter 5).

Table 3.8: AdDesignS™ Pore Surface Diffusion Model input parameters.

Type	Parameter	Notes
Water properties	Pressure, Temperature	Enter manually or keep default values
Adsorbate properties	Name, Molecular Weight, Molar Volume at Normal, Boiling Point, Initial Concentration, Liquid Density, Solubility, Vapor Pressure, Refractive Index, CAS Number	Entered manually or imported through StEPP Export File
Equilibrium parameters	Freundlich adsorption capacity, Freundlick 1/n	Entered manually or estimated within AdDesignS™
Kinetic parameters	Tortuosity (τ), Surface-to-Pore-Diffusion Flux Ratio (SPDFR), Film Mass Transfer Coefficient	Entered manually or estimated within AdDesignS™
Fixed bed properties	Bed Length, Bed Diameter, Bed Mass, Flow Rate, EBCT, Apparent Bed Density, Bed Porosity, Superficial Velocity, Interstitial Velocity	Entered manually or chosen from an adsorber database
Adsorbent properties	Name, Apparent Particle Density, Particle Radius, Particle Porosity, Particle Shape Factor	Entered manually or chosen from an adsorber database
Simulation parameters	Total Run Time, First Point Displayed values, Time Step, Number of Axial Elements	Enter manually or keep default values
Number of collocation points	Axial Direction, Radial Direction	Enter manually or keep default values

CHAPTER 4 DEVELOPMENT OF SCALE-UP APPROACH TO SCALE RSSCT TO FIELD-SCALE

4.1 Introduction

Per- and polyfluoroalkyl substances (PFAS) are a broad class of xenobiotic chemicals receiving extensive public and research attention due to their occurrence worldwide in humans and the environment (Glassmeyer et al 2017; Hu et al 2016; Cousins et al 2019; Ng et al. 2021). Extensive use of PFAS in both consumer and industrial products, and their presence in the environment can be largely attributed to emission from use in and production of these products. Examples include stain repellents, non-stick cookware, lubricants, food packaging costings, cosmetics, and fire-fighting foams (OECD 2018; Wang 2017; Buck 2011). Additional emission sources being highlighted in recent years include treated municipal wastewater discharge, biosolids, and leachate from solid waste landfills (Sun 2016; Guelfo 2018; Brendel 2018; Hu 2016). The persistence of PFAS after release has resulted in contamination of surface water and groundwater, which are used as sources for drinking water treatment plants.

Expanding detection of PFAS in finished drinking water has sparked public concern because of the toxicity and persistence of this class of chemicals. Epidemiological studies have suggested there is a likely link between exposure to PFAS and various adverse health effects including high cholesterol, ulcerative colitis, thyroid disease, testicular cancer, kidney cancer, breast cancer, and pregnancy induced hypertension (Hurley 2018; Grandjean 2012; Kotlarz 2020; Chen et al. 2021; Woodlief et al. 2021). Adverse health effects associated with PFAS has resulted in phasing out of long-chain PFAS. However, the phase out has resulted in a shift to use of shorter-chain PFAS (e.g., perfluoro carboxylic acids with chain length ≤6) and fluorinated alternatives (e.g. per- and polyfluoroalkyl ether acids). To reduce exposure to PFAS both federal

and state-level agencies established health advisory levels, minimum contaminant levels, and reference doses (U.S. EPA 2018; New jersey 2019; USDHHS 2018; U.S. EPA 2021). As more drinking water guidelines are issued, drinking water purveyors are having to develop and implement treatment strategies that are (cost)effective for removal of PFAS present in source waters.

Many conventional and advanced treatment processes (e.g., coagulation, flocculation, sedimentation, filtration, advanced oxidation processes) have been shown to be ineffective for removal of PFAS (Boone 2019; Hopkins 2018; Gebbink 2017). Treatment processes focused on sequestration and capture of micropollutants are quickly evolving to reduce human and environmental exposure to PFAS. Granular activated carbon (GAC) adsorption is being considered widely to fill the treatment gap for PFAS present in source waters (Appleman 2014; Zhi 2015; Vecitis 2009; Sun 2016; Hopkins 2018). The commercial availability and effectiveness of GAC treatment provides water purveyors with a potentially viable option for treatment of contaminated source water. Removal of PFAS has been tested widely at both the bench-scale and field-scale (Rodowa 2020; Hopkins 2018; CFPUA 2017; Zeng 2020; Park 2020; Dickenson 2016). Conducting field-scale adsorption studies is time intensive and requires large volumes of water. As a result, an approach to reduce the time and cost required for determining adsorber performance has been developed called the rapid small-scale column test (RSSCT) (Crittenden 1986, 1987). Two common RSSCT designs used to assess micropollutant removal in source water are constant diffusivity RSSCT (CD-RSSCT) and proportional diffusivity RSSCT (PD-RSSCT). The CD-RSSCT assumes intraparticle diffusivity is independent of particle size and the PD-RSSCT assumes intraparticle diffusivity decreases linearly with particle size. Existing research has demonstrated the CD-RSSCT can be used for determining PFAS

characteristics affecting removal from groundwater (Zeng et al. 2020; Park et al. 2020). Though these works illustrated how different factors effect PFAS removal, there still exists an unknown as to whether RSSCTs can be scaled-up to describe field-scale breakthrough of PFAS. Commonly, the PD-RSSCTs were used as a basis for development of a scale-up approach to predicted performance of field-scale adsorbers (Kennedy et al. 2017; Corwin and Summers 2010). The PD-RSSCT has been shown to describe background organic matter breakthrough well, but generally research has demonstrated the CD-RSSCT provides a better prediction of early micropollutant breakthrough (Summers et al. 1989, Knappe et al. 1997). An alternative approach to scaling RSSCT breakthrough data could potentially be developed compared to the fouling index approach, which was previously developed for scaling PD-RSSCTs (Corwin and Summers 2010). Even though the fouling index approach was demonstrated to be effective in scaling PD-RSSCT breakthrough data, this bench-scale design is still time intensive and requires large volumes of water.

The primary objective of this research was to develop a scale-up approach for the CD-RSSCT, which can be completed in less than one week using significantly less water. To date, the CD-RSSCT has been used to assess GAC performance and estimation of service life. However, a new scale-up approach is required to effectively scale-up ionic PFAS breakthrough data in source waters. The developed scale-up approach would help water providers concerned with PFAS in drinking water predict GAC treatment effectiveness and carbon use rates.

4.2 Materials and methods

4.2.1 Materials

4.2.1.1 Standards

The standards used for this study are described in Chapter 3 Section 3.1.2. PFAS used for spiking influent water for the RSSCT were obtained from Synquest Laboratories Inc. (Alachua, FL) and The Chemours Company (Wilmington, DE).

4.2.1.2 Water samples

RSSCT and pilot-scale tests were conducted in matching waters for coagulated/settled surface water from the Cape Fear Public Utility Authority (Wilmington, NC), and PFAS-impacted groundwater from American Waters (AW). Background water quality parameters and PFAS concentrations for RSSCTs and pilot adsorbers are provided in Chapter 3, Table 3.1 and Table 3.2. For RSSCTs conducted in CFPUA and AW water, 22 PFAS (Table 3.2) were spiked in with concentrations varying from 85 to 158 ngL^{-1}. All pilots were conducted at native PFAS levels (Table 3.2). Pilot and RSSCTs for PFOA removal was assessed from data provided by Jacobs Engineering Group Inc. from Orange County Water District (OCWD).

For the CFPUA and AW RSSCTS, the collected waters were stored in high density polypropylene containers at 4°C prior to use. Additionally, the waters were filtered through a 5µm filter prior to use.

4.2.1.3 Activated carbon

CFPUA RSSCT and pilot testing were performed using two sub-bituminous coal-based carbons (Carbon A and Carbon B) and one enhanced coconut shell-based carbon (Carbon C).

AW RSSCT and pilot were conducted using a sub-bituminous coal-based carbon (Carbon A). OCWD RSSCTs and pilot testing were conducted using three sub-bituminous coal-based carbons (Carbon A, Carbon E, and Carbon G) and one lignite-based carbon (Carbon F). Information about the carbon properties are provided in Chapter 3 (Table 3.3). GAC were used as received for the pilot-scale testing. For the CFPUA RSSCTs, GAC was wet milled with a mortar and pestle, wet sieved, and the fraction in the range of 63 to 74 µm (200x230 U.S. Standard Mesh) was collected for use. Prior to use GAC was dried at 105°C.

4.2.2 Methods

4.2.2.1 Analytical methods

4.2.2.1.1 PFAS analysis

The 22 PFAS spiked into CFPUA surface water for the RSSCTs were quantified by liquid chromatography quadrupole mass spectrometry (LC-MS/MS). Calibration curves were established with standards prepared in ultrapure deionized water. The concentrations of the standards ranged from 1 to 500 ng L^{-1} for all compounds. A full description of the sample analysis method by LC MS/MS (Ultivo, Agilent Technologies Inc.) is provided in Section 3.2.1 and Appendix A.

4.2.2.1.2 Total organic carbon and ultraviolet absorbance

Total organic carbon (TOC) was measured using a TOC analyzer (Model TOC-VCSN, Shimadzu Scientific, Columbia, MD) in accordance with Standard Method 5310C (APHA et al. 2005). Ultraviolet absorbance (UV_{254}) was measured at a wavelength of 254 nm using a spectrophotometer (Hach DR4000, Hach, Loveland, CO) in accordance with Standard Method 5910 (APHA et al. 2005).

4.2.2.2 Rapid small-scale column test

Bench-scale tests were conducted using two common RSSCT designs, the CD-RSSCT and the PD-RSSCT designs (Summers 2014; Crittenden 1987; Crittenden 1986). The CFPUA RSSCTs were conducted with influent water described in Chapter 3 (Table 3.2). RSSCTs were run for ~86,000-120,000 bed volumes and ~70,000-85,000 bed volumes for the CD and PD designs, respectively. The bench-scale and field-scale design parameters are summarized in Tables 3.5-3.7.

The CD-RSSCT were designed in a non-perfect similitude approach with a lower flow rate than what is required for perfect similitude. The reasons for doing this was to 1) shorten the bed depth and 2) further reduce run time. Comparisons for breakthrough for both CD-RSSCT designs were made in AdDesignS using the pore surface diffusion model (PSDM). Simulated breakthroughs were similar for each design indicating a reduce flow rate design could be used to evaluate removal of PFAS at the bench-scale (Appendix B, Figure B.1). The CD-RSSCTs were initially designed using a stainless-steel guard column (I.D. = 0.4 cm, L = 1 cm). Due to the relatively high cost and lack of visual observation of the GAC bed during testing associated with the stainless-steel guard columns, column design switched to using polypropylene tubing (I.D. = 0.318 cm) to hold the GAC bed for CD-RSSCTs. The RSSCT columns for the PD-RSSCT were designed similar to previous research (Kennedy et al. 2017) using a polypropylene tubing setup packed with GAC to achieve a design bed depth and volumes (Table 3.5 and Table 3.6).

Spiked water was stored in a 55-gal drum or 5-gal carboy, depending on experimental water requirements, and pumped through the columns with a HPLC pump (Figure 3.1). Two sampling points were installed to quantify the PFAS concentrations before and after treatment:

an inlet point (2) directly after inlet line from the HPLC pump and an effluent sampling point (4) after the column.

Samples were collected in 40 mL amber vials (ESS, San Leandro, CA) for TOC/UV254 and 15 or 50mL polypropylene containers (Fisher, Waltham, MA) for PFAS. Sampling of the influent occurred at the start and end of the RSSCT. Effluent sampling for the CD-RSSCT occurred 500-1,000 bed volumes for the first 10,000 bed volumes and then every 5,000-10,000 bed volumes for the remainder of the experiment. While for the PD-RSSCT, effluent sampling occurred 2,500 bed volumes for the first 10,000 bed volumes and then every 5,000-10,000 bed volumes for the remainder of the experiment. PFAS and TOC/UV254 samples were then stored at 4°C prior to analyses.

4.2.2.2 Pilot-scale experiments

Pilot-scale testing was conducted at the in two different water sources, water source A and water source C. The pilot-scale GAC adsorbers were designed to mimic the operational conditions of potential future full-scale GAC adsorbers and to study PFAS removal. Influent to the pilot-scale adsorbers for source water A was directly sourced from the effluent of the coagulated/settled water basins. Average background water quality characteristics for each water source is provided in Table 3.1. The influent water contained several PFAS at ng L^{-1} concentrations (Table 3.2). Pilot designs specifications for each GAC tested are provided in Table 3.5 and Table 3.7. The pilot-scale adsorbers were operated to approximately 22,000 and 80,000 bed volumes treated for water source A and C, respectively.

4.2.2.3 AdDesignS: Pore surface diffusion modeling

Description of PFAS breakthrough curves is crucial to the development of a scale-up approach. Potentially both pore and surface diffusion could occur simultaneously within GAC particles. Therefore, the pore-surface diffusion model (PSDM) would provide description of both RSSCT and field-scale adsorbers. The PSDM in AdDesginS has been previously used to curve-fit breakthrough curves of multi-solute systems (Crittenden 1986, Kennedy 2015, Rodowa 2020, Kennedy 2017). Input parameters required include both system design and operating parameters (e.g., particle diameter, bed density, bed diameter, bed depth, flow rate, mass of carbon) and physical/chemical characteristics for adsorbates of interest. Additionally, Freundlich adsorption capacity and adsorption kinetics parameters (e.g., tortuosity, surface-pore diffusion flux ratio) are required but can be adjusted to obtain the best fit for breakthrough data.

4.3 Results and discussion

4.3.1 Effect of GAC particle size in RSSCTs on PFAS breakthrough curves

Initial RSSCTs were conducted to determine whether the GAC particle size used in CD- and PD-RSSCTs affected PFAS breakthrough curves. CD-RSSCTs were conducted with coagulated surface water with a TOC of 2.3 mg L^{-1} and PD-RSSCTs with coagulated surface water from the same source, but with a TOC of 1.3 mg L^{-1}. For CD-RSSCTs, particle sizes of 200x230 and 230x325 U.S. mesh were compared while particle sizes of 100x200 and 200x230 U.S. mesh were compared for PD-RSSCTs. Bed volumes that could be treated to 10, 20, 50% breakthrough are compared in parity plots for 22 PFAS (Figure 4.1)

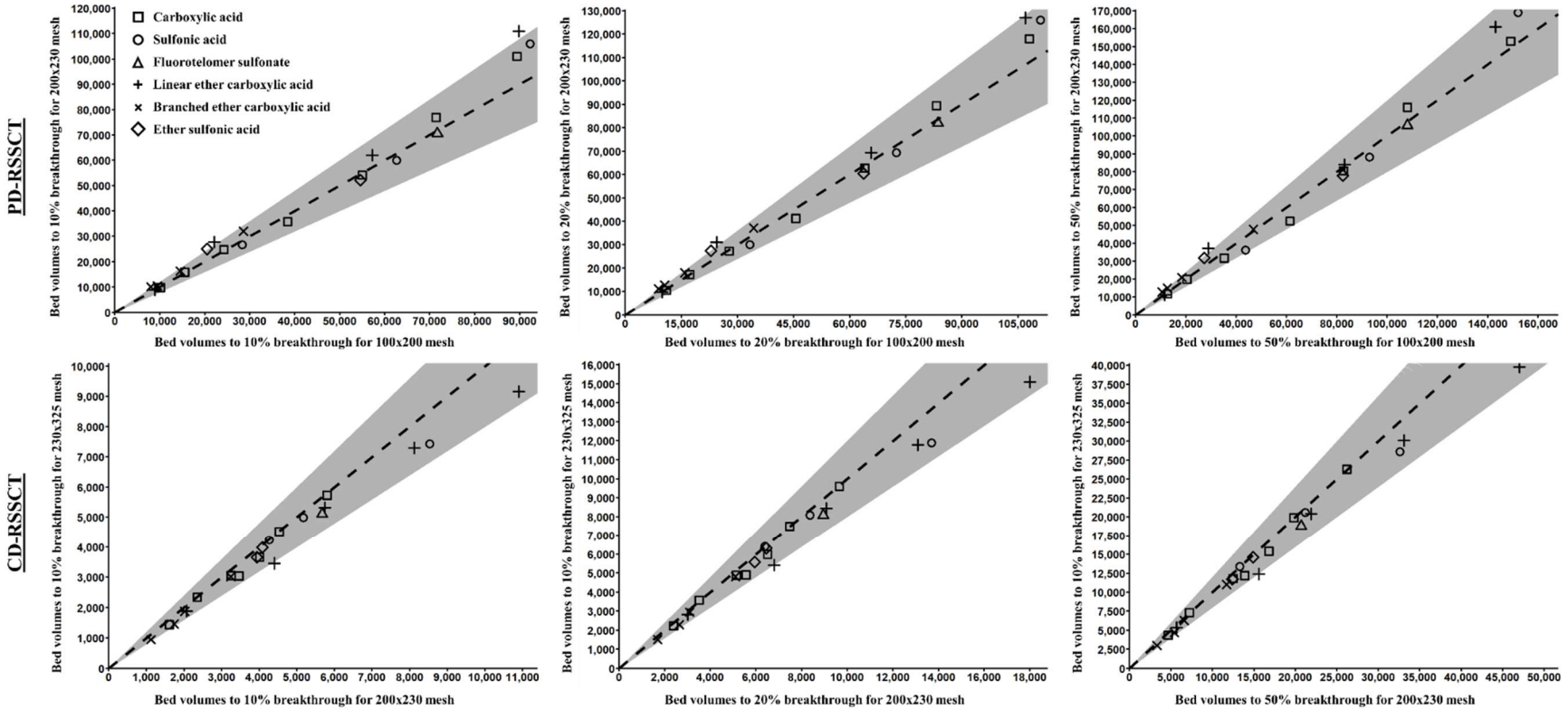

Figure 4.1: Comparison of bed volumes to 10, 20, and 50% breakthrough for PD-RSSCT at 100x200 and 200x2300 mesh sizes in TOC = 1.3 mgL^{-1} coagulated surface water post biofiltration and for CD-RSSCT at 200x230 and 230x325 mesh sizes in TOC = 1.5 mgL^{-1} coagulated surface water. Shaded region indicate 20% deviation from perfect agreement (1:1 dashed line) between the two RSSCT designs. Carbon: A, Simulated EBCT: 10 minutes. Design specifications in Section 3.2.4.

Results in Figure 4.1 demonstrate that similar bed volumes could be treated to 10, 20, and 50% breakthrough for 22 PFAS when employing two different particle sizes in the CD- and PD-RSSCT designs. Additionally, describing the data with the PSDM yielded similar Freundlich adsorption capacity and adsorption kinetic parameters (Appendix B, Table B.9). Results presented in Figure 4.1 demonstrate that intraparticle diffusivity was independent of adsorbent particle size for both CD and PD-RSSCTs in the tested condition. Park et al. (2020) demonstrated similar independence of intraparticle diffusivity on particle size for CD-RSSCTs using mean GAC particle diameters of 0.13, 0.17, and 0.2 mm. These results suggest that scale-up procedures that rely on RSSCT data are not sensitive to the GAC particle diameter used in RSSCT.

4.3.2 Direct comparison of RSSCTs and field-scale adsorbers

To assess whether CD- and/or PD-RSSCTs could directly predict PFAS breakthrough curves obtained at the pilot scale, breakthrough curves were compared for three GACs at an EBCT of ~10 minutes, and for one GAC at an EBCT of ~ 20 minutes. As shown in Figure 4.2, for Carbon A at an EBCT of ~10 min, directly comparable breakthrough curves for the RSSCT and pilot were available for 5 perfluoroalkyl carboxylic acids (PFCAs), 1 perfluoroalkyl sulfonic acid (PFSA), 4 perfluoroalkyl ether carboxylic acids (PFECAs), and 1 polyfluoroalkyl ether sulfonic acid (PFESA). Similarly, 10 PFAS breakthrough curves were available for Carbon B (Figure 4.3) and 7 for Carbon C (Figure 4.4) at an EBCT of ~10 min. Only 8 directly comparable PFAS breakthrough curves were available for Carbon A at an EBCT of ~20 min (Figure 4.5). Well documented by other studies (Hopkins et al. 2018; Rodowa et al. 2020; Park et al. 2020), these data sets illustrate that PFAS adsorbability increases with increasing PFAS chain length

within a given subclass (e.g. PFBA<PFPeA<PFHxA<PFHpA<PFOA for the PFCAs and PFMOAA<PFO2HxA<PFO3OA for the PFECAs), and these trends were observed both in the pilot-scale and bench-scale data (Figure 4.2).

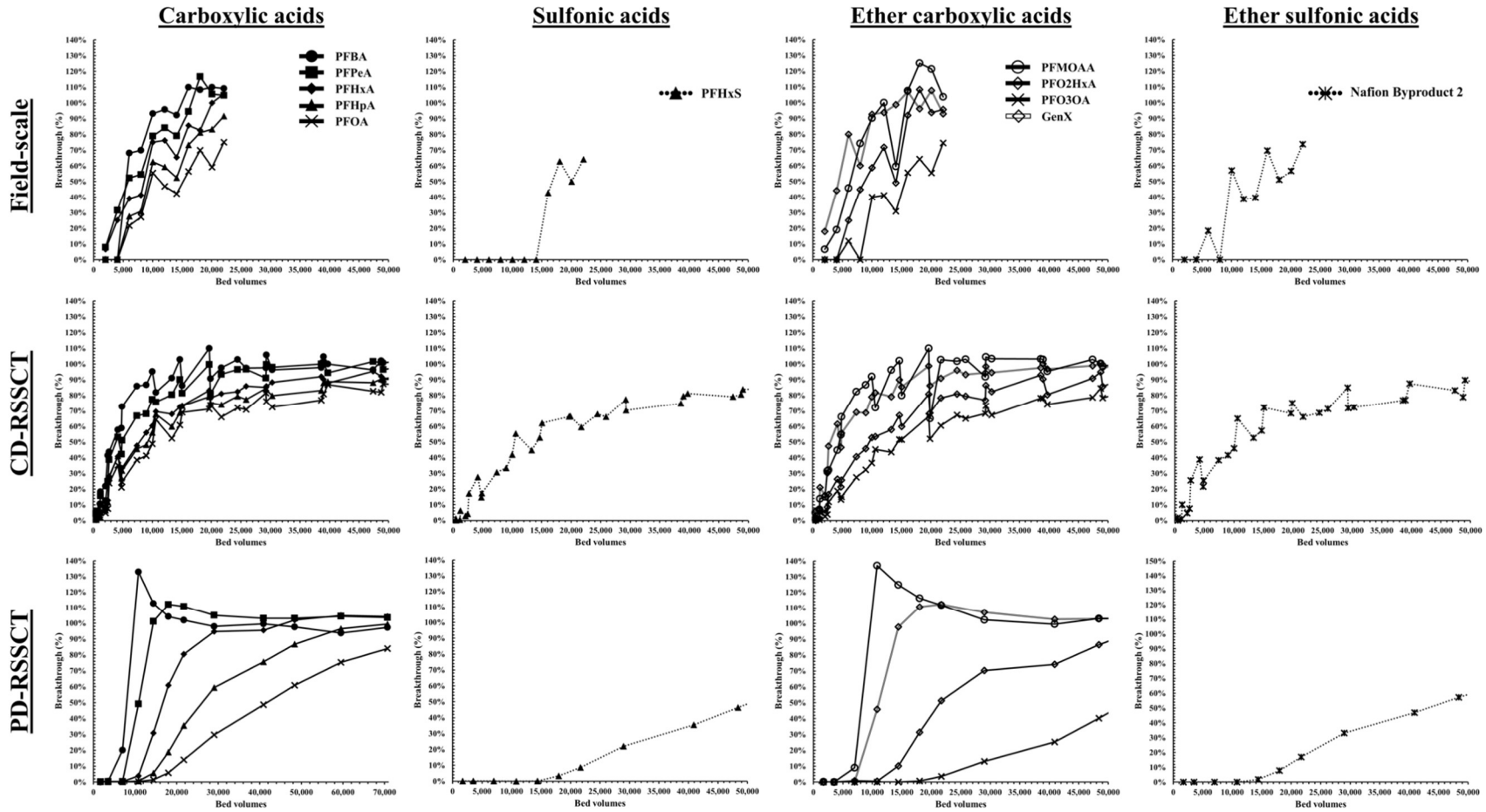

Figure 4.2: Breakthrough curves for PFAS in coagulated/settled surface water (TOC =2.3 mgL^{-1}) for field-scale, CD-RSSCT, and PD-RSSCT. Carbon: Carbon A, Simulated EBCT = 10 minutes.

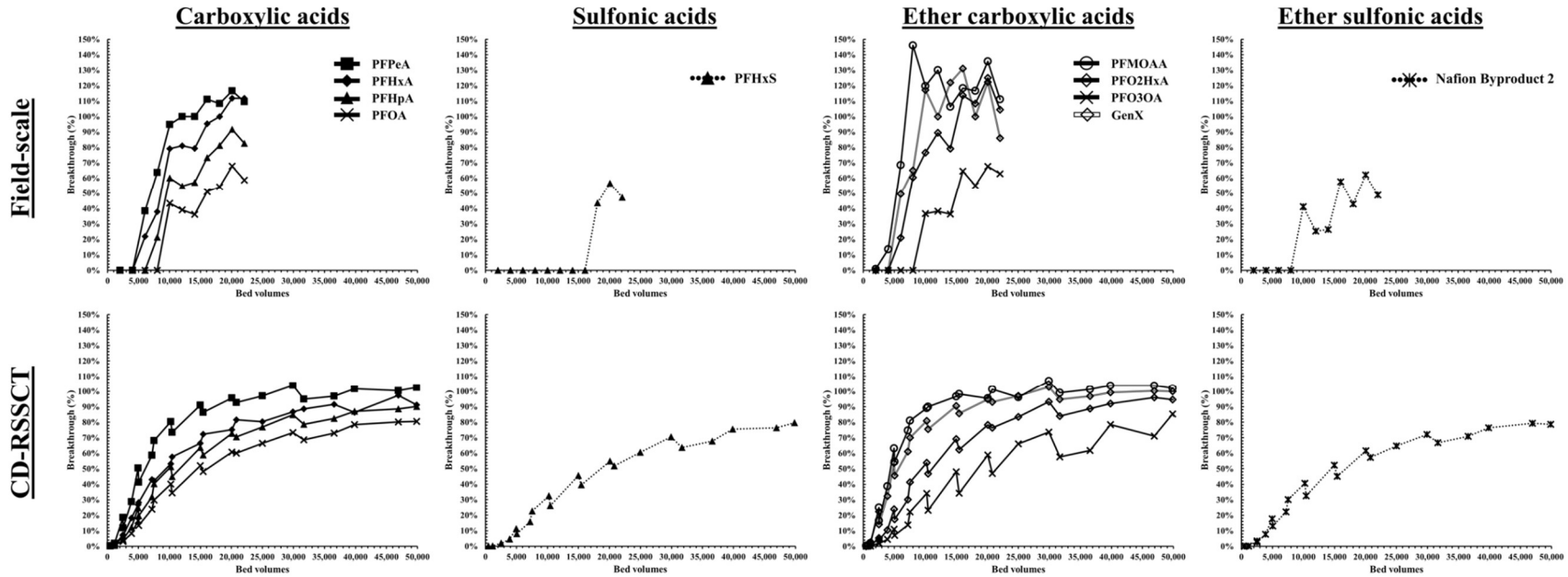

Figure 4.3: Breakthrough curves for PFAS in coagulated/settled surface water (TOC =2.3 mgL^{-1}) for field-scale, CD-RSSCT, and PD-RSSCT. Carbon: Carbon B, Simulated EBCT = 10 minutes.

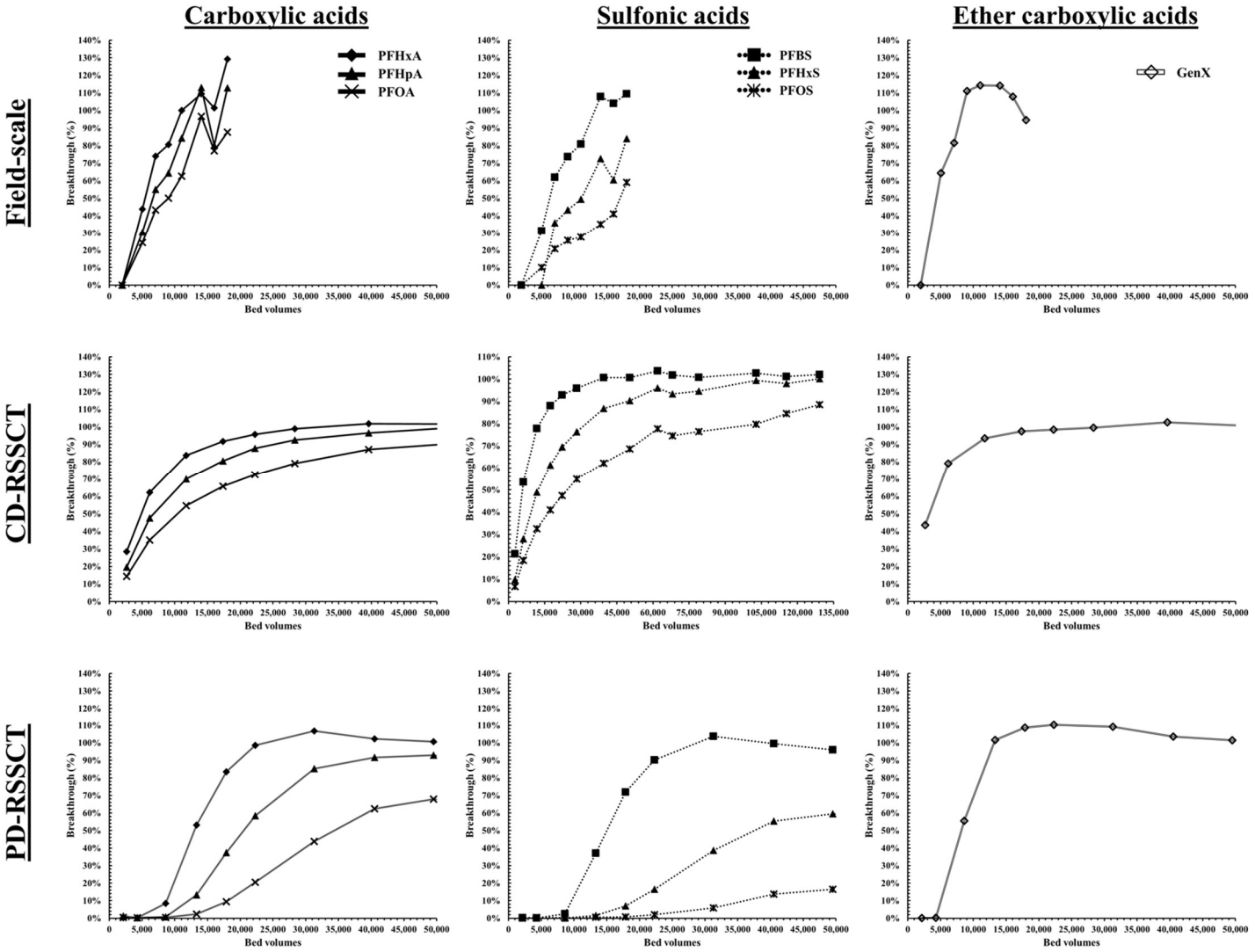

Figure 4.4: Breakthrough curves for PFAS in coagulated/settled surface water (TOC =2.3 mgL^{-1}) for field-scale, CD-RSSCT, and PD-RSSCT. Carbon: Carbon C, Simulated EBCT = 10 minutes.

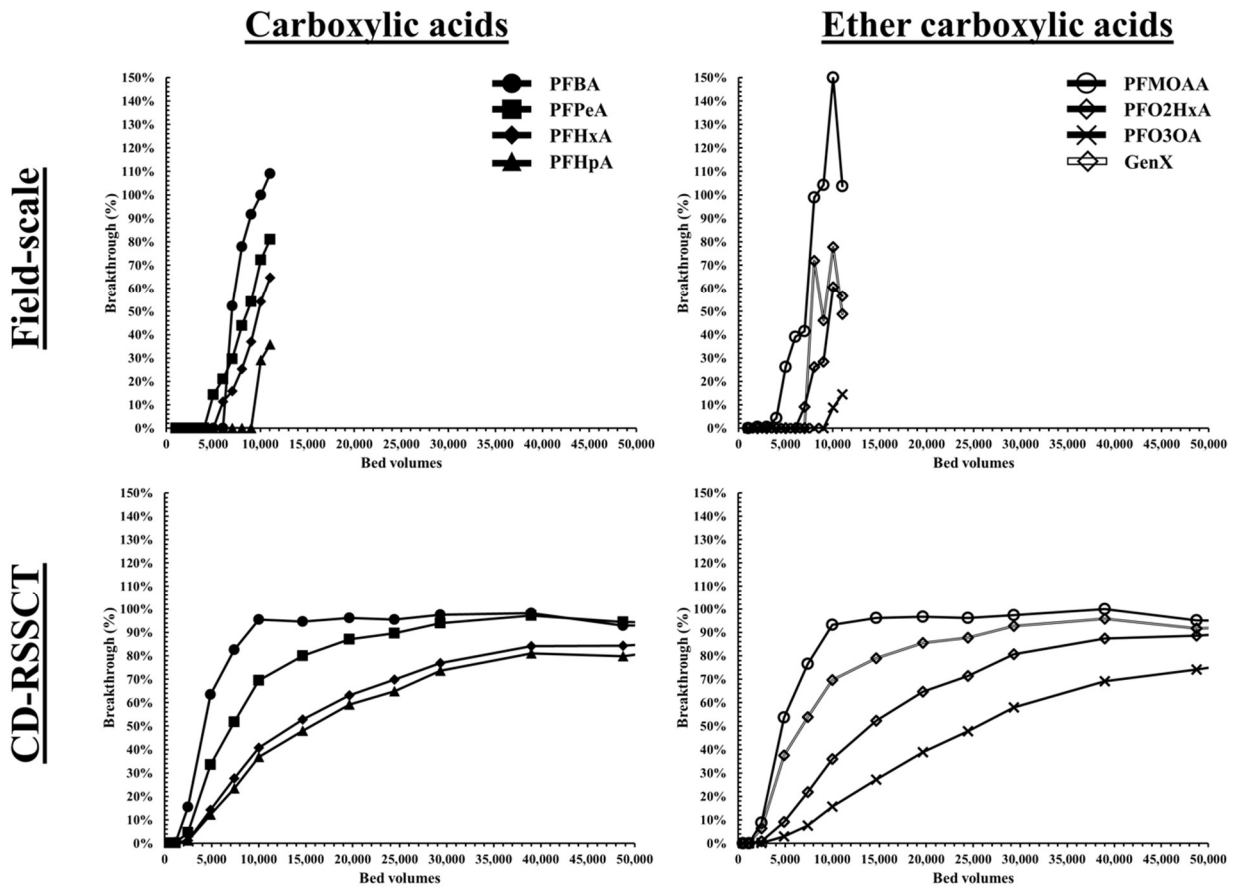

Figure 4.5: Breakthrough curves for PFAS in coagulated/settled surface water (TOC =2.3 mgL^{-1}) for field-scale, CD-RSSCT, and PD-RSSCT. Carbon: Carbon A, Simulated EBCT = 20 minutes.

To make direct comparisons, all raw PFAS breakthrough curve data were described with the PSDM, and results were compared as shown in Figure 4.6 for the PFHxS dataset obtained with Carbon A at an EBCT of ~10 min. The same comparisons were made for all other directly comparable data sets as shown in Figures B.1-B.4.

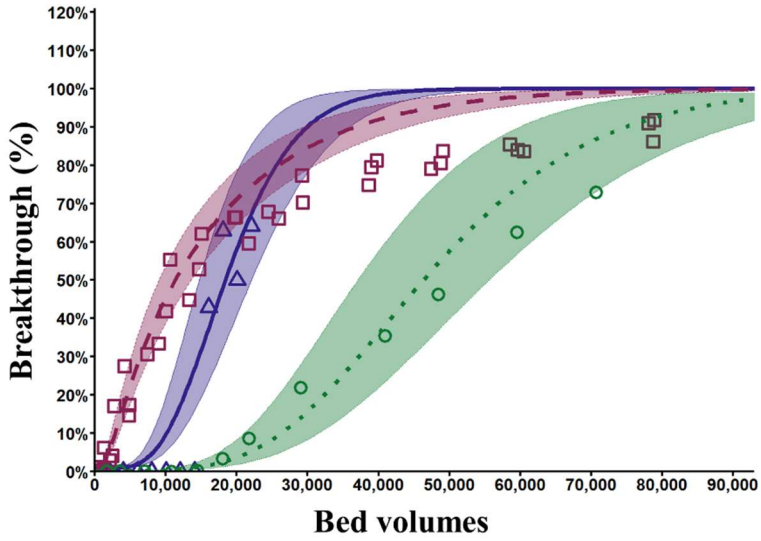

Figure 4.6: Direct comparison of CD-RSSCT (red) and PD-RSSCT (green) data and PSDMs to pilot-scale (blue) breakthrough for PFHxS in coagulate/settled surface water (TOC = 2.3 mg L^{-1}), Carbon: Carbon A, simulated EBCT= 10 minutes. The symbols represent experimental or pilot data; the lines represent best fit PSDM for each data set; the shaded region 20% variance from best fit PSDM.

The comparison illustrated in Figure 4.6 demonstrates that neither PD- nor CD-RSSCT data can be directly used to describe or predict field-scale breakthrough. Similar to breakthrough results for other micropollutants (e.g., pharmaceuticals, personal care products, and herbicides), the PD-RSSCT results overpredicted the onset of breakthrough and adsorption capacity (Kennedy et al. 2017; Summers et al. 2014). Comparison of field-scale and CD-RSSCT breakthrough curves illustrated similar adsorption capacity but dissimilar adsorption kinetics (Figure 4.6 and Figures B.2-B5). The difference in either adsorption capacity and/or adsorption kinetics for PD- or CD-RSSCTs is likely due to the GAC particle size dependence. The results illustrated by the comparison of breakthrough curves (Figure 4.6 and Figures B.2-B5) highlights

that development of a scale-up approach needs to account for the dependence of adsorption capacity and adsorption kinetics on GAC particle size.

4.3.3 Scale-up of freundlich adsorption capacity

To properly compare Freundlich adsorption capacities across all experiments, data sets were curve fit with the PSDM. The resulting Freundlich adsorption capacity parameters (K; Tables B.1-B.3) obtained for the RSSCTs were compared to corresponding field-scale values in Figure 4.7. The comparisons were made for a wide range of PFAS, multiple GAC, and multiple background water matrices.

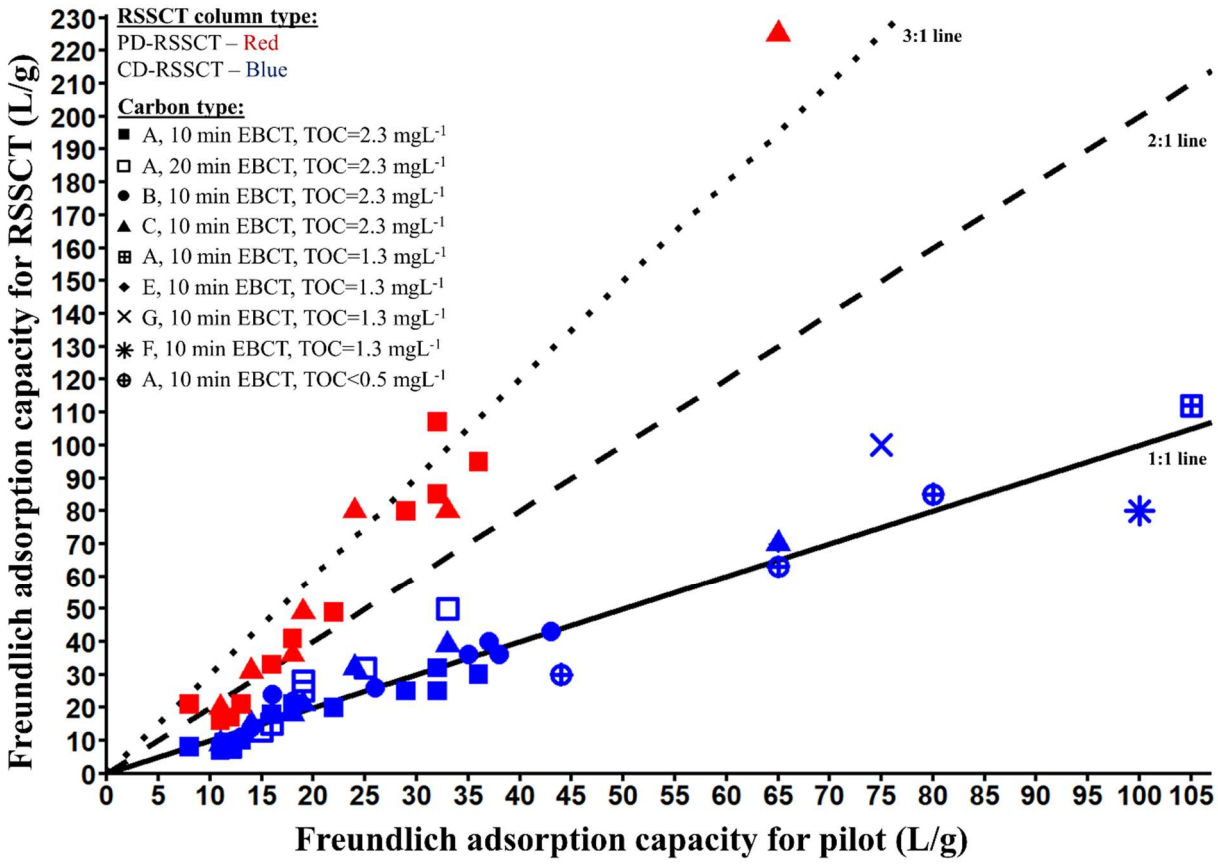

Figure 4.7: Comparison of Freundlich adsorption capacity parameters for CD-RSSCT and PD-RSSCT to field-scale.

Similar to previous research (Kenndey 2017, Summers 2014), the PD-RSSCT overpredict capacity by factor of 2-3 (Figure 4.7). A scale-up approach previously developed by Corwin and Summers (2010) could be used to scale-up PD-RSSCT data to predict field-scale PFAS breakthrough. However, PD-RSSCT are time intensive (>3 months) and require large volumes of water (>55 gal) to achieve breakthrough of many PFAS. The CD-RSSCT design requires less time (~3 days) and a lower water requirement (~5 gals) compared to the PD-RSSCT to achieve breakthrough of the majority of PFAS. The reduction in run time and water requirement makes the CD-RSSCT design ideal basis for developing a scale-up approach to predict field-scale PFAS breakthrough. Another advantage of using the CD-RSSCT design is the direct prediction of field-scale PFAS adsorption capacities (Figure 4.7). As a result, use of the CD-RSSCT design in developing a scale-up approach would only require determining an appropriate manner for scaling adsorption kinetics.

4.3.4 Scaling CD-RSSCT adsorption kinetics to predict field-scale breakthrough

Previous research has demonstrated that scale-up in a proportional diffusivity context using the PSDM is feasible (Summers et al. 2014). The scale-up approach accomplished this by scaling particle size-dependent adsorption kinetics using the normalized intraparticle flux (NTIF). The development of a scale-up approach for predicting field-scale breakthrough from CD-RSSCT data it will require determining exactly how the adsorption kinetics scale with respect to particle size.

The scale-up approach moving forward will assess this dependence of adsorption kinetics on GAC particle size by scaling through the NTIF. The NTIF has a value of 1 for the base case (max pore diffusion flux case in Table 4.1), which translates to surface diffusion being negligible

and pore diffusion being equivalent to liquid diffusion, meaning tortuosity is 1. When diffusion is more tortuous (longer path length) the value of tortuosity increases resulting in a decrease in the NTIF, which is calculated as the inverse of tortuosity (pore diffusion flux case in Table 4.1). Finally, if the intraparticle diffusion occurs at a rate faster than the max pore diffusion flux case then surface diffusion is invoked, and the NTIF is calculated as the sum of the pore and surface diffusion flux contributions (Pore plus surface diffusion flux case Table 4.1). To address the particle size-dependence of intraparticle diffusion, first kinetic parameters for individual breakthrough curves of the CD-RSSCT need to be obtained. For example shown in Figure 4.6, the best fit PSDM of PFHxS breakthrough data was achieved using a tortuosity (τ) of 3 and a surface-pore diffusion flux ratio (SPDFR) of 10^{-30}.

Table 4.1: Different intraparticle diffusion cases for RSSCTs.

Case	Tortuosity (τ)	Surface-pore diffusion flux ratio (SPDFR)	Normalized total intraparticle flux for RSSCT ($NTIF_{RSSCT}$)
Max pore diffusion flux	1	10^{-30}	1
Pore diffusion flux	>1	10^{-30}	$1/\tau$
Pore plus surface diffusion	1	$>10^{-30}$	1+SPDFR

Therefore, the NTIF for PFHxS in the CD-RSSCT falls into the category of pore diffusion flux (Table 4.1) and was calculated to be a value of 0.33. The NTIF for the field-scale can then be determined from NTIF of the CD-RSSCT using Equation 4.1.

$$NTIF_{field-scal} = (scaling\ factor)^X \times NTIF_{RSSCT} \qquad \textit{Equation 4.1}$$

Where the scaling factor represents the ratio of the GAC particle diameters of the field-scale to the RSSCT and the value of X represents proportionality factor (where X=0 is constant diffusivity case and X=1 is the proportional diffusivity case).

For a case where intraparticle diffusivity is expected to vary linearly with particle size (i.e. the proportional diffusivity case) the proportional factor is set to a value of one. As an example, if the $NTIF_{field\text{-}scale}$ (Equation 4.1) is calculated to be greater than one, then the $NTIF_{field\text{-}scale}$ falls into the pore plus surface diffusion category (Table 4.2). The applicable τ and SPDFR values for the field-scale adsorber would be calculated based on the pore-plus surface diffusion case in Table 4.2.

Table 4.2: Determination of scaled adsorption kinetics from scaled NTIF case.

Case	Normalized total intraparticle flux for RSSCT ($NTIF_{field\text{-}scale}$)	Tortuosity (τ)	Surface-pore diffusion flux ratio (SPDFR)
Mass pore diffusion flux	1	1	10^{-30}
Pore diffusion flux	<1	$1/ NTIF_{field\text{-}scale}$	10^{-30}
Pore plus surface diffusion	>1	1	$NTIF_{field\text{-}scale} - 1$

This scale-up approach, in conjunction with CD-RSSCT breakthrough data, allows for determining the dependence of intraparticle diffusivity on GAC particle size. Summers et al. (2014) suggested that intraparticle diffusivity potentially varies neither linearly or constantly with GAC particle size. This can be investigated by varying the proportionality factor in Equation 4.1. The particle-size dependence was investigated by applying proportionality factors of 0, 0.25, 0.5, and 1 for Equation 4.1. Additionally, other works have suggested that intraparticle diffusivity may not be constant with particle size due to the nature of porous materials, which more likely consist of uniformly distributed micropores that branch off from macropores (Matsui et al. 2009, Sontheimer et al.1988). For each proportionality case, scaled adsorption kinetics parameters were calculated for individual PFAS (Tables B.7-B.11). A scaled PSDM for a PFAS was then obtained using the CD-RSSCT adsorption capacity and scaled kinetic parameters as input parameters in AdDesignS. Bed volumes to 10, 20, and 50%

breakthrough for scaled PSDMs were then compared directly to field-scale bed volumes for each proportionality case (Figure 4.8 and Figures B.6 and B.7).

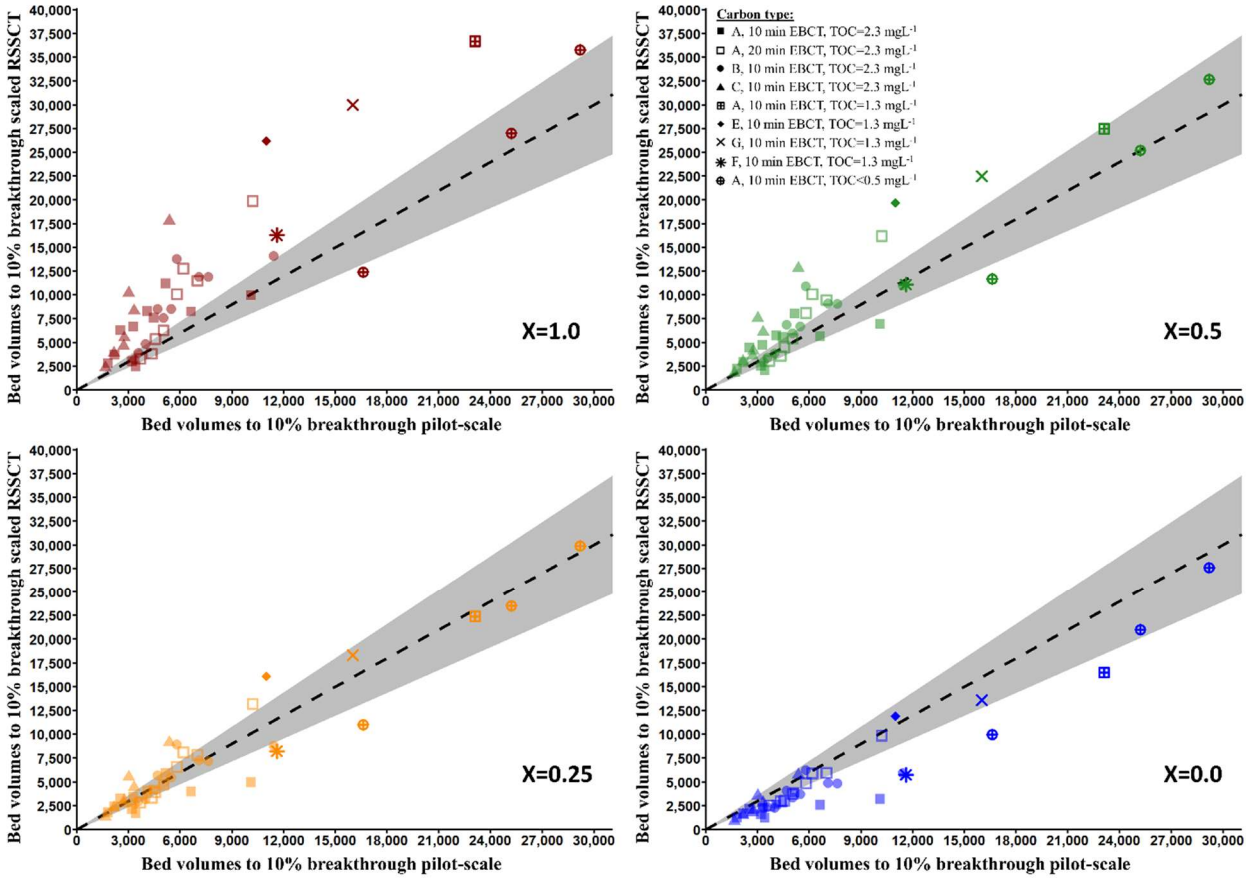

Figure 4.8: Comparison of bed volumes to 10% breakthrough for field-scale and scaled CD-RSSCT. Dashed line represents 1:1 line for pilot breakthrough to 10%. Shaded region around dashed line represents 20% variance for bed volumes to 10% breakthrough for field-scale.

Results in Figure 4.8 demonstrate that scaled CD-RSSCT PSDMs were able to describe onset of field-scale breakthrough for the majority of PFAS when a proportionality value of X=0.25 was applied to Equation 4.1. Under this scaling case 79% of the field-scale data set for bed volumes to 10% breakthrough was well described (Table B.4). While scaling kinetics for the other three cases of X=0, X=0.5, and X=1 were only able to described 67%, 75%, and 36% of bed volumes to 10% breakthrough for the field-scale data set. Bed volumes to 10% breakthrough clustered together for each carbon type in each scaling case suggesting carbon type does not

affect the approach to scaling adsorption kinetics. Additional comparisons were made for bed volumes to 20% and 50% breakthrough, which suggested that adsorption kinetics scaled best when applying a value of X=0.25 (Table B.5 and Table B.6). Applying the proportionality factor of X=0.25 in Equation 4.1, PSDMs were produced to simulate field-scale breakthrough. Generally, the scaled PSDMs were able to predict field-scale breakthrough well (Figure 4.9 and Figures B.20-B.22).

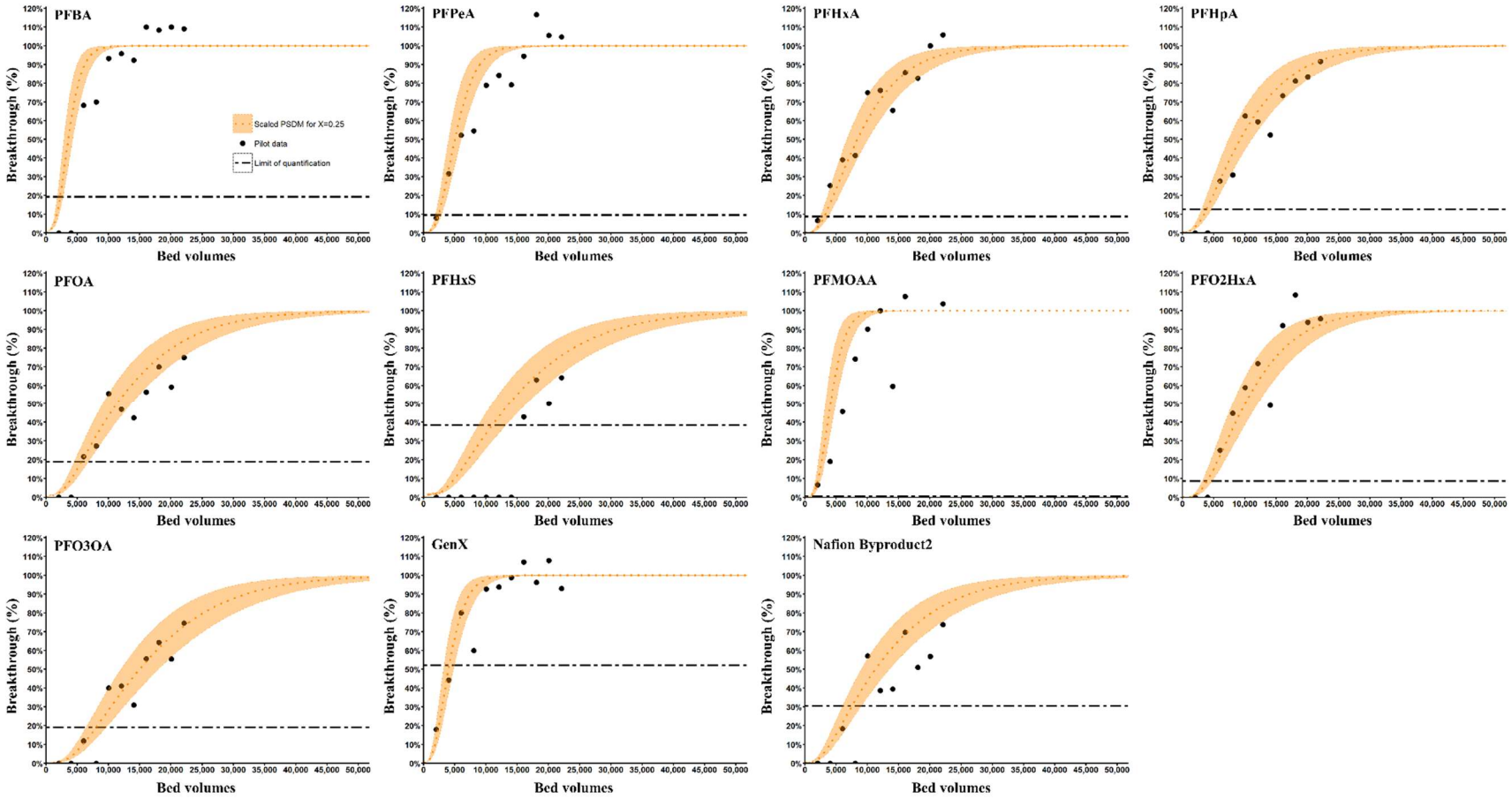

Figure 4.9: Prediction of field-scale breakthrough for PSDMs using scaled kinetics assuming X=0.25. Carbon: Carbon A, TOC=2.3 mgL^{-1}, EBCT=10 minutes.

Crittenden et al. (1987) suggested that three reasons for difference between an RSSCT and pilot were 1) difference in influent concentration, 2) differences in adsorption capacity, and 3) differences in intraparticle diffusivity. Scaled PSDMs in Figure 4.6 demonstrated there is a difference in intraparticle diffusivity for the field-scale and RSSCT. The scaled RSSCT PSDMs suggest that intraparticle diffusivity scales with particle size for a proportionality factor of X=0.25. The PFAS used in this study represent only a small fraction of known PFAS. With the developed scale-up approach, in conjunction with CD-RSSCT data, field-scale PFAS breakthrough could potentially be predicted under similar operating conditions. Additionally, applying a similar proportionality factor to RSSCT design equations should produce matching breakthrough curves for both RSSCT and field-scale.

4.3.5 Validation of scale-up approach

Using data collected from CD-RSSCTs and field-scale adsorbers conducted in two groundwaters with TOCs of 1.6 mgL^{-1} and <0.5 mgL^{-1}, the developed scale-up approach was applied. The scale-up was conducted for PFOA breakthrough data for four different carbons a wastewater-impacted groundwater and Carbon A breakthrough data for three PFAS in groundwater (Table 3.7 and Table 3.5, respectively). Extracted bed volumes to 10% breakthrough from scaled PSDM results were compared to field-scale adsorber results (Figure 4.10).

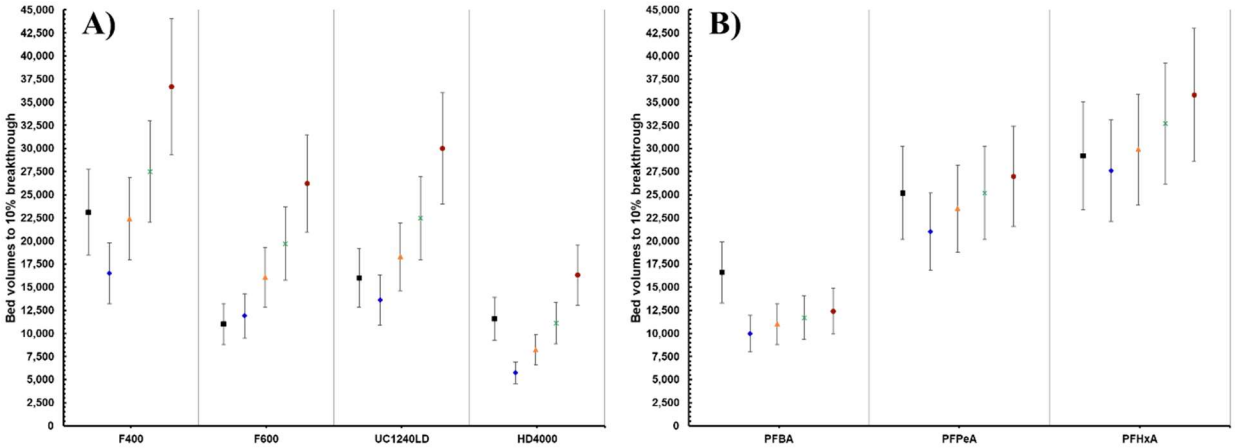

Figure 4.10: Comparison of bed volumes to 10% breakthrough for scaled CD-RSSCT PSDM and field-scale. A) Validation for wastewater-impacted groundwater with TOC=1.6 mgL^{-1}, B) Validation for groundwater with TOC<0.5mgL^{-1}, EBCT: 10 minutes, Pilot data represented by black squares with +/- 20% variance, Scaled CD-RSSCT for X=0.0 (blue diamond), X=0.25 (orange triangle) X=0.5 (green x), and X=1.0 (red circle) with +/-20% variance.

Validation of the scale-up approach in both groundwaters demonstrates that scaling kinetics using a proportionality factor of X=0.25 described field-scale breakthrough for a wide range of GAC and several PFAS. These results suggest that the scale-up approach is not influenced by the background water matrix, as demonstrated by the description of field-scale breakthrough curves in two lower TOC water matrices.

Furthermore, the dependence of intraparticle diffusivity on GAC particle size could be investigated by applying the proportionality factor of X=0.25 to RSSCT design equations. An RSSCT would be designed according to Equation 4.2, where a value of X=0.25 is applied. Additionally, the diffusion coefficient describing intraparticle diffusivity would be defined as Equation 4.3.

$$\left[\frac{EBCT_{RSSCT}}{EBCT_{field-scale}}\right] = \left[\frac{d_{RSSCT}}{d_{field-scal}}\right]^{2-X} \qquad \textit{Equation 4.2}$$

$$\left[\frac{D_{RSSCT}}{D_{field-scale}}\right] = \left[\frac{d_{RSSCT}}{d_{field-scal}}\right]^{X} \qquad \textit{Equation 4.3}$$

In Equation 4.3, the diffusion coefficients for the RSSCT and field-scale are represented by D_{RSSCT} and $D_{field\text{-}scale}$, respectively. An RSSCT for Carbon A was designed according to Equation 4.2, where X = 0.25 to assess whether field-scale PFAS breakthrough could be predicted. Breakthrough curves were directly compared between RSSCT and field-scale (Figure 4.11).

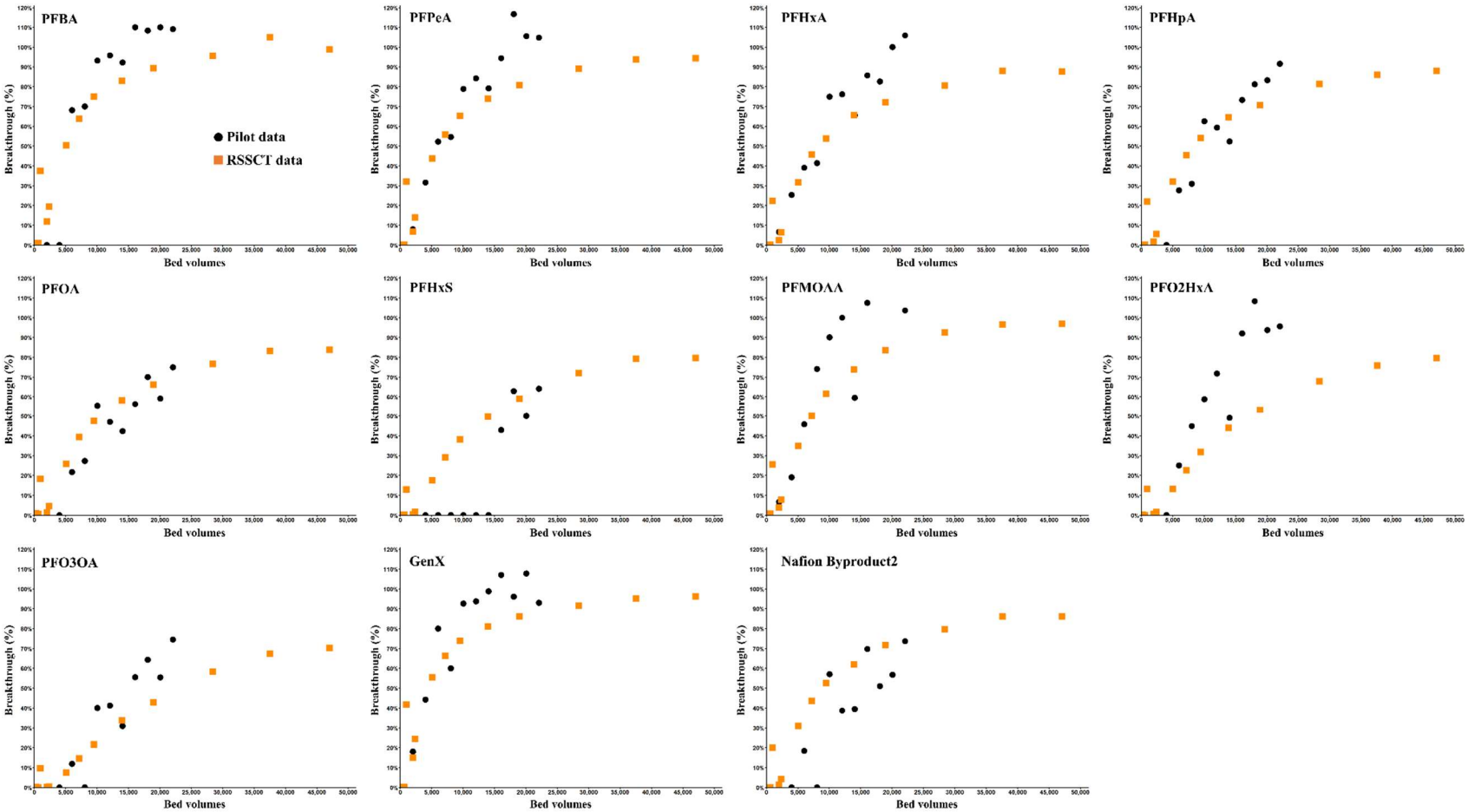

Figure 4.11: Direct comparison of RSSCT designed using equation 2 for X=0.25 (orange) and field-scale (black) data sets in coagulate/settled surface water (TOC = 2.3 mg L^{-1}), Carbon: Carbon A, simulated EBCT= 10 minutes.

Results in Figure 4.11 show that conducting a RSSCT designed according to Equation 4.2 can produce breakthrough curves for PFAS that describe field-scale breakthrough. The description of field-scale breakthrough curves suggests that intraparticle diffusivity dependence on GAC particle size scales well for a proportionality value of X=0.25.

4.4 Conclusions

CD-RSSCT and field-scale testing were conducted in three different water matrices, for six different GAC, and two EBCT to develop and validate a new scale-up approach that can predict field-scale breakthrough curves from CD-RSSCT data. By investigating the dependence of intraparticle diffusivity on GAC particle size, this research was able to demonstrate that for the majority of PFAS, the scale-up approach described field-scale breakthrough well when applying a proportionality value of X=0.25 for Equation 4.1. These results have highlighted that intraparticle diffusivity scale neither linearly nor constantly with GAC particle size. The scale-up approach was validated by predicting bed volumes to 10% breakthrough for the majority of PFAS in two groundwaters, with TOCs of 1.6 mgL^{-1} and <0.5 mgL^{-1}, for four carbons tested. The developed scale-up approach allows for expedited prediction of GAC performance at the field-scale by conducting a CD-RSSCT. Additionally, the prescribed scale-up approach within this research could be used to scale-up existing CD-RSSCT to rapidly develop field-scale predictions. The results of this work also suggest that a RSSCT designed using a proportionality factor of X=0.25 can predict field-scale breakthrough well. Ultimately, the developed scale-up approach can provide drinking water providers with an approach to rapidly estimate GAC service life by conducting CD-RSSCTs, which take a few days to conduct compared to several months for a field-scale adsorber.

CHAPTER 5 FACTORS INFLUENCING GAC REMOVAL OF PFAS

5.1 Introduction

Per- and polyfluoroalkyl substances (PFAS) is a diverse class of chemicals that include: 1) perfluoroalkyl carboxylic acids (PFCA), 2) perfluoroalkyl sulfonic acids (PFSA), 3) per- and polyfluoroalkylether acids (PFEA), 4) precursor of perfluoroalkyl acids (OECD 2018; Kwiatkowski et al. 2020; Buck et al. 2011). The unique physicochemical characteristics of PFAS include chemical/thermal stability, and hydrophobicity-lipophilicity. As such, PFAS are used in consumer and industrial products including non-stick coatings, fire-fighting foams, cosmetics, food packaging materials, and stain repellents (OECD 2018; Wang et al. 2017; Cousins et al. 2019). Through both industrial and consumer applications of PFAS, emissions of PFAS to the environment as increased resulting in widespread detection in the environment and humans (Ahrens 2011; Wang et al. 2017; Ng et al. 2021; Andrews et al. 2020; Muir et al. 2021; De Silva et al. 2020; Yao et al. 2021). In response to these occurrences, major fluorochemical manufacturers agreed to phase out the production of long-chain PFAS. This shift in use of long-chain PFAS has led industry to use other structurally similar PFAS including shorter-chain homologs (fluorinated carboxylates with chain lengths less than 7 and fluorinated sulfonates with chain lengths less than 6) or less studied fluorinated alternatives including per- and polyfluoroalkyl ether acids (PFEA, incorporate different numbers of ether oxygen linkages) (Brendel et al. 2018; ECA 2019; Kwiatkowski et al. 2020; Liu et al. 2018). The continued emission and persistence of PFAS has resulted in human exposure and adverse health effects to several bodily systems (Hurley 2018; Grandjean 2012; Kotlarz 2020; De Silva et al. 2021; Woodlief et al. 2021). One of the many exposure pathways potentially leading to adverse health

effects is ingestion of contaminated drinking water (De Silva et al. 2021; Vertergern and Cousins 2009; Ng et al. 2021).

The extensive use of PFAS coupled with their persistent nature, represents a continued threat to drinking water treatment systems as demonstrated by the continued detection in drinking water (Gyllenhammer et al. 2019; Boone 2019; Hopkins 2018; Gebbink 2017; Vestergern and Cousins 2009; Appleman et al. 2014; Hu et al. 2016). The occurrence and associated adverse health effects has led regulatory agencies are introducing stricter drinking water standards and guidelines to protect humans from exposure to PFAS present in drinking water sources (NJDEP 2018; EPA 2019; ECHA 2020; EPA 2021; ITRC 2020). Drinking water providers are having to keep pace with the ever changing regulatory landscape to meet standards and guidelines. As many conventional and advanced drinking water treatment processes are ineffective for the removal of PFAS, other treatment strategies are being investigated and employed to reduce PFAS levels in treated drinking water (Appleman et al. 2014; Pan et al. 2016; Franke et al. 2019; Bruton and Sedlak 2017; Crone et al. 2019). Success has often been found in using granular activated carbon (GAC) to treat for micropollutants in drinking water (Appleman 2013; USEPA 2018; Kennedy et al. 2015; Golovko et al. 2020; Hansen et al. 2010). Adsorption of PFAS to GAC has demonstrated removal is dependent on many physicochemical characteristics of PFAS, water quality parameters, and adsorber design (Zeng et al. 2019; Park et al. 2020; Rodowa et al. 2020; Gagliano et al. 2020; Cantoni et al. 2021). Studies have mainly focused the removal efficacy PFOA and PFOS, and other homologs from water likely due to the historical production and use of these chemicals. However, the increased detection of novel PFEAs in water sources requires similar studies to evaluate whether removal of PFEAs by GAC is as effective as previous results for other PFAS.

Traditionally, pilot-scale testing would be conducted to assess the removal of PFAS from source water while testing the effects of adsorbent type and empty bed contact time. Conducting pilot-scale tests are time intensive and costly. Evaluation of micropollutant removal by GAC can now be conducted through the more practical use of rapid small-scale column tests (Crittenden et al. 1986; Crittenden et al. 1989; Summers et al. 2014). RSSCTs have been extensively adopted to simulate the breakthrough of PFAS and other micropollutants in full-scale adsorbers. Chapter 4 results demonstrated the application of the CD-RSSCT could be used to predict PFAS breakthrough at the full-scale after scaling the intraparticle diffusivity. The benefit of evaluating removal of replacement PFAS using the CD-RSSCT include 1) shorter experimental run time, 2) smaller quantities of water, and 3) collection of scalable adsorption kinetics parameters. The benefits of conducting and scaling CD-RSSCTs allow for the rapid evaluation of field-scale conditions (e.g., carbon type, organic matter type and concentration, novel PFAS, and empty bed contact time).

This study aimed to evaluate factors (e.g., GAC type, background NOM concentration, adsorber empty bed contact time, and PFAS physiochemical characteristics) influencing removal of traditional PFAS and novel PFEA (Table 5.1) from drinking water by GAC. RSSCTs were conducted in drinking water matrices affected by PFAS contamination. Estimation of PFAS removal efficiency at the field-scale were based on scaled RSSCT breakthrough data. Results of obtained from this research aim to better guide water providers understand factors that potentially influence removal efficiency of PFAS by GAC from contaminated source water.

5.2 Materials and methods

5.2.1 Materials

5.2.1.1 Waters

Influent waters for the RSSCT experiments were collected from two different drinking waters sources (Table 3.1; Water A and Water C). Water A was collected from a drinking water treatment plant that treats surface water. Water C was collected from a drinking water treatment plant that treats groundwater. Water quality parameters for each water are provided in Section 3.1.1, Table 3.1. Waters were filtered through a 5 um cartridge filter prior to being spiked with PFAS. PFAS and total organic carbon (TOC) concentrations were measured at the beginning and end of each RSSCT to verify water quality parameters were consistent during the experiments. The average concentrations of individual PFAS are provided in Section 3.1.2, Table 3.2.

5.2.1.2 Adsorbents

RSSCTs were conducted using one of four carbons. Carbons tested included two sub-bituminous coal-based carbons (Carbon A and Carbon B), one enhanced coconut shell-based carbon (Carbon C), and one lignite-based carbon (Carbon D). Information about the carbon properties are provided in the Section 3.1.1, Table 3.3. For all the RSSCTs, GAC was wet milled with a mortar and pestle, wet sieved, and the fraction in the range of 63 to 74 µm (200x230 U.S. Standard Mesh) was collected for use. Prior to use GAC was dried at 105°C.

5.2.1.3 Adsorbates

In this study a total of 22 PFAS (Table 5.1) were assessed in RSSCT experiments, including seven perfluorocarboxylic acids (PFCAs), three perfluorosulfonic acids (PFSAs), one

fluorotelomer sulfonate (FTS), nine per- and polyfluoroalkyl ether carboxylic acids (PFECAs), two per- and polyfluoroalkyl ether sulfonic acids (PFESAs). All PFAS tested were sourced from Synquest Laboratories Inc. (Alachua, FL), Fluoryx Laboratories (Carson City, NV), and The Chemours Company (Wilmington, DE).

Table 5.1: Physicochemical characteristics of PFAS.

Compound	CAS # (hyperlinked to US EPA Chemicals Dashboard)	Molecular weight	Molar volume	logD	Chain length	# of Ether oxygen linkage(s)
Carboxylic acid						
PFBA	375-22-4	214	127	-1.22	4	--
PFPeA	2706-90-3	264	155	-0.52	5	--
PFHxA	307-24-4	314	182	0.18	6	--
PFHpA	375-85-9	364	210	0.88	7	--
PFOA	335-67-1	414	237	1.58	8	--
PFNA	375-95-1	464	265	2.28	9	--
PFDA	335-76-2	514	292	2.98	10	--
Sulfonic acid						
PFBS	375-73-5	300	162	0.25	5	--
PFHxS	355-46-4	400	217	1.65	7	--
PFOS	1763-23-1	500	272	3.05	9	--
Fluorotelomer sulfonate						
6:2FTS	27619-97-2	427	250	1.54	9	--
Linear ether carboxylic acid						
PFMOAA	674-13-5	180	106	-1.19	4	1
PFO2HxA	39492-88-1	246	140	0.27	6	2
PFO3OA	39492-89-2	312	174	1.73	8	3
PFO4DA	39492-90-5	378	208	3.18	10	4
PFO5DoA	39492-91-6	444	242	4.64	12	5
Branched ether carboxylic acid						
PMPA	13140-29-9	230	134	-0.45	5	1
PEPA	267239-61-2	280	161	-0.23	6	1
GenX	13252-13-6	330	189	0.47	7	1
HydroEve	773804-62-9	428	245	1.66	10	2
Linear ether sulfonic acid						
NVHOS	801209-99-4	298	164	0.05	6	1
Branched ether sulfonic acid						
NafionBP2	749836-20-2	464	252	2.43	10	2

5.2.2 Methods

5.2.2.1 Analytical methods

5.2.2.1.1 PFAS analysis

The 22 PFAS spiked into source water A and source water C (Section 3.1.2, Table 3.2) for the RSSCTs were quantified by liquid chromatography quadrupole mass spectrometry (LC-MS/MS). Calibration curves were established with standards prepared in ultrapure deionized water. The concentrations of the standards ranged from 1 to 500 ng L^{-1} for all compounds. A full description of the sample analysis method by LC MS/MS (Ultivo, Agilent Technologies Inc.) is provided in Section 3.2.1 and Appendix A.

5.2.2.1.2 Total organic carbon and ultraviolet absorbance

Total organic carbon (TOC) was measured using a TOC analyzer (Model TOC-VCSN, Shimadzu Scientific, Columbia, MD) in accordance with Standard Method 5310C (APHA et al. 2005). Ultraviolet absorbance (UV_{254}) was measured at a wavelength of 254 nm using a spectrophotometer (Hach DR4000, Hach, Loveland, CO) in accordance with Standard Method 5910 (APHA et al. 2005).

5.2.2.2 Rapid small-scale column testing

RSSCTs were conducted using the constant diffusivity RSSCT (CD-RSSCT, Figure 3.1) design to simulate full-scale empty bed contact times of 10- and 20-min. Details of the CD-RSSCT design and operation are provided in Section 3.2.4. The CD-RSSCT approach is beneficial because of the reduction in water, quantity of adsorbent, and time to achieve micropollutant breakthrough compared to a PD-RSSCT or pilot-scale column. Demonstrated in

Chapter 4, by conducting a CD-RSSCT with influent water matching the field-scale conditions, the Freundlich adsorption capacity of the CD-RSSCT matched well the field-scale capacity and adsorption kinetics could be scaled to predicted field-scale adsorption kinetics. The developed scale-up approach in Chapter 4 allows for rapidly investigating factors influencing PFAS breakthrough at the field-scale.

Operational parameters for RSSCTs and field-scale adsorbers are provided in Section 3.2.4, Table 3.5. For all RSSCTs, carbons were prepared according to GAC preparation described in Section 3.2.3. The GAC particle size used in all RSSCTs was 200x230 U.S. Standard Mesh. Prior to use all carbons were dried at 105°C. The CD-RSSCTs were design using a similar approach to previous research (Kennedy et al. 2017; Chapter 4 of this work). Use of polypropylene tubing to build RSSCTs is relatively inexpensive and permits visual observation of the GAC bed during testing. Activated carbon was loaded into the 0.318 cm diameter column as a slurry to achieve a calculated bed depth based on design equations. The ratio of the column diameter to particle diameter was designed to be greater than a ratio of 10:1, which is sufficient for preventing wall effects (Knappe et al. 1999). Spiked water was stored in 5-gal carboys and pumped through the column with a HPLC pump. Samples were collected for TOC/UV254 in 40 mL amber vials (Environmental Sampling Supply, Carol Stream, IL) and for PFAS in 15 mL polypropylene falcon tubes (Thermo Fisher Scientific, Waltham, MA). Sampling of the RSSCT influent occurred at the beginning and end of the experiment. Sampling of the RSSCT effluent occurred initially every 500-1,000 bed volumes for the first 10,000 bed volumes and then every 5,000-10,000 bed volumes for the reminder of the RSSCT experiment.

5.2.2.3 Data analysis

To compare PFAS breakthrough curves at the field-scale, CD-RSSCT results were scaled according to the approach presented in Chapter 4. Adsorption capacity and adsorption kinetics parameters for individual PFAS breakthrough curves can be estimated from the pore-surface diffusion model (PSDM) fit (AdDesignS, Michigan Technological University, Houghton, MI). Previous research has demonstrated use of a PSDM fit can describe micropollutant adsorption capacity and adsorption kinetics (Kennedy et al. 2015; Summers et al. 2014; Fotta 2012; Rodowa et al. 2020; Crittenden et al. 1986). After Freundlich adsorption capacity and kinetics parameters were obtained using AdDesignS, kinetics were scaled using the approach described in Chapter 4 of this work, which was demonstrated to be effective for predicting field-scale breakthrough. Evaluation of factors influencing PFAS breakthrough were then made by comparing scaled breakthrough curves and breakthrough to specific treatment objectives (e.g., 10%, 20%, 50% breakthrough).

Additionally, carbon use rate (CUR) has been used as a metric for evaluating GAC performance. The CUR metric is expressed as the mass of GAC required to treat a volume of water to a desired treatment objective (Equation 5.1).

$$CUR = \frac{M_{GAC}}{BV \times V_{bed}} \qquad \textit{Equation 5.1}$$

In Equation 5.1, M_{GAC} represents the mass of GAC (units of mg or lbs), BV is bed volumes to a desired treatment objective (e.g., 10 or 20% breakthrough), and V_{bed} is the volume of the bed (units of L or gals). From Equation 5.1, the conclusion can be made that more efficient use of the GAC is achieved when an adsorber can treat larger volume of water resulting in lower CUR values. Knappe et al. (2017) proposed CUR limits for determining the feasibility of GAC to remove contaminants cost-effectively. GAC is considered feasible if the CUR is less than 0.2 lbs

GAC/1000 gallons of water treated (well adsorbed contaminant), while a CUR at or above 0.6 lbs GAC/1000 gallons water treated (weakly adsorbed contaminant) is unfeasible due to high GAC costs.

5.3 Results and discussion

5.3.1 Effect of PFAS structure

PFAS vary structurally within a class of more than 5,000 chemicals and changes to the structure can affect both physical and chemical characteristics. For example, PFAS vary in chain length and molar volume (Table 5.1). Additionally, PFAS differ in the functional head group (e.g., carboxylate, sulfonate) at the end of the fluorinated chain. The various structural differences among PFAS are expected to influence adsorption potential. This research investigated the effect of PFAS structure on breakthrough for several classes of PFAS in RSSCTs that employed different GACs. In Figure 5.1 breakthrough curves for 22 different PFAS tested are compared for Carbon A at a simulated EBCT of 10 minutes in a water of TOC = 2.3 mgL^{-1}. Similar comparisons were prepared for Carbon A (EBCT = 20 minutes), Carbon B (EBCT = 10 minutes), Carbon C (EBCT = 10 minutes), and Carbon D (EBCT = 10 minutes) in Figure C.1-C.4 of Appendix C. To investigate trends in breakthrough with respect to various physicochemical properties (e.g., chain length, molar volume, logD), bed volumes to 10, 20, and 50% breakthrough were extracted from these data sets. Figure 5.2 illustrates how molar volume affects bed volumes to 10% breakthrough for the carbons tested in this study. Additional figures were prepared for bed volumes to 20% and 50% breakthrough (Appendix C, Figures C.5 and C.6).

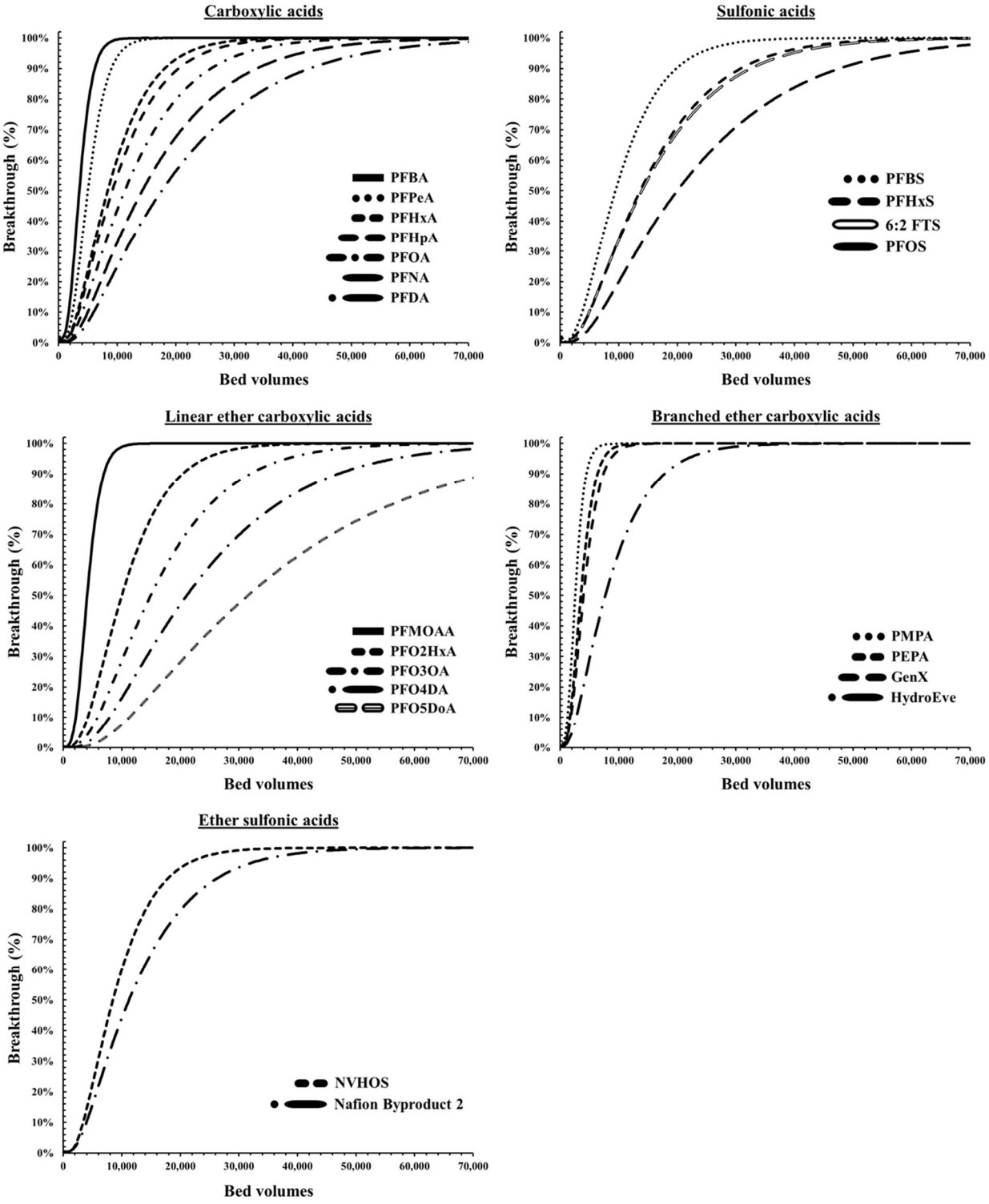

Figure 5.1: Breakthrough curves for different classes of PFAS. Carbon: Carbon A, EBCT=10 minutes, TOC= 2.3 mgL^{-1}.

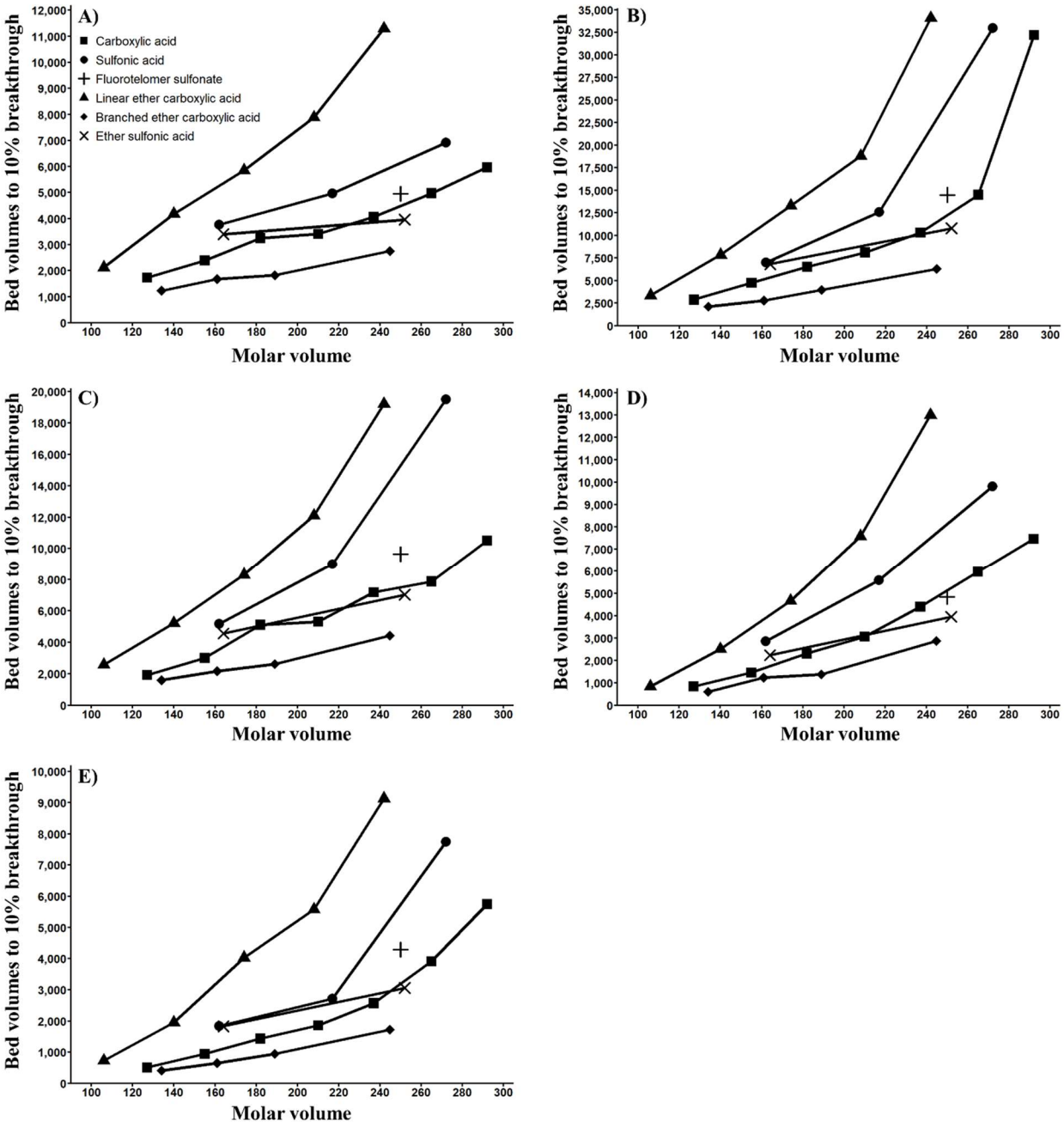

Figure 5.2: Effect of molar volume on bed volumes to 10% breakthrough. TOC = 2.3 mgL^{-1}; A) Carbon A, EBCT = 10 minutes, B) Carbon A, EBCT = 20 minutes, C) Carbon B, EBCT = 10 minutes, D) Carbon C, EBCT = 10 minutes, E) Carbon D, EBCT = 10 minutes.

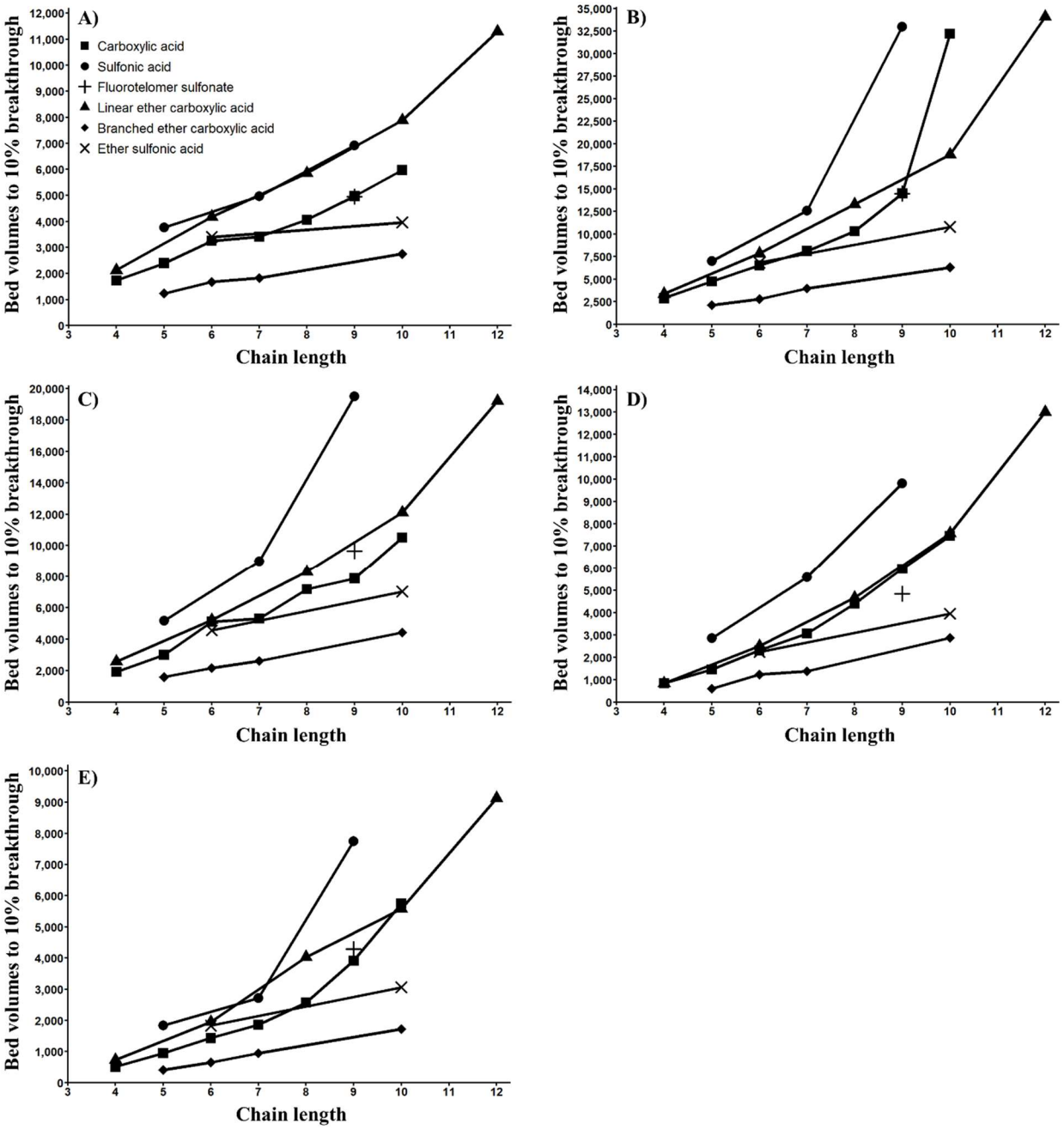

Figure 5.3: Effect of chain length on bed volumes to 10% breakthrough. TOC = 2.3 mgL^{-1}; A) Carbon A, EBCT = 10 minutes, B) Carbon A, EBCT = 20 minutes, C) Carbon B, EBCT = 10 minutes, D) Carbon C, EBCT = 10 minutes, E) Carbon D, EBCT = 10 minutes.

For PFAS classes, which more than two compounds were tested, the bed volumes to 10% breakthrough increased with increasing molar volume (Figure 5.2) and chain length (Figure 5.3). For example, breakthrough of PFBA, a four-carbon chain length PFCA (molar volume = 127), occurred at ~1,700 bed volumes compared to PFHxA, a six carbon chain length PFCA (molar volume = 140), which occurred at ~3,300 bed volumes. For other PFAS classes including PFSA, PFECA, and PFESA similar increases in bed volumes to 10% breakthrough occurred with increasing molar volume and chain length. The increase in bed volumes to 10% breakthrough (Figure 5.2) with respect to PFAS molar volume indicates that increasing overall molecular size enhances PFAS affinity to GAC. The increased affinity to GAC suggests that increasing molar volume by addition of CF_2 or OCF_2 group, increased the hydrophobicity of the PFAS. Similar results were demonstrated for Carbon A at an EBCT of 20 minutes and three additional GAC (Carbon B, Carbon C, and Carbon D) in Figures 5.2 and 5.3. The improved removal efficiency with increasing molecular size for PFAS has been previously demonstrated by other research for PFCA and PFSA compounds (Rodowa et al. 2020; Appleman et al. 2014; Dudley et al. 2015, Zeng et al. 2020; Park et al. 2020; Kempsity 2014; Cantoni et al. 2021). For example, Rodowa et al. (2020) demonstrated similar increase in adsorbability with increasing chain length for PFCAs. Larger molecular PFAS are more hydrophobic than smaller molecular PFAS because of the addition of additional fluorinated carbons. As a result, increasing chain length PFAS prefer to partition into the solid phase than the aqueous phase. Additionally, previous research has suggested that the head group moiety of a PFAS can influence the affinity to GAC. These studies demonstrated that for PFAS of equivalent chain length sulfonic acid PFAS had a higher affinity for GAC than carboxylic acid PFAS (Dudley et al. 2015; Rodowa et al. 2020; Cantoni et al. 2021; Higgins and Luthy 2006; Park et al. 2020). When comparing results for PFCA and PFSA

(Figure 5.2 and 5.3), the PFSA 1) break through at later bed volumes to 10% breakthrough compared to PFCA, and 2) have a higher adsorption capacity compared to PFCA. Regarding the influence acidic functional group on PFEAs, a similar effect is noticeable when comparing HydroEve (ether carboxylic acid) and Nafion Byproduct 2 (ether sulfonic acid). Bed volumes to 10% breakthrough were greater for Nafion Byproduct 2 (Bed volumes to 10% breakthrough = ~4,000) compared to HydroEve (Bed volumes to 10% breakthrough = ~2,800). These results suggest that effect of acidic functional group is similar across PFAS subclasses. Research has suggested that the molecular size and/or electrostatic interactions associated with a PFAS containing a sulfonic acid head group could potentially result increased hydrophobicity compared to a PFAS with a carboxylic acid functional head group (Higgin and Luthy et al. 2006). Xiao et al. (2013) hypothesized that a concept of hard and soft bases could explain the increased adsorption of sulfonic acid group compared carboxylic acid group. Potentially a greater electron-donor characteristic of PFAS with a sulfonic acid moiety compared to carboxylic acid moiety could explain the difference adsorption potential.

Literature has also previously suggested that branching of PFAS reduces affinity to GAC resulting in earlier breakthrough (Park et al. 2020; Rodowa et al. 2020; McCleaf et al. 2014; Eschauzier et al. 2012). In Figure 5.4, branched PFECA (e.g., PMPA, PEPA, and GenX) breakthrough earlier than similar chain length PFCA (e.g., PFPeA, PFHxA, and PFHpA) for removal by Carbon A in a TOC of 2.3 mgL-1 surface water at an EBCT of 10 minutes.

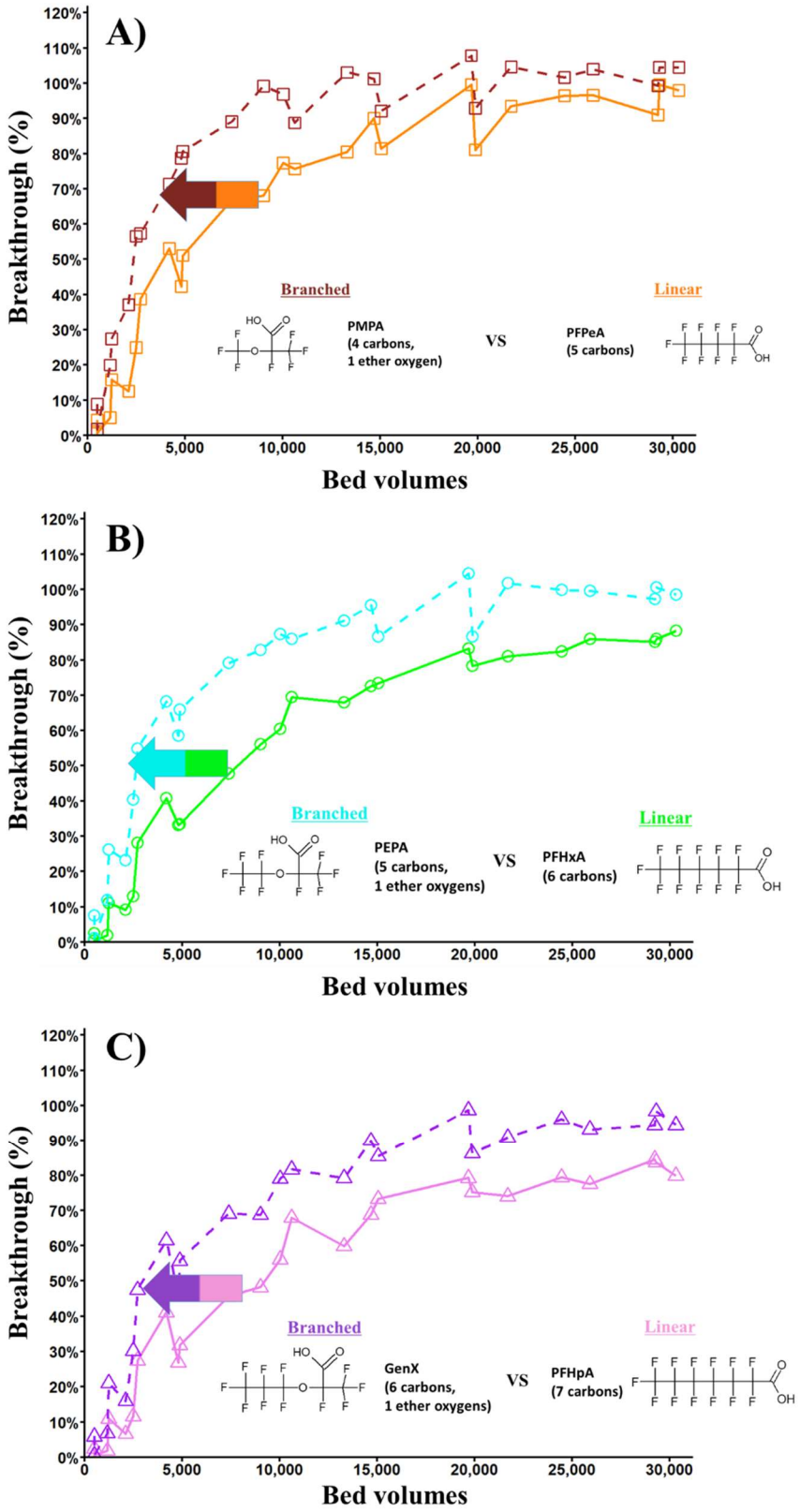

Figure 5.4: Effect of branching on PFAS breakthrough. A) PMPA vs PFPeA, B) PEPA vs PFHxA, C) GenX vs PFHpA. Carbon: Carbon A, EBCT = 10 minutes, TOC = 2.3 mgL^{-1}.

Results in Figure 5.4 demonstrate that branching of the alkyl chain results earlier breakthrough compared to a similar chain length unbranched PFAS. For example, in Figure 5.4B PEPA (branched) breakthrough earlier than PFHxA (unbranched). These decrease in breakthrough was observed for several other PFAS pairs (e.g., PMPA < PFPeA and GenX < PFHpA). This result was also demonstrated in for three additional GAC (Figures C.9-C.12) and for two additional background TOC concentrations (Figures C.13-C.16). These findings are in agreement with Sun et al. (2016), which demonstrated removal of branched PFAS by PAC was less than unbranched PFAS.

In addition to the previous mentioned factors affecting PFAS breakthrough, the incorporation of ether oxygen linkages was investigated. Comparison of raw RSSCT breakthrough data (Figure 5.5) were made for similar chain length PFAS with and without ether oxygen linkages. The addition of a single ether oxygen linkage illustrated little change in breakthrough when comparing PFMOAA and PFBA (Figure 5.5A). Similarly, PFECAs with multiple ether oxygen linkages demonstrated little change in breakthrough curves (Figures 5.5B and 5.5C). Similar breakthrough curves for PFAS with and without ether oxygen linkages were also demonstrated for several GAC (Figure C.17-C.20) and in two additional influent TOC concentration waters (Figures C.21-C.24). These results are expected, as there is little change in the hydrophobicity of PFAS with the incorporation of ether oxygen linkages as indicated by logD values (Table 5.1).

These interpretations of sulfonate vs carboxylate and incorporation of ether oxygen groups on adsorption potential still need to be corroborated by experimentally determined physicochemical properties, for which there is currently either 1) limited data or 2) significant uncertainty in measurements (Rayne and Forest 2009; Gomis et al. 2015).

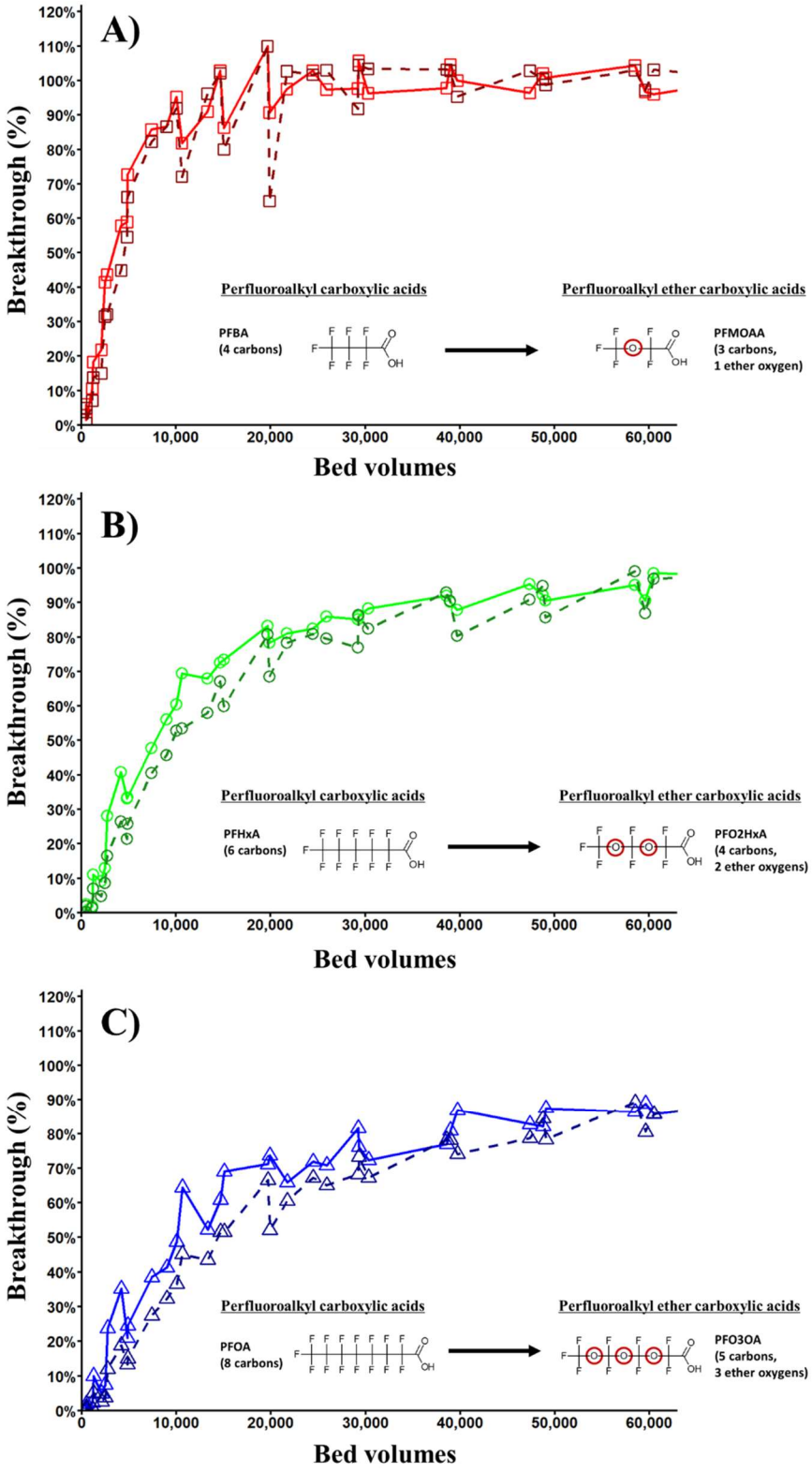

Figure 5.5: Effect of incorporation of ether oxygen linkage on PFAS breakthrough. No ether oxygen linkage (Solid line), Ether oxygen linkage (dashed line). A) PFBA vs PFMOAA, B) PFHxA vs PFO2HxA, C) PFOA vs PFO3OA. Carbon: Carbon A, EBCT = 10 minutes, TOC = 2.3 mgL^{-1}.

5.3.2 Effect of carbon type

Adsorbent materials can vary widely in pore structure and surface chemistry. These characteristics associated with each adsorbent are expected to influence removal efficiency. The production of GAC from a variety of raw materials (e.g., bituminous coal, coconut shell, and lignite) and activation process (e.g., thermal or chemical) can produce differing surface chemistry and pore structure. Previous research has demonstrated for a variety of micropollutants that GAC selection can affect adsorption kinetics and adsorption capacity (Wu et al. 2020; Du et al. 2014; Crittenden et al. 2011; Summers et al. 2011; Punyapalakul et al. 2013; Du et al. 2015; Appleman et al. 2013; Knappe 2006; Cantoni et al. 2021). The highly porous nature of GAC gives rise to an internal pore structure that can consist of 1) primary micropores (<8 Å width), 2) secondary micropores (8-20 Å width), 3) mesopores (20-500 Å width), and 4) macropores (>500 Å width). Previous research has suggested that adsorbents containing a higher fraction of micropores than mesopores are less efficient for removal of micropollutants (Kennedy et al. 2015; Du et al. 2014; Appleman et al. 2013). The decrease in effectiveness is suggested to be a result of pore blockage and competition for high energy adsorption sites. Several studies have evaluated the removal of traditional PFAS (e.g., PFOA and PFOS) by GAC. Results from these studies illustrated that similar to other micropollutants, generally high meso- and macroporous adsorbents were most effective for removal of PFAS (Kothawala et al. 2017; McCleaf et al. 2017). This work conducted RSSCTs to assess the influence of GAC characteristics on the removal of a variety of PFAS including short-chain PFAS and novel PFEAs. RSSCTs were conducted in the same influent water for two reagglomerated subbituminous coal-based carbons (Carbons A and B), one enhanced coconut shell-based carbon (Carbon C), and one lignite-based carbon (Carbon D). Characteristics for these carbons are provided in Section 3.1.3, Table 3.3.

Ratios of bed volumes to 10% breakthrough for a selected GAC to bed volumes to 10% breakthrough for Carbon A are compared for RSSCTs conducted in a coagulated surface water with a TOC of 2.3 mg L^{-1} (Figure 5.6).

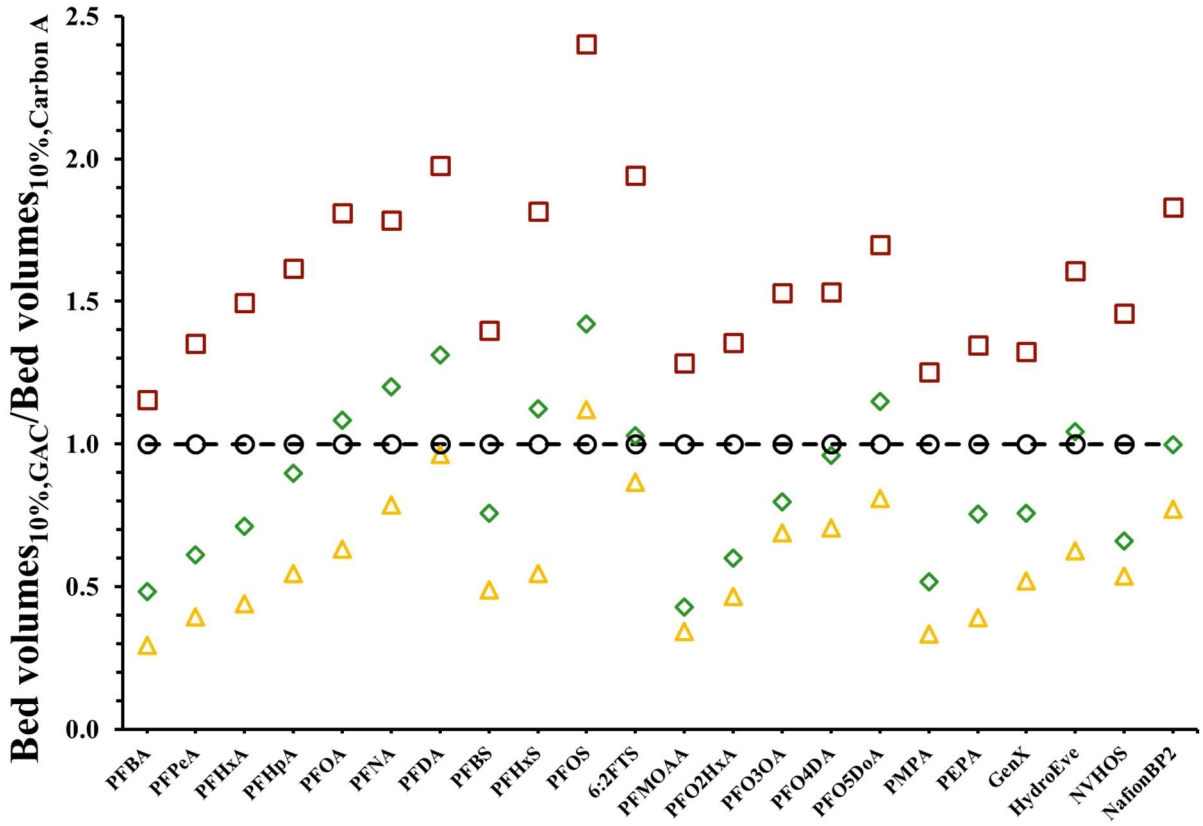

Figure 5.6: Effect of carbon selection on bed volumes to 10% breakthrough with Carbon A used as a basis for comparison. Carbon: A (Black), B (Red), C (Green), D (Orange); EBCT= 10minutes; TOC=2.3 mg L^{-1}.

In Figure 5.6 if bed volumes to 10% breakthrough are exactly the same as Carbon A then the ratio of bed volumes, for a given PFAS tested, would be a value of one. Increase or decrease in this this ratio of bed volumes to 10% breakthrough would indicate a greater number of bed volumes to smaller number of bed volumes could be treated to 10% breakthrough, respectively. For example, comparison of bed volume ratios for PFHxA (Figure 5.6) indicates better performance of Carbon B compared to Carbon A because the ratio of bed volumes to 10% breakthrough is greater than one. While for both Carbon C and Carbon D the ratios are less than

one, which indicates these carbons treated less bed volumes to 10% breakthrough compared to Carbon A. Ratios comparing bed volumes to 10% breakthrough for individual GAC to Carbon A in Figure 5.6 illustrates that for the majority of PFAS, higher removal efficiency occurred in the following order: Carbon B > Carbon A > Carbon C > Carbon D. Though Carbon A and Carbon B are both reagglomerated sub-bituminous coal-based carbon and contain similar pore size distributions (Figure 5.7), Carbon B has a higher removal efficiency than carbon A (Figure 5.6). The better performance for Carbon B versus Carbon A could be explained by the slightly higher pore volume in the secondary micropore width range (Figure 5.7 and Table 3.3). Appleman et al. (2015) demonstrated a similar trend between two coal-based carbons, with more favorable adsorption of PFAS being attributed to a difference in microporosity structure.

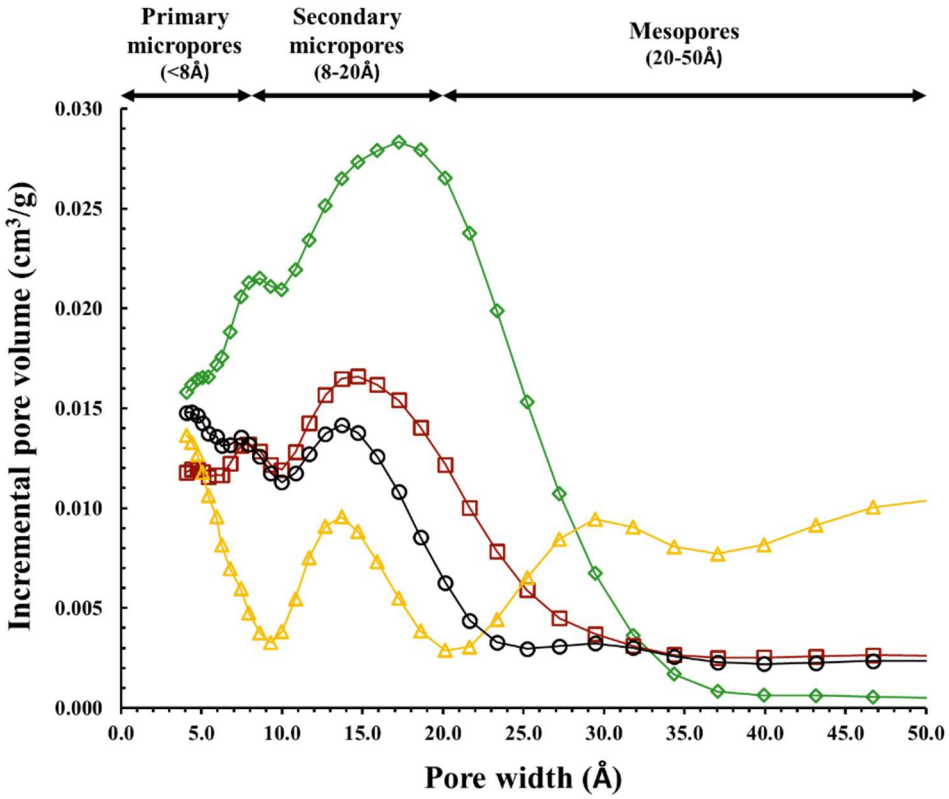

Figure 5.7: Comparison of pore size distributions of GACs tested. Carbon A (black circles), Carbon B (red squares), Carbon C (green diamonds), and Carbon D (yellow triangles).

Figure 5.7 illustrates the pore size distributions for the four carbons studied in this research. The pore size distribution for Carbons A, B, and C show pore volume is concentrated in the <30 Å pore width range with pore volume peaking in the 8 to 20 Å pore width range. While for Carbon D the pore structure was less focused in the micropore region and spread out over the <8 to 50 Å pore width range with significant pore volume in mesopore range (20-50 Å). These differences in pore size distribution for three of the GAC (Carbons A, B, and D) could explain the breakthrough order of PFAS illustrated by results in Figure 5.6. Considering PFAS are small in molecular size, with diameters estimated from molar volume ranging from 7.0 to 9.7 Å, the presence of pore volume in the secondary micorpore region is important for removal. Several studies have suggested preferential adsorption of organic pollutants occurs when the pore width is approximately 1.7-2.0 times the targeted molecules second widest dimension (Kasaika et al., Li et al. 2002; Newcombe et al. 2002, Pelekani et al. 1999). To assess in which pore diameter PFAS preferentially adsorb, bed volumes to 10% breakthrough were correlated with GAC pore volume in selected pore width ranges for each tested GAC. A trial-and-error approach similar to that used by Li et al. (2002) and Ebie et al. (1995) was employed to determine the pore width range that controlled adsorption for individual PFAS present in the influent water. Pore volume was summed for a selected pore width range and then plotted against bed volumes to 10% breakthrough for each GAC tested. The resulting correlations to determine the pore width range controlling adsorption are shown in Figure 5.8 for four PFAS, with additional plots for all other PFAS provided in Appendix C Figures C.9-C.13.

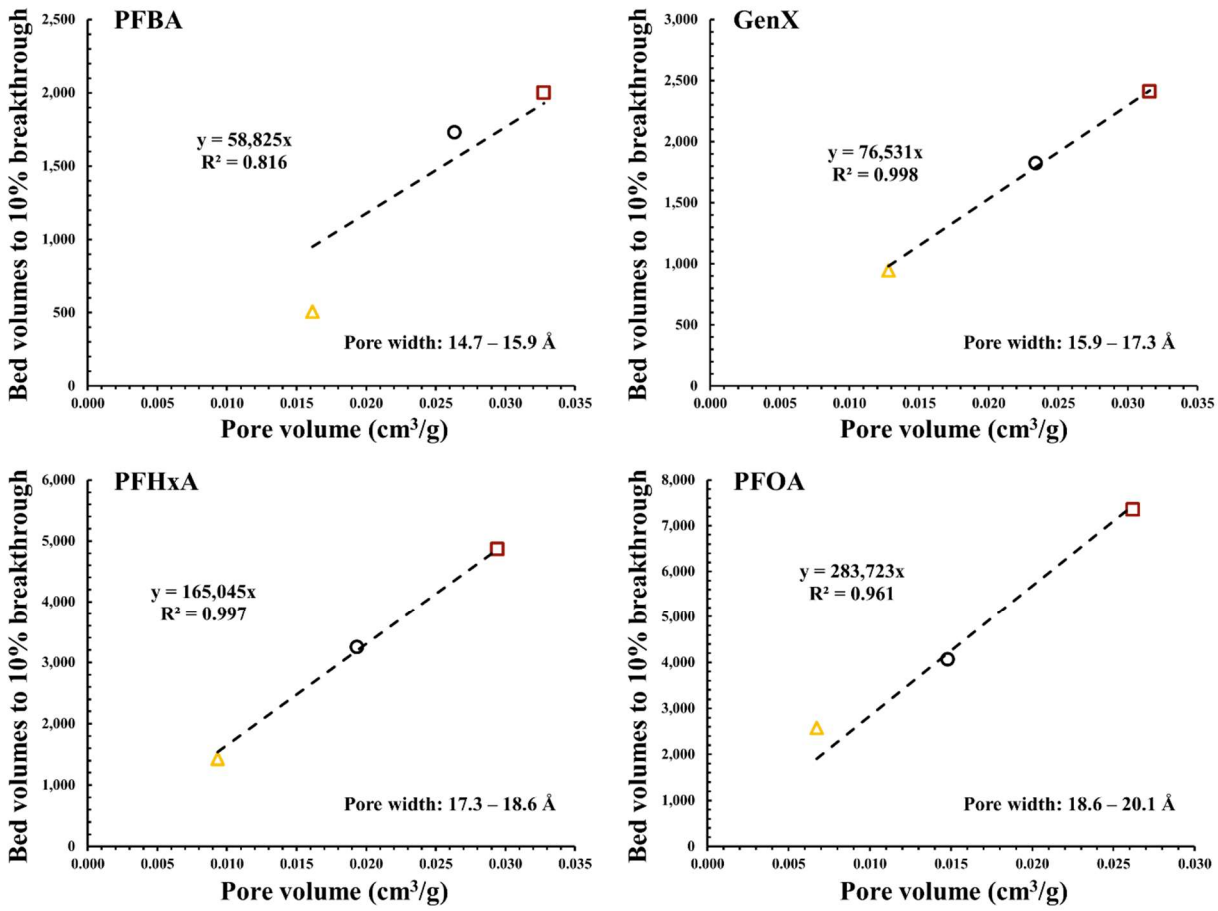

Figure 5.8: Relationships between bed volumes to 10% breakthrough and pore volumes in the secondary micropore range in coagulated/settled surface water. Carbon A (black circle), Carbon B (red square), Carbon D (yellow triangle).

Results presented in Figure 5.8 demonstrate that available pore volume in the 9.30-9.98, 15.9-17.3, 17.3-18.6, and 18.6-20.1 Å pore width range for PFBA, GenX, PFHxA, and PFOA, respectively, controlled adsorption. For each PFAS studied in this research, results suggest that these micropollutants adsorb primarily in pore widths that are 1.9 to 2.2 times the targeted PFAS molecular diameter. A correlation between molecular diameter and mean pore width is shown in Figure. 5.9.

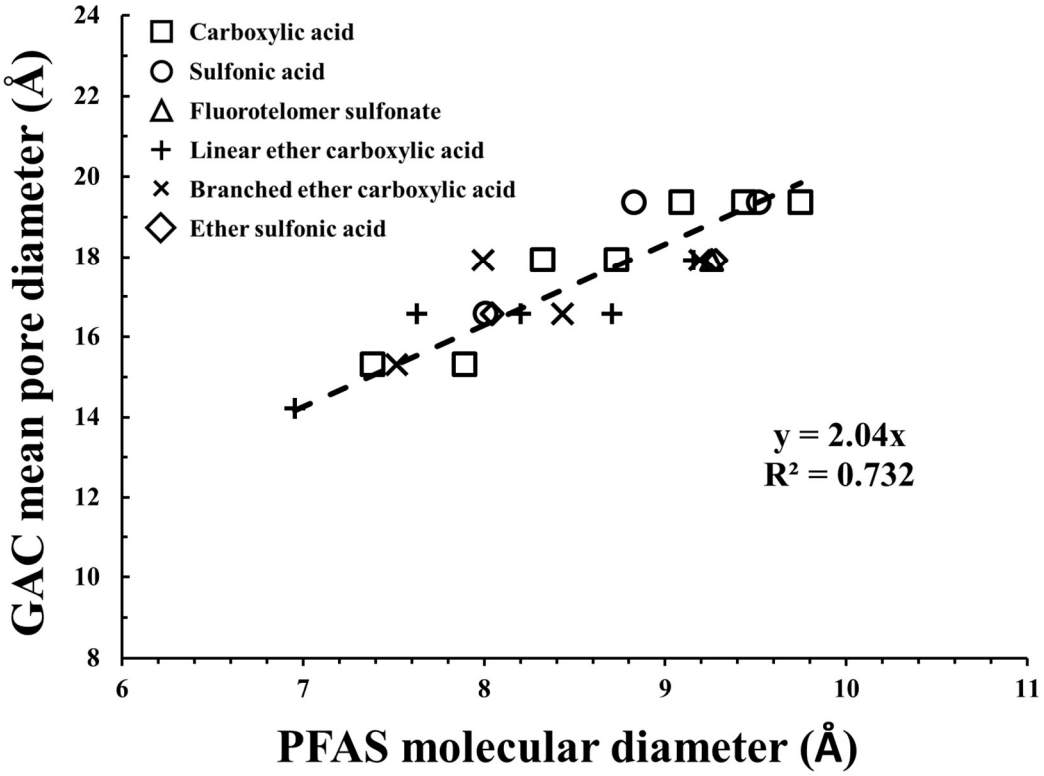

Figure 5.9: Correlation between molecular diameter of PFAS and preferred mean pore diameter for adsorption based on results from Figure 5.8 and Figure C.9 and C.13. For data collected from adsorption in coagulated surface water, TOC = 2.3 mgL^{-1}.

Results in Figure 5.9 suggest there is a linear correlation between PFAS molecular diameter and preferred GAC mean pore width for adsorption. These results align well with the range of preferred pore size for adsorption of micropollutants previously suggested by Kasaoka et al. (1989) and Li et al. (2002). The change in micropore size distribution of GAC altered the performance of a GAC to remove a targeted PFAS. Additionally, Zhi et al. (2015) suggested based on results for several GAC that if microporosity was important then increased micropore volume would be expected to result in increased adsorption. Other studies comparing GAC produced from different base materials (e.g., coal based, coconut shell based, lignite based) also suggested the importance of increasing micropore volume for the removal of micropollutants (Du et al. 2014; Appleman et al. 2013; McNamara et al. 2018; Zeng et al. 2020; Cantoni et al.

2021). Of the four GAC tested in this research, Carbon C pore size distribution did not correlate with the other carbons for determining pore width range controlling PFAS removal. This result suggests that due to limited mesopore volume for Carbon C this GAC demonstrated reduced GAC performance. McNamara et al. (2018) showed a similar result for a coconut shell-based carbon. They attributed the lower removal efficiency of coconut shell-based carbons to a poor transport pore structure produced by the higher percentage of micropore compared to the reagglomerated subbituminous coal-based carbon that contained more well-developed mesopores allowing transport the micropores. This suggests that while micropores are important to adsorption of small molecule PFAS, the mesopore structure is key to facilitating transport to the micropores of GAC, which is supported by this and other research (Li et al. 2002; Newcombe et al. 2002).

Additionally, to rapidly assess the pore width controlling PFAS adsorption correlations where prepared between collision cross-section for [M-H-CO2] ($CCS_{[M-H-CO2]}$) mean pore diameter and collision cross-section for [M-H] ($CCS_{[M-H]}$) (Figure 5.10). The CCS is a molecular descriptor of PFAS surface area (Dodds et al. 2020). Correlating CCS and mean pore width provides potentially a rapid approach to assessing 1) mean pore width required for effective removal of novel PFAS and 2) information for selecting GAC to test the removal of PFAS present in source water.

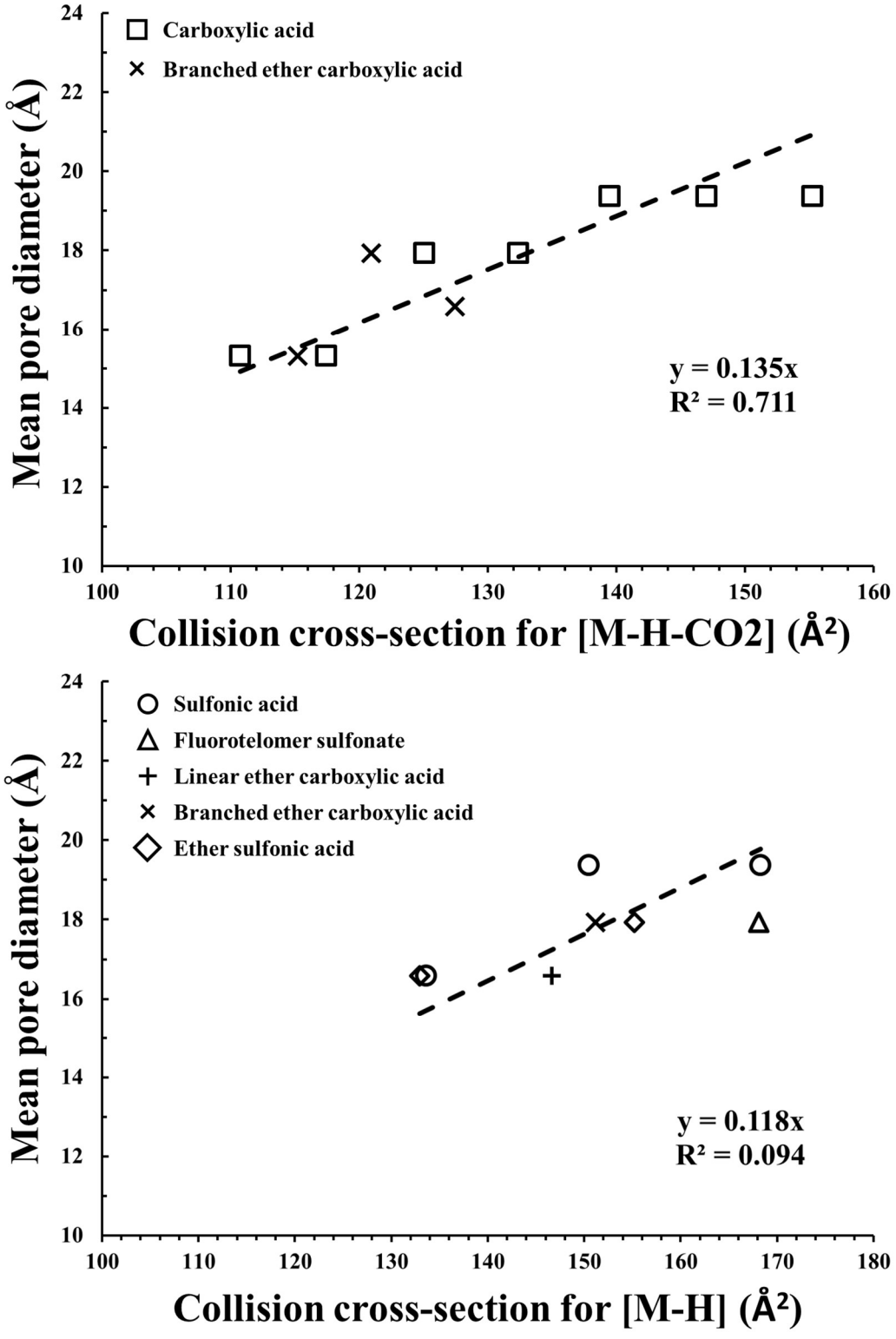

Figure 5.10: Correlation for collision cross-sections and mean pore diameter with relationships for PFAS with estimated collision cross-section for [M-H-CO2] (Top) and [M-H] (bottom). Based on results for preferred adsorption of PFAS in mean pore diameter in Figure 5.8 and Figure C.9-C13. TOC = 2.3 mgL^{-1} and EBCT=10 minutes.

Figure 5.10 illustrates a correlation developed for $CCS_{[M-H-CO2]}$ and mean pore diameter, while a mean pore diameter did not correlate with $CCS_{[M-H]}$. These correlations are just one suggestion for estimating preferred mean pore width controlling PFAS adsorption based on accurately and rapidly measured physicochemical characteristics of PFAS. Development of these correlations has the potential to improve the process of selecting a GAC to be tested for PFAS removal at both the bench-scale and field-scale.

In a lower background NOM concentraion surface water (TOC = 1.3 mg L^{-1}), results suggest that Carbon C becomes more competitive for removal of longer-chain PFAS compared to Carbon A (Figure 5.11).

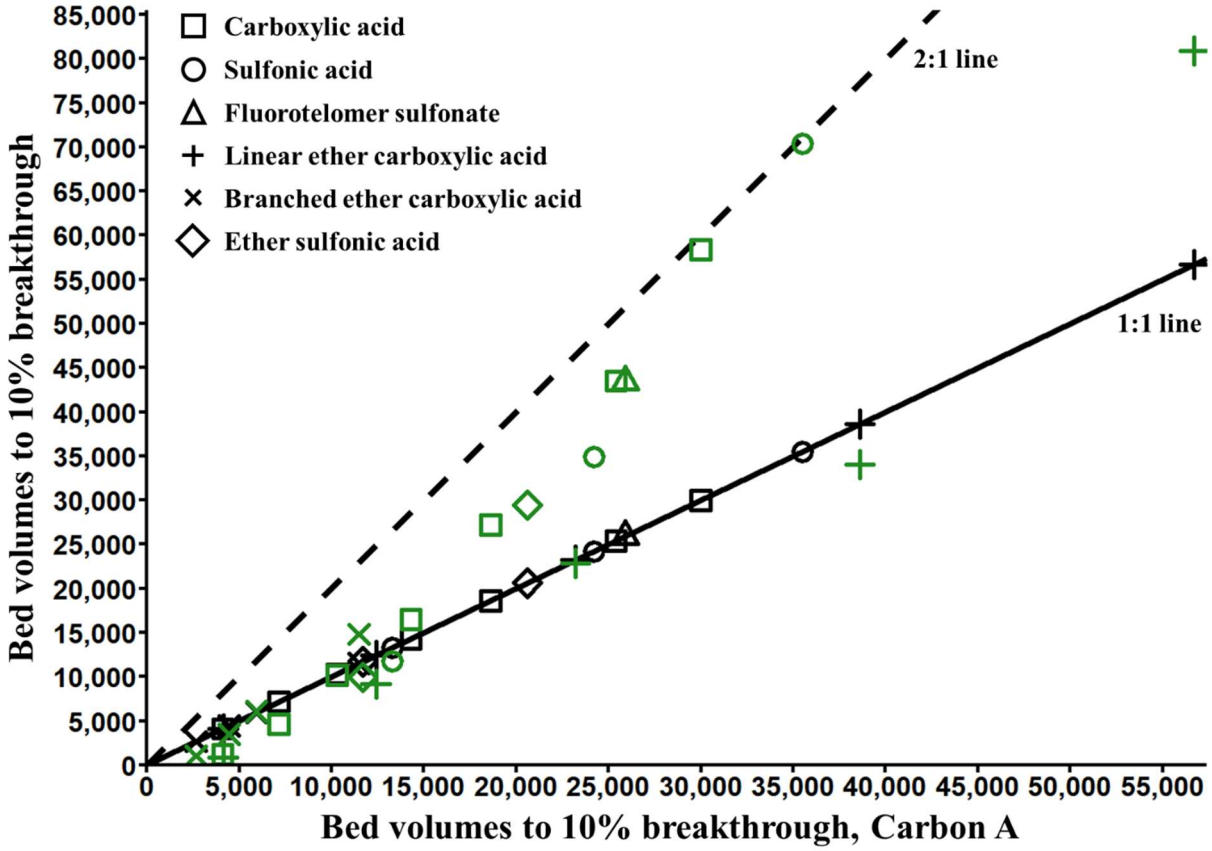

Figure 5.11: Effect of carbon selection on bed volumes to 10% breakthrough. Carbon: Carbon A (Black), Carbon C (Green); EBCT= 10minutes; TOC=1.3 mg L^{-1}.

The improved removal efficiency of longer-chain PFAS for Carbon C to Carbon A suggests that reducing background organic matter results in less pore blockage, allowing for access to the higher-energy adsorption sites in the microporous structure. These results corroborate previous research by McNamara et al. (2018) that pore blockage of mesopores inhibits transport to micropores. Therefore, by reducing concentration of background NOM less pore blockage occurs allowing long-chain PFAS to be transported to adsorption sites in the highly microporous coconut shell-based carbon (Carbon C).

The collection of breakthrough data for these adsorbents is important for assessing GAC use rates and the potential cost associated with a selection of GAC for removal of PFAS present in source water. Though Carbon B provides a greater removal efficiency compared to other carbons tested (Figure 5.6), from a GAC use rate perspective the majority of PFAS would still require high GAC use rate (>0.6 lbs/1000 gals) to treat for PFAS in in source water with a TOC = 2.3 mgL^{-1} (Figure 5.12). If drinking water providers consider a GAC use rate below 0.4 lbs/1000 gals feasible then removal of many long-chain of PFAS tested could be removed from contaminated source water. Additionally, utilities might consider coupling these results for effect of carbon type on GAC use rate with the effect of background organic matter on GAC use rate. The information for PFAS present in source water and source water quality conditions would provide a more well-rounded picture on the feasibility of GAC to treat for PFAS in source water.

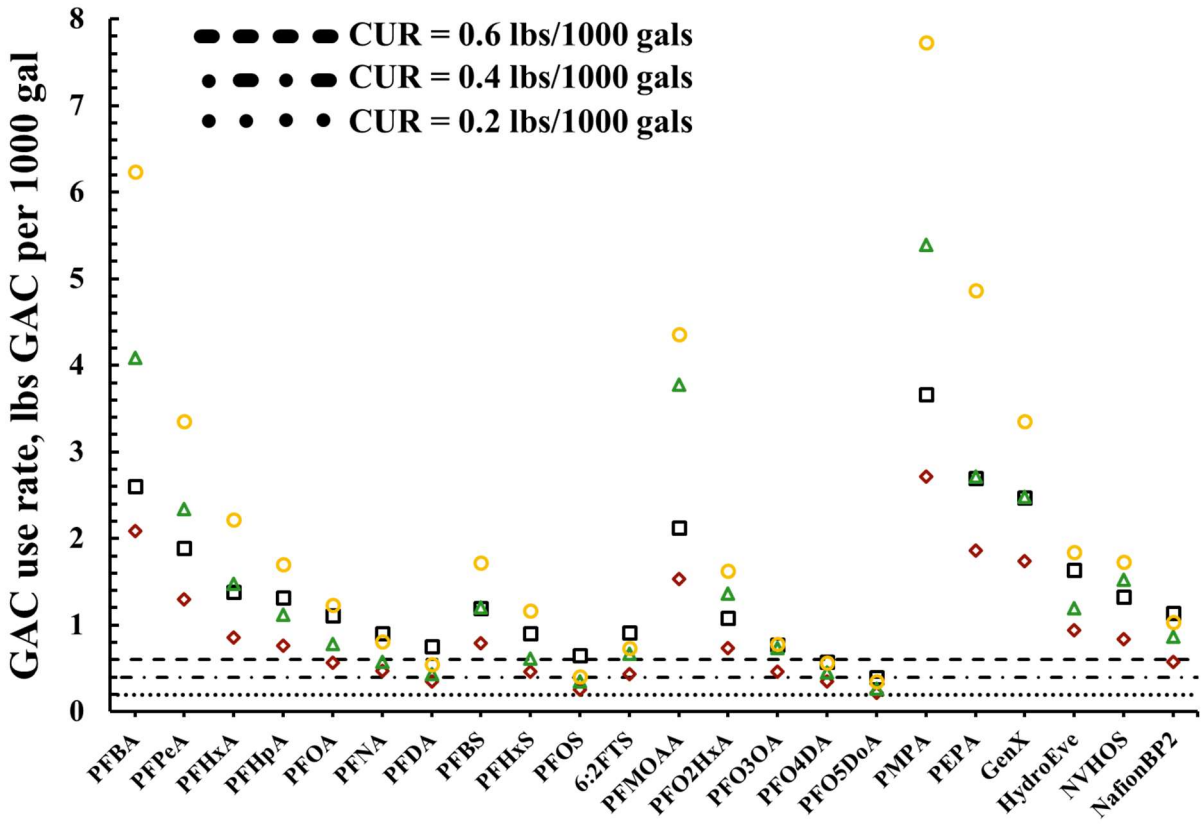

Figure 5.12: Comparison of GAC use rates calculated for individual PFAS removed by four different carbons. Carbon A (black circles), Carbon B (red squares), Carbon C (green diamonds), and Carbon D (yellow triangles). EBCT = 10 minutes, TOC = 2.3 mgL^{-1}.

5.3.3 Effect of empty bed contact time

The EBCT is an important design parameter for full-scale GAC adsorbers and can be increased or decreased by adjusting the bed depth and/or hydraulic loading rate (HLR). This research investigated the effect of EBCT on breakthrough by increasing the bed depth while maintaining a constant HLR. Increasing the bed depth while maintaining a constant HLR is expected to allow for the development of a constant mass transfer zone. Hand et al. (1984) referred to this phenomenon as constant pattern, which assuming the adsorber is designed above a minimum Stanton value should produce a constant pattern mass transfer zone with increasing EBCT and demonstrate no improved removal by increasing EBCT. However, results vary among research suggesting that increasing EBCT can improve and have no effect on GAC performance

(Kempsity 2014; Kennedy et al 2015; Summers et al. 2014, Park et al. 2020, Rodowa et al. 2020; Murray et al. 2021). For example, Kennedy et al. (2015) demonstrated a 52% increase in bed volumes to 10% breakthrough by doubling the EBCT from seven to 15 minutes. While Summers et al. (2014) demonstrated that doubling EBCT exhibited no improvement in GAC performance for removal of volatile organic compounds. Recently, Murray et al. (2021) demonstrated for several PFAS that increasing EBCT enhanced adsorption of PFAS. The previous research suggests that improved GAC performance by increasing EBCT is influenced by the adsorption kinetics associated with individual contaminants. In this work, the effect of increasing EBCT was investigated to determine whether 1) constant pattern was achieved and 2) whether EBCT affected breakthrough of PFAS. Comparisons were prepared for both RSSCTs and field-scale adsorbers at EBCTs of 10 and 20 minutes (0.056 and 0.112 min for RSSCT, respectively) in Figures 5.13 and 5.14.

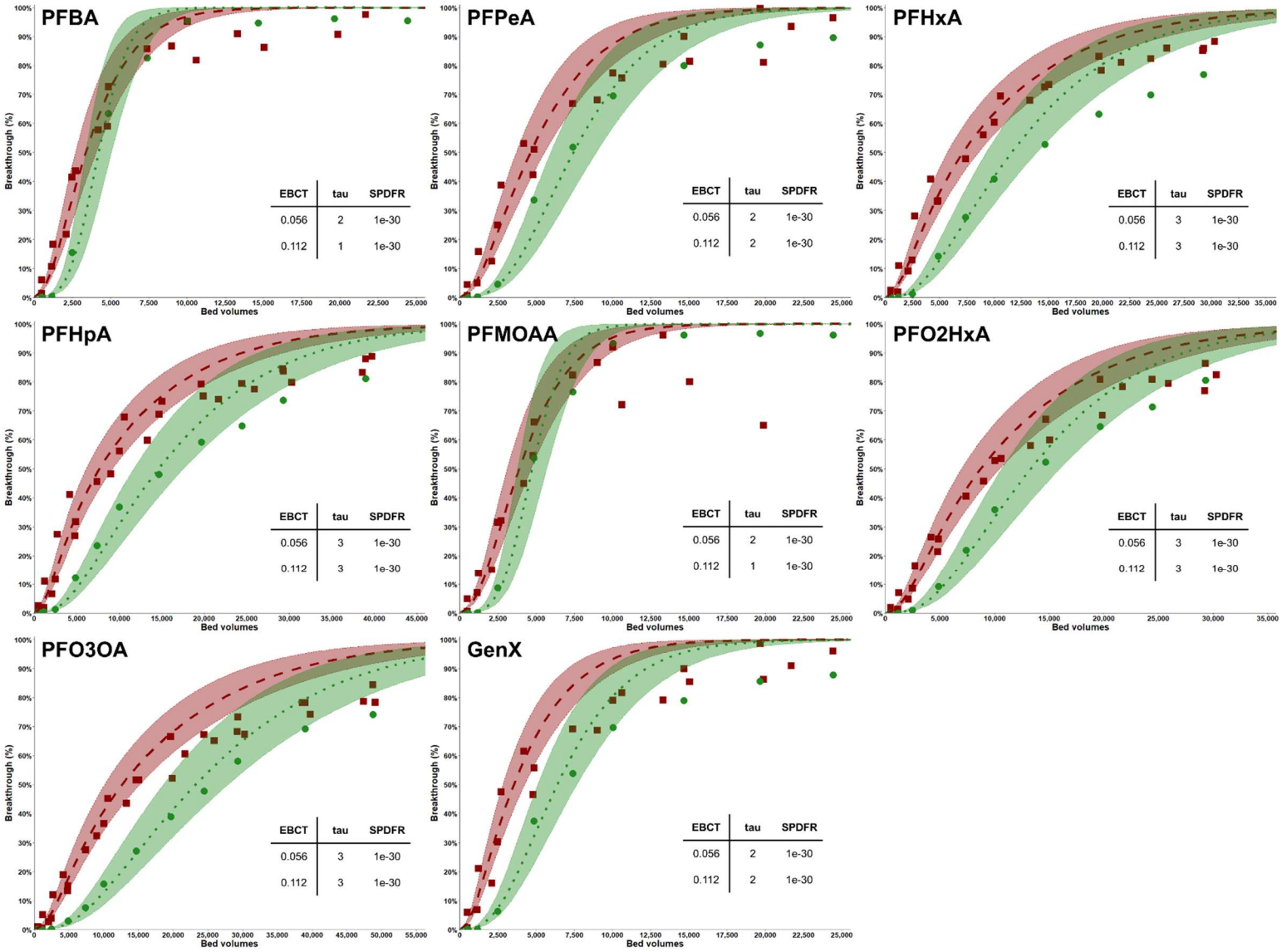

Figure 5.13: Comparison of breakthrough curves for individual PFAS in RSSCT designed for EBCTs of 0.056 (Red squares and dashed line) and 0.112 (Green circles and dotted line) minutes. Shaded region represents +/- 20% variance of PSDM line. Carbon: Carbon A, TOC = 2.3 mgL^{-1}.

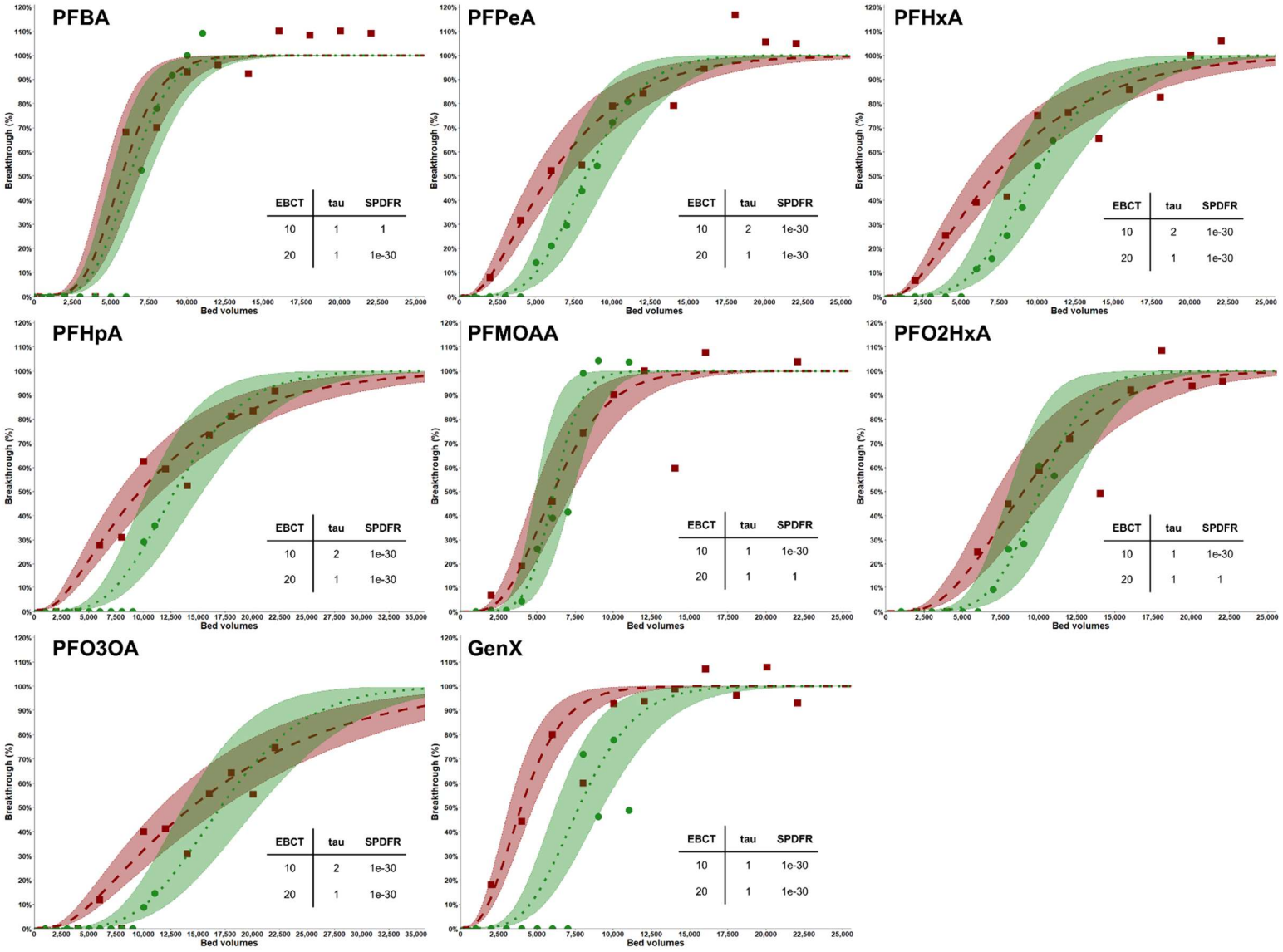

Figure 5.14: Comparison of breakthrough curves for individual PFAS in RSSCT designed for EBCTs of 10 (Red squares and dashed line) and 20 (Green circles and dotted line) minutes. Shaded region represents +/- 20% variance of PSDM line. Carbon: Carbon A, TOC = 2.3 mgL^{-1}.

These results illustrate that self-sharpening and development of a constant pattern mass transfer zone occurs in both RSSCT and field-scale breakthrough curves (Figure 5.13 and 5.14). This is supported by 1) an increase in bed volumes to 10 and 20 % breakthrough (Figures 5.15 and 5.16) and 2) an increase in the Stanton number towards the line denoting constant pattern (Figure 5.17). The self-sharpening phenomena that is illustrated by both bench-scale and field-scale experiments (Figure 5.17) indicates a gradual development of constant pattern mass transfer zone, which was previously suggested to form by Hand et al. (1984). Hand et al. (1984) numerically solved for the case required for constant pattern to exist when assuming a linear isotherm (1/n = 1). Under a linear isotherm condition for a Biot number the dashed line represents a minimum Stanton number required to develop constant pattern (Figure 5.17). Plotting Biot and Stanton values for RSSCT and field-scale PFAS breakthrough curves in Figure 5.17, the results suggest that a constant pattern is developing in the GAC adsorber by increasing the EBCT from 10 to 20 minutes.

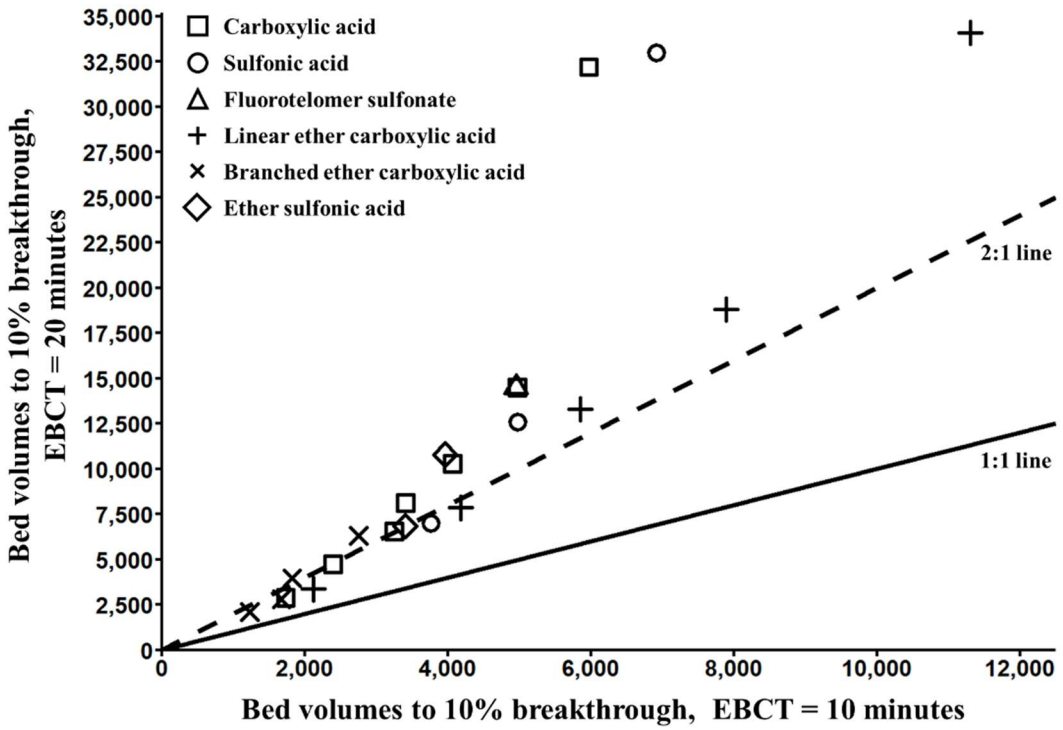

Figure 5.15: Effect of empty bed contact time on bed volumes to 10% breakthrough. Carbon: A; TOC =2.3 mg L^{-1}.

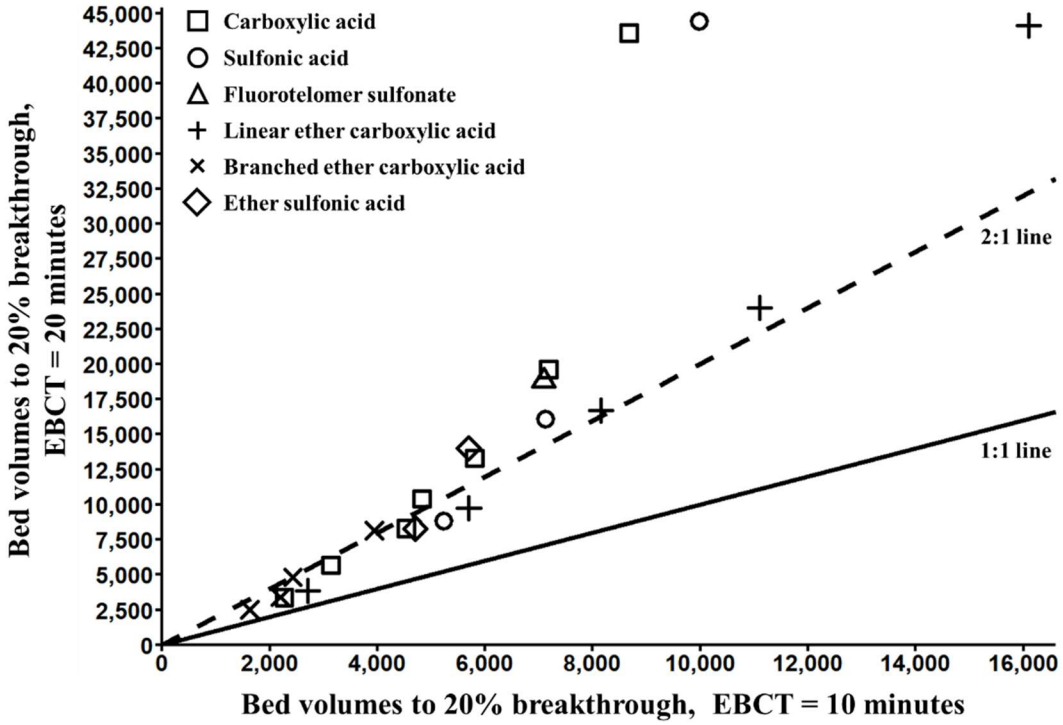

Figure 5.16: Effect of empty bed contact time on bed volumes to 20% breakthrough. Carbon: A; TOC =2.3 mg L^{-1}.

Results in Figure 5.17 illustrate the development of constant pattern mass transfer zone for a variety of PFAS with varying adsorption kinetics. These results suggest that adsorption kinetics influence formation of a constant pattern mass transfer zone. For example, Biot and Stanton values plotted from data by Knappe et al. (2017) suggest that lower molecular weight volatile organic compounds with faster adsorption kinetics develop a constant pattern mass transfer zone when increasing EBCT from 5 to 22 minutes. Comparing these results to data collected for PFAS demonstrates that the slower adsorption kinetic PFAS require longer EBCT in order to develop a constant pattern mass transfer zone. These results suggest that increasing EBCT is beneficial for contaminates with slower adsorption kinetics.

Other studies have demonstrated that increasing EBCT either yielded the same or later bed volumes to breakthrough (Knappe et al. 1997; Corwin and Summers 2012; Kennedy and Summers 2015, Park et al. 2020; Murray et al. 2021). Park et al. 2020 investigated the effect of EBCT on PFAS removal in a groundwater (TOC = 0.78 mg L^{-1}), results for PFBA, PFPeA and PFHxA for EBCT of 5, 10 , and 20 minutes demonstrated that increasing EBCT increased the bed volumes that could be treated to 10% breakthrough. These results are consistent with results obtained in this work suggesting that slower adsorption kinetic PFAS exhibited greater self-sharpening of the breakthrough curve with increasing EBCT. Additionally, Rodowa et al. (2020) demonstrated that increasing EBCT improved the number of bed volumes that could be treated to 10% breakthrough.

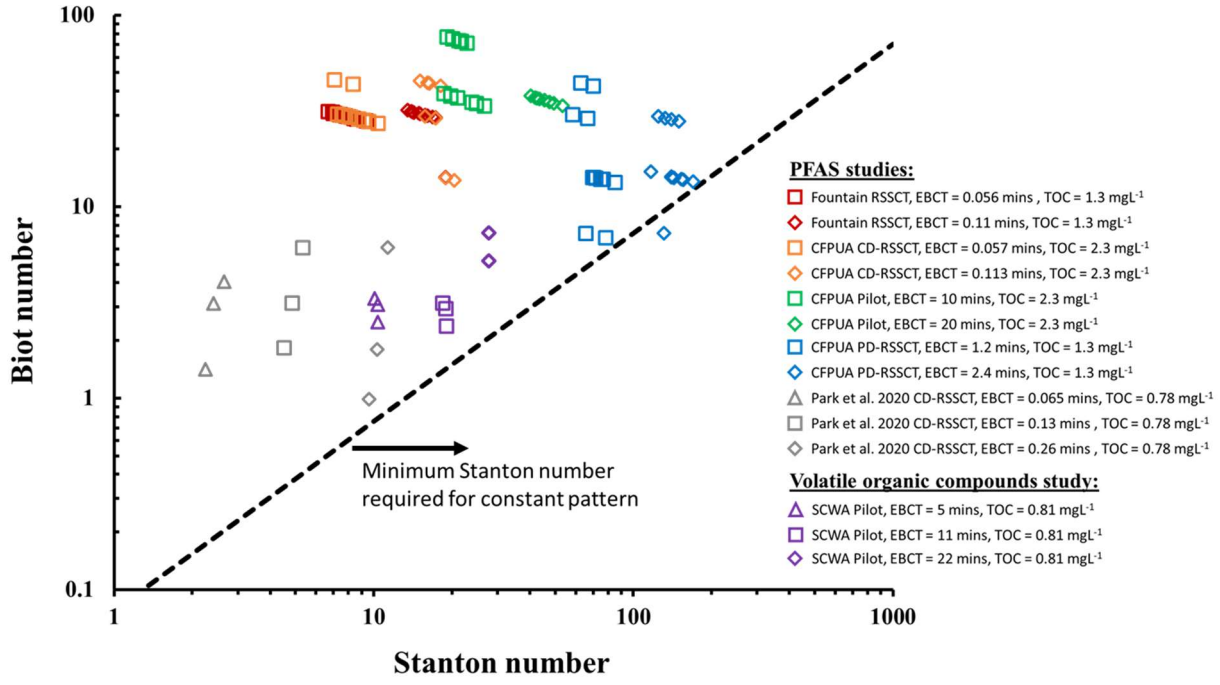

Figure 5.17: Determination of constant pattern mass transfer zone formation in RSSCTs and pilot adsorbers. Source water A and B was tested with Carbon A, EBCT = 10 and 20 minutes, TOC = 2.3 mgL^{-1}; Fountain RSSCTs Carbon: F400; SCWA water was tested for F830S GAC, EBCT = 5 and 11 minutes, TOC = 0.81 mgL^{-1} (Knappe et al. 2017); Part et al. (2020) Carbon: F400, EBCT = 5, 10, 20 minutes, TOC = 0.78 mgL^{-1}.

5.3.4 Effect of background matrix

Background NOM is present in drinking water treatment at varying concentrations and for different characteristics. Research has established that competition from background NOM reduces the adsorption capacity of GAC to effectively adsorb target micropollutants (Corwin and Summers 2012; Summers et al. 2010; Sontheimer et al. 1988; Inyang and Dickenson 2017; Dudley et al. 2015). The presence of background organic matter adversely affects the removal of micropollutants by direct competition for adsorption sites and decreasing the intraparticle diffusion rate via pore blockage. Previous research has demonstrated that removal efficiency of both long- and short-chain PFAS is affected in the presence of background organic matter (Gagliano et al. 2020; McCleaf et al. 2017; Kothawala et al. 2017; Appleman et al. 2013). The removal of alternative PFAS (e.g., PFEA) from waters impacted by increasing background

organic matter is expected to exhibit similar reduction in adsorption capacity. By conducting RSSCTs in three separate source waters of different TOC concentrations (<0.5, 1.3, and 2.3 mg L^{-1}) bed volumes to 10% breakthrough can be compared to assess the effect of background organic matter concentration on PFAS removal efficiency (Figure 5.18).

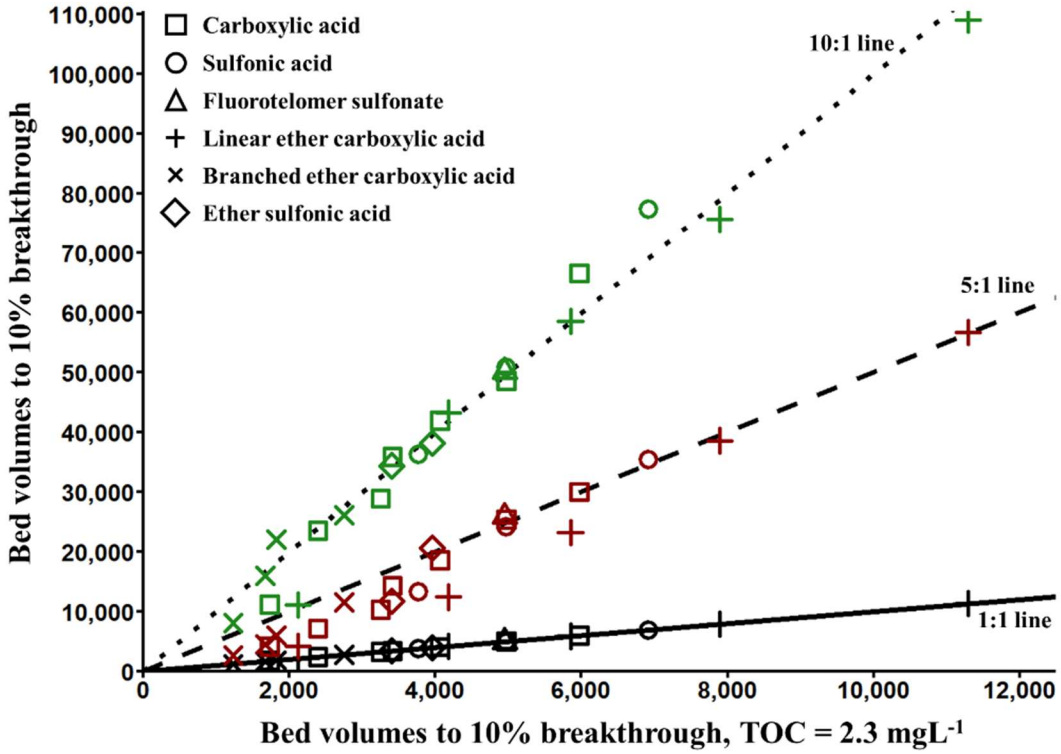

Figure 5.18: Effect of background organic matter concentration on breakthrough to 10%. Carbon: Carbon A, TOCs: <0.5 mgL^{-1} (green), 1.3 mgL^{-1} (red), 2.3 mgL^{-1} (black).

In Figure 5.18, results demonstrate that a reduction in influent TOC concentration from 2.3 mg L^{-1} to <0.5 mg L^{-1} increased GAC service life. For the majority of compounds there is approximately a factor of ~10 increase in bed volumes to 10% breakthrough by reducing influent TOC to <0.5 mgL^{-1}. For a few short-chain PFAS the decrease in influent TOC concentration only enhanced removal by a factor of ~6. A similar increase in GAC service life was exhibited for an enhanced coconut shell-based carbon tested in similar waters as Carbon C (Figure 5.19).

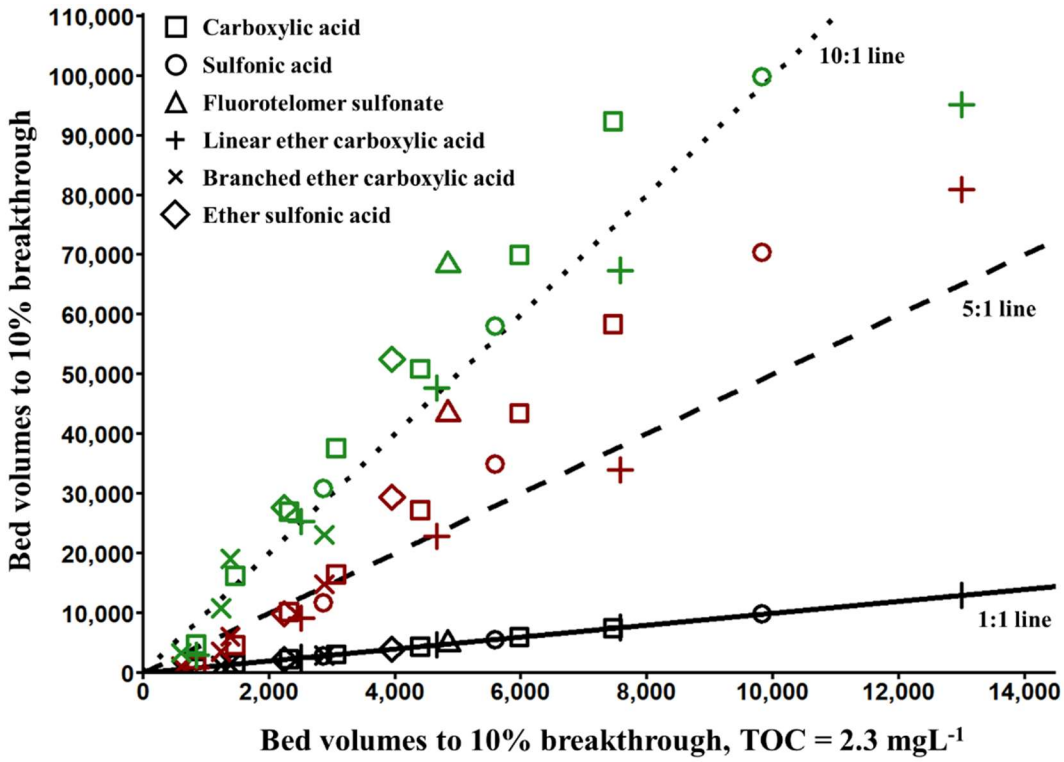

Figure 5.19: Effect of background organic matter concentration on breakthrough to 10%. Carbon: Carbon C, TOCs: <0.5 mgL^{-1} (green), 1.3 mgL^{-1} (red), 2.3 mgL^{-1} (black).

The decrease in GAC service life in high influent TOC concentration is likely due to either 1) pore blockage, 2) direct site competition, or 3) electrostatic interactions (Kennedy and Summers 2015; Reinert 2013; Corwin and Summers 2010; Inyang and Dickenson 2017, McCleaf et al. 2017; Appleman et la. 2014). Inyang and Dickenson (2017) suggested that PFOA adsorption to biochar was reduced due to the NOM blocking or directly competing for the high-energy pore sites. Appleman et al. (2014) demonstrated a similar effect of increasing TOC concentration in influent water on the adsorption of PFAS to GAC. Results in Figures 5.18 and 5.19 suggest that increasing influent TOC concentration results in pore blockage and reduced access to preferred adsorption sites in the micropore width range. Comparison of bed volumes to 10% breakthrough also demonstrates that PFEA compounds are equally affected by background organic matter content when compared to traditional PFAS (e.g., PFCAs and PFSAs).

Additionally, results from Figures 5.18 and 5.19 demonstrate that decreasing influent TOC concentration improved PFAS removal by a similar factor for Carbon A and Carbon C. This could indicate that the reduction of organic matter allowed for more accessibility to the larger fraction of high-energy microporous structure in both Carbon A and Carbon C. These results suggest that control of background NOM concentration is important to improving the GAC service live. Additionally, GAC use rates were calculated for individual PFAS from data collected in the different water sources. These values are plotted in Figure 5.20 against different GAC use rate thresholds.

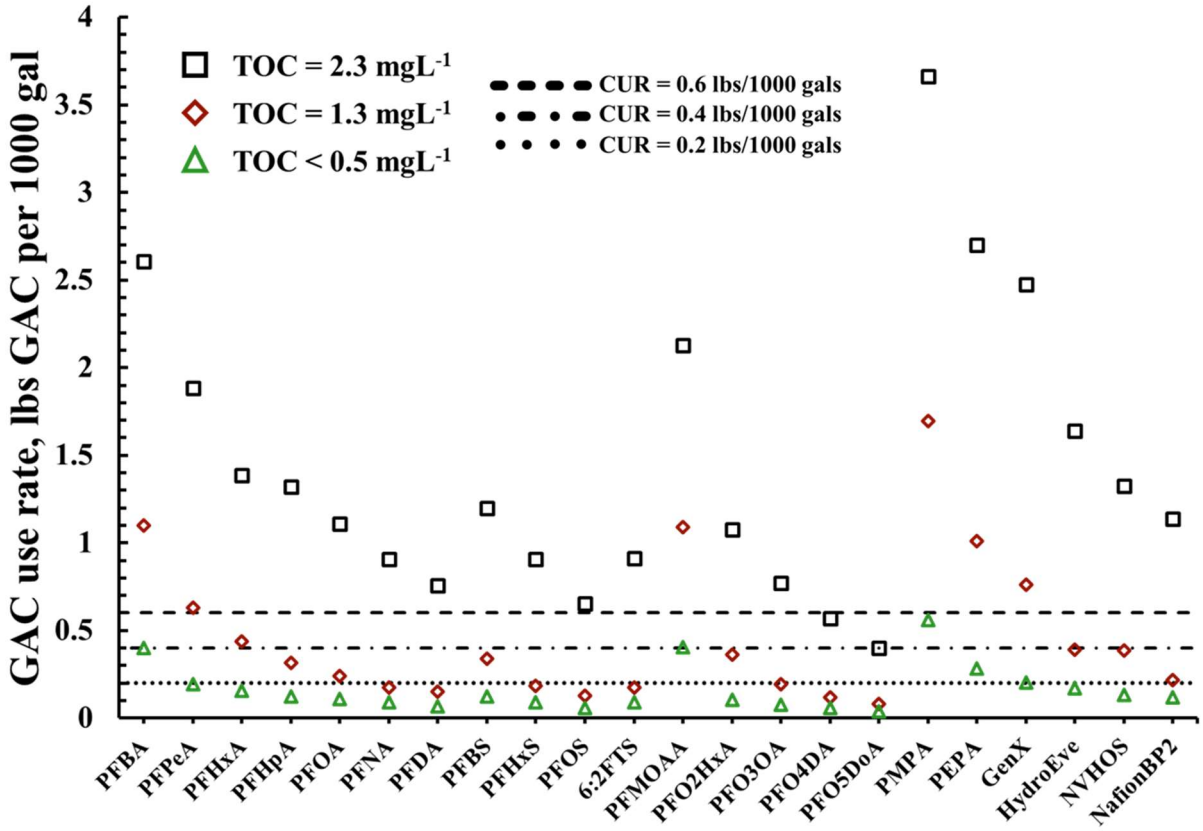

Figure 5.20: Comparison of GAC use rates for individual compounds in three different TOC waters. Carbon: Carbon A; EBCT = 10 minutes.

Results in Figure 5.20 demonstrates from a cost perspective the importance of reducing influent TOC concentration. Knappe and Summers (2012) suggested treatment by GAC would

be feasible if the GAC use rate is less than or equal to 0.2 lbs. GAC per 1000 gallons of water treated. They also suggested that dependent on the utility, GAC could be considered feasible if the utility is willing to consider a CUR less than 0.6 lbs. GAC per 1000 gallons of water treated when treating for weakly adsorbing micropollutants. For a treatment objective of 10% breakthrough, the removal of the majority of PFAS by GAC in the TOC of 2.3 mgL^{-1} water would be unfeasible as GAC use rates would be higher than 0.6 lbs GAC per 1000 gallons of water treated. However, a reduction in background NOM concentration from a TOC of 2.3 mgL^{-1} to a TOC of 1.3 mgL^{-1} would result in 72% of the PFAS requiring a GAC use rate less than 0.6 lbs per 1000 gals of water treated, assuming the utility was trying to maintain a treatment objective of 10% breakthrough. While in the groundwater with a TOC less than 0.5 mgL^{-1}, 81% of PFAS can be treated to 10% breakthrough with a GAC use rate CUR less or equal to 0.2 lbs GAC per 1000 gallons of water treated. Additionally, a utility could consider higher treatment objective (e.g., removal to 20% breakthrough) to reduce the GAC use rate while meeting desired removal for targeted PFAS.

5.4 Conclusions

RSSCTs were conducted to assess a variety of factors that could potentially influence removal efficiency. These experiments aimed to determine for a wide range of PFAS the influence of 1) PFAS physicochemical characteristics, 2) GAC type, 3) influent background NOM concentration, and 4) empty bed contact time. Breakthrough curves for a wide range of PFAS corroborated previous research that increasing chain length increased adsorption potential of PFCA and PFSA, but also novel PFEAs. Results from RSSCTs also demonstrated that incorporation of ether oxygen linkages had little effect on PFAS breakthrough curves. This work

also aimed to understand the effect of different GAC types on removal of a wide range of PFAS. PFAS removal for GAC generally followed the ranking of Carbon B > Carbon A > Carbon C > Carbon D. Results suggest that GAC with high pore volume in the secondary micropore range controls PFAS adsorption. Additionally, correlations for PFAS molecular diameter vs GAC mean pore width and PFAS CCS vs GAC mean pore width suggest that estimations made from these correlations could predict preferred mean pore width for adsorption of other PFAS. For RSSCTs conducted in different TOC source waters, the results demonstrated that a reduction in TOC concentration from 2.3 mgL^{-1} to <0.5 mgL^{-1} increased removal to 10% breakthrough by approximately a factor of 10 for the majority of PFAS. This work also investigated the influence of EBCT on removal efficiency and determined that increasing EBCT from 10 to 20 minutes increased bed volumes to 10% breakthrough. Additionally, this work illustrated that PFAS with slower adsorption kinetics could benefit from increasing EBCT as a constant pattern mass transfer zone forms. Ultimately, the investigation of these factors influencing PFAS removal by GAC provide key information which can be leveraged by water utility to achieve treatment objectives for PFAS present in source water.

CHAPTER 6 CONCLUSIONS AND FUTURE RESEARCH

6.1 Hypothesis conclusions

Based on the hypotheses developed for this research, the following conclusions were reached.

Hypothesis 1: Based on previous research conducted with neutral organic contaminants, the PD-RSSCT design will effectively predict PFAS adsorption kinetics in field-scale GAC contactors, but adsorption capacity will be overpredicted by PD-RSSCTs.

Results in Chapter 4 demonstrated that neither the PD-RSSCT nor the CD-RSSCT design yielded data that could directly predict field-scale PFAS breakthrough curves. From an adsorption capacity perspective, the PD-RSSCT overpredicted field-scale PFAS adsorption capacity by a factor of about 2-3, while the CD-RSSCT yielded PFAS adsorption capacities that closely matched field-scale adsorption capacities for the evaluated PFASs, GACs, and background water matrices. From an adsorption kinetics perspective, neither the CD-RSSCT nor the PD-RSSCT yielded PFAS breakthrough curves that matched the shape of field-scale PFAS breakthrough curves. As a result, a scale-up approach involving the pore surface diffusion model (PSDM) was developed to scale adsorption kinetics. Overall, a proportionality factor of X=0.25 most effectively described the dependence of intraparticle PFAS flux on GAC particle size. It is therefore recommended to conduct either (1) CD-RSSCTs and adjust the resulting PFAS breakthrough curve with the PSDM to account for the GAC particle size-dependence of PFAS adsorption kinetics or (2) RSSCTs designed with a proportionality factor of X=0.25, in which case PFAS breakthrough curves can directly predict field-scale breakthrough.

Hypothesis 2: PFAS adsorbability increases with increasing chain length, while incorporation of ether oxygen groups and branching of PFAS will translate into decreased adsorbability.

Results in Chapter 5 illustrated that several physicochemical characteristics of PFAS influence adsorbability. For PFAS within a given subclass, adsorbability increased with increasing chain length. This trend is well known for widely studied PFCAs and PFSAs, and results here showed that the adsorbability of monoether PFEAs and multiether PFEAs also increased with increasing chain length. Incorporation of an ether oxygen linkage was expected to decrease the adsorbability of PFAS. However, results comparing PFAS of equivalent chain length with and without ether oxygen linkages (e.g. PFHxA and PFO2HxA) demonstrated that the incorporation of one or more ether oxygen linkages resulted in similar adsorbability. This result was demonstrated for RSSCTs conducted with 1) different EBCTs, 2) different GACs, and 3) different background water matrices. Structurally PFAS can be branched or linear. Recognizing that linear PFCAs and PFECAs of equivalent chain length exhibited similar adsorbability, differences in adsorbability between linear PFCAs and branched PFECAs of equivalent chain length should be a result of the branching. Results comparing linear PFCAs and branched PFECAs of equivalent chain length (e.g., GenX and PFHpA) demonstrated that branching decreased adsorbability.

Hypothesis 3: Based on results of prior research for the adsorption of natural organic matter (NOM) and the similarity of size and charge between PFAS and NOM, GAC with substantial pore volume in the secondary micropores (8 Å< dp < 20 Å) and small mesopores will be most effective for PFAS removal.

Results from Chapter 5 demonstrated that GAC pore structure influences GAC use rates for PFAS removal. RSSCTs conducted using two sub-bituminous coal-based carbons (Carbon A and Carbon B), one enhanced coconut shell-based carbon (Carbon C), and one lignite carbon (Carbon D) showed removal efficiency of PFAS generally followed the trend Carbon B > Carbon A > Carbon C > Carbon D. Through a trial-and-error process, correlations were developed between GAC pore volume and bed volumes of water that could be treated to reach 10% breakthrough of each PFAS. The correlations developed between PFAS adsorbability and pore volume of GACs A, B, and D suggested adsorption is controlled by the pore volume in the secondary micropore range (8-20 Å). Breakthrough of PFAS for Carbon C did not follow the pore volume trend exhibited by the other three GACs. This could be due to smaller pore volume in the mesopore range (20-500 Å), which can exacerbate pore blockage resulting from DOM adsorption. A second correlation was developed between mean pore diameter, in which PFAS preferentially adsorb, and PFAS molecular diameter. This correlation suggested that PFAS adsorption takes place preferentially in pores with a mean pore width that is about twice the molecular diameter of a PFAS (r2=0.732). Therefore, it is recommended that selection criteria for GAC consider 1) pore volume in the pore width range ~2 times the molecular diameter of the target PFAS, and 2) pore volume in the mesopore range to limit pore blockage.

Hypothesis 4: Higher concentrations of DOM will increase carbon use rates for PFAS removal because of increased direct adsorption competition, pore blockage, and electrostatic repulsion.

Results from Chapter 5 showed that increasingly larger bed volumes of water could be treated prior to onset of PFAS breakthrough as influent DOC concentrations decreased from 2.3 mg L-1 to <0.5 mg L-1. A decrease in DOC concentration from 2.3 mgL-1 to <0.5 mgL-1 resulted in a factor of ~10 decrease in GAC use rates for the majority of PFAS. For short-chain PFAS (e.g., PFBA, PFMOAA, and PMPA) GAC use rate only decreased by a factor of ~6 for a similar decrease in influent DOM concentration. For a GAC use rate of 0.4 lb of GAC/1000 gallons of water treated, corresponding to ~11,000 bed volumes of water treated, only PFO5DoDA, the longest-chain PFAS that was evaluated, could be removed to >90% when the DOC was 2.3 mg L-1. In contrast, 21 out of the 22 targeted PFAS could be removed by >90% at the same GAC use rate when the DOC concentration was <0.5 mg L-1. It is therefore recommended to reduce influent DOC concentrations prior to GAC treatment to reduce GAC use rates for PFAS removal.

Hypothesis 5: Increasing empty bed contact time (EBCT) from 10 to 20 minutes will decrease GAC use rates for a treatment goal of >90% PFAS removal because the longer EBCT promotes the development of a shorter mass transfer zone within the adsorber bed.

Results presented in Chapter 5 illustrate that increasing the EBCT from 10 to 20 minutes for the evaluated pilot and RSSCT conditions decreased GAC use rates by a factor of ~2 for the majority of PFAS and a 90% removal criterion. The decrease in GAC use rate was smaller for a 50% removal criterion, highlighting that the increase in EBCT led to a shorter mass transfer zone

for individual PFAS in the GAC bed. Additionally, a comparison of values of the Biot and Stanton numbers from a wide range of available RSSCT and pilot studies suggested that increasing EBCT was especially beneficial for adsorbates with slower adsorption kinetics (e.g. PFAS) that require longer EBCTs to establish constant pattern breakthrough curves.

6.2 Future research

- Validate the developed scale-up approach with a wider range of GACs and background water matrices (e.g., organic matter types).
- Further investigate the constant pattern phenomenon to determine under what water quality conditions or adsorber designs an increase in EBCT is effective in reducing GAC use rates.
- Develop a correlation for estimating adsorption kinetics of novel PFAS by linking adsorption kinetic parameters to physicochemical characteristics of PFAS (e.g., collision cross section, logD, chain length).
- Determine factor(s) resulting in discrepancy in PFAS adsorption capacities when using similar GAC particle size in PD- and CD-RSSCTs.

REFERENCES

Wang, Zhanyun, et al. "A Never-Ending Story of Per-and Polyfluoroalkyl Substances (PFASs)?." Environmental Science & Technology 52.5 (2018): 3325-3325.

Hopkins, Zachary R., et al. "Recently detected drinking water contaminants: GenX and other per-and polyfluoroalkyl ether acids." Journal-American Water Works Association 110.7 (2018): 13-28.

Hu, Xindi C., et al. "Detection of poly-and perfluoroalkyl substances (PFASs) in US drinking water linked to industrial sites, military fire training areas, and wastewater treatment plants." Environmental science & technology letters 3.10 (2016): 344-350.

Gebbink, Wouter A., Laura Van Asseldonk, and Stefan PJ Van Leeuwen. "Presence of emerging per-and polyfluoroalkyl substances (PFASs) in river and drinking water near a fluorochemical production plant in the Netherlands." Environmental science & technology 51.19 (2017): 11057-11065.

Banzhaf, Stefan, et al. "A review of contamination of surface-, ground-, and drinking water in Sweden by perfluoroalkyl and polyfluoroalkyl substances (PFASs)." Ambio 46.3 (2017): 335-346.

Crone, Brian C., et al. "Occurrence of per-and polyfluoroalkyl substances (PFAS) in source water and their treatment in drinking water." Critical reviews in environmental science and technology 49.24 (2019): 2359-2396.

Andrews, David Q., and Olga V. Naidenko. "Population-Wide Exposure to Per-and Polyfluoroalkyl Substances from Drinking Water in the United States." Environmental Science & Technology Letters 7.12 (2020): 931-936.

Kaboré, Hermann A., et al. "Worldwide drinking water occurrence and levels of newly-identified perfluoroalkyl and polyfluoroalkyl substances." Science of The Total Environment 616 (2018): 1089-1100.

Boone, J. Scott, et al. "Per-and polyfluoroalkyl substances in source and treated drinking waters of the United States." Science of the Total Environment 653 (2019): 359-369.

Kolpin, Dana W., et al. "A Comprehensive Statewide Spatiotemporal Stream Assessment of Per- and Polyfluoroalkyl Substances (PFAS) in an Agricultural Region of the United States." Environmental Science & Technology Letters (2021).

US EPA. (2021).“Fifth Unregulated Contaminant Monitoring Rule.” US EPA, 3 Nov. 2021, www.epa.gov/dwucmr/fifth-unregulated-contaminant-monitoring-rule.

ITRC. (2020). “8 Basis of Regulations – PFAS — Per- and Polyfluoroalkyl Substances.” ITRC, Sept. 2020, pfas-1.itrcweb.org/8-basis-of-regulations.

ECHA, 2020. “Perfluoroalkyl Chemicals (PFAS) - ECHA.” echa.europa.eu/hot-topics/perfluoroalkyl-chemicals-pfas.

Wang, Zhanyun, et al. "A New OECD Definition for Per-and Polyfluoroalkyl Substances." Environmental science & technology (2021).

Crittenden, John C., John K. Berrigan, and David W. Hand. "Design of rapid small-scale adsorption tests for a constant diffusivity." Journal (Water Pollution Control Federation) (1986): 312-319.

Crittenden, John C., et al. "Design of rapid fixed-bed adsorption tests for nonconstant diffusivities." Journal of Environmental Engineering 113.2 (1987): 243-259.

Glassmeyer, Susan T., et al. "Nationwide reconnaissance of contaminants of emerging concern in source and treated drinking waters of the United States." Science of the Total Environment 581 (2017): 909-922.

US EPA. (2019). “EPA Releases PFAS Groundwater Guidance for Federal Cleanup Programs, Fulfilling PFAS Action Plan Commitment.” US EPA, 20 Dec. 2019, www.epa.gov/newsreleases/epa-releases-pfas-groundwater-guidance-federal-cleanup-programs-fulfilling-pfas-action.

US EPA. (2021). “PFAS Strategic Roadmap: EPA’s Commitments to Action 2021–2024.” US EPA, 3 Nov. 2021, www.epa.gov/pfas/pfas-strategic-roadmap-epas-commitments-action-2021-2024.

Xiao, Feng. "Emerging poly-and perfluoroalkyl substances in the aquatic environment: A review of current literature." Water research 124 (2017): 482-495.

Braun, Joseph M., et al. "Prenatal perfluoroalkyl substance exposure and child adiposity at 8 years of age: The HOME study." Obesity 24.1 (2016): 231-237.

Barry, Vaughn, Andrea Winquist, and Kyle Steenland. "Perfluorooctanoic acid (PFOA) exposures and incident cancers among adults living near a chemical plant." Environmental health perspectives 121.11-12 (2013): 1313-1318.

Cousins, Ian T., et al. "The concept of essential use for determining when uses of PFASs can be phased out." Environmental Science: Processes & Impacts 21.11 (2019): 1803-1815.

Yao, Jingzhi, et al. "Novel perfluoroalkyl ether carboxylic acids (PFECAs) and sulfonic acids (PFESAs): occurrence and association with serum biochemical parameters in residents living near a fluorochemical plant in China." Environmental Science & Technology 54.21 (2020): 13389-13398.

Yao, Jingzhi, et al. "Occurrence of Novel Perfluoroalkyl Ether Carboxylic Acids in River Water and Human Urine Quantified by a Simple Liquid–Liquid Microextraction Approach Coupled with LC–MS/MS." Environmental Science & Technology Letters 8.9 (2021): 773-778.

Conley, Justin M., et al. "Adverse maternal, fetal, and postnatal effects of hexafluoropropylene oxide dimer acid (GenX) from oral gestational exposure in Sprague-Dawley rats." Environmental health perspectives 127.3 (2019): 037008.

Conley, Justin M., et al. "Hexafluoropropylene oxide-dimer acid (HFPO-DA or GenX) alters maternal and fetal glucose and lipid metabolism and produces neonatal mortality, low birthweight, and hepatomegaly in the Sprague-Dawley rat." Environment International 146 (2021): 106204.

Lohmann, Rainer, et al. "Are fluoropolymers really of low concern for human and environmental health and separate from other PFAS?." Environmental Science & Technology 54.20 (2020): 12820-12828.

Woodlief, Tracey, et al. "Immunotoxicity of Per-and Polyfluoroalkyl Substances: Insights into Short-Chain PFAS Exposure." Toxics 9.5 (2021): 100.

Chen, Jiamiao, et al. "Chronic exposure to PFO4DA and PFO5DoDA, two perfluoroalkyl ether carboxylic acids (PFECAs), suppresses hepatic stress signals and disturbs glucose and lipid metabolism in male mice." Journal of Hazardous Materials 411 (2021): 124963.

De Silva, Amila O., et al. "PFAS exposure pathways for humans and wildlife: a synthesis of current knowledge and key gaps in understanding." Environmental Toxicology and Chemistry 40.3 (2021): 631-657.

Fenton, Suzanne E., et al. "Per-and polyfluoroalkyl substance toxicity and human health review: Current state of knowledge and strategies for informing future research." Environmental toxicology and chemistry 40.3 (2021): 606-630.

Järnberg, Ulf, et al. " Perfluoroalkylated acids and related compounds (PFAS) in the Swedish environment—Chemistry, sources, exposures." Stockholm University and Orebro University. (2007).

Ritscher, Amélie, et al. "Zürich statement on future actions on per-and polyfluoroalkyl substances (PFASs)." Environmental health perspectives 126.8 (2018): 084502.

OECD. (2018). "Toward a new comprehensive global database of per-and polyfluoroalkyl substances (PFASs): Summary report on updating the OECD 2007 list of per-and polyfluoroalkyl substances (PFASs)."

OECD. (2013). “Synthesis Paper on Per-and Polyfluorinated Chemicals (PFCS).” OECD, 2013, www.oecd.org/env/ehs/risk-management/PFC_FINAL-Web.pdf.

Kwiatkowski, Carol F., et al. "Scientific basis for managing PFAS as a chemical class." Environmental Science & Technology Letters 7.8 (2020): 532-543.

Bell, Caitlin H., et al., eds. Emerging contaminants handbook. CRC Press, 2019.

Buck, Robert C., et al. "Perfluoroalkyl and polyfluoroalkyl substances in the environment: terminology, classification, and origins." Integrated environmental assessment and management 7.4 (2011): 513-541.

Herzke, Dorte, Elisabeth Olsson, and Stefan Posner. "Perfluoroalkyl and polyfluoroalkyl substances (PFASs) in consumer products in Norway–A pilot study." Chemosphere 88.8 (2012): 980-987.

Muir, Derek, and Luc T. Miaz. "Spatial and temporal trends of perfluoroalkyl substances in global ocean and coastal waters." Environmental Science & Technology (2021).

C8 Science Panel. "The Science Panel Website." (2017).

Fei, Chunyuan, et al. "Perfluorinated chemicals and fetal growth: a study within the Danish National Birth Cohort." Environmental health perspectives 115.11 (2007): 1677-1682.

Melzer, David, et al. "Association between serum perfluorooctanoic acid (PFOA) and thyroid disease in the US National Health and Nutrition Examination Survey." Environmental health perspectives 118.5 (2010): 686-692.

Steenland, Kyle, et al. "Predictors of PFOA levels in a community surrounding a chemical plant." Environmental health perspectives 117.7 (2009): 1083-1088.

U.S. EPA. (2010/15) "PFOA Stewardship Program Guidance on Reporting Emissions and product Content." https://www.epa.gov/sites/production/files/2015-10/documents/pfoaguidance.pdf (accessed Jan. 2019)

Sheng, Nan, et al. "Cytotoxicity of novel fluorinated alternatives to long-chain perfluoroalkyl substances to human liver cell line and their binding capacity to human liver fatty acid binding protein." Archives of toxicology 92.1 (2018): 359-369.

Strynar, Mark, et al. "Identification of novel perfluoroalkyl ether carboxylic acids (PFECAs) and sulfonic acids (PFESAs) in natural waters using accurate mass time-of-flight mass spectrometry (TOFMS)." Environmental science & technology 49.19 (2015): 11622-11630.

McCord, James P., et al. "Emerging Chlorinated Polyfluorinated Polyether Compounds Impacting the Waters of Southwestern New Jersey Identified by Use of Nontargeted Analysis." Environmental Science & Technology Letters 7.12 (2020): 903-908.

US EPA, (2017) “Risk Management for Per- and Polyfluoroalkyl Substances (PFAS) under TSCA.”, www.epa.gov/assessing-and-managing-chemicals-under-tsca/risk-management-and-polyfluoroalkyl-substances-pfas.

Sun, Mei, et al. "Legacy and emerging perfluoroalkyl substances are important drinking water contaminants in the Cape Fear River Watershed of North Carolina." Environmental science & technology letters 3.12 (2016): 415-419.

Guelfo, Jennifer L., et al. "Evaluation and management strategies for per-and polyfluoroalkyl substances (PFASs) in drinking water aquifers: perspectives from impacted US Northeast communities." Environmental health perspectives 126.6 (2018): 065001.

Brendel, Stephan, et al. "Short-chain perfluoroalkyl acids: environmental concerns and a regulatory strategy under REACH." Environmental Sciences Europe 30.1 (2018): 1-11.

Davis, Katherine L., et al. "Transport of ammonium perfluorooctanoate in environmental media near a fluoropolymer manufacturing facility." Chemosphere 67.10 (2007): 2011-2019.

Lindstrom, Andrew B., Mark J. Strynar, and E. Laurence Libelo. "Polyfluorinated compounds: past, present, and future." Environmental science & technology 45.19 (2011): 7954-7961.

McCord, James, and Mark Strynar. "Identification of per-and polyfluoroalkyl substances in the cape fear river by high resolution mass spectrometry and nontargeted screening." Environmental science & technology 53.9 (2019): 4717-4727.

Gebbink, Wouter A., Laura Van Asseldonk, and Stefan PJ Van Leeuwen. "Presence of emerging per-and polyfluoroalkyl substances (PFASs) in river and drinking water near a fluorochemical production plant in the Netherlands." Environmental science & technology 51.19 (2017): 11057-11065.

Anderson, R. Hunter, et al. "Occurrence of select perfluoroalkyl substances at US Air Force aqueous film-forming foam release sites other than fire-training areas: Field-validation of critical fate and transport properties." Chemosphere 150 (2016): 678-685.

Murakami, Michio, et al. "Occurrence and sources of perfluorinated surfactants in rivers in Japan." Environmental science & technology 42.17 (2008): 6566-6572.

Wang, Zhanyun, et al. "Global emission inventories for C4–C14 perfluoroalkyl carboxylic acid (PFCA) homologues from 1951 to 2030, Part I: production and emissions from quantifiable sources." Environment international 70 (2014): 62-75.

Appleman, Timothy D., et al. "Nanofiltration and granular activated carbon treatment of perfluoroalkyl acids." Journal of hazardous materials 260 (2013): 740-746.

Quiñones, Oscar, and Shane A. Snyder. "Occurrence of perfluoroalkyl carboxylates and sulfonates in drinking water utilities and related waters from the United States." Environmental science & technology 43.24 (2009): 9089-9095.

Exner, Martin, and Harald Färber. "Perfluorinated surfactants in surface and drinking waters (9 pp)." Environmental Science and Pollution Research 13.5 (2006): 299-307.

Takagi, Sokichi, et al. "Fate of perfluorooctanesulfonate and perfluorooctanoate in drinking water treatment processes." Water research 45.13 (2011): 3925-3932.

Thompson, Jack, Geoff Eaglesham, and Jochen Mueller. "Concentrations of PFOS, PFOA and other perfluorinated alkyl acids in Australian drinking water." Chemosphere 83.10 (2011): 1320-1325.

Heydebreck, Franziska, et al. "Alternative and legacy perfluoroalkyl substances: differences between European and Chinese river/estuary systems." Environmental science & technology 49.14 (2015): 8386-8395.

Pan, Yitao, et al. "Worldwide distribution of novel perfluoroether carboxylic and sulfonic acids in surface water." Environmental science & technology 52.14 (2018): 7621-7629.

Nakayama, Shoji, et al. "Perfluorinated compounds in the Cape Fear drainage basin in North Carolina." Environmental science & technology 41.15 (2007): 5271-5276.

Shiwaku, Yoko, et al. "Spatial and temporal trends in perfluorooctanoic and perfluorohexanoic acid in well, surface, and tap water around a fluoropolymer plant in Osaka, Japan." Chemosphere 164 (2016): 603-610.

New Jersey Department of Environmental Protection (NJDEP). 2014. Occurence of Perfluorinated Chemicals in Untreated New Jersey Drinking Water Sources, Final Report. April.https://www.nj.gov/dep/watersupply/pdf/pfc-study.pdf

Betts, K. S. "Perfluoroalkyl acids: What is the evidence telling us?." Environmental health perspectives 115.7 (2007): A344-A344.

Kotlarz, Nadine, et al. "Measurement of novel, drinking water-associated PFAS in blood from adults and children in Wilmington, North Carolina." Environmental health perspectives 128.7 (2020): 077005.

International Agency for Research on Cancer. (2016) IARC Monograph: PFOA “Possibly Carcinogenic to Humans”. https://monographs.iarc.fr/wp-content/uploads/2018/06/mono110-01.pdf (accessed May 2019)

U.S. N. T. P. (2016). "Immunotoxicity associated with exposure to Perfluorooctanoic Acid or Perfluorooctane Sulfonate." Research Triangle Park, NC: Office of Health Assessment and Translation, National Toxicology Program (NTP), National Institute of Environmental Health Sciences, National Institutes of Health, US Department of Health and Human Services.

Grandjean, Philippe, et al. "Serum vaccine antibody concentrations in children exposed to perfluorinated compounds." Jama 307.4 (2012): 391-397.

Saikat, Sohel, et al. "The impact of PFOS on health in the general population: a review." Environmental Science: Processes & Impacts 15.2 (2013): 329-335.

Mastrantonio, Marina, et al. "Drinking water contamination from perfluoroalkyl substances (PFAS): an ecological mortality study in the Veneto Region, Italy." The European Journal of Public Health 28.1 (2018): 180-185.

He, Xiaowei, et al. "PFOA is associated with diabetes and metabolic alteration in US men: National Health and Nutrition Examination Survey 2003–2012." Science of the total environment 625 (2018): 566-574.

Renner, Rebecca. (2006). "The long and the short of perfluorinated replacements." Environmental science & technology 40: 12-13.

Glynn, Anders, et al. "Perfluorinated alkyl acids in blood serum from primiparous women in Sweden: serial sampling during pregnancy and nursing, and temporal trends 1996–2010." Environmental science & technology 46.16 (2012): 9071-9079.

Wang, Zhanyun, et al. "Hazard assessment of fluorinated alternatives to long-chain perfluoroalkyl acids (PFAAs) and their precursors: status quo, ongoing challenges and possible solutions." Environment international 75 (2015): 172-179.

Hoppin, J., et al. (2018). "The GenX Exposure Study: Center for Human Health and the Environment." https://chhe.research.ncsu.edu/the-genx-exposurestudy/.

Hoppin, J., et al. "An overview of emerging PFAS in drinking water worldwide." Environmental Epidemiology 3 (2019): 162-163.

Shi, Yali, et al. "Tissue distribution and whole body burden of the chlorinated polyfluoroalkyl ether sulfonic acid F-53B in crucian carp (Carassius carassius): Evidence for a highly bioaccumulative contaminant of emerging concern." Environmental science & technology 49.24 (2015): 14156-14165.

Guo, Hua, et al. "Comparative hepatotoxicity of novel PFOA alternatives (perfluoropolyether carboxylic acids) on male mice." Environmental science & technology 53.7 (2019): 3929-3937.

Richards, Alicia Carolyn. GenX Inhibits P-glycoprotein and Breast Cancer Resistance Protein Transport Activity and Expression at the Blood-brain Barrier in Sprague-Dawley Rats. Diss. The University of North Carolina at Chapel Hill, 2018.

Blum, Arlene, et al. "The Madrid statement on poly-and perfluoroalkyl substances (PFASs)." Environmental health perspectives 123.5 (2015): A107-A111.

Ng, Carla, et al. "Addressing Urgent Questions for PFAS in the 21st Century." Environmental Science & Technology 55.19 (2021): 12755-12765.

Post, Gloria B., Jessie A. Gleason, and Keith R. Cooper. "Key scientific issues in developing drinking water guidelines for perfluoroalkyl acids: Contaminants of emerging concern." PLoS biology 15.12 (2017): e2002855.

Pachkowski, Brian, Gloria B. Post, and Alan H. Stern. "The derivation of a Reference Dose (RfD) for perfluorooctane sulfonate (PFOS) based on immune suppression." Environmental research 171 (2019): 452-469.

Post, Gloria B. "Recent US state and federal drinking water guidelines for per-and polyfluoroalkyl substances." Environmental Toxicology and Chemistry 40.3 (2021): 550-563.

NH DES. (2019). Water Quality Standards, Monitoring, Compliance, Reporting, and Public Notification for Certain Perfluorochemicals (Accessed March 2019). https://www4.des.state.nh.us/nh-pfas-investigation/wp-content/uploads/Summary-of-Comments-Responses-with-Attachments.pdf

ATSDR. (2021). Toxicological Profile for Perfluoroalkyls Draft for Public Comment June 2018 (Accessed June 2021). https://www.atsdr.cdc.gov/toxprofiles/tp200.pdf

VT DHS. (2019). Perfluoroalkyl and polyfluoroalkyl substances (PFAS) in drinking water (Accessed March 2019). https://www.healthvermont.gov/environment/drinking-water/perfluoroalkyl-and-polyfluoroalkyl-substances-pfas-drinking-water

NC DHHS. (2017). Questions and answers regarding North Carolina Department of Health and Human Services Updated Risk Assessment of GenX (Perfluoro-22-propoxypropanoic acid) (Accessed March 2019) https://epi.dph.ncdhhs.gov/oee/pfas/NC%20DHHS%20Health%20Goal%20Q&A.pdf

MN DEP. (2019). “Perfluoroalkyl Substances (PFAS) - EH: Minnesota Department of Health.” Perfluoroalkyl Substances (PFAS), 2019, www.health.state.mn.us/communities/environment/hazardous/topics/pfcs.html#guidancerelease.

Vecitis, Chad D., et al. "Treatment technologies for aqueous perfluorooctanesulfonate (PFOS) and perfluorooctanoate (PFOA)." Frontiers of Environmental Science & Engineering in China 3.2 (2009): 129-151.

Rahman, Mohammad Feisal, Sigrid Peldszus, and William B. Anderson. "Behaviour and fate of perfluoroalkyl and polyfluoroalkyl substances (PFASs) in drinking water treatment: A review." Water research 50 (2014): 318-340.

Houtz, Erika F., and David L. Sedlak. "Oxidative conversion as a means of detecting precursors to perfluoroalkyl acids in urban runoff." Environmental science & technology 46.17 (2012): 9342-9349.

Zhang, Chuhui, et al. "Fate of per-and polyfluoroalkyl ether acids in the total oxidizable precursor assay and implications for the analysis of impacted water." Environmental science & technology letters 6.11 (2019): 662-668.

LaZerte, J. D., et al. "Pyrolyses of the Salts of the Perfluoro Carboxylic Acids1." Journal of the American Chemical Society 75.18 (1953): 4525-4528.

Hori, Hisao, et al. "Efficient decomposition of environmentally persistent perfluorocarboxylic acids by use of persulfate as a photochemical oxidant." Environmental Science & Technology 39.7 (2005): 2383-2388.

Moriwaki, Hiroshi, et al. "Sonochemical decomposition of perfluorooctane sulfonate and perfluorooctanoic acid." Environmental science & technology 39.9 (2005): 3388-3392.

Yamamoto, Takashi, et al. "Photodegradation of perfluorooctane sulfonate by UV irradiation in water and alkaline 2-propanol." Environmental science & technology 41.16 (2007): 5660-5665.

Bruton, Thomas A., and David L. Sedlak. "Treatment of aqueous film-forming foam by heat-activated persulfate under conditions representative of in situ chemical oxidation." Environmental Science & Technology 51.23 (2017): 13878-13885.

Lu, Dingnan, et al. "Treatment train approaches for the remediation of per-and polyfluoroalkyl substances (PFAS): A critical review." Journal of hazardous materials 386 (2020): 121963.

Huang, Shan, and Peter R. Jaffé. "Defluorination of perfluorooctanoic acid (PFOA) and perfluorooctane sulfonate (PFOS) by Acidimicrobium sp. strain A6." Environmental science & technology 53.19 (2019): 11410-11419.

Kucharzyk, Katarzyna H., et al. "Novel treatment technologies for PFAS compounds: A critical review." Journal of environmental management 204 (2017): 757-764.

Murray, Conner C., et al. "Removal of per-and polyfluoroalkyl substances using super-fine powder activated carbon and ceramic membrane filtration." Journal of hazardous materials 366 (2019): 160-168.

Steinle-Darling, Eva, and Martin Reinhard. "Nanofiltration for trace organic contaminant removal: structure, solution, and membrane fouling effects on the rejection of perfluorochemicals." Environmental science & technology 42.14 (2008): 5292-5297.

Stratton, Gunnar R., et al. "Plasma-based water treatment: efficient transformation of perfluoroalkyl substances in prepared solutions and contaminated groundwater." Environmental science & technology 51.3 (2017): 1643-1648.

Wang, Li, et al. "Electron beam treatment for potable water reuse: Removal of bromate and perfluorooctanoic acid." Chemical Engineering Journal 302 (2016): 58-68.

Ternes, Thomas A., et al. "Removal of pharmaceuticals during drinking water treatment." Environmental science & technology 36.17 (2002): 3855-3863.

Rossner, Alfred, Shane A. Snyder, and Detlef RU Knappe. "Removal of emerging contaminants of concern by alternative adsorbents." Water research 43.15 (2009): 3787-3796.

Corwin, Christopher J., and R. Scott Summers. "Controlling trace organic contaminants with GAC adsorption." Journal-American Water Works Association 104.1 (2012): E36-E47.

Summers, R. Scott, Detlef RU Knappe, and Vernon L. Snoeyink. "Adsorption of organic compounds by activated carbon." Water quality and treatment: A handbook on drinking water, 6th Edition. Edited by JK Edzwald. McGraw-Hill (2011).

Reinert, Allison Marie. "Granular Activated Carbon Adsorption of Micropollutants from Surface Water: Field-scale Adsorber Performance and Scale-up of Bench-scale Data." (2013).

Crittenden, John C., et al. MWH's water treatment: principles and design. John Wiley & Sons, 2012.

Hansen, Mona C., et al. "Sorption of perfluorinated compounds from contaminated water to activated carbon." Journal of Soils and Sediments 10.2 (2010): 179-185.

Dudley, Leigh-Ann. "Removal of Perfluorinated Compounds by Powdered Activated Carbon, Superfine Powder Activated Carbon, and Anion Exchange Resin." (2012).

Piai, Laura, et al. "Diffusion of hydrophilic organic micropollutants in granular activated carbon with different pore sizes." Water research 162 (2019): 518-527.

Zhi, Yue, and Jinxia Liu. "Adsorption of perfluoroalkyl acids by carbonaceous adsorbents: Effect of carbon surface chemistry." Environmental pollution 202 (2015): 168-176.

Park, Minkyu, et al. "Adsorption of perfluoroalkyl substances (PFAS) in groundwater by granular activated carbons: Roles of hydrophobicity of PFAS and carbon characteristics." Water research 170 (2020): 115364.

Arevalo Perez, Elisa Carolina. "Removal of Perfluorinated Compounds by Anion Exchange: Factors Affecting Resin Performance and Regeneration." (2014).

Dudley, Leigh-Ann, Elisa C. Arevalo, and Detlef RU Knappe. "Removal of Perfluoroalkyl Substances by PAC Adsorption and Anion Exchange [Project# 4344]." (2015).

Senevirathna, S. T. M. L. D., et al. "A comparative study of adsorption of perfluorooctane sulfonate (PFOS) onto granular activated carbon, ion-exchange polymers and non-ion-exchange polymers." Chemosphere 80.6 (2010): 647-651.

Carter, Kimberly E., and James Farrell. "Removal of perfluorooctane and perfluorobutane sulfonate from water via carbon adsorption and ion exchange." Separation Science and Technology 45.6 (2010): 762-767.

Rodowa, Alix E., et al. "Pilot scale removal of per-and polyfluoroalkyl substances and precursors from AFFF-impacted groundwater by granular activated carbon." Environmental Science: Water Research & Technology 6.4 (2020): 1083-1094.

Belkouteb, Nadine, et al. "Removal of per-and polyfluoroalkyl substances (PFASs) in a full-scale drinking water treatment plant: Long-term performance of granular activated carbon (GAC) and influence of flow-rate." Water Research 182 (2020): 115913.

Franke, Vera, et al. "Efficient removal of per-and polyfluoroalkyl substances (PFASs) in drinking water treatment: nanofiltration combined with active carbon or anion exchange." Environmental Science: Water Research & Technology 5.11 (2019): 1836-1843.

CFPUA (Cape Fear Public Utility Authority), 2017. GenX Information. CFPUA, Wilmington, N.C. www.cfpua.org/CivicAlerts.aspx?CID=18 (accessed Dec. 16, 2017)

Bansal, Roop Chand, Jean-Baptiste Donnet, and Fritz Stoeckli. "Marcel Dekker, A review of: Active carbon." Inc, New York 482 (1988).

Zhang, Wei, et al. "Selecting activated carbon for water and wastewater treatability studies." Environmental Progress 26.3 (2007): 289-298.

Moore, Brian C., et al. "GAC pore structure in Cincinnati during full-scale treatment/reactivation." Journal-American Water Works Association 95.2 (2003): 103-112.

Summers, R. S., et al. "Evaluation of available scale-up approaches for the design of GAC contactors." Denver, CO: Water Research Foundation Report 4235 (2014).

Corwin, Christopher J., and R. Scott Summers. "Scaling trace organic contaminant adsorption capacity by granular activated carbon." Environmental science & technology 44.14 (2010): 5403-5408.

Inyang, Mandu, and Eric RV Dickenson. "The use of carbon adsorbents for the removal of perfluoroalkyl acids from potable reuse systems." Chemosphere 184 (2017): 168-175.

McCleaf, Philip, et al. "Removal efficiency of multiple poly-and perfluoroalkyl substances (PFASs) in drinking water using granular activated carbon (GAC) and anion exchange (AE) column tests." Water research 120 (2017): 77-87.

Li, Lei, Patricia A. Quinlivan, and Detlef RU Knappe. "Effects of activated carbon surface chemistry and pore structure on the adsorption of organic contaminants from aqueous solution." Carbon 40.12 (2002): 2085-2100.

Carter, Margaret C., Walter J. Weber Jr, and Kevin P. Olmstead. "Effects of background dissolved organic matter on TCE adsorption by GAC." Journal-American Water Works Association 84.8 (1992): 81-91.

Pelekani, C., and V. L. Snoeyink. "Competitive adsorption in natural water: role of activated carbon pore size." Water research 33.5 (1999): 1209-1219.

Li, Qilin, et al. "Pore blockage effect of NOM on atrazine adsorption kinetics of PAC: the roles of PAC pore size distribution and NOM molecular weight." Water research 37.20 (2003): 4863-4872.

Kennedy, Anthony Myers. Granular Activated Carbon Adsorption of Organic Micropollutants: Scale-Up and Effect of Background Dissolved Organic Matter. Diss. University of Colorado at Boulder, 2013.

Sontheimer, Heinrich, John C. Crittenden, and R. Scott Summers. Activated carbon for water treatment. Vol. 90. Karlsruhe, Germany: DVGW-Forschungsstelle, Engler-Bunte-Institut, Universitat Karlsruhe (TH), 1988.

Matsui, Yoshihiko, Detlef RU Knappe, and Ryuichi Takagi. "Pesticide adsorption by granular activated carbon adsorbers. 1. Effect of natural organic matter preloading on removal rates and model simplification." Environmental science & technology 36.15 (2002): 3426-3431.

Schideman, Lance C., et al. "Application of a three-component competitive adsorption model to evaluate and optimize granular activated carbon systems." Water research 41.15 (2007): 3289-3298.

Crittenden, John C., et al. "Predicting GAC performance with rapid small-scale column tests." Journal-American Water Works Association 83.1 (1991): 77-87.

Summers, R. Scott, et al. "Bench-scale evaluation of GAC for NOM control." Journal-American Water Works Association 87.8 (1995): 69-80.

Kennedy, Anthony M., et al. "Full-and pilot-scale GAC adsorption of organic micropollutants." Water research 68 (2015): 238-248.

Crittenden, J. C., et al. "Prediction of GAC performance using rapid small-scale column tests." AWWARF report 90549 (1989).

Hurley, Susan, et al. "Breast cancer risk and serum levels of per-and poly-fluoroalkyl substances: A case-control study nested in the California Teachers Study." Environmental Health 17.1 (2018): 1-19.

Zeng, Chao, et al. "Removing per-and polyfluoroalkyl substances from groundwaters using activated carbon and ion exchange resin packed columns." AWWA Water Science 2.1 (2020): e1172.

Dickenson, E., and Chr Higgins. "Treatment mitigation strategies for poly-and perfluoroalkyl substances." Water Research Foundation Web Report 4322 (2016).

Kennedy, Anthony M., et al. "Prediction of full-scale GAC adsorption of organic micropollutants." Environmental Engineering Science 34.7 (2017): 496-507.

Summers, R. Scott, et al. "The influence of background organic matter on GAC adsorption." Journal-American Water Works Association 81.5 (1989): 66-74.

Knappe, Detlef RU, et al. "The effect of preloading on rapid small-scale column test predictions of atrazine removal by GAC adsorbers." Water research 31.11 (1997): 2899-2909.

Matsui, Yoshihiko, et al. "Branched pore kinetic model analysis of geosmin adsorption on super-powdered activated carbon." Water research 43.12 (2009): 3095-3103.

Ahrens, Lutz. "Polyfluoroalkyl compounds in the aquatic environment: a review of their occurrence and fate." Journal of Environmental Monitoring 13.1 (2011): 20-31.

Liu, Yanna, et al. "Nontarget mass spectrometry reveals new perfluoroalkyl substances in fish from the Yangtze River and Tangxun Lake, China." Environmental science & technology 52.10 (2018): 5830-5840.

Vestergren, Robin, and Ian T. Cousins. "Tracking the pathways of human exposure to perfluorocarboxylates." Environmental science & technology 43.15 (2009): 5565-5575.

Gyllenhammar, Irina, et al. "Perfluoroalkyl acids (PFAAs) in children's serum and contribution from PFAA-contaminated drinking water." Environmental science & technology 53.19 (2019): 11447-11457.

Schaefer, Charles E., et al. "Electrochemical treatment of perfluorooctanoic acid (PFOA) and perfluorooctane sulfonic acid (PFOS) in groundwater impacted by aqueous film forming foams (AFFFs)." Journal of Hazardous Materials 295 (2015): 170-175.

Golovko, Oksana, et al. "Sorption Characteristics and Removal Efficiency of Organic Micropollutants in Drinking Water Using Granular Activated Carbon (GAC) in Pilot-Scale and Full-Scale Tests." Water 12.7 (2020): 2053.

Hansen, Mona C., et al. "Sorption of perfluorinated compounds from contaminated water to activated carbon." Journal of Soils and Sediments 10.2 (2010): 179-185.

Gagliano, Erica, et al. "Removal of poly-and perfluoroalkyl substances (PFAS) from water by adsorption: Role of PFAS chain length, effect of organic matter and challenges in adsorbent regeneration." Water research 171 (2020): 115381.

Cantoni, Beatrice, et al. "Perfluoroalkyl substances (PFAS) adsorption in drinking water by granular activated carbon: Influence of activated carbon and PFAS characteristics." Science of The Total Environment 795 (2021): 148821.

Fotta, Meredith Elyse. "Effect of Granular Activated Carbon Type on Adsorber Performance and Scale-Up Approaches for Volatile Organic Compound Removal." (2012).

Knappe, D. R. U., et al. "Evaluation of Henry's Law Constants and Freundlich Adsorption Constants for VOCs." Water Research Foundation, Denver, CO (2017).

Kempisty, David M. Adsorption of volatile and perfluorinated compounds from groundwaters using granular activated carbon. Diss. University of Colorado at Boulder, 2014.

Higgins, Christopher P., and Richard G. Luthy. "Sorption of perfluorinated surfactants on sediments." Environmental science & technology 40.23 (2006): 7251-7256.

Xiao, Feng, Matt F. Simcik, and John S. Gulliver. "Mechanisms for removal of perfluorooctane sulfonate (PFOS) and perfluorooctanoate (PFOA) from drinking water by conventional and enhanced coagulation." Water research 47.1 (2013): 49-56.

Eschauzier, Christian, et al. "Impact of treatment processes on the removal of perfluoroalkyl acids from the drinking water production chain." Environmental science & technology 46.3 (2012): 1708-1715.

Rayne, Sierra, and Kaya Forest. "Perfluoroalkyl sulfonic and carboxylic acids: A critical review of physicochemical properties, levels and patterns in waters and wastewaters, and treatment methods." Journal of Environmental Science and Health Part A 44.12 (2009): 1145-1199.

Gomis, Melissa Ines, et al. "A modeling assessment of the physicochemical properties and environmental fate of emerging and novel per-and polyfluoroalkyl substances." Science of the Total Environment 505 (2015): 981-991.

Wu, Congyue, et al. "Exploring the factors that influence the adsorption of anionic PFAS on conventional and emerging adsorbents in aquatic matrices." Water Research 182 (2020): 115950.

Du, Ziwen, et al. "Adsorption behavior and mechanism of perfluorinated compounds on various adsorbents—A review." Journal of hazardous materials 274 (2014): 443-454.

Du, Ziwen, et al. "Removal of perfluorinated carboxylates from washing wastewater of perfluorooctanesulfonyl fluoride using activated carbons and resins." Journal of hazardous materials 286 (2015): 136-143.

Punyapalakul, Patiparn, et al. "Effects of surface functional groups and porous structures on adsorption and recovery of perfluorinated compounds by inorganic porous silicas." Separation Science and Technology 48.5 (2013): 775-788.

Knappe, D. R. U. "Surface chemistry effects in activated carbon adsorption of industrial pollutants." Interface Science and Technology. Vol. 10. Elsevier, 2006. 155-177.

Kothawala, Dolly N., et al. "Influence of dissolved organic matter concentration and composition on the removal efficiency of perfluoroalkyl substances (PFASs) during drinking water treatment." Water research 121 (2017): 320-328.

Li, Lei, Patricia A. Quinlivan, and Detlef RU Knappe. "Effects of activated carbon surface chemistry and pore structure on the adsorption of organic contaminants from aqueous solution." Carbon 40.12 (2002): 2085-2100.

Newcombe, G., et al. "Simultaneous adsorption of MIB and NOM onto activated carbon: II. Competitive effects." Carbon 40.12 (2002): 2147-2156.

Ebie, Kunio. "Effect of pore size distribution of activated carbon on the adsorption of humic substances and trace organic compounds." Water Supply 13 (1995): 65-70.

Kasaoka, S., et al. "Preparation of activated fibrous carbon from phenolic fabric and its molecular-sieve properties." Int Chem Eng 29.1 (1989): 101-114.

McNamara, James D., et al. "Comparison of activated carbons for removal of perfluorinated compounds from drinking water." Journal-American Water Works Association 110.1 (2018): E2-E14.

Dodds, James N., et al. "Rapid characterization of per-and polyfluoroalkyl substances (PFAS) by ion mobility spectrometry–mass spectrometry (IMS-MS)." Analytical chemistry 92.6 (2020): 4427-4435.

Hand, David W., John C. Crittenden, and William E. Thacker. "Simplified models for design of fixed-bed adsorption systems." Journal of Environmental Engineering 110.2 (1984): 440-456.

Murray, Conner C., et al. "PFAS treatment with granular activated carbon and ion exchange resin: Comparing chain length, empty bed contact time, and cost." Journal of Water Process Engineering 44 (2021): 102342.

Appleman, Timothy D., et al. "Treatment of poly-and perfluoroalkyl substances in US full-scale water treatment systems." Water research 51 (2014): 246-255.

APPENDICES

Appendix A: Analytical method

Materials

All materials used for sample collection and analysis have been previously checked for their suitability for PFAS analysis and were found to not contribute to measurable additions or losses of PFASs except for the filters. The following materials were used for sample preparation and analysis:

a. 15 mL polypropylene conical centrifuge tubes with polypropylene screw caps (Corning Falcon P/N 352097)
b. Genesee Scientific, Reach Olympus Classic Pipet Tips, plastic, 1-10 µL capacity (P/N 24-120R), checked to be PFAS-free
c. Genesee Scientific, Olympus Class Pipet Tips, plastic, 10-200 µL capacity (P/N 24-151R), checked to be PFAS-free
d. Genesee Scientific, Reach Olympus Pipet Tips, plastic, 100-1000 µL capacity (P/N 24-165R), checked to be PFAS-free
e. Eppendorf epTIPS Pipette tips, plastic, 50-1000 µL capacity (P/N 022492055), checked to be PFAS-free
f. Chemglass, Norm-ject polypropylene syringe, 30mL capacity (P/N CG-3081-05), checked to be PFAS-free
g. GE Healthcare Whatman™ GD/X Glass Micro Fiber (GMF) Syringe Filters, 0.45 µm (P/N 68942504)
h. Thermo Scientific™ 9mm Plastic Screw Thread Vials, 2 mL capacity (P/N 03-376-900)
i. Thermo Scientific™ 9 mm Autosampler Vial Screw Thread Caps (P/N 03-376-483)
j. 24-component native PFAS standard mix (2.0 µg/mL in methanol), Wellington Laboratories P/N PFCA-24PAR
k. Individual PFEA standards (HFPO-DA, ADONA, F-53B major) (50.0 µg/mL in methanol), Wellington Laboratories P/N HFPO-DA, NaDONA, 9Cl-PF3ONS
l. Individual PFECA/PFESA/PFES-CA standards (1 mg/mL in water), Chemours (not commercially available)
m. 19-component mass-labelled PFAS standard mix (1.0 µg/mL in methanol), Wellington Laboratories P/N MPFCA-24ES
n. Mass-labelled HFPO-DA (50 µg/mL in methanol), Wellington P/N M3HFPO-DA

Sample preparation

a. Using clean pipette tips, transfer 1,620 µL of sample from the 15-mL centrifuge tube to a new autosampler vial and add 180 µL of the internal standard mix.
b. Cap the vial with a screw cap and vortex the vial for 10 seconds.

The same sample preparation procedure was applied to method blanks, calibration standards, and quality control samples.

Table A.1: PFAS analyte acronyms, precursor and product ion m/z values, fragmentor and collision energies, and capillary voltages – (1) quantitation ion, (2) confirmation ion (note: only one transition is available for PFBA and PFPeA).

Name (Acronym)	Precursor Ion	Confirmation Ion	Fragmentor (V)	Collision Energy (V)	Capillary Voltage (V)	Internal standard
High Temperature Ion Source Compounds						
NVHOS (1)	296.9	79.9	140.0	48.0	1500	MPFBS
NVHOS (2)	269.9	135.1	140.0	24.0	1500	MPFBS
Nafion Byproduct 4 (1)	440.9	197.0	140.0	32.0	1500	MPFBS
Nafion Byproduct 4 (2)	440.9	241.0	140.0	20.0	1500	MPFBS
Nafion Byproduct 2 (1)	462.9	263.0	140.0	24.0	2000	MPFHxS
Nafion Byproduct 2 (2)	462.9	213.0	140.0	32.0	2000	MPFHxS
6:2FTS (1)	427.0	406.9	160.0	20.0	2000	M6:2 FTS
6:2 FTS (1)	427.0	80.9	160.0	40.0	2000	M6:2 FTS
PFBS (1)	298.9	79.9	140.0	40.0	1500	MPFBS
PFBS (2)	298.9	98.8	140.0	28.0	1500	MPFBS
PFHxS (1)	398.9	79.8	166.0	68.0	2000	MPFHxS
PFHxS (2)	398.9	98.9	166.0	36.0	2000	MPFHxS
PFOS (1)	498.9	79.7	170.0	76.0	2000	MPFOS
PFOS (2)	498.9	98.8	170.0	44.0	2000	MPFOS
Low Temperature Ion Source Compounds						
PFBA (1)	213.0	169.0	84.0	0.0	1500	MPFBA
PFPeA (1)	263.0	219.0	80.0	0.0	1500	MPFPeA
PFHxA (1)	313.0	268.9	94.0	0.0	2000	MPFHxA
PFHxA (2)	313.0	119.0	94.0	16.0	2000	MPFHxA
PFHpA (1)	363.0	319.0	100.0	0.0	2000	MPFHpA
PFHpA (2)	363.0	169.1	100.0	8.0	2000	MPFHpA
PFOA (1)	413.0	369.0	103.0	0.0	2000	MPFOA
PFOA (2)	413.0	168.9	103.0	12.0	2000	MPFOA
PFNA (1)	463.0	418.9	100.0	0.0	2000	MPFNA
PFNA (2)	463.0	219.0	100.0	8.0	2000	MPFNA
PFDA (1)	513.0	469.0	120.0	0.0	4000	MPFDA
PFDA (2)	513.0	269.0	120.0	8.0	4000	MPFDA
PFMOAA (1)	179.0	85.0	79.0	4.0	1500	MPFBA
PFMOAA (2)	179.0	135.0	79.0	0.0	1500	MPFBA
PMPA (1)	229.0	184.9	89.0	0.0	1500	MPFBA
PMPA (2)	229.0	85.1	89.0	16.0	1500	MPFBA
PEPA (1)	235.0	135.0	100.0	16.0	1500	MGenX
PEPA (2)	279.0	235.0	100.0	0.0	1500	MGenX
GenX (1)	285.0	169.0	108.0	0.0	2000	MGenX
GenX (2)	329.0	169.1	108.0	4.0	2000	MGenX
PFO2HxA (1)	245.0	85.0	95.0	0.0	1500	MGenX
PFO2HxA (2)	201.0	85.0	95.0	0.0	1500	MGenX

Table A.1: (continued).

PFO3OA (1)	311.0	85.0	105.0	0.0	2000	MGenX
PFO3OA (2)	311.0	151.0	105.0	0.0	2000	MGenX
HydroEve (1)	427.0	283.0	100.0	4.0	2000	MGenX
HydroEve (2)	427.0	262.9	100.0	12.0	2000	MGenX
PFO4DA (1)	376.9	85.0	110.0	0.0	2000	MGenX
PFO4DA (2)	376.9	150.9	110.0	0.0	2000	MGenX
PFO5DoA (1)	442.9	84.8	110.0	0.0	2000	MGenX
PFO5DoA (2)	442.9	150.8	110.0	0.0	2000	MGenX
Internal Standards						
MPFBA	217.0	172.0	85.0	0.0	1500	
MPFPeA	268.0	223.0	55.0	0.0	1500	
MPFHxA	318.0	273.0	95.0	0.0	2000	
MPFHpA	367.0	322.0	60.0	0.0	2000	
MPFOA	421.0	376.0	105.0	0.0	2000	
MPFNA	472.0	427.0	105.0	0.0	2000	
MFPDA	519.0	474.0	110.0	0.0	4000	
MGenX	287.0	169.0	108.0	0.0	2000	
MPFBS	302.0	79.9	120.0	40.0	1500	
MPFHxS	402.0	81.0	170.0	56.0	2000	
MPFOS	507.0	81.0	190.0	60.0	2000	
M6:2FTS	429.0	409.0	165.0	20.0	2000	

Appendix B: Scale-up of RSSCT plots

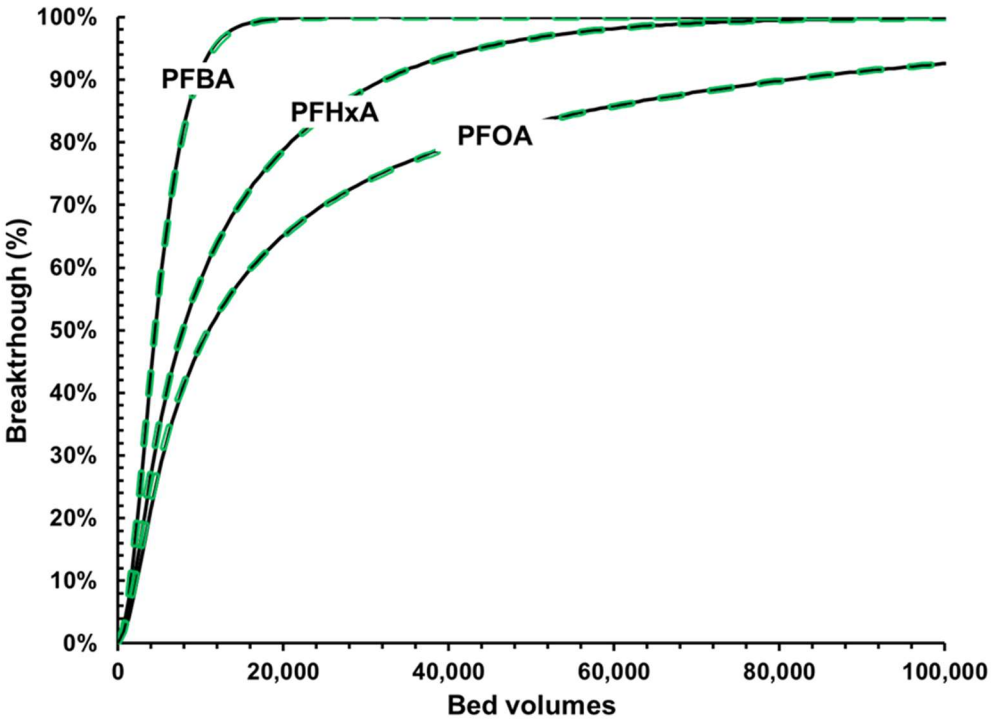

Figure B.1: Comparison of simulated breakthrough curves using pore surface diffusion model for two constant diffusivity column designs. The black lines represent breakthrough for a RSSCT designed under perfect similitude and the green dashed lines represent breakthrough for a RSSCT designed under reduced hydraulic loading condition.

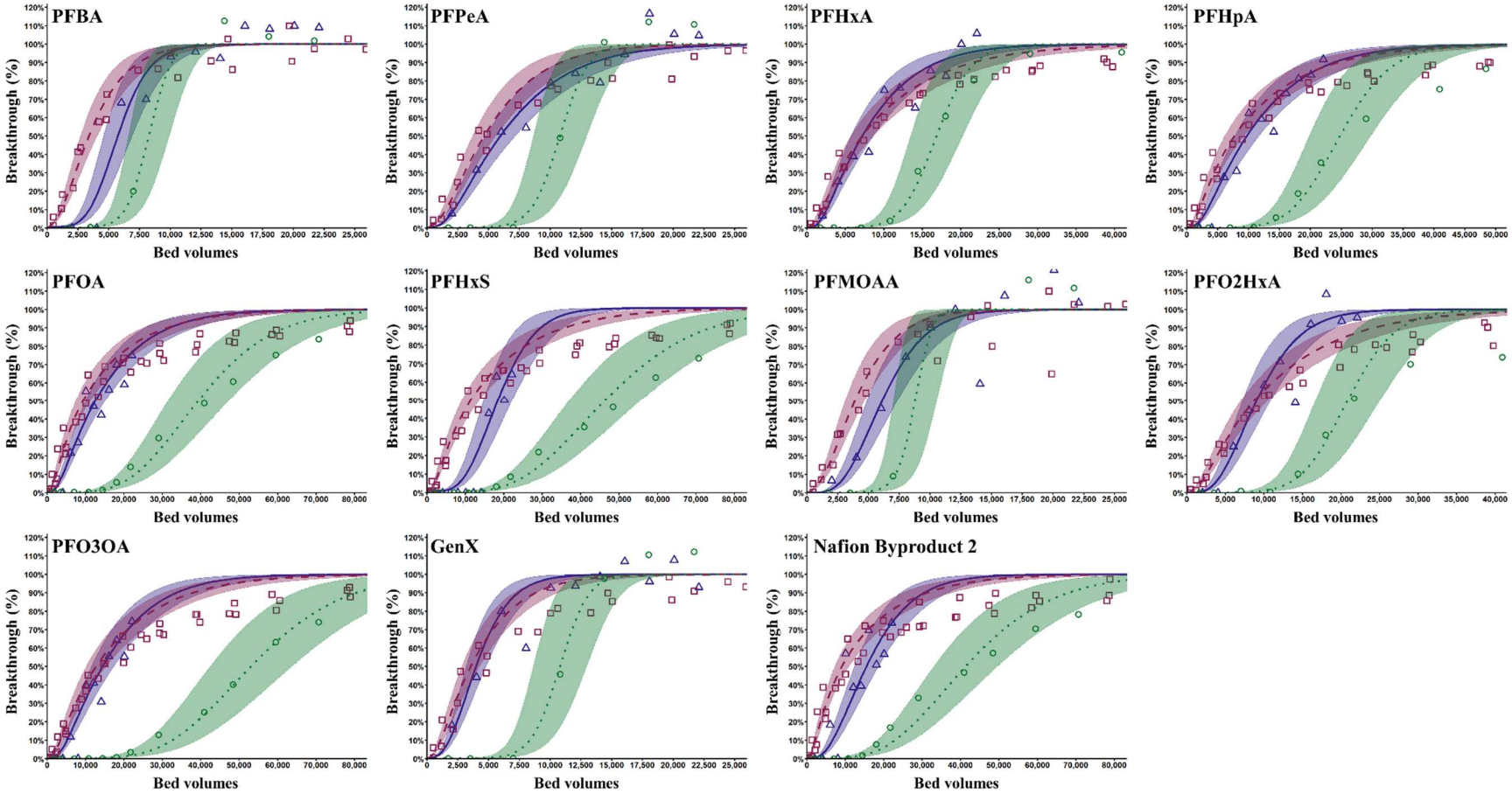

Figure B.2: Direct comparison of CD-RSSCT (red), PD-RSSCT (green), and pilot-scale (blue) breakthrough for PFAS in coagulate/settled surface water (TOC = 2.3 mg L-1), Carbon: Carbon A, simulated EBCT= 10 minutes. The symbols represent experimental or pilot data; the lines represent best fit PSDM for each data set; the shaded region 20% variance from best fit PSDM.

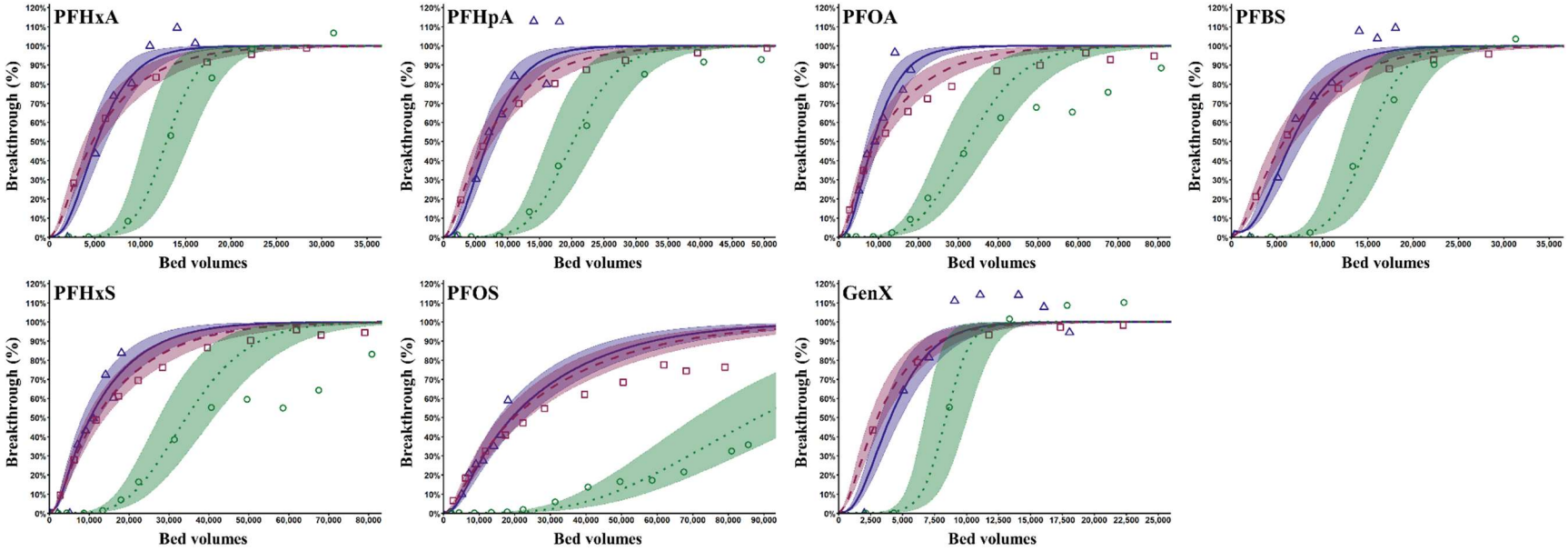

Figure B.3: Direct comparison of CD-RSSCT (red), PD-RSSCT (green), and pilot-scale (blue) breakthrough for PFAS in coagulate/settled surface water (TOC = 2.3 mg L-1), Carbon: Carbon C, simulated EBCT= 10 minutes. The symbols represent experimental or pilot data; the lines represent best fit PSDM for each data set; the shaded region 20% variance from best fit PSDM.

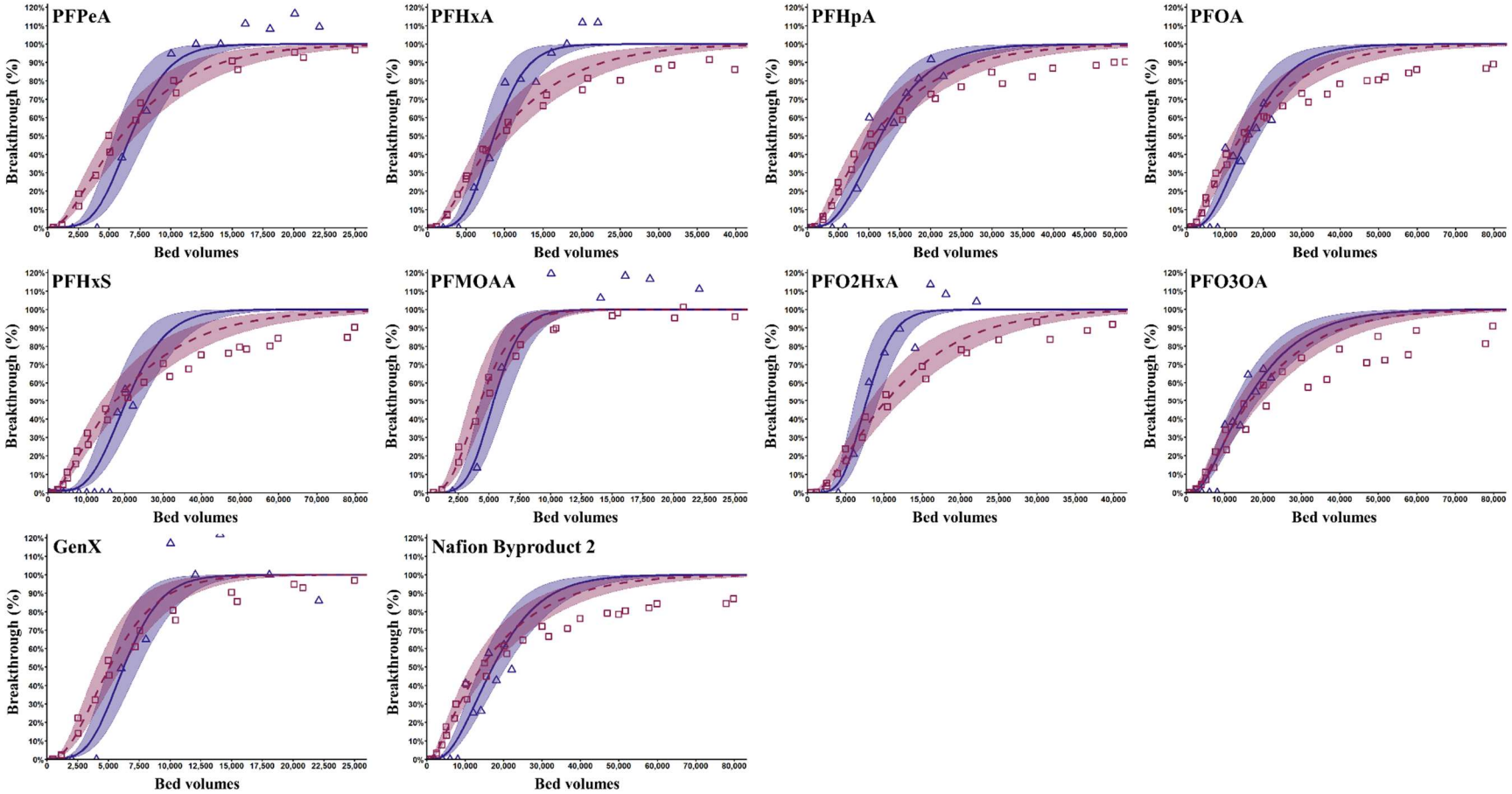

Figure B.4: Direct comparison of CD-RSSCT (red) and pilot-scale (blue) breakthrough for PFAS in coagulate/settled surface water (TOC = 2.3 mg L-1), Carbon: Carbon B, simulated EBCT= 10 minutes. The symbols represent experimental or pilot data; the lines represent best fit PSDM for each data set; the shaded region 20% variance from best fit PSDM.

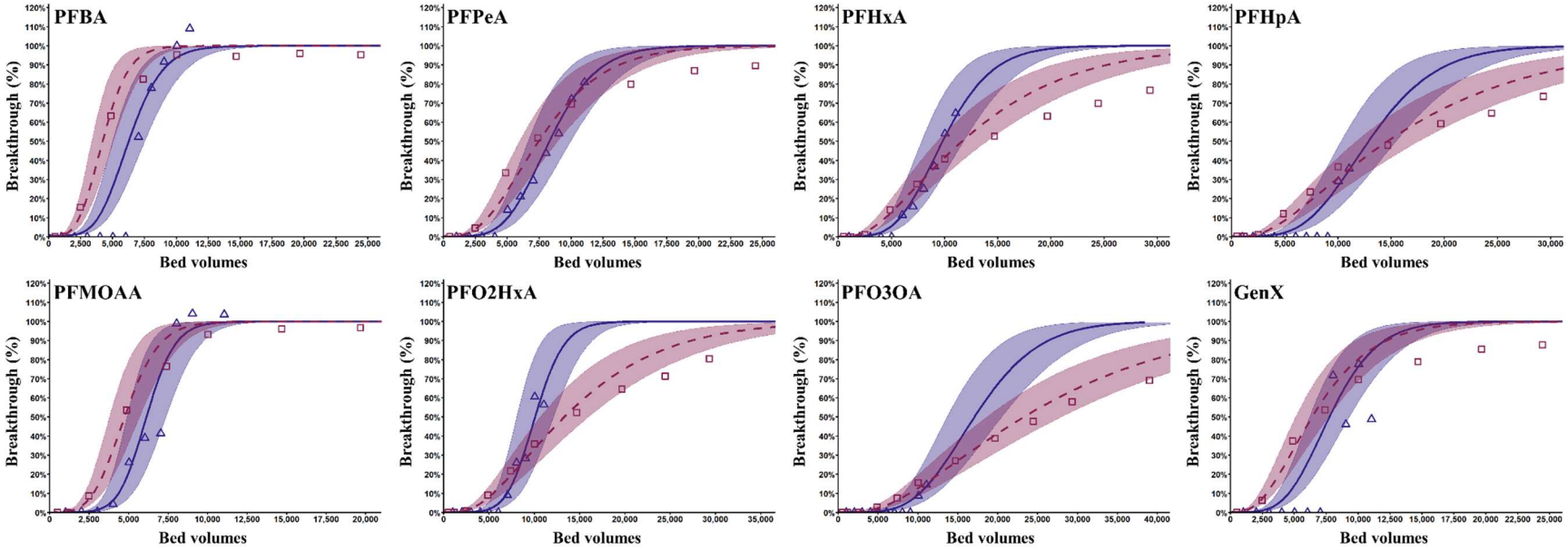

Figure B.5: Direct comparison of CD-RSSCT (red) and pilot-scale (blue) breakthrough for PFAS in coagulate/settled surface water (TOC = 2.3 mg L-1), Carbon: Carbon A, simulated EBCT= 20 minutes. The symbols represent experimental or pilot data; the lines represent best fit PSDM for each data set; the shaded region 20% variance from best fit PSDM.

Table B.1: AdDesignS inputs for Freundlich adsorption capacity and kinetic parameters for best fit PSDMs for field-scale and CD-RSSCT, TOC =2.3 mgL^{-1}. Carbon: Carbon A, EBCT = 10 and 20 min.

Compound	Carbon A, simulated EBCT = 10 min						Carbon A, simulated EBCT = 20 min					
	Field-scale			CD-RSSCT			Field-scale			CD-RSSCT		
	Freundlich adsorption capacity (L/g)	Tortuosity	Surface pore diffusion flux ratio	Freundlich adsorption capacity (L/g)	Tortuosity	Surface pore diffusion flux ratio	Freundlich adsorption capacity (L/g)	Tortuosity	Surface pore diffusion flux ratio	Freundlich adsorption capacity (L/g)	Tortuosity	Surface pore diffusion flux ratio
PFBA	11	1.0	1.0	7	2.0	1E-30	12	1.0	1E-30	8	1.0	1E-30
PFPeA	13	2.0	1E-30	10	2.0	1E-30	16	1.0	1E-30	15	2.0	1E-30
PFHxA	16	2.0	1E-30	18	3.0	1E-30	19	1.0	1E-30	25	3.0	1E-30
PFHpA	22	2.0	1E-30	20	3.0	1E-30	25	1.0	1E-30	32	3.0	1E-30
PFOA	29	2.0	1E-30	25	3.0	1E-30						
PFBS												
PFHxS	36	1.0	1.0	30	3.0	1E-30						
PFOS												
PFMOAA	12	1.0	1E-30	8	2.0	1E-30	11.5	1.0	1.0	9	1.0	1E-30
PFO2HxA	18	1.0	1E-30	21	3.0	1E-30	19	1.0	1.0	28	3.0	1E-30
PFO3OA	32	2.0	1E-30	32	3.0	1E-30	33	1.0	1E-30	50	3.0	1E-30
GenX	8	1.0	1E-30	8	2.0	1E-30	15	1.0	1E-30	13	2.0	1E-30
Nafion Byproduct 2	32	1.0	1E-30	25	3.0	1E-30						

Table B.2: AdDesignS inputs for Freundlich adsorption capacity and kinetic parameters for best fit PSDMs for field-scale and CD-RSSCT, TOC =2.3 mgL^{-1}. Carbon: Carbon B and Carbon D, EBCT = 10.

Compound	Carbon B, simulated EBCT = 10 min						Carbon C, simulated EBCT = 10 min					
	Field-scale			CD-RSSCT			Field-scale			CD-RSSCT		
	Freundlich adsorption capacity (L/g)	Tortuosity	Surface pore diffusion flux ratio	Freundlich adsorption capacity (L/g)	Tortuosity	Surface pore diffusion flux ratio	Freundlich adsorption capacity (L/g)	Tortuosity	Surface pore diffusion flux ratio	Freundlich adsorption capacity (L/g)	Tortuosity	Surface pore diffusion flux ratio
PFBA												
PFPeA	14	1.0	1.0	14	2.0	1E-30						
PFHxA	18	1.0	1.0	22	2.0	1E-30	14	1.0	1E-30	15	2.0	1E-30
PFHpA	26	1.0	1E-30	26	2.0	1E-30	19	1.0	1E-30	21	2.0	1E-30
PFOA	35	1.0	1E-30	36	2.0	1E-30	24	1.0	1E-30	32	2.0	1E-30
PFBS							18	1.0	1E-30	18	2.0	1E-30
PFHxS	43	1.0	1.0	43	2.0	1E-30	33	2.0	1E-30	39	2.0	1E-30
PFOS							65	2.0	1E-30	70	2.0	1E-30
PFMOAA	11	1.0	1.0	9	1.0	1E-30						
PFO2HxA	16	1.0	1.0	24	2.0	1E-30						
PFO3OA	37	2.0	1E-30	40	2.0	1E-30						
GenX	13	1.0	1.0	11	1.0	1E-30	11	1.0	1E-30	9	2.0	1E-30
Nafion Byproduct 2	38	1.0	1E-30	36	2.0	1E-30						

Table B.3: AdDesignS inputs for Freundlich adsorption capacity and kinetic parameters for best fit PSDMs for field-scale and PD-RSSCT, TOC =2.3 mgL^{-1}. Carbon: Carbon A and Carbon D, EBCT = 10.

Compound	Carbon A, simulated EBCT = 10 min						Carbon C, simulated EBCT = 10 min					
	Field-scale			PD-RSSCT			Field-scale			PD-RSSCT		
	Freundlich adsorption capacity (L/g)	Tortuosity	Surface pore diffusion flux ratio	Freundlich adsorption capacity (L/g)	Tortuosity	Surface pore diffusion flux ratio	Freundlich adsorption capacity (L/g)	Tortuosity	Surface pore diffusion flux ratio	Freundlich adsorption capacity (L/g)	Tortuosity	Surface pore diffusion flux ratio
PFBA	11	1.0	1.0	16	1.0	1E-30						
PFPeA	13	2.0	1E-30	21	1.0	1E-30						
PFHxA	16	2.0	1E-30	33	2.0	1E-30	31	2.0	1E-30	31	2.0	1E-30
PFHpA	22	2.0	1E-30	49	3.0	1E-30	49	3.0	1.0	49	3.0	1.0
PFOA	29	2.0	1E-30	80	6.0	1E-30	80	4.0	1E-30	80	4.0	1E-30
PFBS							36	2.0	1E-30	36	2.0	1E-30
PFHxS	36	1.0	1.0	95	7.0	1E-30	80	3.0	1E-30	80	3.0	1E-30
PFOS							225	7.0	1E-30	225	7.0	1E-30
PFMOAA	12	1.0	1E-30	17	1.0	1.0						
PFO2HxA	18	1.0	1E-30	41	3.0	1E-30						
PFO3OA	32	2.0	1E-30	107	6.0	1E-30						
GenX	8	1.0	1E-30	21	1.0	1E-30	20	1.0	1E-30	20	1.0	1E-30
Nafion Byproduct 2	32	1.0	1E-30	85	7.0	1E-30						

Table B.4: AdDesignS inputs for Freundlich adsorption capacity and kinetic parameters for best fit PSDMs for field-scale and CD-RSSCT, TOC <0.5 mgL^{-1}. Carbon: Carbon A, EBCT = 10.

Compound	Carbon A, simulated EBCT = 10 min					
	Field-scale			CD-RSSCT		
	Freundlich adsorption capacity (L/g)	Tortuosity	Surface pore diffusion flux ratio	Freundlich adsorption capacity (L/g)	Tortuosity	Surface pore diffusion flux ratio
PFBA	44	1.0	3.0	30	1.0	1.0
PFPeA	65	1.0	5.0	63	1.0	1.0
PFHxA	80	1.0	3.0	85	1.0	0.5

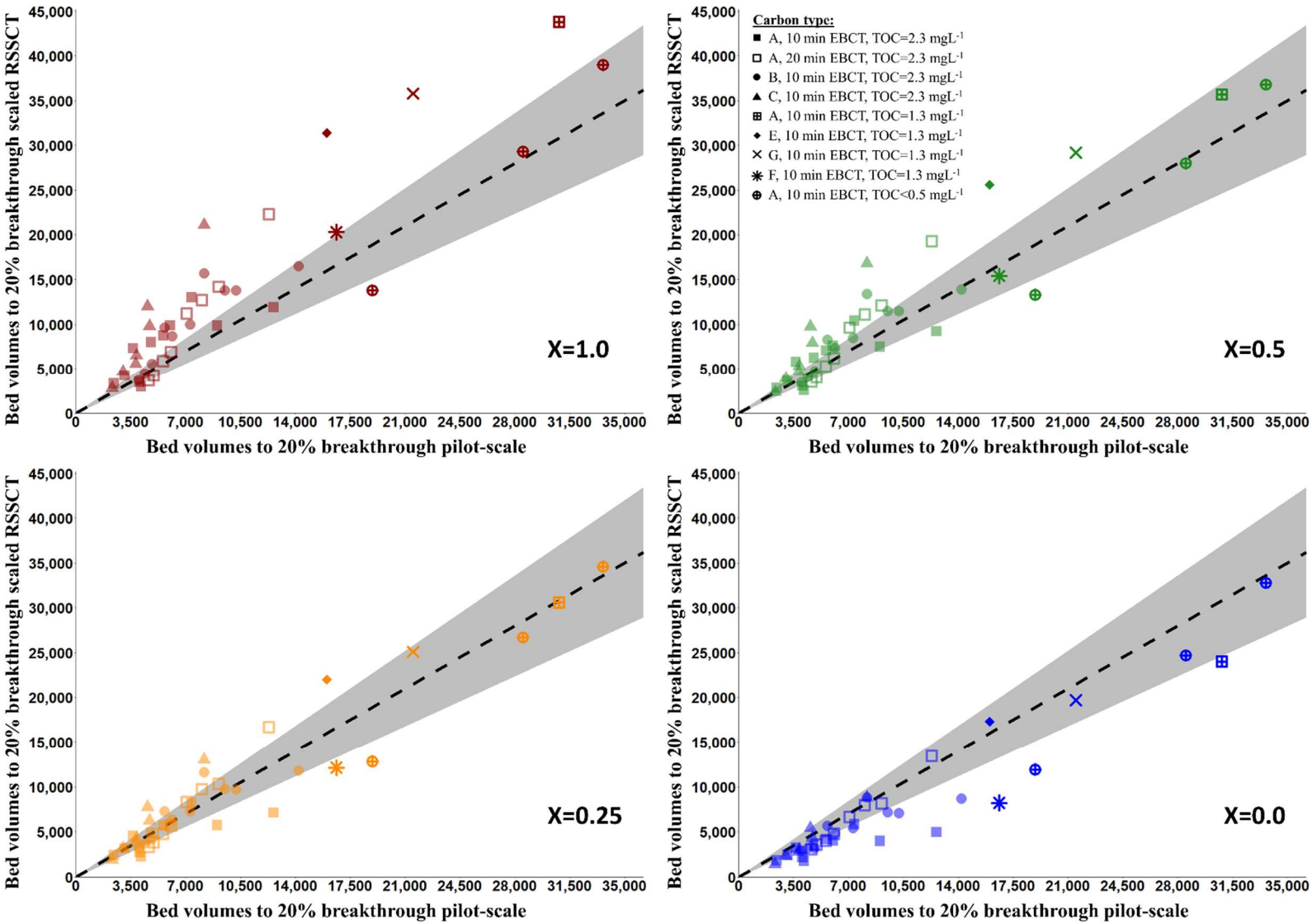

Figure B.6: Comparison of bed volumes to 20% breakthrough for field-scale and scaled CD-RSSCT. Dashed line represents 1:1 line for pilot breakthrough to 10%. Shaded region around dashed line represents 20% variance bed volumes to 10% breakthrough for pilot-scale.

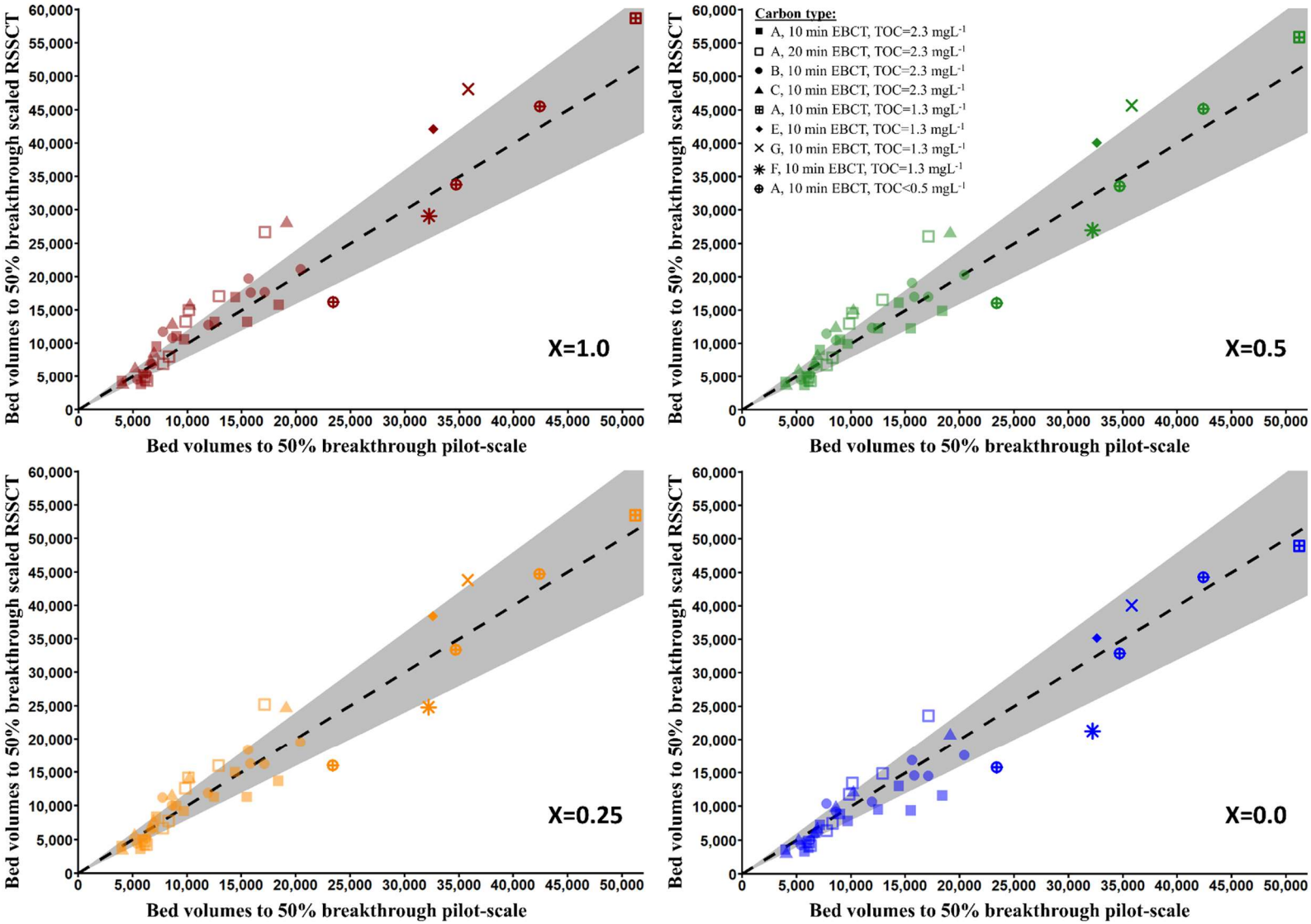

Figure B.7: Comparison of bed volumes to 50% breakthrough for field-scale and scaled CD-RSSCT. Dashed line represents 1:1 line for pilot breakthrough to 10%. Shaded region around dashed line represents 20% variance bed volumes to 10% breakthrough for pilot-scale.

Table B.5: Overview of PFAS for each scaling case compared to field-scale bed volumes to 10% breakthrough.

Case	Carbon A, 10 min EBCT		Carbon A, 20 min EBCT		Carbon B, 10 min EBCT		Carbon C, 10 min EBCT		Overall	
	Number of compounds good prediction	% total	Number of compounds good prediction	% total	Number of compounds good prediction	% total	Number of compounds good prediction	% total	Number of compounds good prediction	% total
X = 0.0	5	45%	7	88%	7	70%	5	71%	24	67%
X = 0.25	7	64%	8	100%	9	90%	5	71%	29	81%
X = 0.5	8	73%	6	75%	9	90%	4	57%	27	75%
X = 1.0	4	36%	4	50%	4	40%	1	14%	13	36%

Table B.6: Overview of PFAS for each scaling case compared to field-scale bed volumes to 20% breakthrough.

Case	Carbon A, 10 min EBCT		Carbon A, 20 min EBCT		Carbon B, 10 min EBCT		Carbon C, 10 min EBCT		Overall	
	Number of compounds good prediction	% total	Number of compounds good prediction	% total	Number of compounds good prediction	% total	Number of compounds good prediction	% total	Number of compounds good prediction	% total
X = 0.0	7	64%	7	88%	8	80%	6	86%	28	78%
X = 0.25	8	73%	8	100%	10	100%	5	71%	31	86%
X = 0.5	9	82%	7	88%	9	90%	4	57%	29	81%
X = 1.0	6	55%	4	50%	8	80%	2	29%	20	56%

Table B.7: Overview of PFAS for each scaling case compared to field-scale bed volumes to 50% breakthrough.

Case	Carbon A, 10 min EBCT		Carbon A, 20 min EBCT		Carbon B, 10 min EBCT		Carbon C, 10 min EBCT		Overall	
	Number of compounds good prediction	% total	Number of compounds good prediction	% total	Number of compounds good prediction	% total	Number of compounds good prediction	% total	Number of compounds good prediction	% total
X = 0.0	7	64%	8	100%	10	100%	7	100%	32	89%
X = 0.25	10	91%	8	100%	10	100%	7	100%	35	97%
X = 0.5	10	91%	7	88%	10	100%	7	100%	34	94%
X = 1.0	10	91%	7	88%	9	90%	6	86%	32	89%

Table B.8: AdDesignS inputs for Freundlich adsorption capacity and kinetic parameters for field-scale and scaled CD-RSSCT, Carbon: Carbon A, EBCT: 10 minutes, TOC =2.3 mgL^{-1}.

Compound	Field-scale			PSDM Scaling X=0.0			PSDM Scaling X=0.25			PSDM Scaling X=0.5			PSDM Scaling X=1.0		
	Freundlich adsorption capacity (L/g)	Tortuosity	Surface pore diffusion flux ratio	Freundlich adsorption capacity (L/g)	Tortuosity	Surface pore diffusion flux ratio	Freundlich adsorption capacity (L/g)	Tortuosity	Surface pore diffusion flux ratio	Freundlich adsorption capacity (L/g)	Tortuosity	Surface pore diffusion flux ratio	Freundlich adsorption capacity (L/g)	Tortuosity	Surface pore diffusion flux ratio
PFBA	11	1.0	1.0	7	2.0	1E-30	7	1.0	1E-30	7	1.0	0.8	7	1.0	5.7
PFPeA	13	2.0	1E-30	10	2.0	1E-30	10	1.0	1E-30	10	1.0	0.8	10	1.0	5.7
PFHxA	16	2.0	1E-30	18	3.0	1E-30	18	1.6	1E-30	18	1.0	0.2	18	1.0	3.5
PFHpA	22	2.0	1E-30	20	3.0	1E-30	20	1.6	1E-30	20	1.0	0.2	20	1.0	3.5
PFOA	29	2.0	1E-30	25	3.0	1E-30	25	1.6	1E-30	25	1.0	0.2	25	1.0	3.5
PFHxS	36	1.0	1.0	30	3.0	1E-30	30	1.6	1E-30	30	1.0	0.2	30	1.0	3.5
PFMOAA	12	1.0	1E-30	8	2.0	1E-30	8	1.0	1E-30	8	1.0	0.8	8	1.0	5.7
PFO2HxA	18	1.0	1E-30	21	3.0	1E-30	21	1.6	1E-30	21	1.0	0.2	21	1.0	3.5
PFO3OA	32	2.0	1E-30	32	3.0	1E-30	32	1.6	1E-30	32	1.0	0.2	32	1.0	3.5
GenX	8	1.0	1E-30	8	2.0	1E-30	8	1.0	1E-30	8	1.0	0.8	8	1.0	5.7
Nafion Byproduct 2	32	1.0	1E-30	25	3.0	1E-30	25	1.6	1E-30	25	1.0	0.2	25	1.0	3.5

Table B.9: AdDesignS inputs for Freundlich adsorption capacity and kinetic parameters for field-scale and scaled CD-RSSCT, Carbon: Carbon A, EBCT: 20 minutes, TOC =2.3 mgL^{-1}.

Compound	Field-scale			PSDM Scaling X=0.0			PSDM Scaling X=0.25			PSDM Scaling X=0.5			PSDM Scaling X=1.0		
	Freundlich adsorption capacity (L/g)	Tortuosity	Surface pore diffusion flux ratio	Freundlich adsorption capacity (L/g)	Tortuosity	Surface pore diffusion flux ratio	Freundlich adsorption capacity (L/g)	Tortuosity	Surface pore diffusion flux ratio	Freundlich adsorption capacity (L/g)	Tortuosity	Surface pore diffusion flux ratio	Freundlich adsorption capacity (L/g)	Tortuosity	Surface pore diffusion flux ratio
PFBA	12	1.0	1E-30	8	1.0	1E-30	8	1.0	0.9	8	1.0	2.7	8	1.0	12.4
PFPeA	16	1.0	1E-30	15	2.0	1E-30	15	1.0	1E-30	15	1.0	0.8	15	1.0	5.7
PFHxA	19	1.0	1E-30	25	3.0	1E-30	25	1.6	1E-30	25	1.0	0.2	25	1.0	3.5
PFHpA	25	1.0	1E-30	32	3.0	1E-30	32	1.6	1E-30	32	1.0	0.2	32	1.0	3.5
PFMOAA	11.5	1.0	1.0	9	1.0	1E-30	9	1.0	0.9	9	1.0	2.7	9	1.0	12.4
PFO2HxA	19	1.0	1.0	28	3.0	1E-30	28	1.6	1E-30	28	1.0	0.2	28	1.0	3.5
PFO3OA	33	1.0	1E-30	50	3.0	1E-30	50	1.6	1E-30	50	1.0	0.2	50	1.0	3.5
GenX	15	1.0	1E-30	13	2.0	1E-30	13	1.0	1E-30	13	1.0	0.8	13	1.0	5.7

Table B.10: AdDesignS inputs for Freundlich adsorption capacity and kinetic parameters for field-scale and scaled CD-RSSCT, Carbon: Carbon B, EBCT: 10 minutes, TOC =2.3 mgL^{-1}.

	Field-scale			PSDM Scaling X=0.0			PSDM Scaling X=0.25			PSDM Scaling X=0.5			PSDM Scaling X=1.0		
Compound	Freundlich adsorption capacity (L/g)	Tortuosity	Surface pore diffusion flux ratio	Freundlich adsorption capacity (L/g)	Tortuosity	Surface pore diffusion flux ratio	Freundlich adsorption capacity (L/g)	Tortuosity	Surface pore diffusion flux ratio	Freundlich adsorption capacity (L/g)	Tortuosity	Surface pore diffusion flux ratio	Freundlich adsorption capacity (L/g)	Tortuosity	Surface pore diffusion flux ratio
PFPeA	14	1.0	1.0	14	2.0	1E-30	14	1.0	1E-30	1.0	0.8	1.0	14	1.0	5.7
PFHxA	18	1.0	1.0	22	2.0	1E-30	22	1.0	1E-30	1.0	0.8	1.0	22	1.0	5.7
PFHpA	26	1.0	1E-30	26	2.0	1E-30	26	1.0	1E-30	1.0	0.8	1.0	26	1.0	5.7
PFOA	35	1.0	1E-30	36	2.0	1E-30	36	1.0	1E-30	1.0	0.8	1.0	36	1.0	5.7
PFHxS	43	1.0	1.0	43	2.0	1E-30	43	1.0	1E-30	1.0	0.8	1.0	43	1.0	5.7
PFMOAA	11	1.0	1.0	9	1.0	1E-30	9	1.0	0.9	1.0	2.7	1.0	9	1.0	12.4
PFO2HxA	16	1.0	1.0	24	2.0	1E-30	24	1.0	1E-30	1.0	0.8	1.0	24	1.0	5.7
PFO3OA	37	2.0	1E-30	40	2.0	1E-30	40	1.0	1E-30	1.0	0.8	1.0	40	1.0	5.7
GenX	13	1.0	1.0	11	1.0	1E-30	11	1.0	0.9	1.0	2.7	1.0	11	1.0	12.4
Nafion Byproduct 2	38	1.0	1E-30	36	2.0	1E-30	36	1.0	1E-30	1.0	0.8	1.0	36	1.0	5.7

Table B.11: AdDesignS inputs for Freundlich adsorption capacity and kinetic parameters for field-scale and scaled CD-RSSCT, Carbon: Carbon C, EBCT: 10 minutes, TOC =2.3 mgL^{-1}.

	Field-scale			PSDM Scaling X=0.0			PSDM Scaling X=0.25			PSDM Scaling X=0.5			PSDM Scaling X=1.0		
Compound	Freundlich adsorption capacity (L/g)	Tortuosity	Surface pore diffusion flux ratio	Freundlich adsorption capacity (L/g)	Tortuosity	Surface pore diffusion flux ratio	Freundlich adsorption capacity (L/g)	Tortuosity	Surface pore diffusion flux ratio	Freundlich adsorption capacity (L/g)	Tortuosity	Surface pore diffusion flux ratio	Freundlich adsorption capacity (L/g)	Tortuosity	Surface pore diffusion flux ratio
PFHxA	14	1.0	1E-30	15	2.0	1E-30	15	1.0	1E-30	15	1	1.0	15	1	6.7
PFHpA	19	1.0	1E-30	21	2.0	1E-30	21	1.0	1E-30	21	1	1.0	21	1	6.7
PFOA	24	1.0	1E-30	32	2.0	1E-30	32	1.0	1E-30	32	1	1.0	32	1	6.7
PFBS	18	1.0	1E-30	18	2.0	1E-30	18	1.0	1E-30	18	1	1.0	18	1	6.7
PFHxS	33	2.0	1E-30	39	2.0	1E-30	39	1.0	1E-30	39	1	1.0	39	1	6.7
PFOS	65	2.0	1E-30	70	2.0	1E-30	70	1.0	1E-30	70	1	1.0	70	1	6.7
GenX	11	1.0	1E-30	9	2.0	1E-30	9	1.0	1E-30	9	1	1.0	9	1	6.7

Table B.12: AdDesignS inputs for Freundlich adsorption capacity and kinetic parameters for field-scale and scaled CD-RSSCT, Carbon: Carbon A, EBCT: 10 minutes, TOC <0.5 mgL^{-1}.

Compound	Field-scale			PSDM Scaling X=0.0			PSDM Scaling X=0.25			PSDM Scaling X=0.5			PSDM Scaling X=1.0		
	Freundlich adsorption capacity (L/g)	Tortuosity	Surface pore diffusion flux ratio	Freundlich adsorption capacity (L/g)	Tortuosity	Surface pore diffusion flux ratio	Freundlich adsorption capacity (L/g)	Tortuosity	Surface pore diffusion flux ratio	Freundlich adsorption capacity (L/g)	Tortuosity	Surface pore diffusion flux ratio	Freundlich adsorption capacity (L/g)	Tortuosity	Surface pore diffusion flux ratio
PFBA	44	1.0	3.0	30	1.0	1.0	30	1.0	2.8	30	1.0	6.3	30	1.0	25.7
PFPeA	65	1.0	5.0	63	1.0	1.0	63	1.0	2.8	63	1.0	6.3	63	1.0	25.7
PFHxA	80	1.0	3.0	85	1.0	0.5	85	1.0	1.9	85	1.0	4.5	85	1.0	19.0

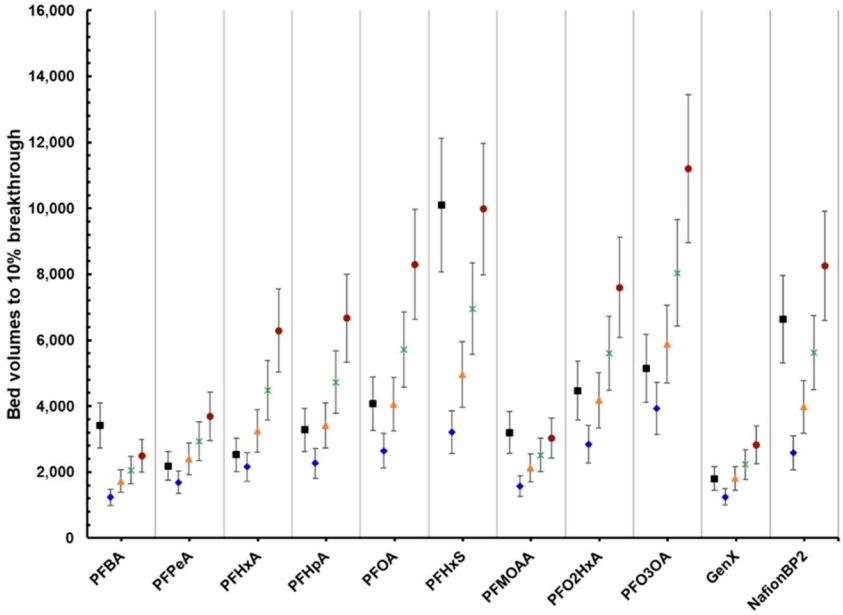

Figure B. 8: Comparison of bed volumes to 10% breakthrough for scaled CD-RSSCT PSDM and field-scale. Carbon: Carbon A, EBCT: 10 minutes, Pilot data represented by black squares with +/-20% variance, Scaled CD-RSSCT for X=0.0 (blue diamond), X=0.25 (orange triangle) X=0.5 (green x), X=1.0 (red circle) with +/-20% variance.

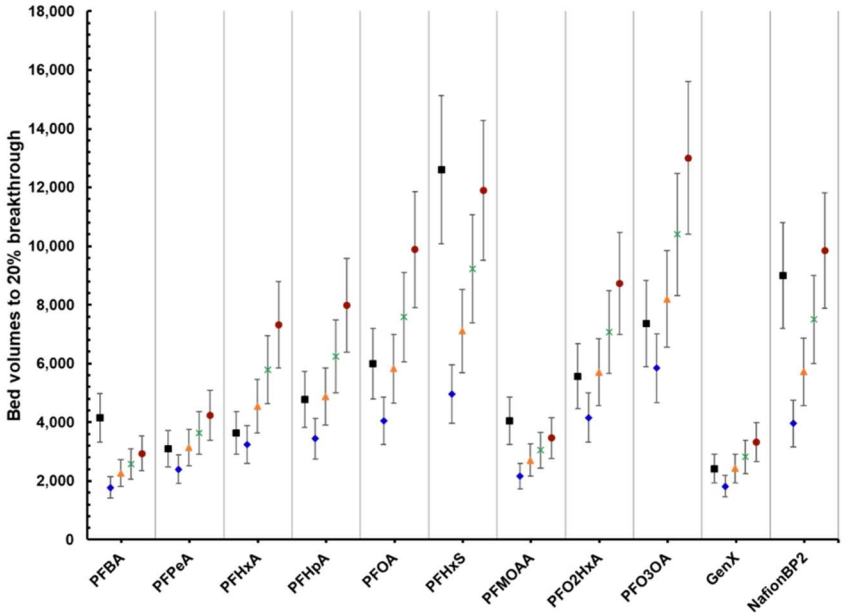

Figure B.9: Comparison of bed volumes to 20% breakthrough for scaled CD-RSSCT PSDM and field-scale. Carbon: Carbon A, EBCT: 10 minutes, Pilot data represented by black squares with +/-20% variance, Scaled CD-RSSCT for X=0.0 (blue diamond), X=0.25 (orange triangle) X=0.5 (green x), X=1.0 (red circle) with +/-20% variance.

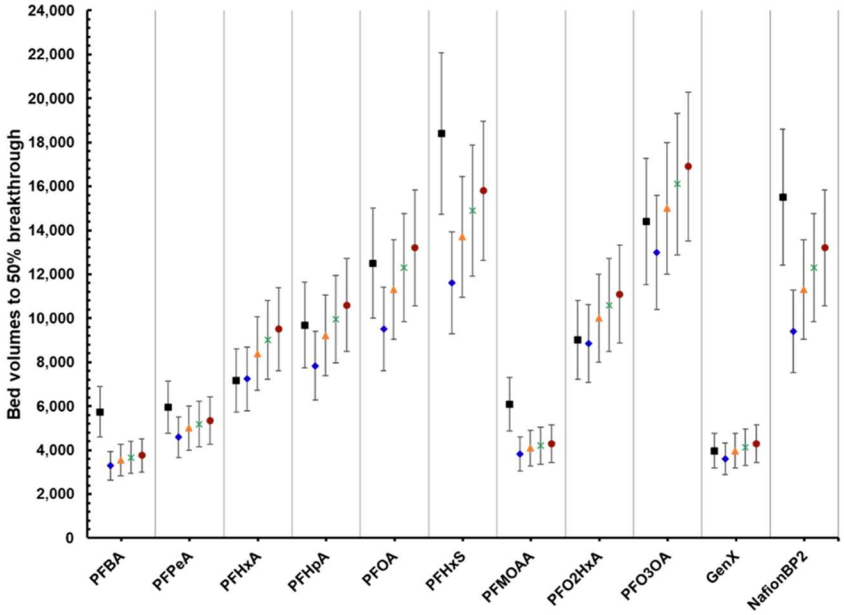

Figure B.10: Comparison of bed volumes to 50% breakthrough for scaled CD-RSSCT PSDM and field-scale. Carbon: Carbon A, EBCT: 10 minutes, Pilot data represented by black squares with +/-20% variance, Scaled CD-RSSCT for X=0.0 (blue diamond), X=0.25 (orange triangle) X=0.5 (green x), X=1.0 (red circle) with +/-20% variance.

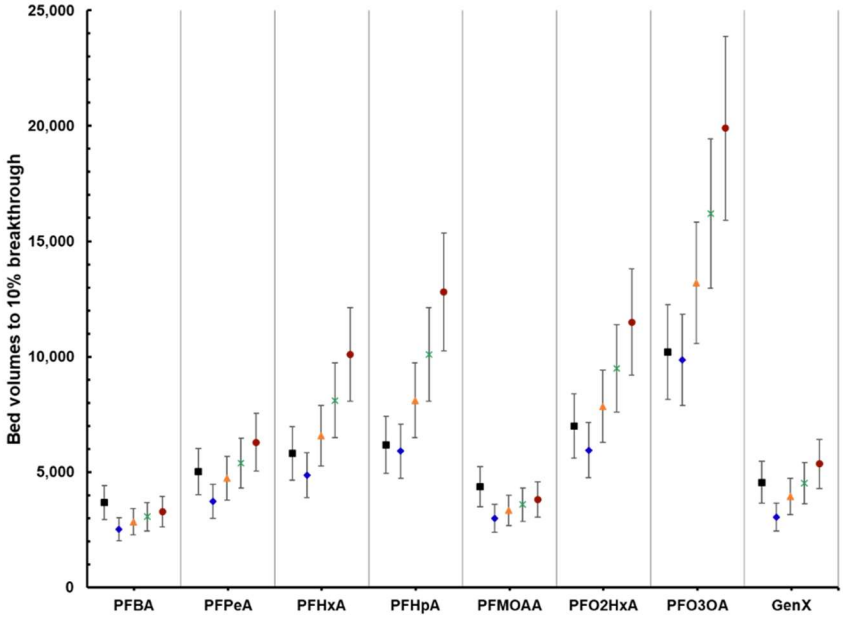

Figure B.11: Comparison of bed volumes to 10% breakthrough for scaled CD-RSSCT PSDM and field-scale. Carbon: Carbon A, EBCT: 20 minutes, Pilot data represented by black squares with +/-20% variance, Scaled CD-RSSCT for X=0.0 (blue diamond), X=0.25 (orange triangle) X=0.5 (green x), X=1.0 (red circle) with +/-20% variance.

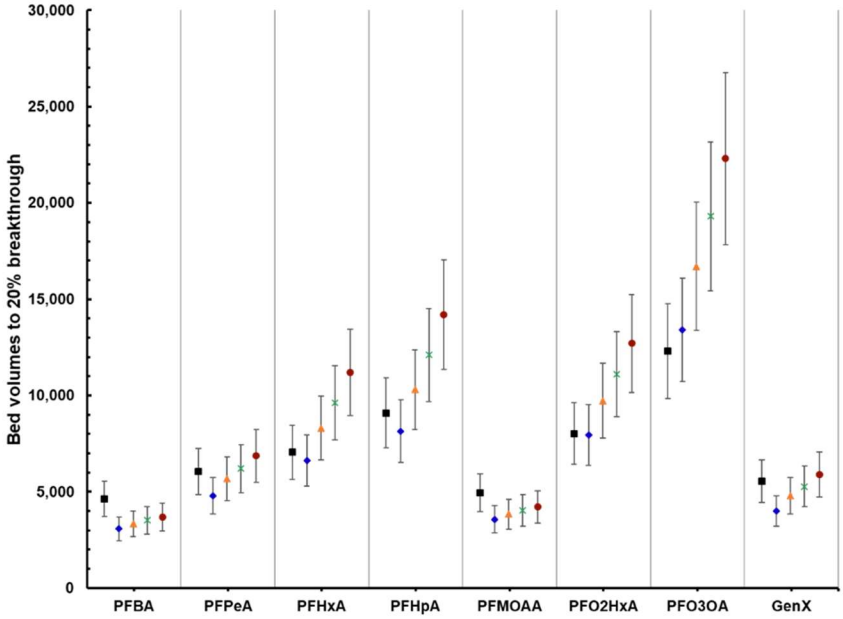

Figure B.12: Comparison of bed volumes to 20% breakthrough for scaled CD-RSSCT PSDM and field-scale. Carbon: Carbon A, EBCT: 20 minutes, Pilot data represented by black squares with +/-20% variance, Scaled CD-RSSCT for X=0.0 (blue diamond), X=0.25 (orange triangle) X=0.5 (green x), X=1.0 (red circle) with +/-20% variance.

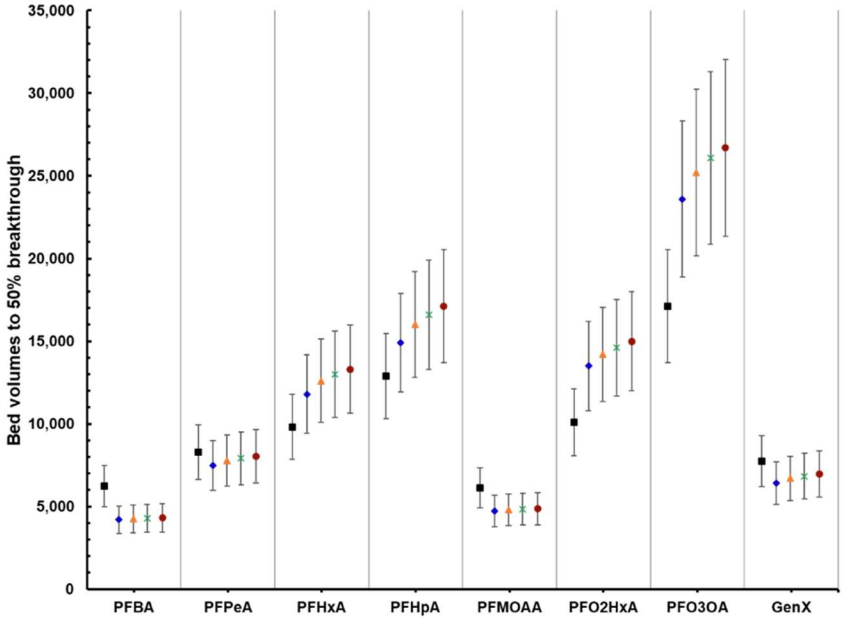

Figure B.13: Comparison of bed volumes to 50% breakthrough for scaled CD-RSSCT PSDM and field-scale. Carbon: Carbon A, EBCT: 20 minutes, Pilot data represented by black squares with +/-20% variance, Scaled CD-RSSCT for X=0.0 (blue diamond), X=0.25 (orange triangle) X=0.5 (green x), X=1.0 (red circle) with +/-20% variance.

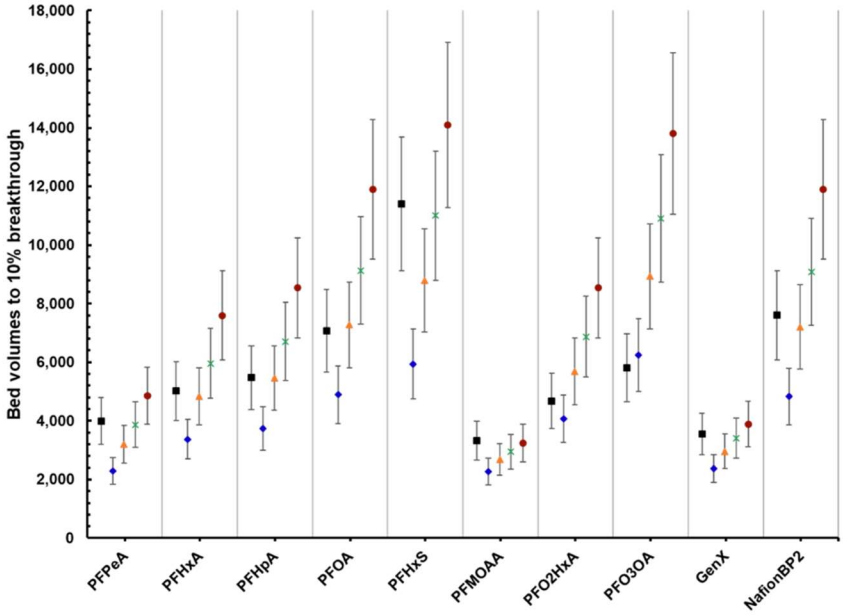

Figure B. 14: Comparison of bed volumes to 10% breakthrough for scaled CD-RSSCT PSDM and field-scale. Carbon:Carbon B, EBCT: 10 minutes, Pilot data represented by black squares with +/-20% variance, Scaled CD-RSSCT for X=0.0 (blue diamond), X=0.25 (orange triangle) X=0.5 (green x), X=1.0 (red circle) with +/-20% variance.

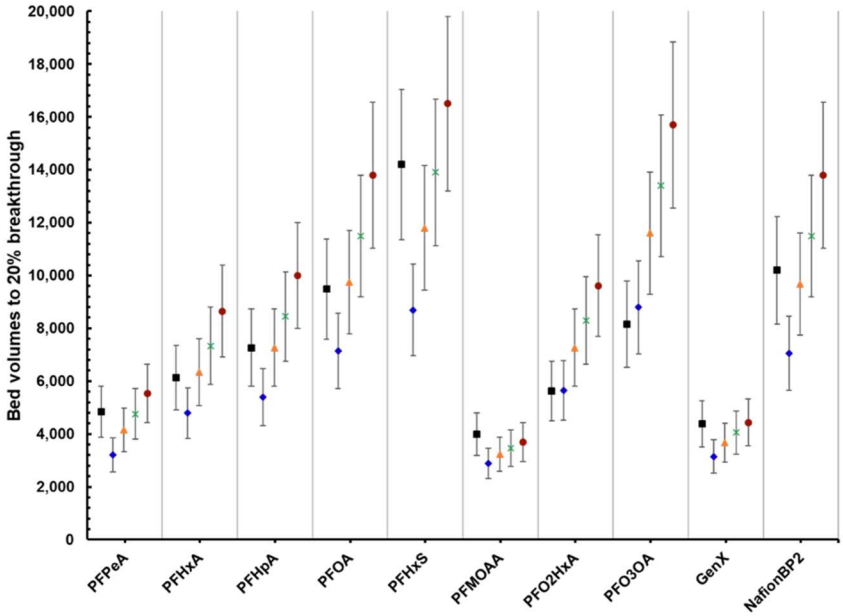

Figure B.15: Comparison of bed volumes to 20% breakthrough for scaled CD-RSSCT PSDM and field-scale. Carbon:Carbon B, EBCT: 10 minutes, Pilot data represented by black squares with +/-20% variance, Scaled CD-RSSCT for X=0.0 (blue diamond), X=0.25 (orange triangle) X=0.5 (green x), X=1.0 (red circle) with +/-20% variance.

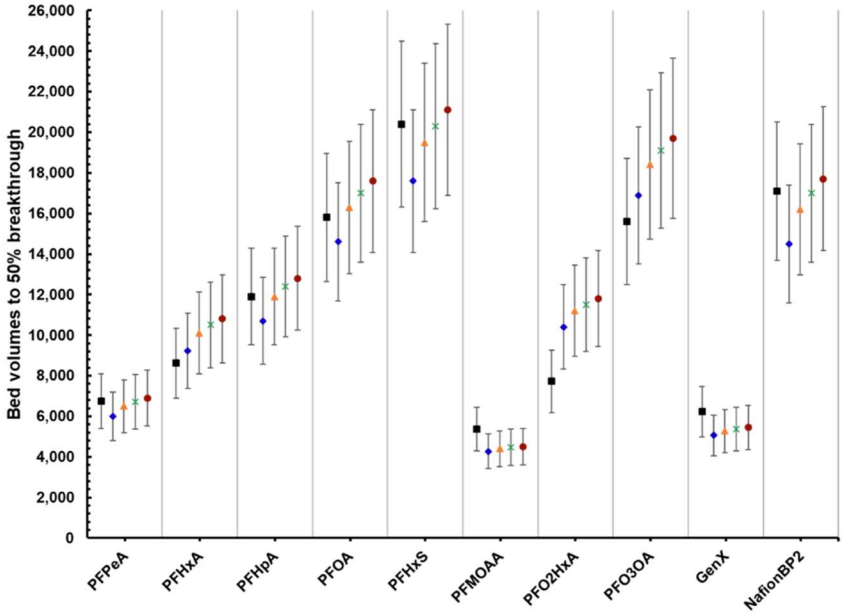

Figure B.16: Comparison of bed volumes to 50% breakthrough for scaled CD-RSSCT PSDM and field-scale. Carbon:Carbon B, EBCT: 10 minutes, Pilot data represented by black squares with +/-20% variance, Scaled CD-RSSCT for X=0.0 (blue diamond), X=0.25 (orange triangle) X=0.5 (green x), X=1.0 (red circle) with +/-20% variance.

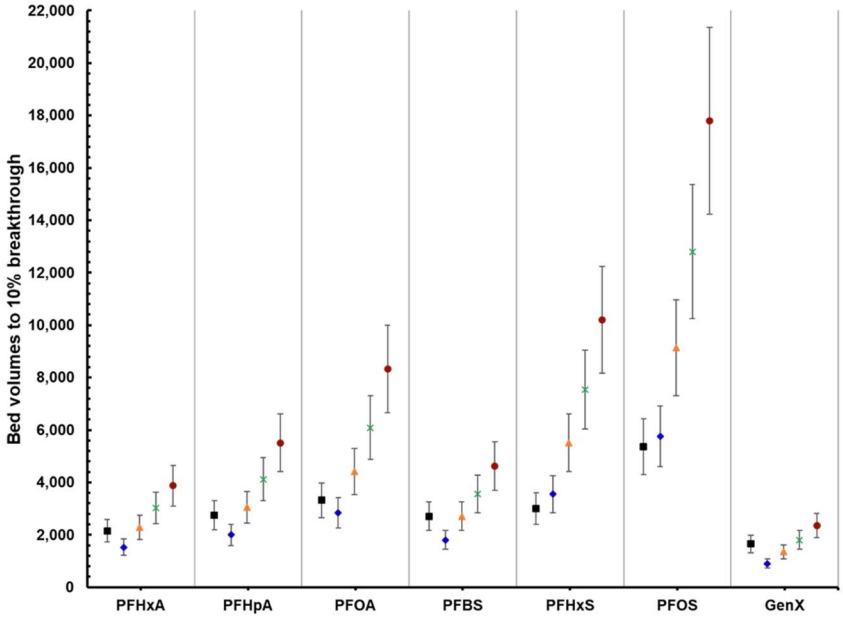

Figure B.17: Comparison of bed volumes to 10% breakthrough for scaled CD-RSSCT PSDM and field-scale. Carbon Carbon C, EBCT: 10 minutes, Pilot data represented by black squares with +/-20% variance, Scaled CD-RSSCT for X=0.0 (blue diamond), X=0.25 (orange triangle) X=0.5 (green x), X=1.0 (red circle) with +/-20% variance.

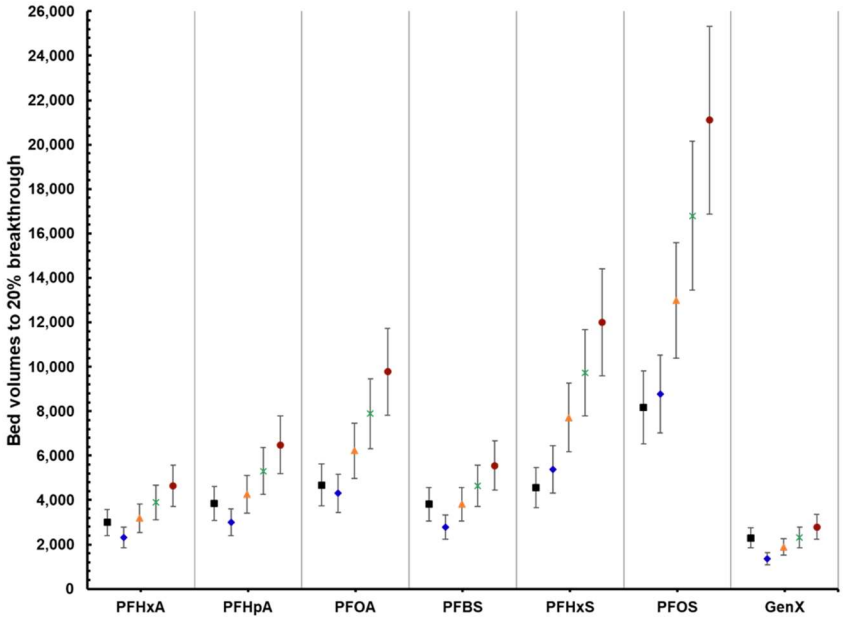

Figure B.18: Comparison of bed volumes to 20% breakthrough for scaled CD-RSSCT PSDM and field-scale. Carbon Carbon C, EBCT: 10 minutes, Pilot data represented by black squares with +/-20% variance, Scaled CD-RSSCT for X=0.0 (blue diamond), X=0.25 (orange triangle) X=0.5 (green x), X=1.0 (red circle) with +/-20% variance.

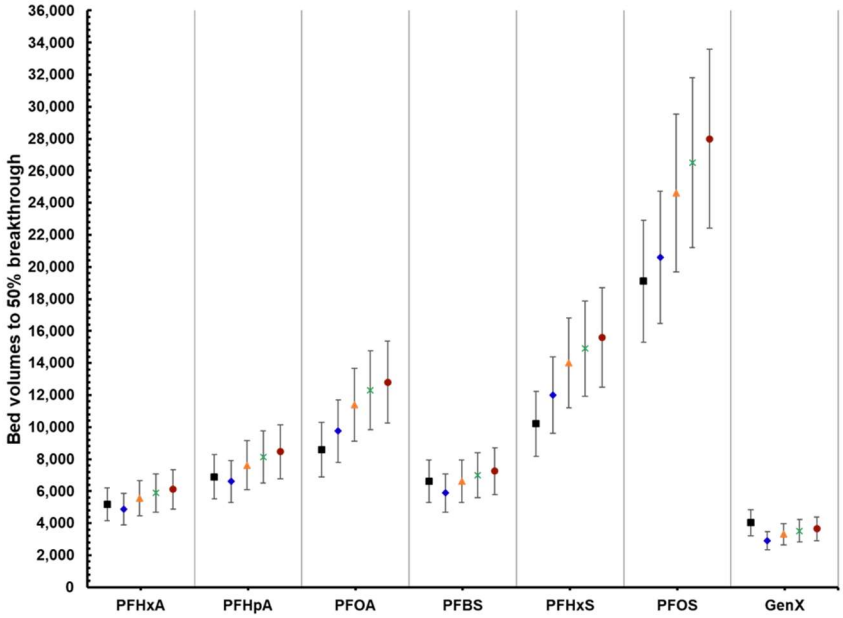

Figure B.19: Comparison of bed volumes to 50% breakthrough for scaled CD-RSSCT PSDM and field-scale. Carbon Carbon C, EBCT: 10 minutes, Pilot data represented by black squares with +/-20% variance, Scaled CD-RSSCT for X=0.0 (blue diamond), X=0.25 (orange triangle) X=0.5 (green x), X=1.0 (red circle) with +/-20% variance.

Table B.13: AdDesignS inputs for Freundlich adsorption capacity and kinetic parameters to compare RSSCT particle size effect, Carbon: Carbon A, EBCT: 10 minutes. TOC = 1.3 mgL^{-1}.

Compound	PD-RSSCT, 100x200 mesh			PD-RSSCT, 200x230 mesh			CD-RSSCT, 200x230 mesh			CD-RSSCT, 230x325 mesh		
	Freundlich adsorption capacity (L/g)	Tortuosity	Surface pore diffusion flux ratio	Freundlich adsorption capacity (L/g)	Tortuosity	Surface pore diffusion flux ratio	Freundlich adsorption capacity (L/g)	Tortuosity	Surface pore diffusion flux ratio	Freundlich adsorption capacity (L/g)	Tortuosity	Surface pore diffusion flux ratio
PFBA	24	1.0	1.0	23	1.0	1.0	10	2.0	1E-30	9	2.0	1E-30
PFPeA	39	1.0	1E-30	39	1.0	1E-30	16	2.0	1E-30	16	2.0	1E-30
PFHxA	68	2.0	1E-30	62	1.0	1E-30	32	3.0	1E-30	30	3.0	1E-30
PFHpA	120	3.0	1E-30	104	3.0	1E-30	37	3.0	1E-30	32	3.0	1E-30
PFOA	160	2.0	1E-30	170	3.0	1E-30	46	3.0	1E-30	42	3.0	1E-30
PFNA	210	2.0	1E-30	230	3.0	1E-30	56	3.0	1E-30	56	3.0	1E-30
PFDA	295	3.0	1E-30	305	3.0	1E-30	76	3.0	1E-30	76	3.0	1E-30
PFBS	85	3.0	1E-30	71	2.0	1E-30	30	2.0	1E-30	30	2.0	1E-30
PFHxS	180	2.0	1E-30	175	3.0	1E-30	57	3.0	1E-30	55	3.0	1E-30
PFOS	300	3.0	1E-30	340	4.0	1E-30	80	2.0	1E-30	70	2.0	1E-30
6:2 FTS	210	2.0	1E-30	210	3.0	1E-30	50	2.0	1E-30	45	2.0	1E-30
PFMOAA	22	1.0	1E-30	22	1.0	1E-30	12	2.0	1E-30	11	2.0	1E-30
PFO2HxA	55	1.0	1E-30	73	2.0	1E-30	38	3.0	1E-30	30	3.0	1E-30
PFO3OA	160	2.0	1E-30	165	2.0	1E-30	56	3.0	1E-30	52	3.0	1E-30
PFO4DA	280	3.0	1E-30	320	3.0	1E-30	88	3.0	1E-30	80	3.0	1E-30
PFO5DoA	--	--	--	--	--	--	130	3.0	1E-30	110	3.0	1E-30
PMPA	20	1.0	1E-30	25	1.0	1E-30	7	2.0	1E-30	6	2.0	1E-30
PEPA	24	1.0	1E-30	29	1.0	1E-30	12	2.0	1E-30	10	2.0	1E-30
GenX	35	1.0	1.0	41	1.0	1E-30	15	2.0	1E-30	14	2.0	1E-30
HydroEve	92	3.0	1E-30	95	3.0	1E-30	28	2.0	1E-30	26	2.0	1E-30
NVHOS	52	1.0	1E-30	62	1.0	1E-30	28	2.0	1E-30	26	2.0	1E-30
Nafion Byproduct 2	160	2.0	1E-30	155	3.0	1E-30	36	2.0	1E-30	35	2.0	1E-30

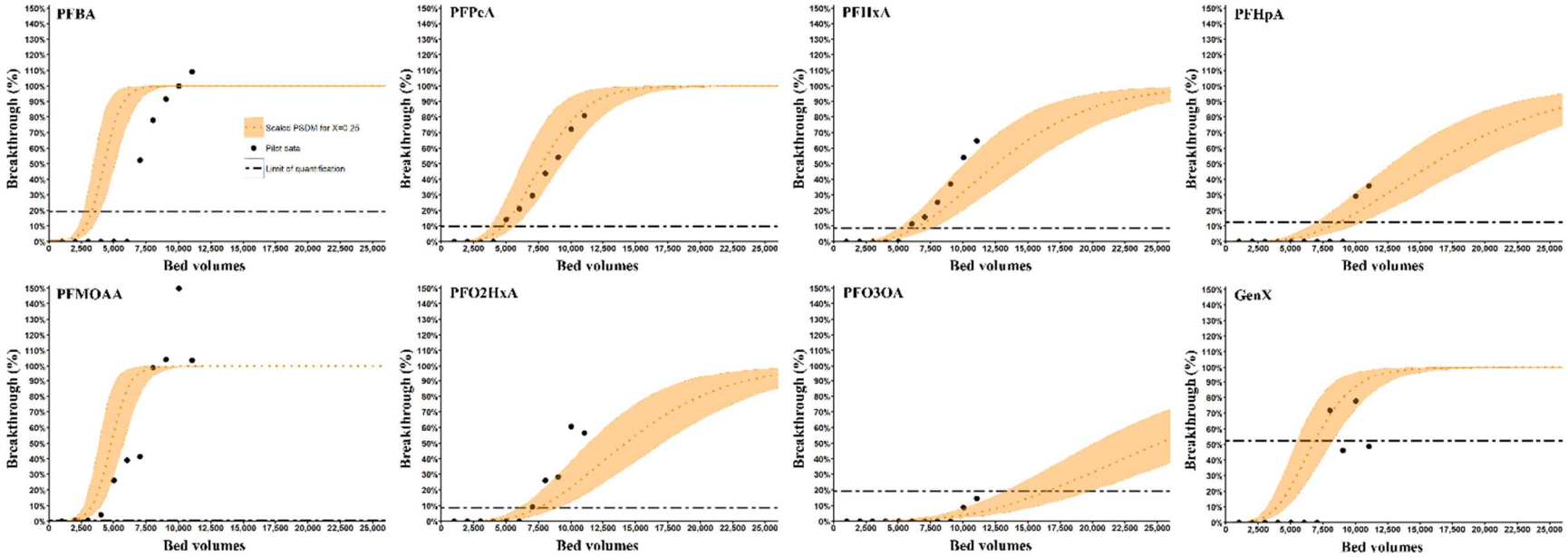

Figure B.20: Prediction of field-scale breakthrough for PSDMs using scaled kinetics assuming X=0.25. Carbon: Carbon A, TOC=2.3 mgL-1, EBCT=20 minutes.

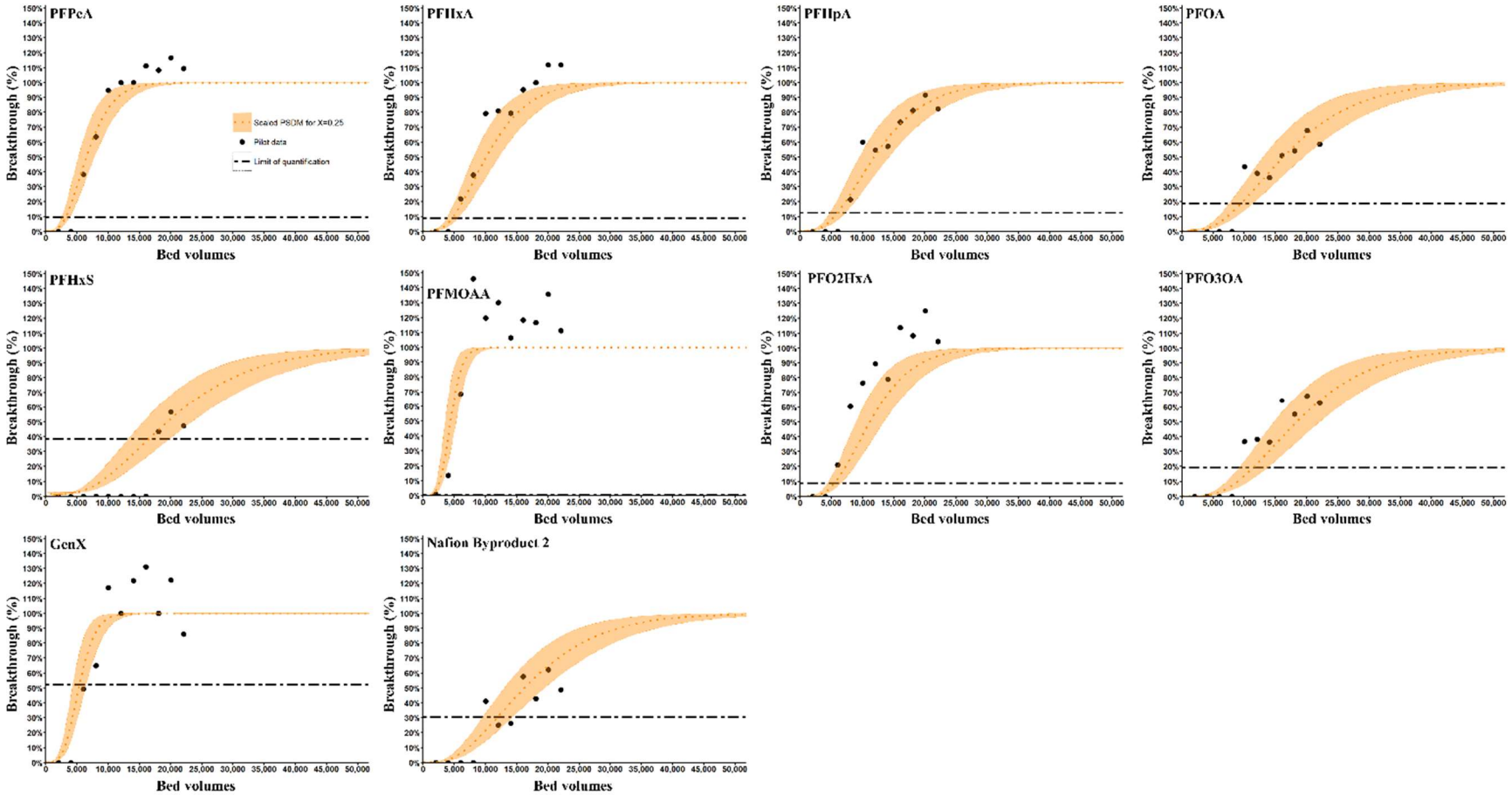

Figure B.21: Prediction of field-scale breakthrough for PSDMs using scaled kinetics assuming X=0.25. Carbon: Carbon B, TOC=2.3 mgL-1, EBCT=10 minutes.

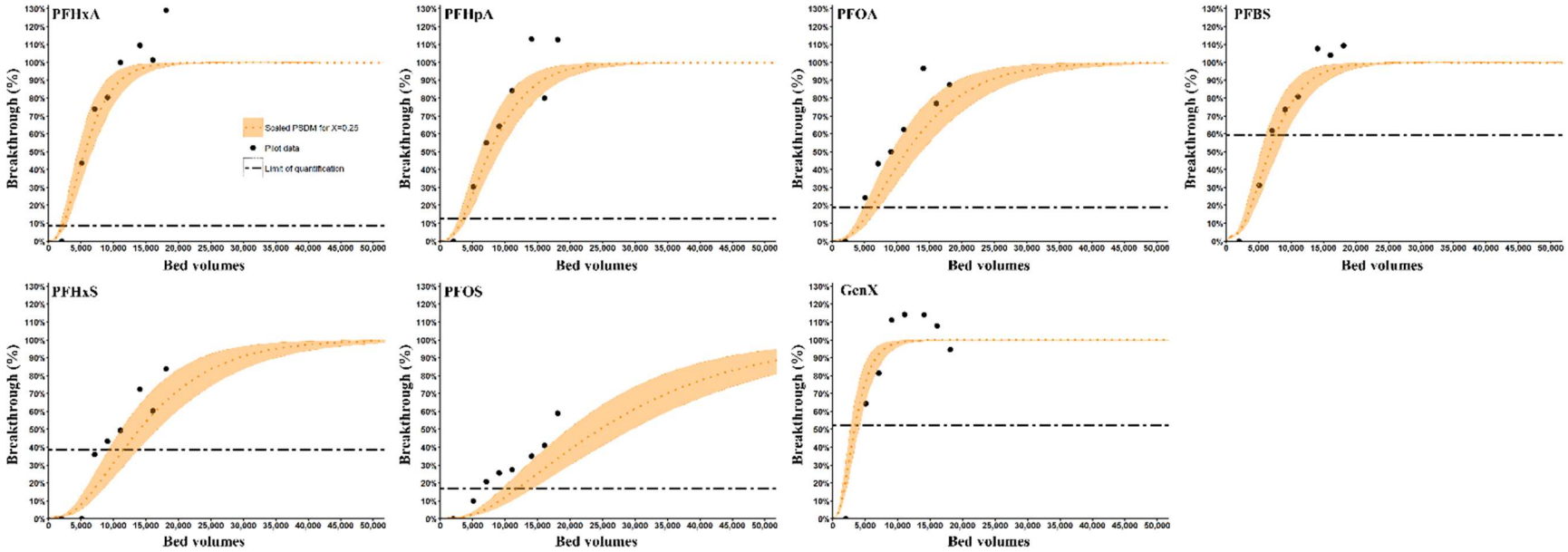

Figure B.22: Prediction of field-scale breakthrough for PSDMs using scaled kinetics assuming X=0.25. Carbon: Carbon C, TOC=2.3 mgL-1, EBCT=10 minutes.

Appendix C: Factors effecting PFAS removal

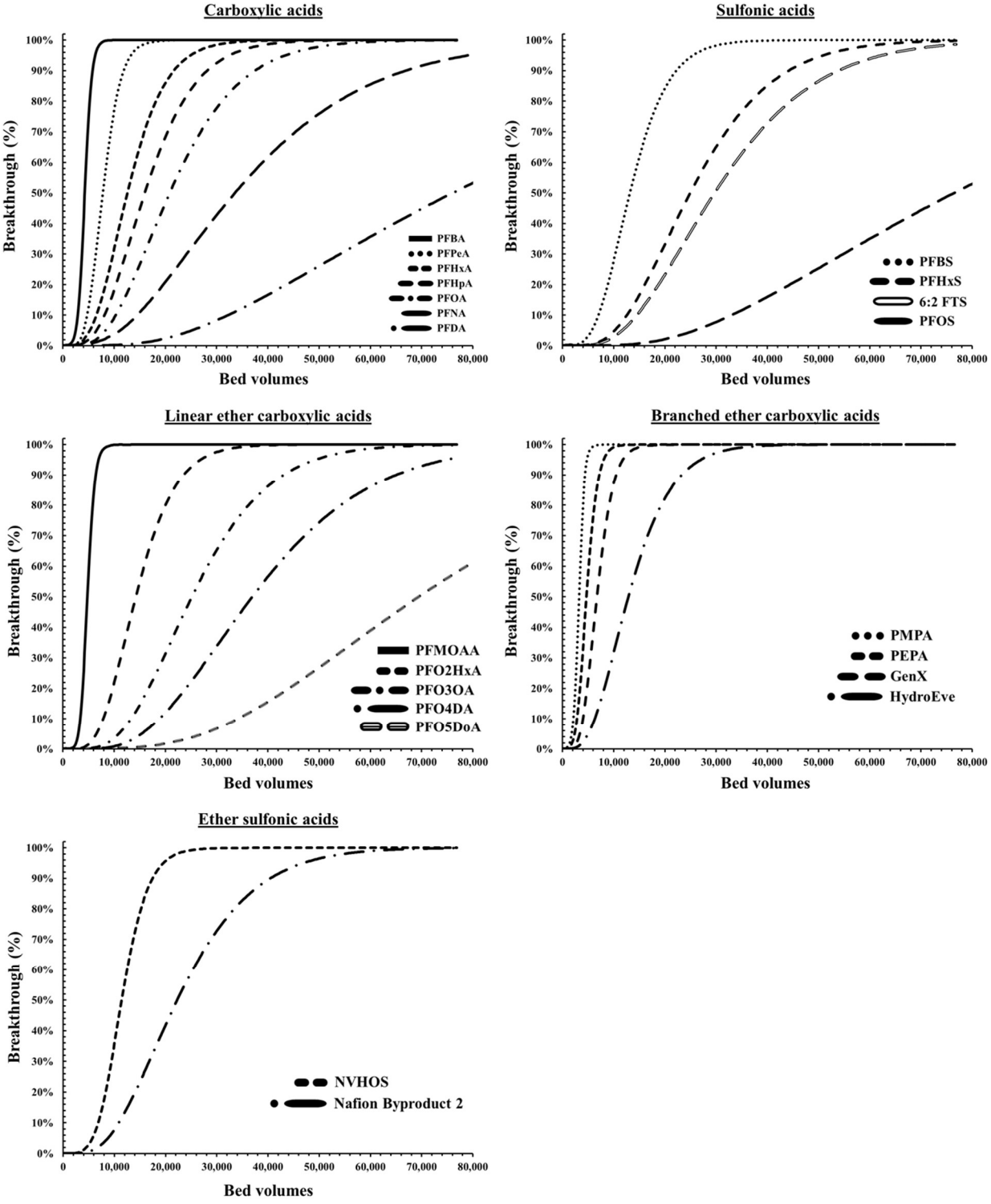

Figure C.1: Breakthrough curves for different classes of PFAS. Carbon: Carbon A, EBCT=20 minutes, TOC= 2.3 mgL^{-1}.

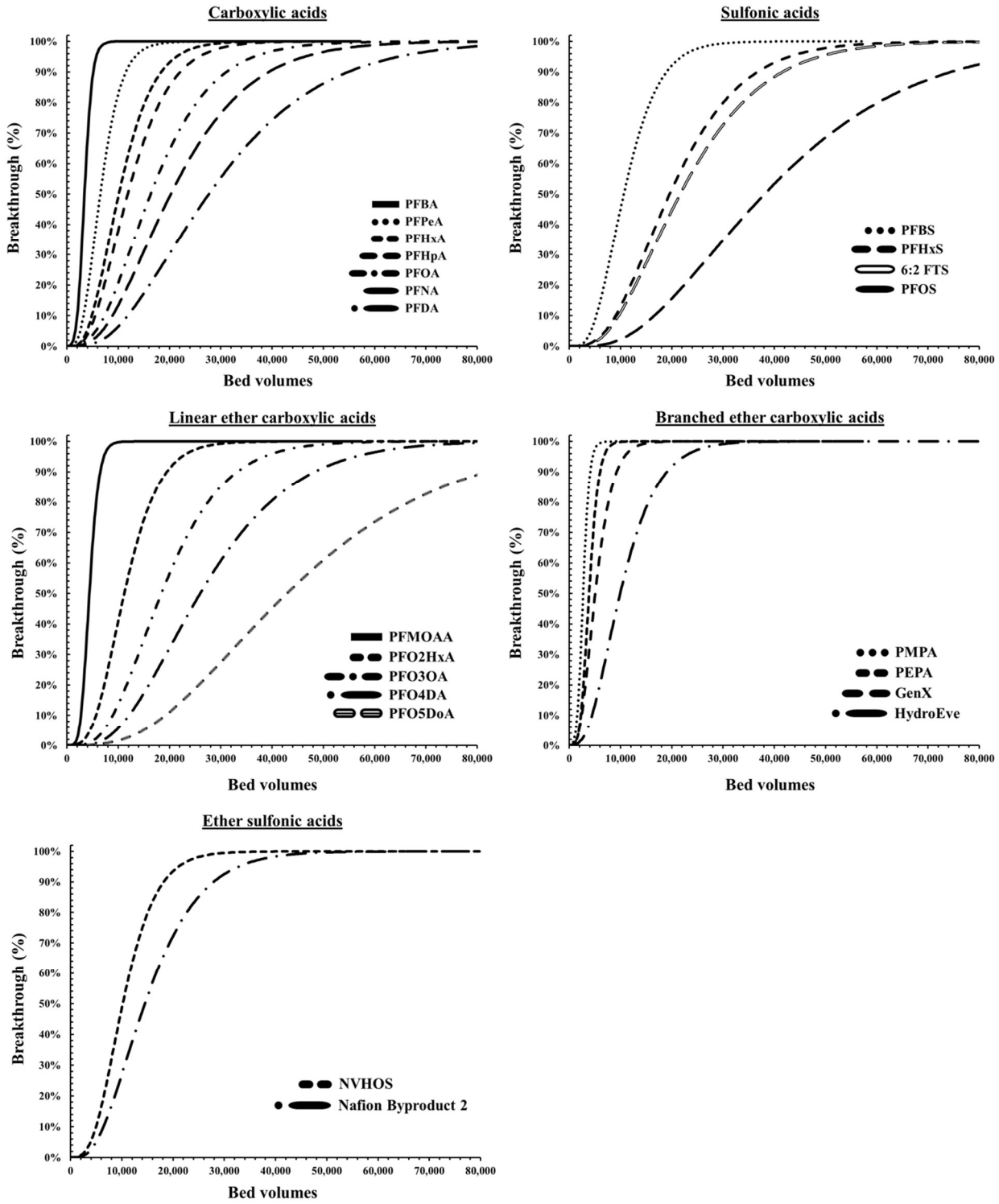

Figure C.2: Breakthrough curves for different classes of PFAS. Carbon: Carbon B, EBCT=10 minutes, TOC= 2.3 mgL^{-1}.

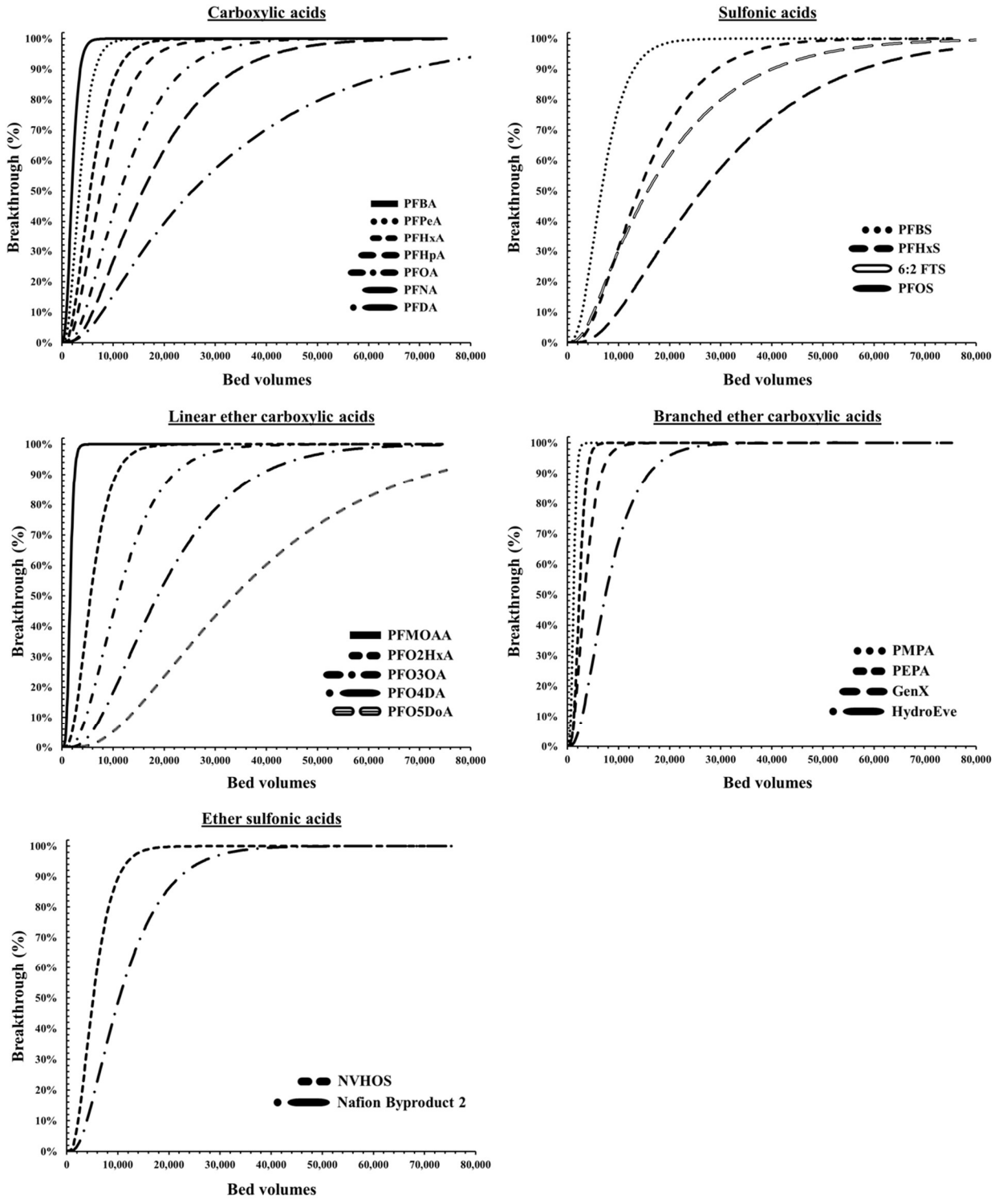

Figure C.3: Breakthrough curves for different classes of PFAS. Carbon: Carbon C, EBCT=10 minutes, TOC= 2.3 mgL^{-1}.

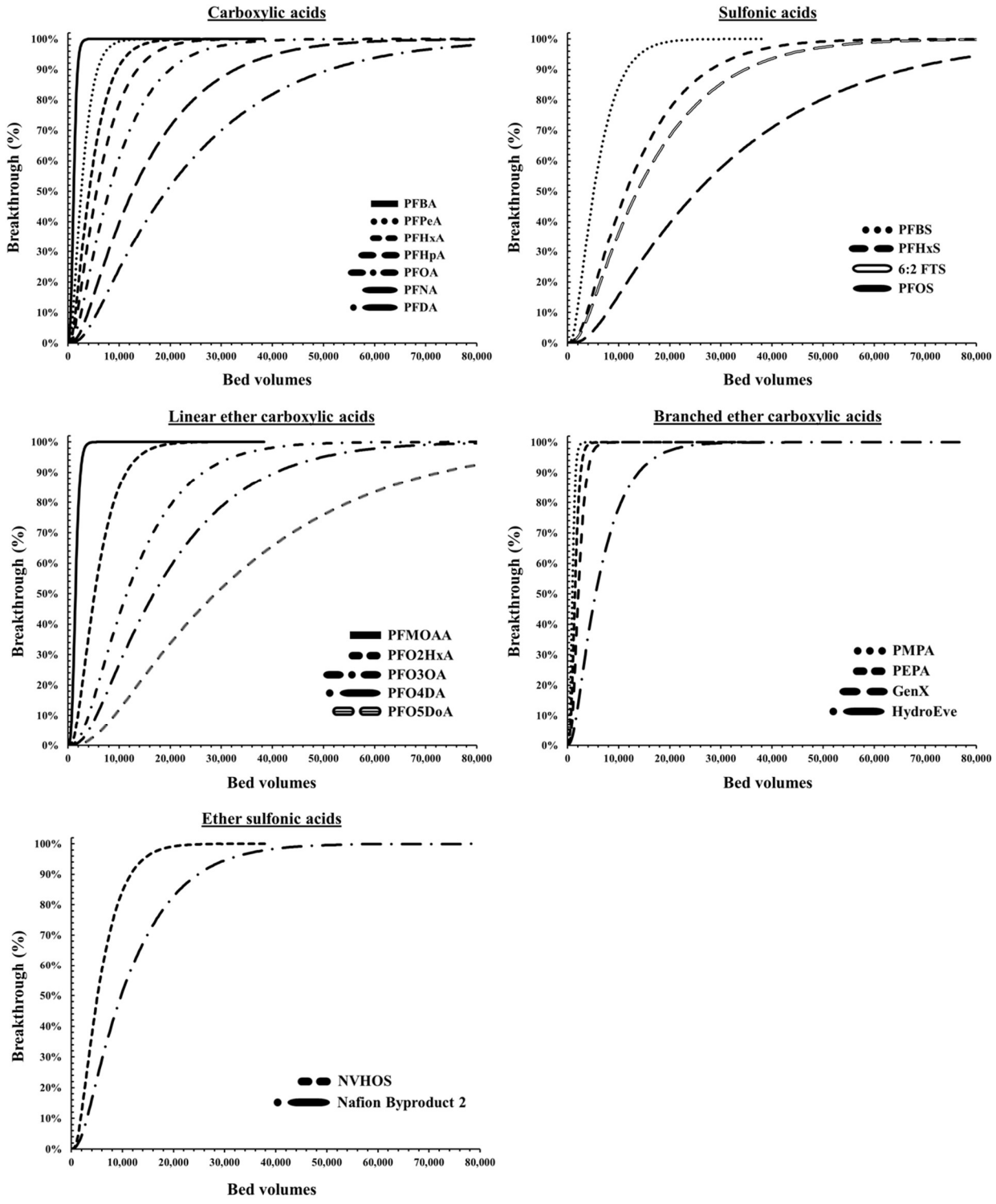

Figure C.4: Breakthrough curves for different classes of PFAS. Carbon: Carbon D, EBCT=10 minutes, TOC= 2.3 mgL^{-1}.

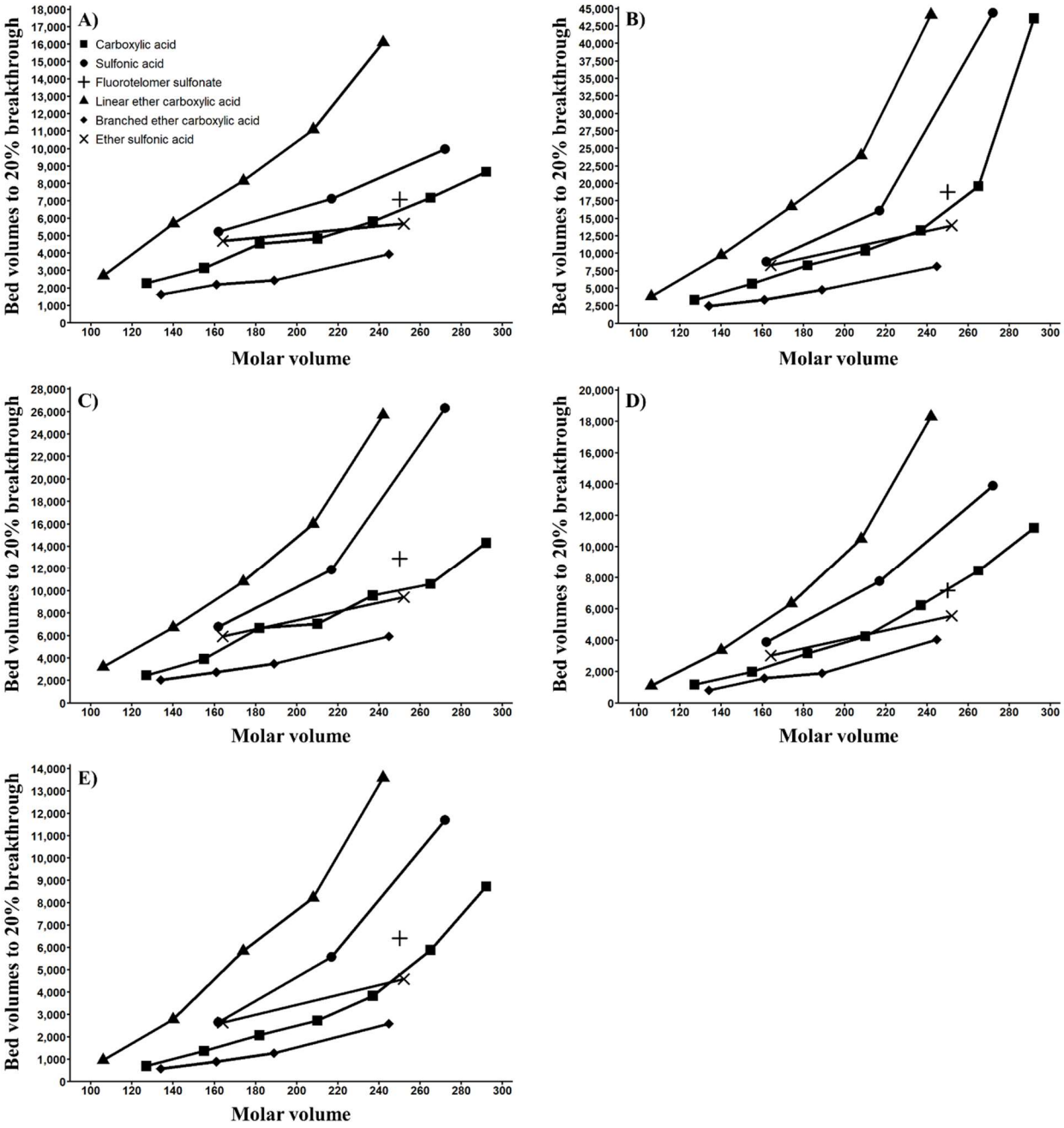

Figure C.5: Effect of molar volume on bed volumes to 20% breakthrough. TOC = 2.3 mgL^{-1}; A) Carbon A, EBCT = 10 minutes, B) Carbon A, EBCT = 20 minutes, C) Carbon B, EBCT = 10 minutes, D) Carbon C, EBCT = 10 minutes, E) Carbon D, EBCT = 10 minutes.

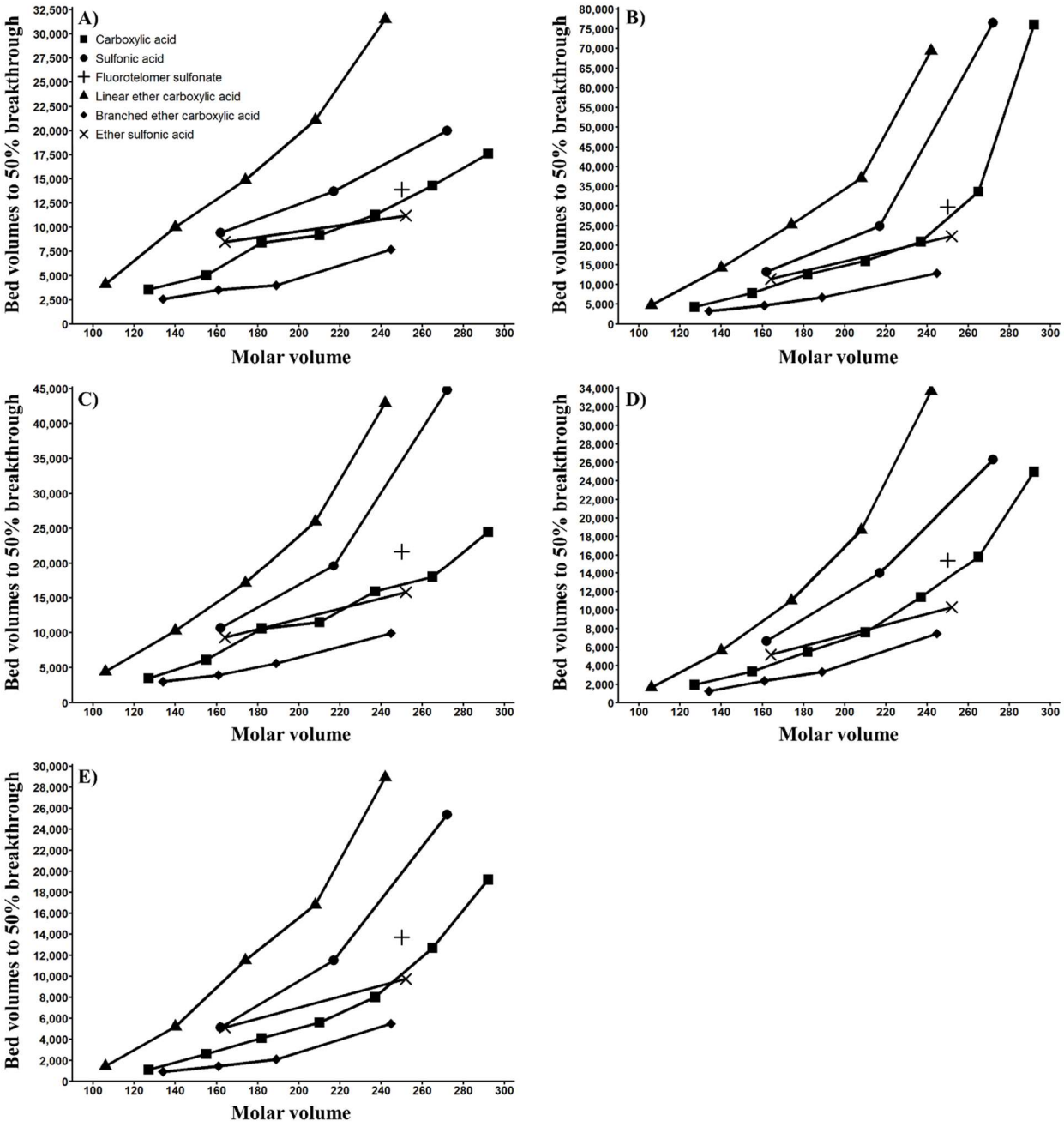

Figure C.6: Effect of molar volume on bed volumes to 50% breakthrough. TOC = 2.3 mgL^{-1}; A) Carbon A, EBCT = 10 minutes, B) Carbon A, EBCT = 20 minutes, C) Carbon B, EBCT = 10 minutes, D) Carbon C, EBCT = 10 minutes, E) Carbon D, EBCT = 10 minutes.

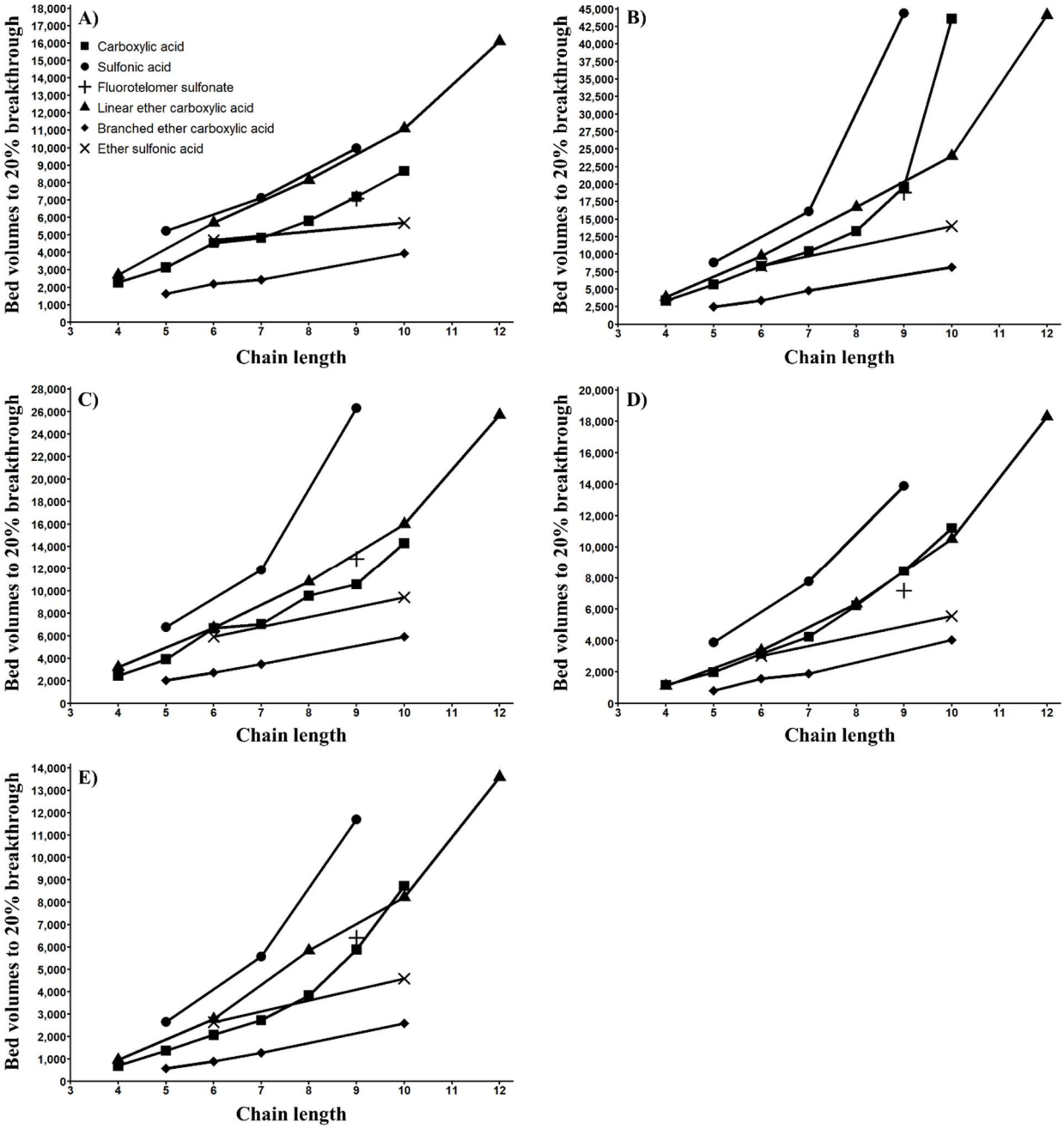

Figure C.7: Effect of chain length on bed volumes to 20% breakthrough. TOC = 2.3 mgL^{-1}; A) Carbon A, EBCT = 10 minutes, B) Carbon A, EBCT = 20 minutes, C) Carbon B, EBCT = 10 minutes, D) Carbon C, EBCT = 10 minutes, E) Carbon D, EBCT = 10 minutes.

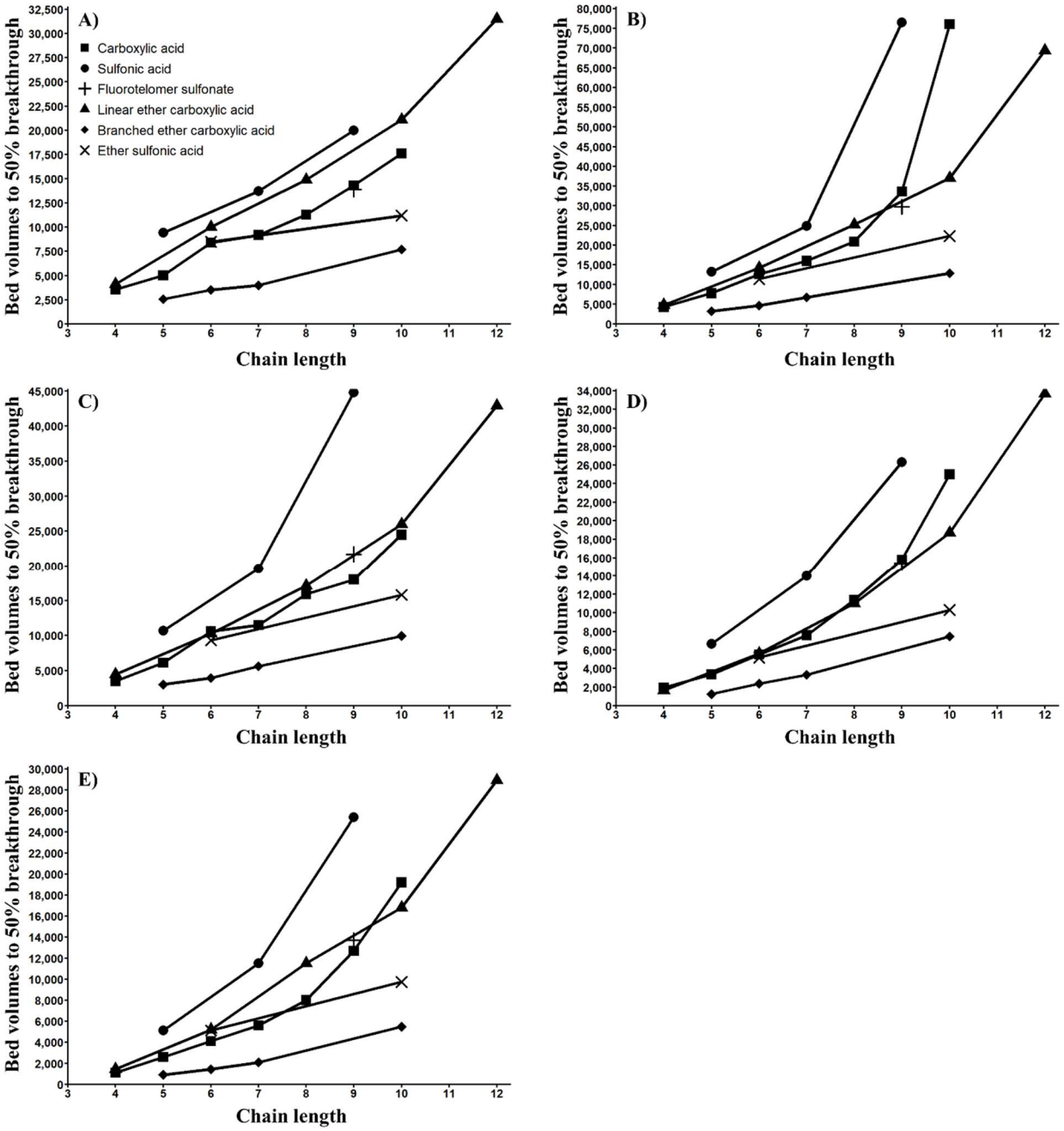

Figure C.8: Effect of chain length on bed volumes to 50% breakthrough. TOC = 2.3 mgL^{-1}; A) Carbon A, EBCT = 10 minutes, B) Carbon A, EBCT = 20 minutes, C) Carbon B, EBCT = 10 minutes, D) Carbon C, EBCT = 10 minutes, E) Carbon D, EBCT = 10 minutes.

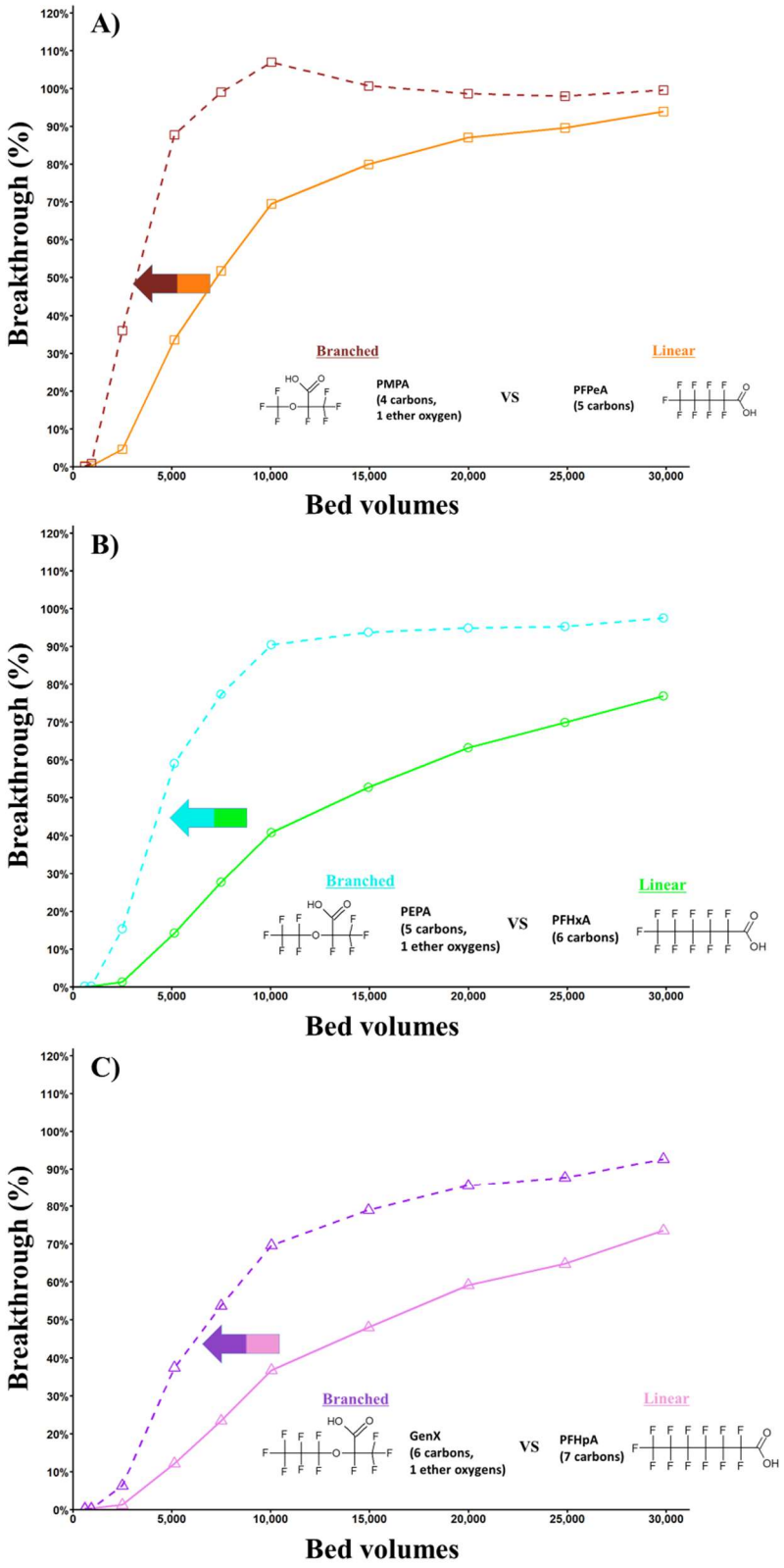

Figure C.9: Effect of branching on PFAS breakthrough. A) PMPA vs PFPeA, B) PEPA vs PFHxA, C) GenX vs PFHpA. Carbon: Carbon A, EBCT = 20 minutes, TOC = 2.3 mgL^{-1}.

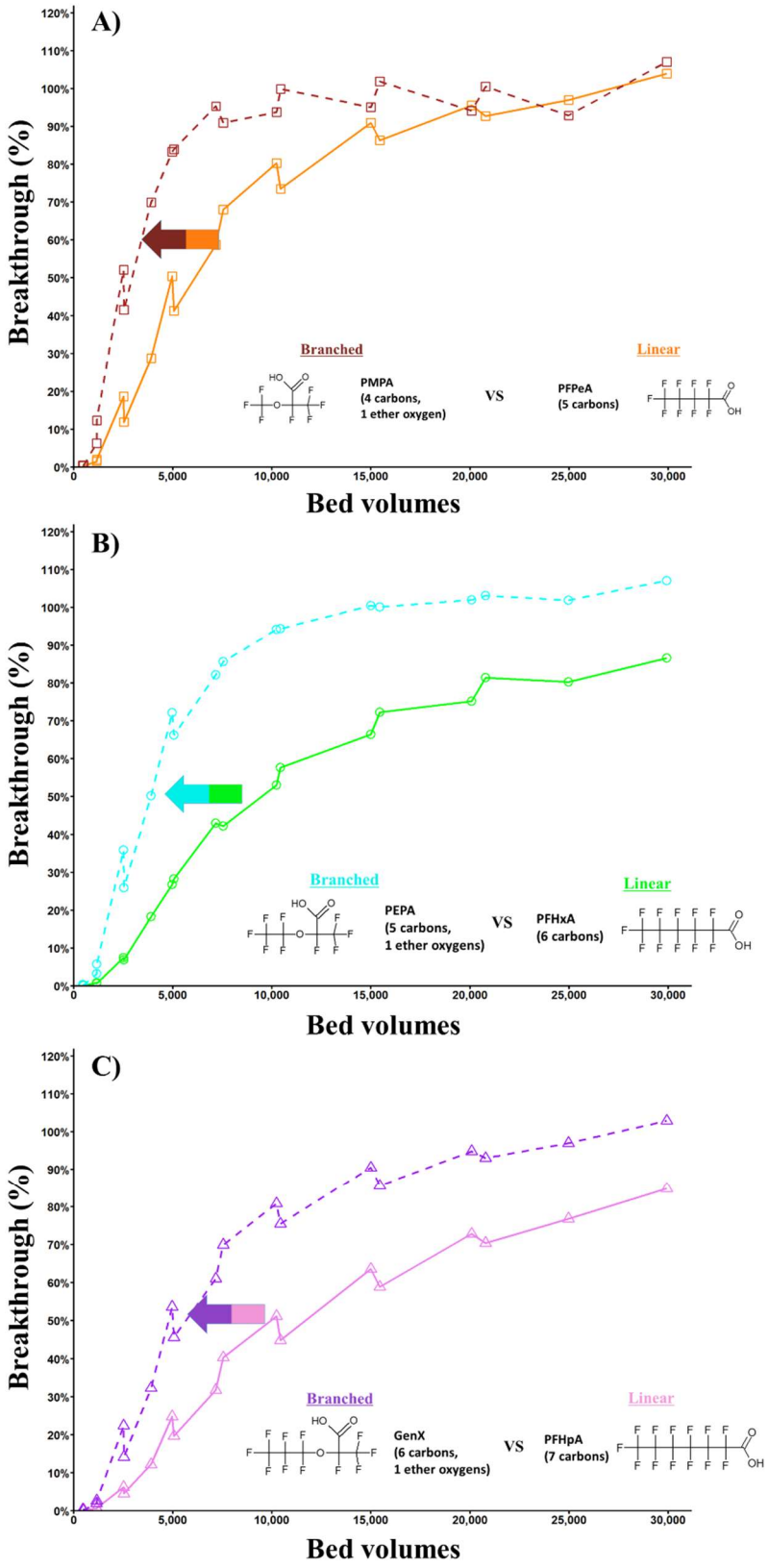

Figure C.10: Effect of branching on PFAS breakthrough. A) PMPA vs PFPeA, B) PEPA vs PFHxA, C) GenX vs PFHpA. Carbon: Carbon B, EBCT = 10 minutes, TOC = 2.3 mgL^{-1}.

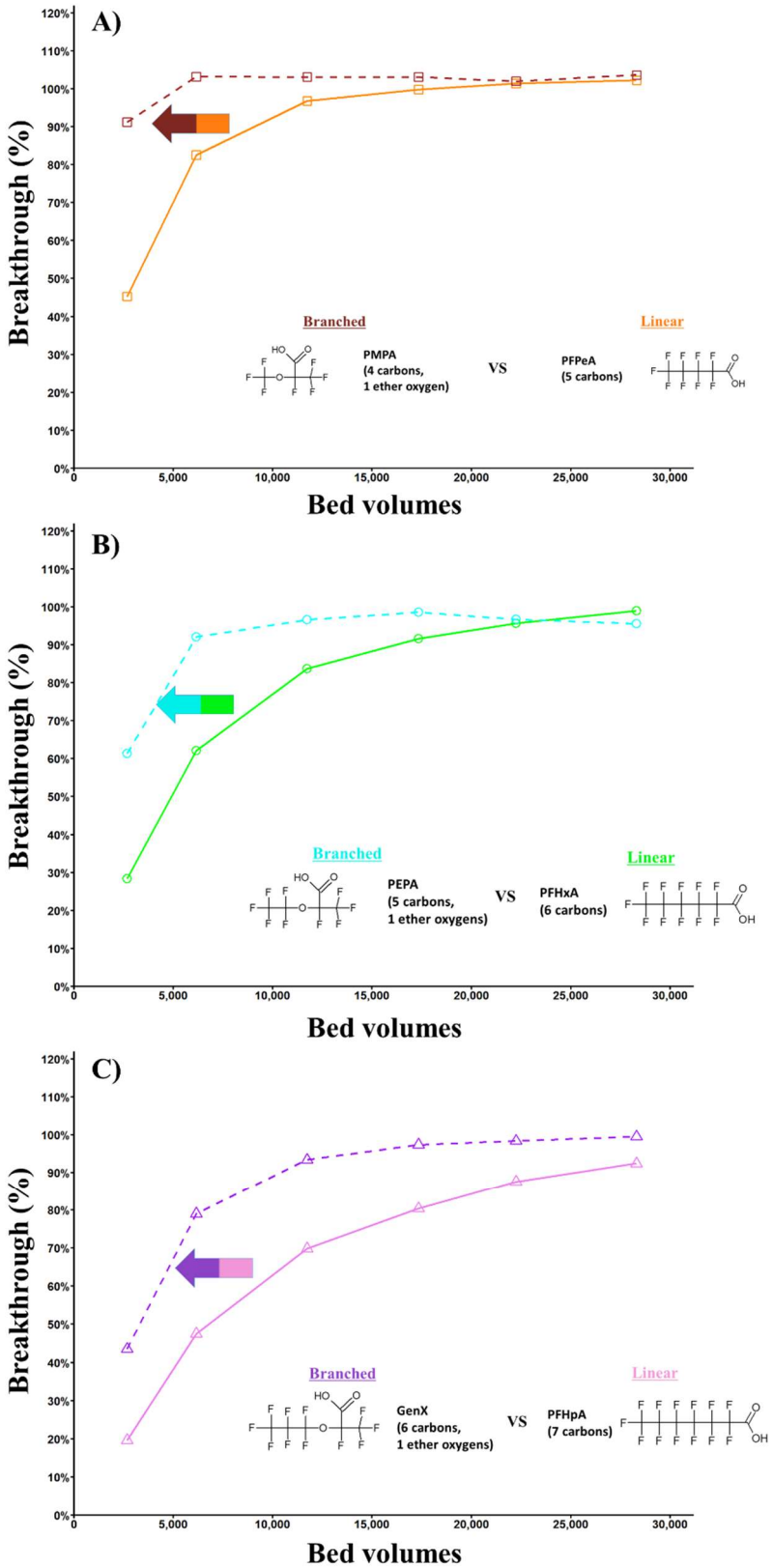

Figure C.11: Effect of branching on PFAS breakthrough. A) PMPA vs PFPeA, B) PEPA vs PFHxA, C) GenX vs PFHpA. Carbon: Carbon C, EBCT = 10 minutes, TOC = 2.3 mgL^{-1}.

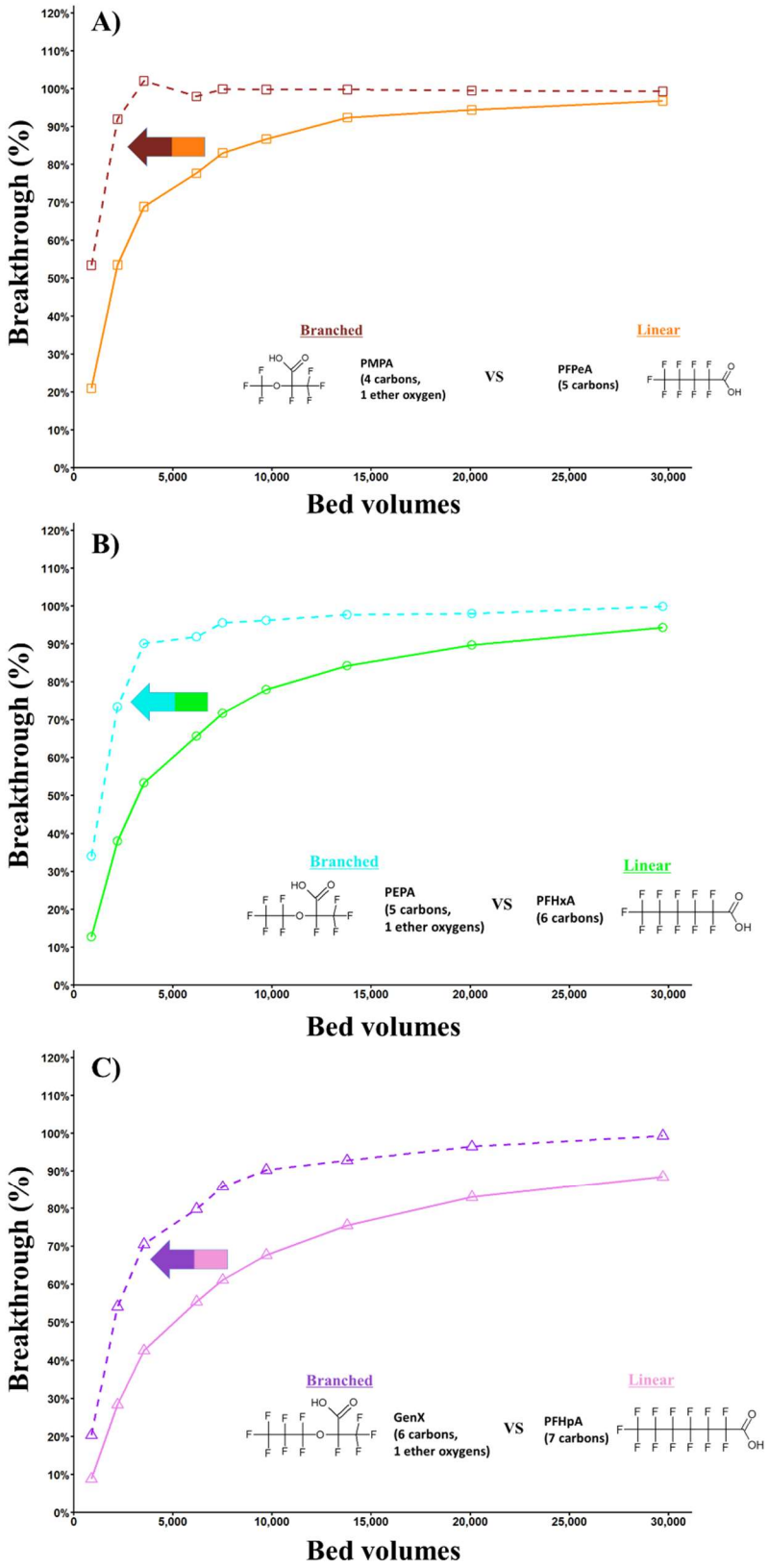

Figure C.12: Effect of branching on PFAS breakthrough. A) PMPA vs PFPeA, B) PEPA vs PFHxA, C) GenX vs PFHpA. Carbon: Carbon D, EBCT = 10 minutes, TOC = 2.3 mgL^{-1}.

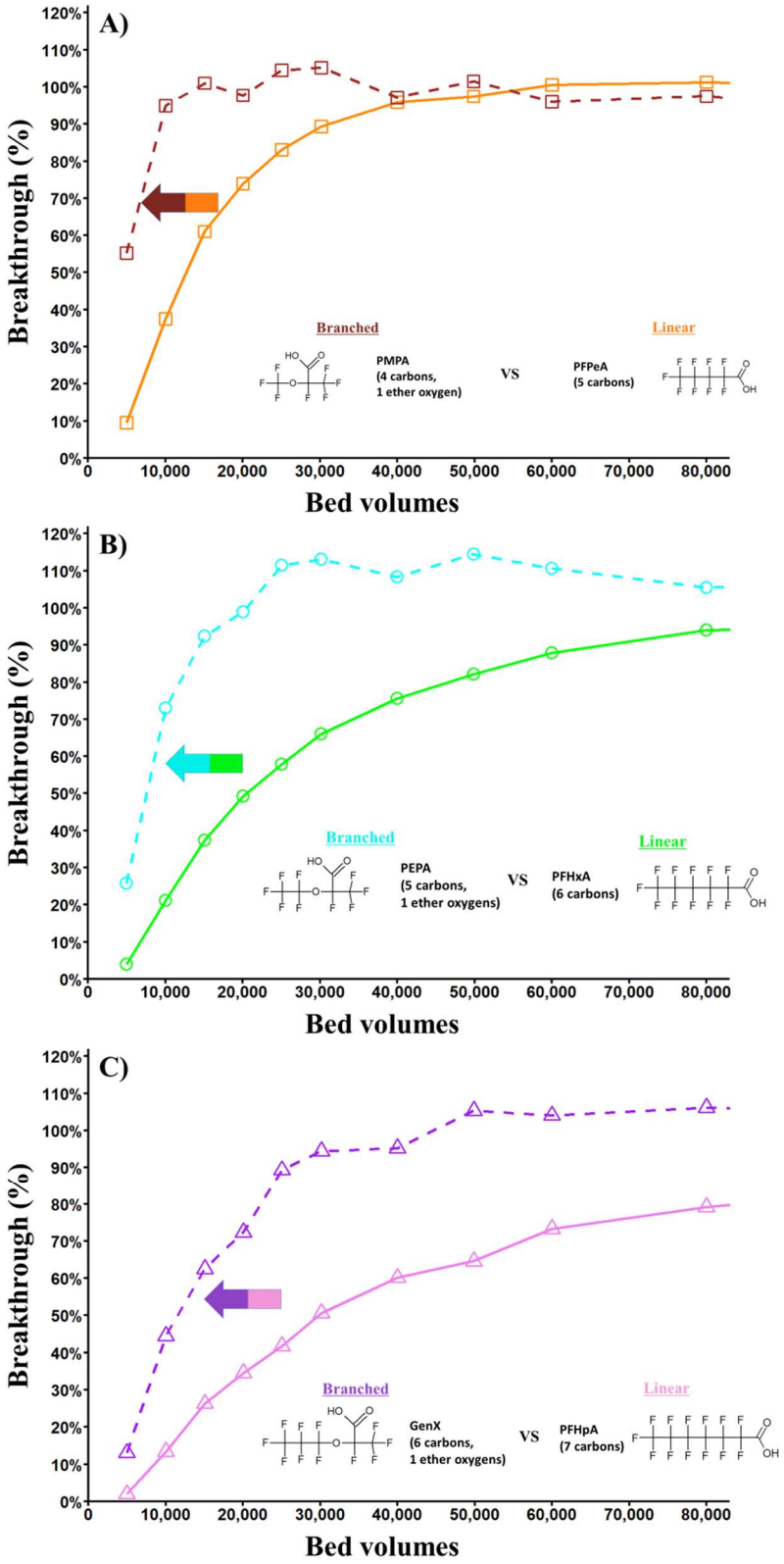

Figure C.13: Effect of branching on PFAS breakthrough. A) PMPA vs PFPeA, B) PEPA vs PFHxA, C) GenX vs PFHpA. Carbon: Carbon A, EBCT = 10 minutes, TOC = 1.3 mgL^{-1}.

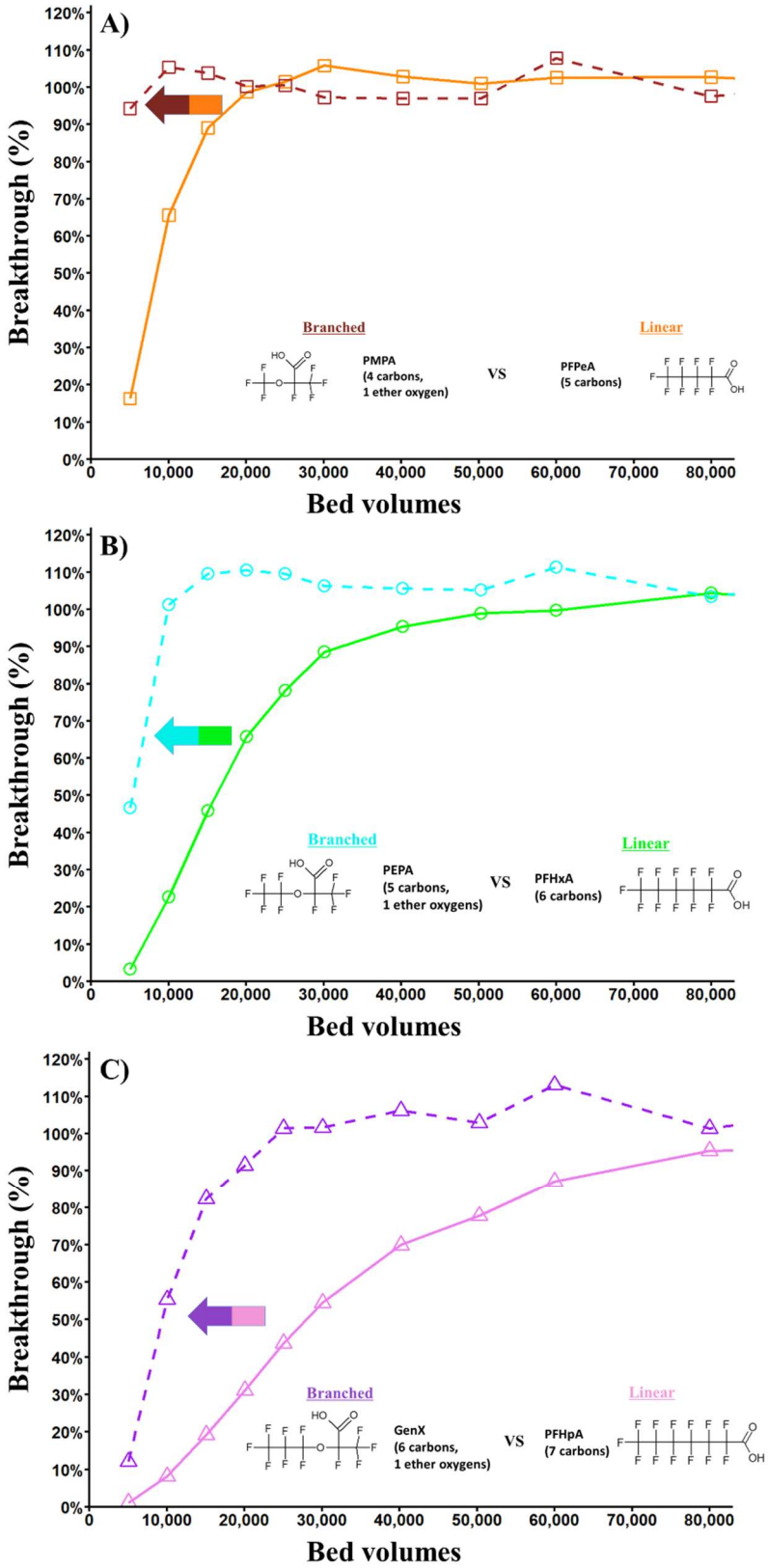

Figure C.14: Effect of branching on PFAS breakthrough. A) PMPA vs PFPeA, B) PEPA vs PFHxA, C) GenX vs PFHpA. Carbon: Carbon C, EBCT = 10 minutes, TOC = 1.3 mgL^{-1}.

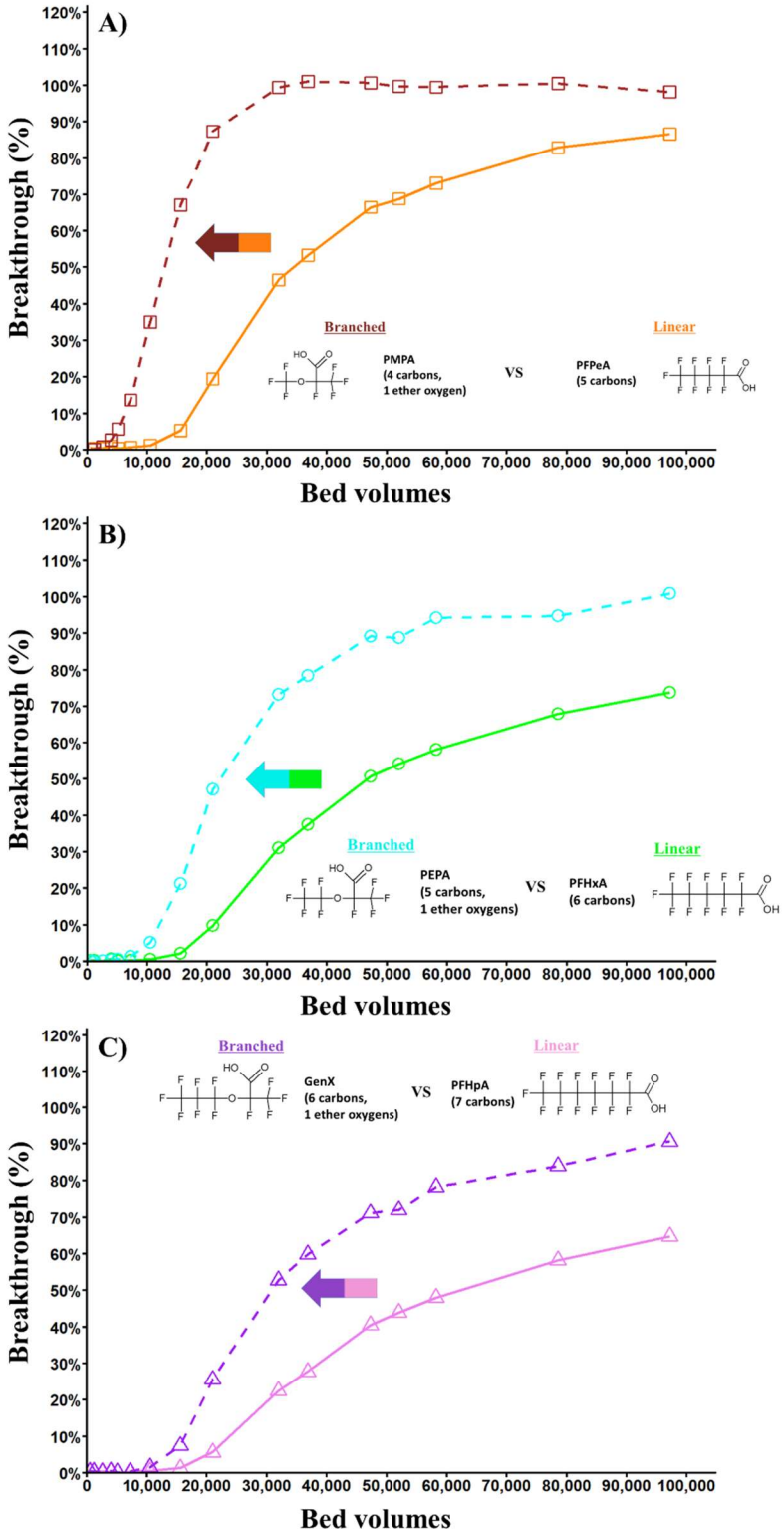

Figure C.15: Effect of branching on PFAS breakthrough. A) PMPA vs PFPeA, B) PEPA vs PFHxA, C) GenX vs PFHpA. Carbon: Carbon A, EBCT = 10 minutes, TOC < 0.5 mgL^{-1}.

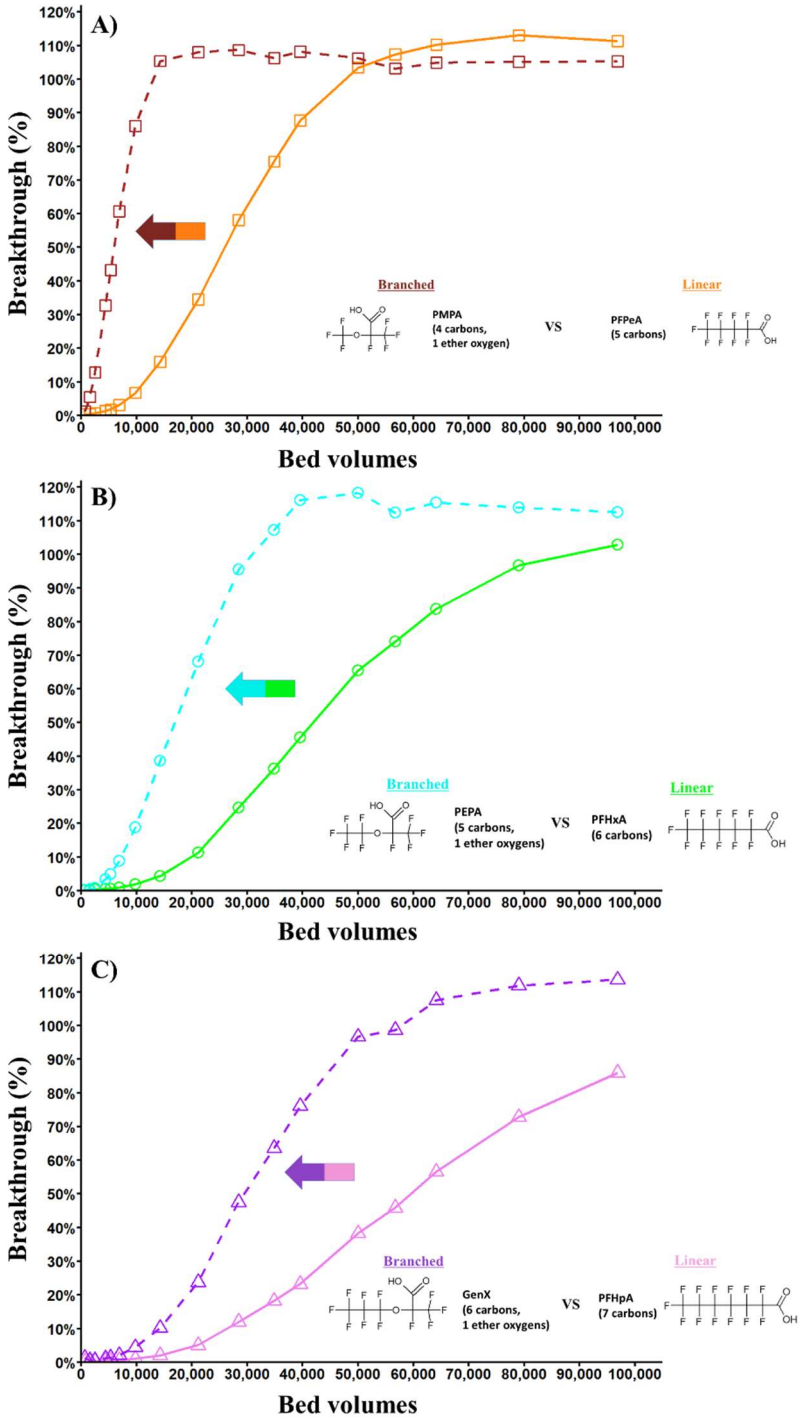

Figure C.16: Effect of branching on PFAS breakthrough. A) PMPA vs PFPeA, B) PEPA vs PFHxA, C) GenX vs PFHpA. Carbon: Carbon C, EBCT = 10 minutes, TOC < 0.5 mgL^{-1}.

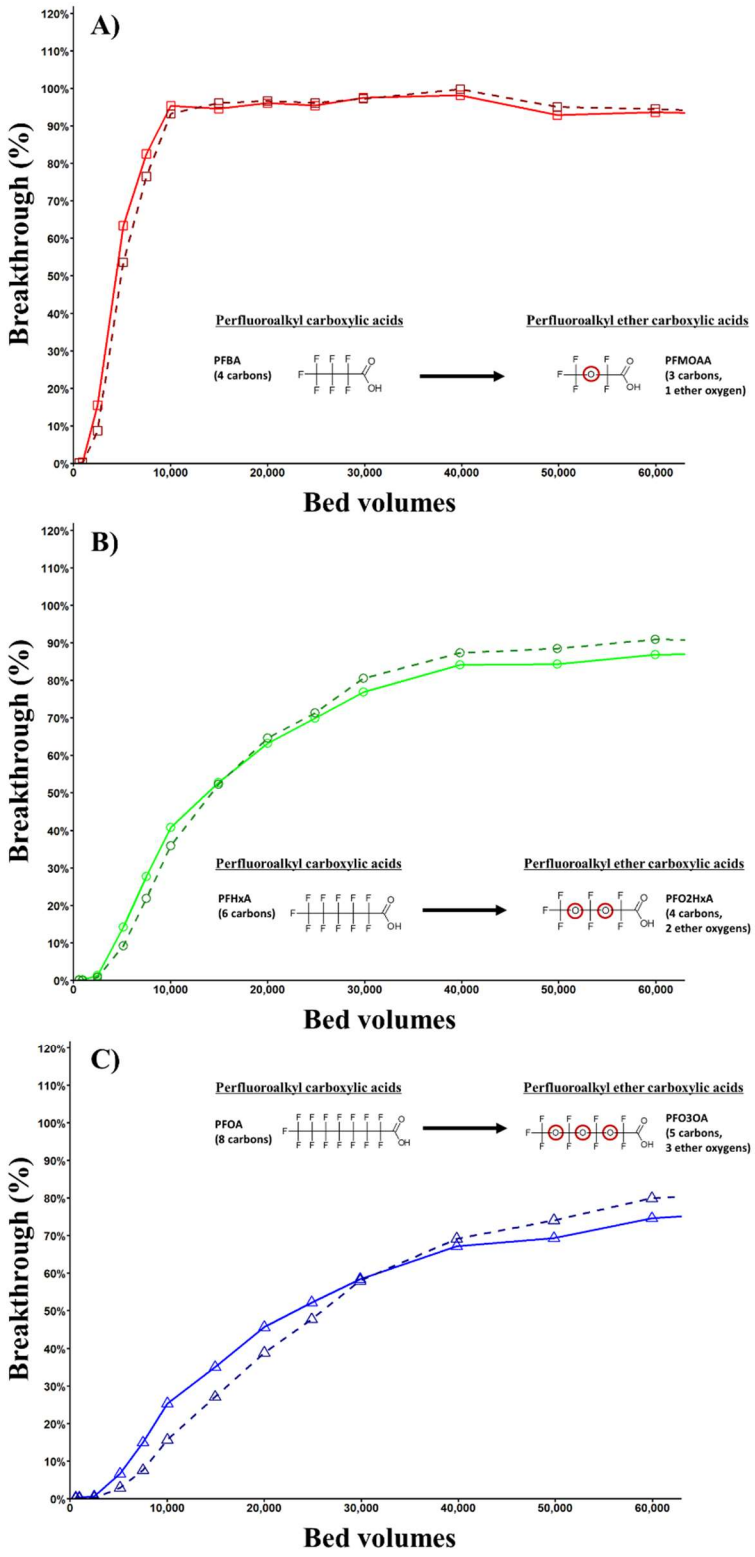

Figure C.17: Effect of incorporation of ether oxygen linkage on PFAS breakthrough. No ether oxygen linkage (Solid line), Ether oxygen linkage (dashed line). A) PFBA vs PFMOAA, B) PFHxA vs PFO2HxA, C) PFOA vs PFO3OA. Carbon: Carbon A, EBCT = 20 minutes, TOC = 2.3 mgL^{-1}.

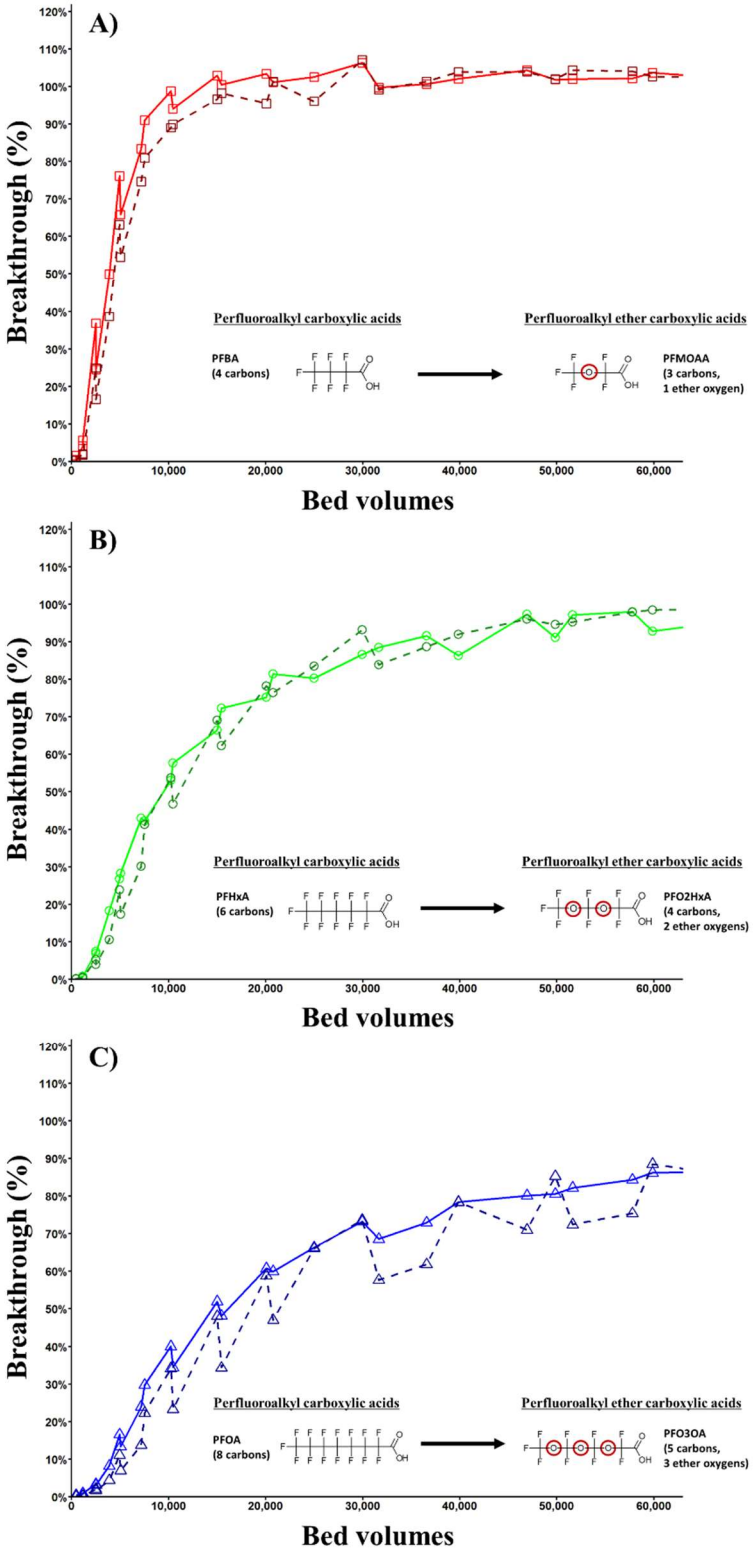

Figure C.18: Effect of incorporation of ether oxygen linkage on PFAS breakthrough. No ether oxygen linkage (Solid line), Ether oxygen linkage (dashed line). A) PFBA vs PFMOAA, B) PFHxA vs PFO2HxA, C) PFOA vs PFO3OA. Carbon: Carbon B, EBCT = 10 minutes, TOC = 2.3 mgL^{-1}.

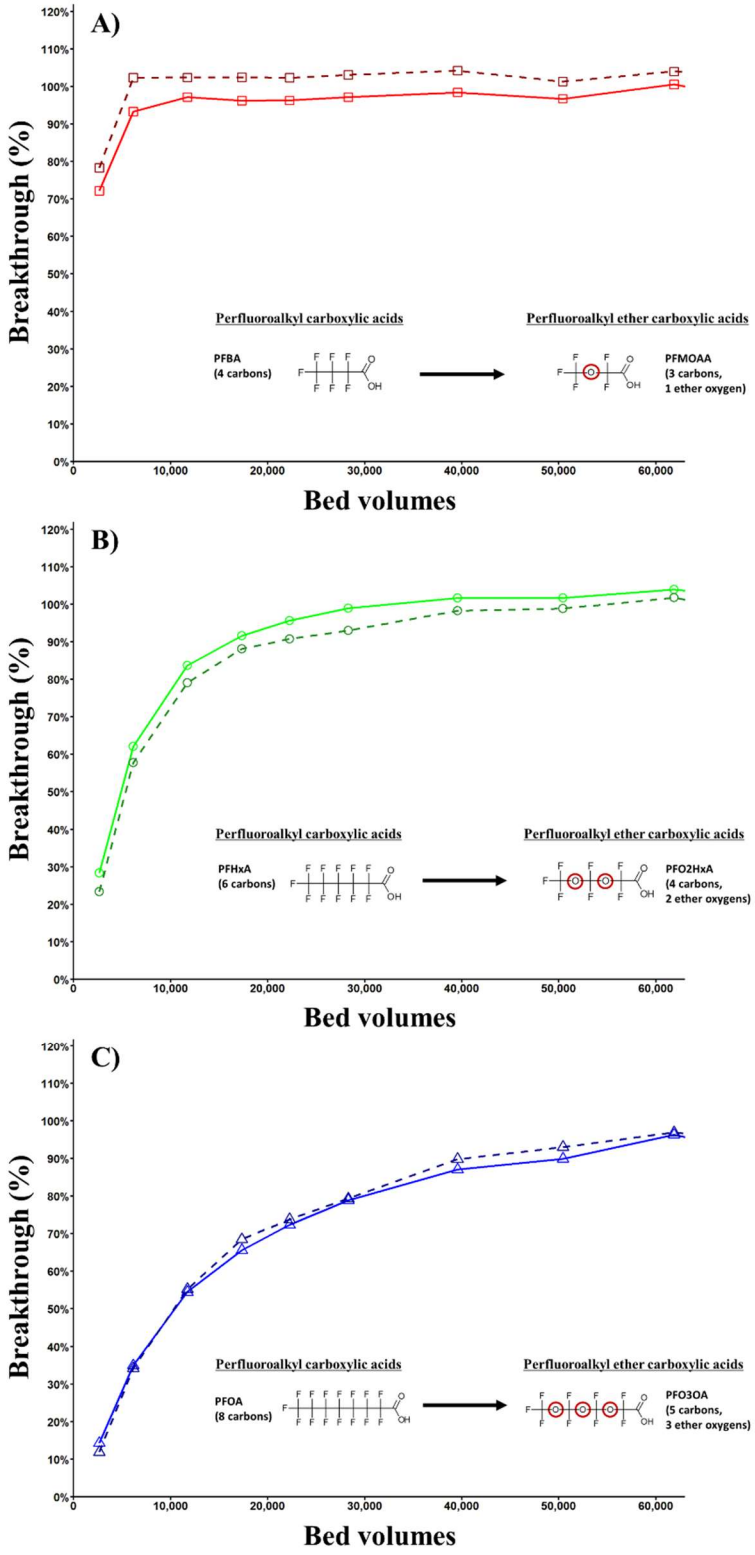

Figure C.19: Effect of incorporation of ether oxygen linkage on PFAS breakthrough. No ether oxygen linkage (Solid line), Ether oxygen linkage (dashed line). A) PFBA vs PFMOAA, B) PFHxA vs PFO2HxA, C) PFOA vs PFO3OA. Carbon: Carbon C, EBCT = 10 minutes, TOC = 2.3 mgL^{-1}.

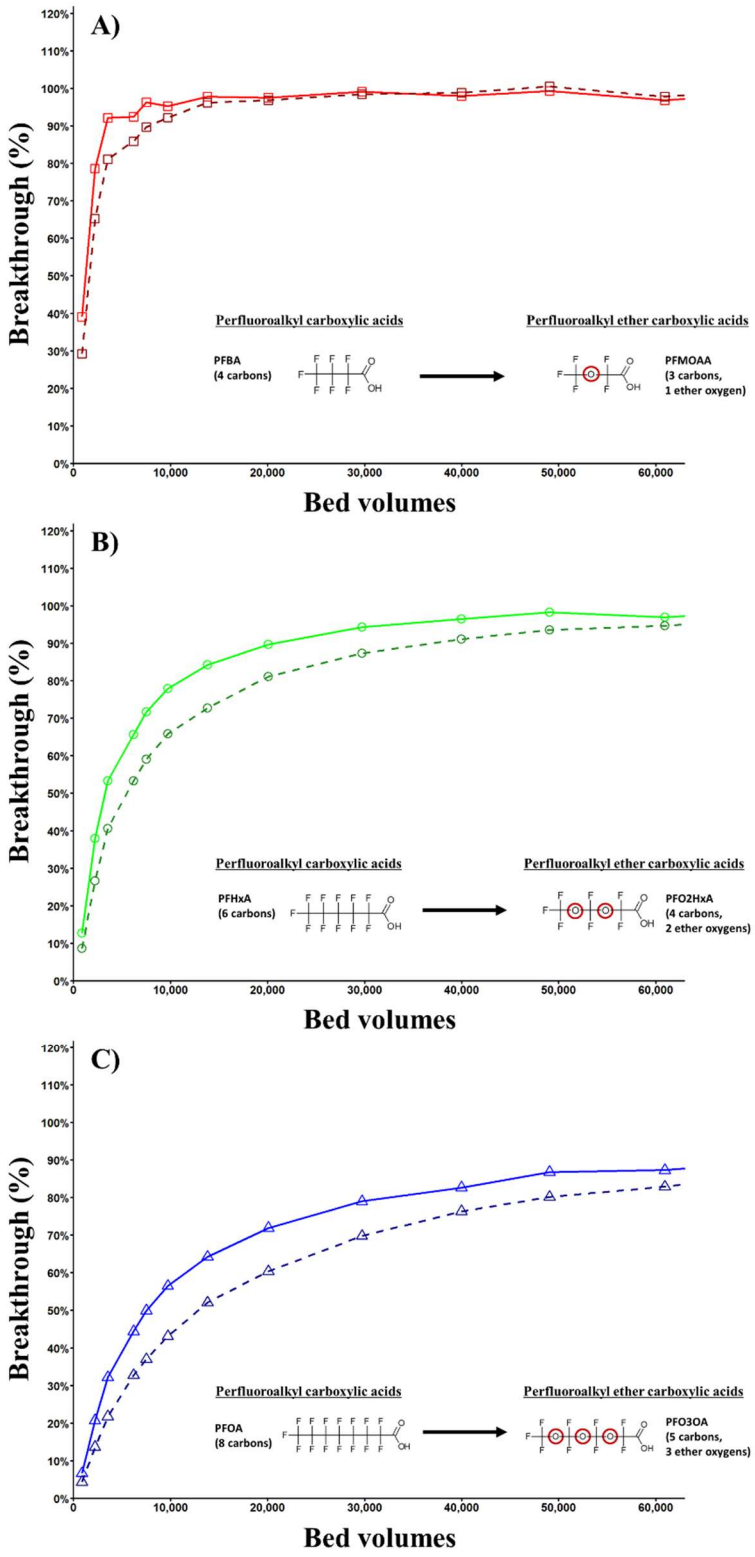

Figure C.20: Effect of incorporation of ether oxygen linkage on PFAS breakthrough. No ether oxygen linkage (Solid line), Ether oxygen linkage (dashed line). A) PFBA vs PFMOAA, B) PFHxA vs PFO2HxA, C) PFOA vs PFO3OA. Carbon: Carbon D, EBCT = 10 minutes, TOC = 2.3 mgL^{-1}.

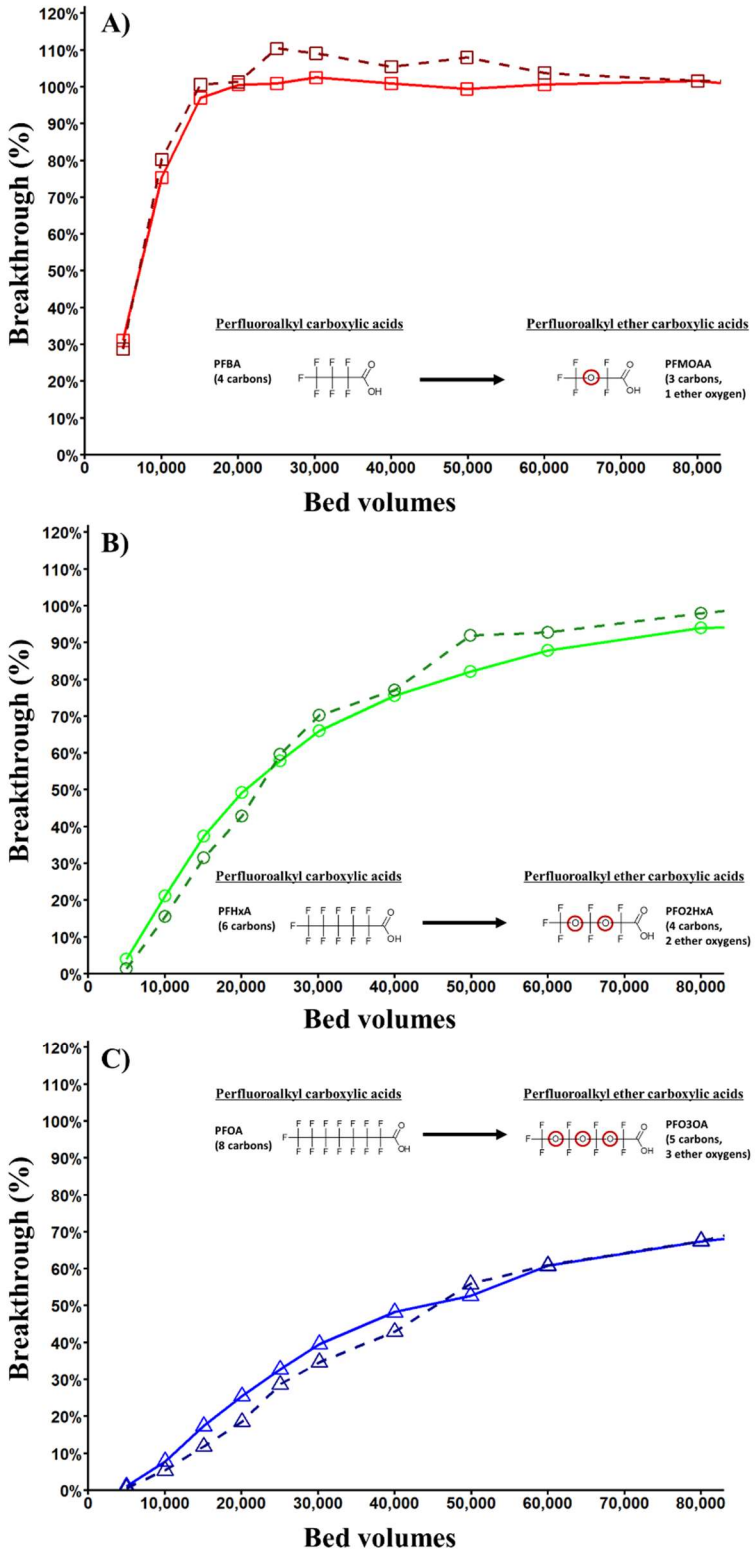

Figure C.21: Effect of incorporation of ether oxygen linkage on PFAS breakthrough. No ether oxygen linkage (Solid line), Ether oxygen linkage (dashed line). A) PFBA vs PFMOAA, B) PFHxA vs PFO2HxA, C) PFOA vs PFO3OA. Carbon: Carbon A, EBCT = 10 minutes, TOC = 1.3 mgL^{-1}.

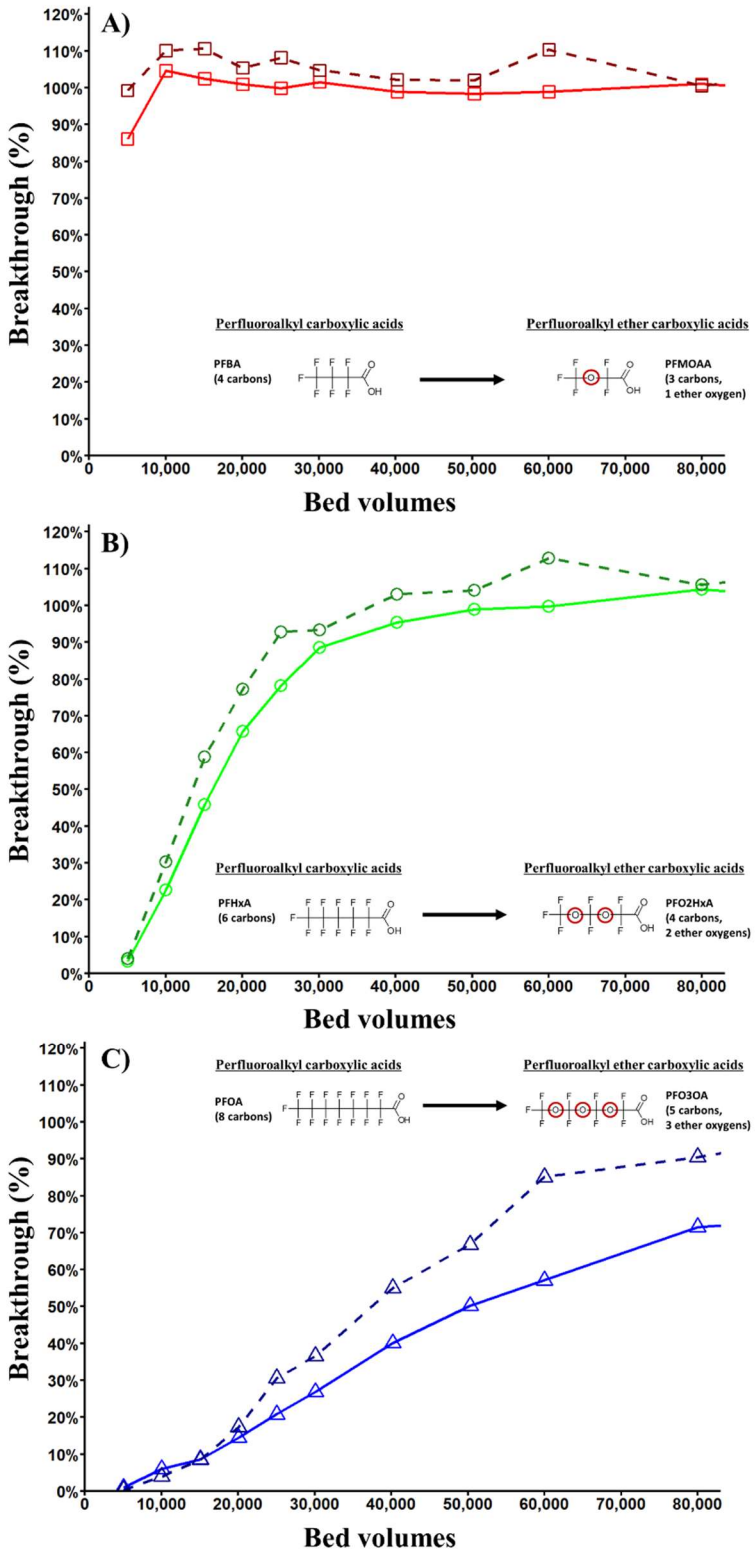

Figure C.22: Effect of incorporation of ether oxygen linkage on PFAS breakthrough. No ether oxygen linkage (Solid line), Ether oxygen linkage (dashed line). A) PFBA vs PFMOAA, B) PFHxA vs PFO2HxA, C) PFOA vs PFO3OA. Carbon: Carbon C, EBCT = 10 minutes, TOC = 1.3 mgL^{-1}.

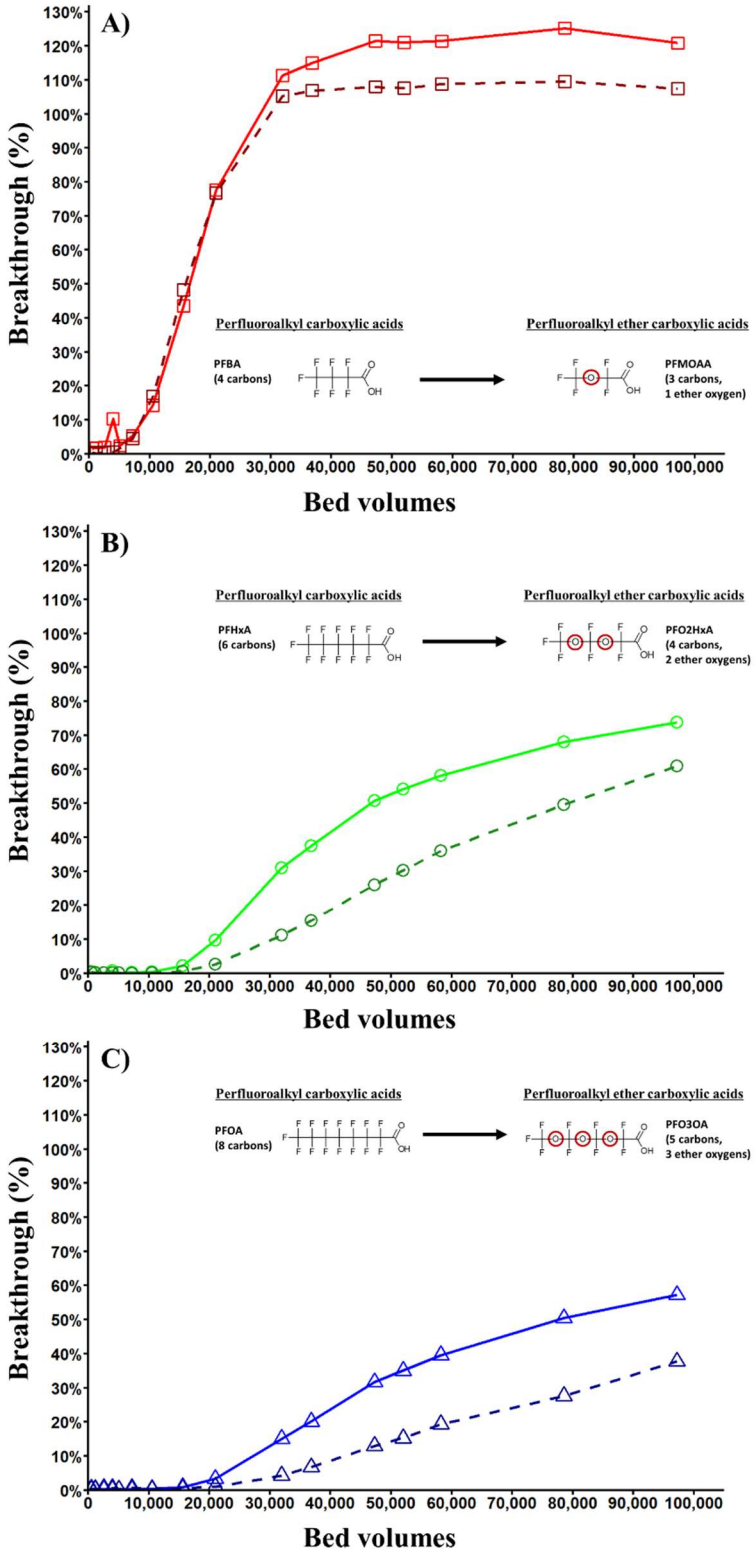

Figure C.23: Effect of incorporation of ether oxygen linkage on PFAS breakthrough. No ether oxygen linkage (Solid line), Ether oxygen linkage (dashed line). A) PFBA vs PFMOAA, B) PFHxA vs PFO2HxA, C) PFOA vs PFO3OA. Carbon: Carbon A, EBCT = 10 minutes, TOC < 0.5 mgL^{-1}.

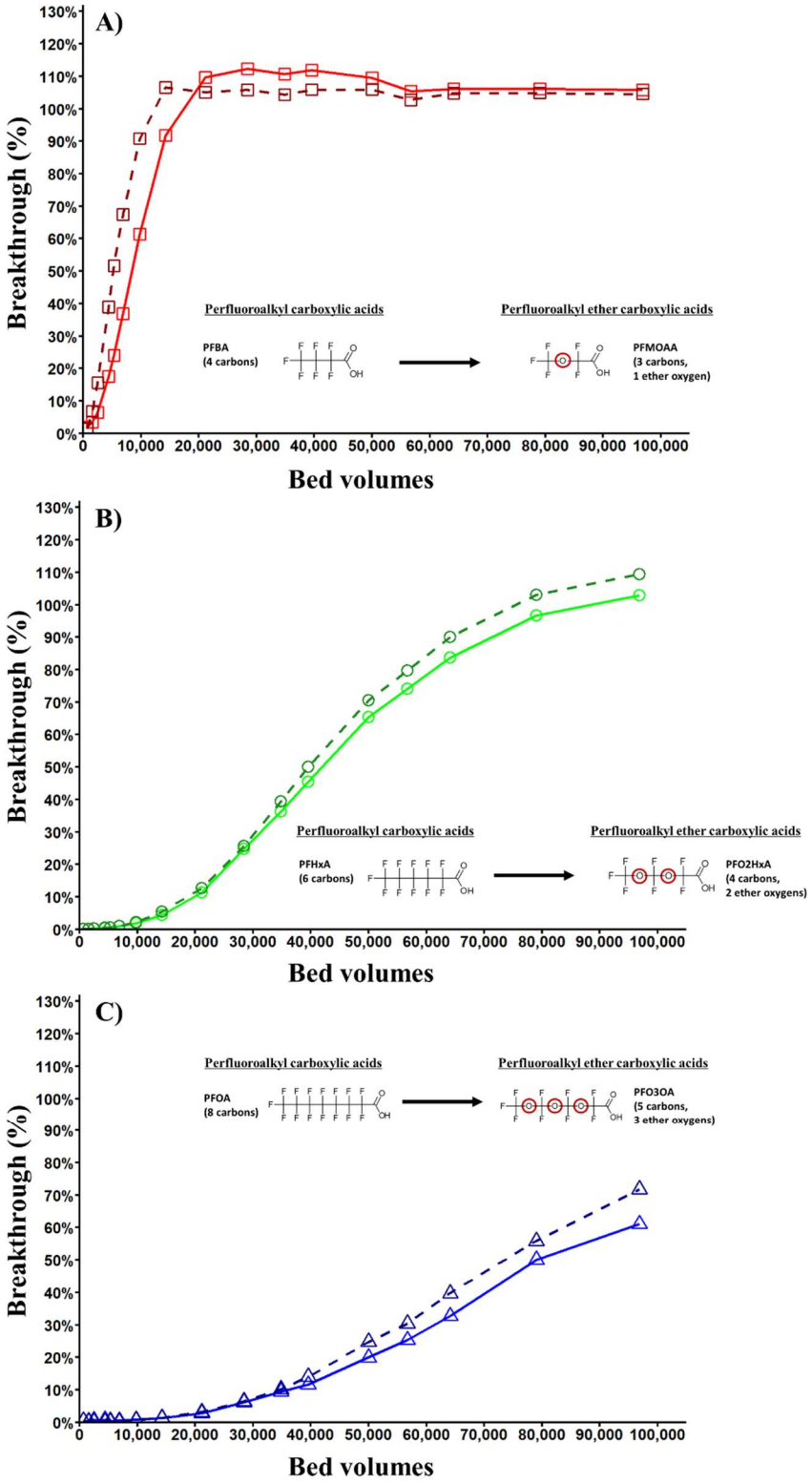

Figure C.24: Effect of incorporation of ether oxygen linkage on PFAS breakthrough. No ether oxygen linkage (Solid line), Ether oxygen linkage (dashed line). A) PFBA vs PFMOAA, B) PFHxA vs PFO2HxA, C) PFOA vs PFO3OA. Carbon: Carbon C, EBCT = 10 minutes, TOC < 0.5 mgL^{-1}.

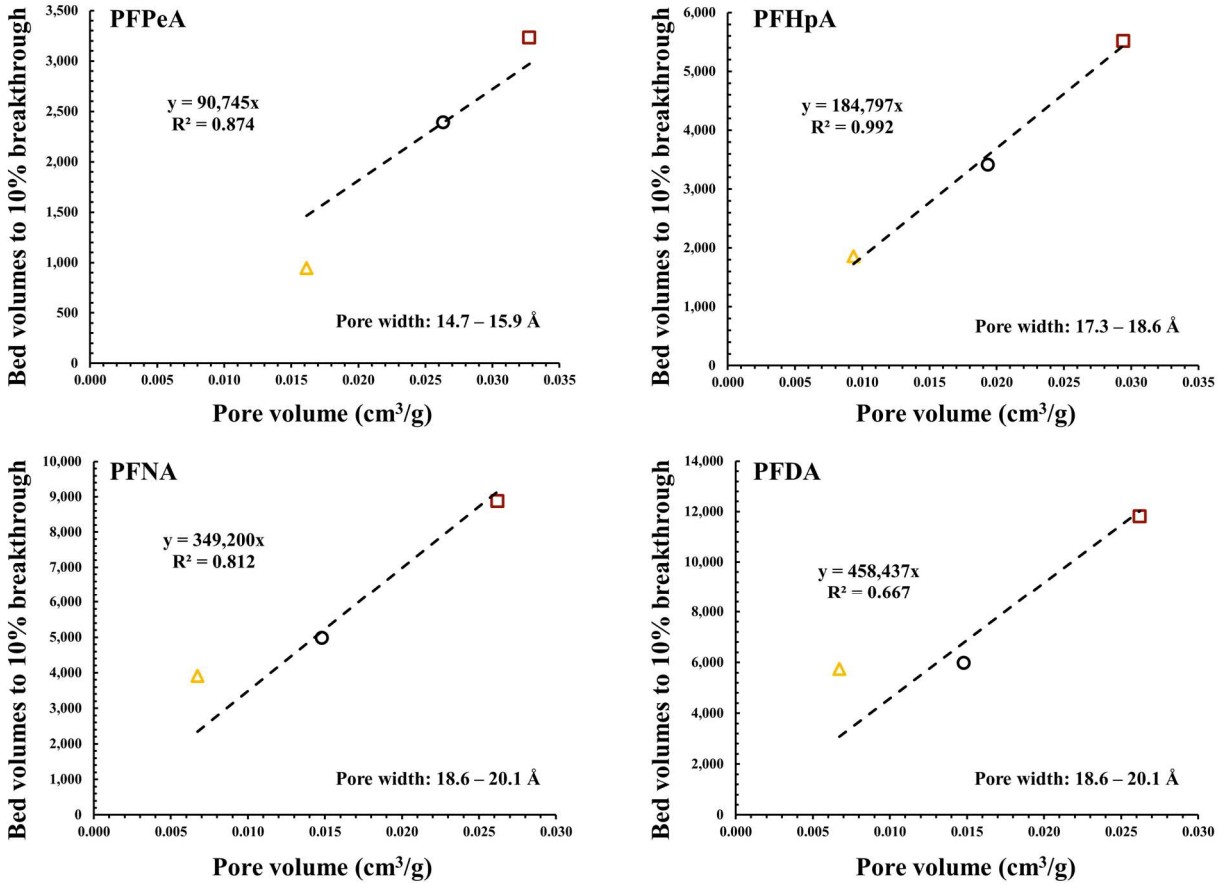

Figure C.25: Relationships between bed volumes to 10% breakthrough and pore volumes in the secondary micropore range in coagulated/settled surface water. Carbon A (black circle), Carbon B (red square), Carbon D (yellow triangle).

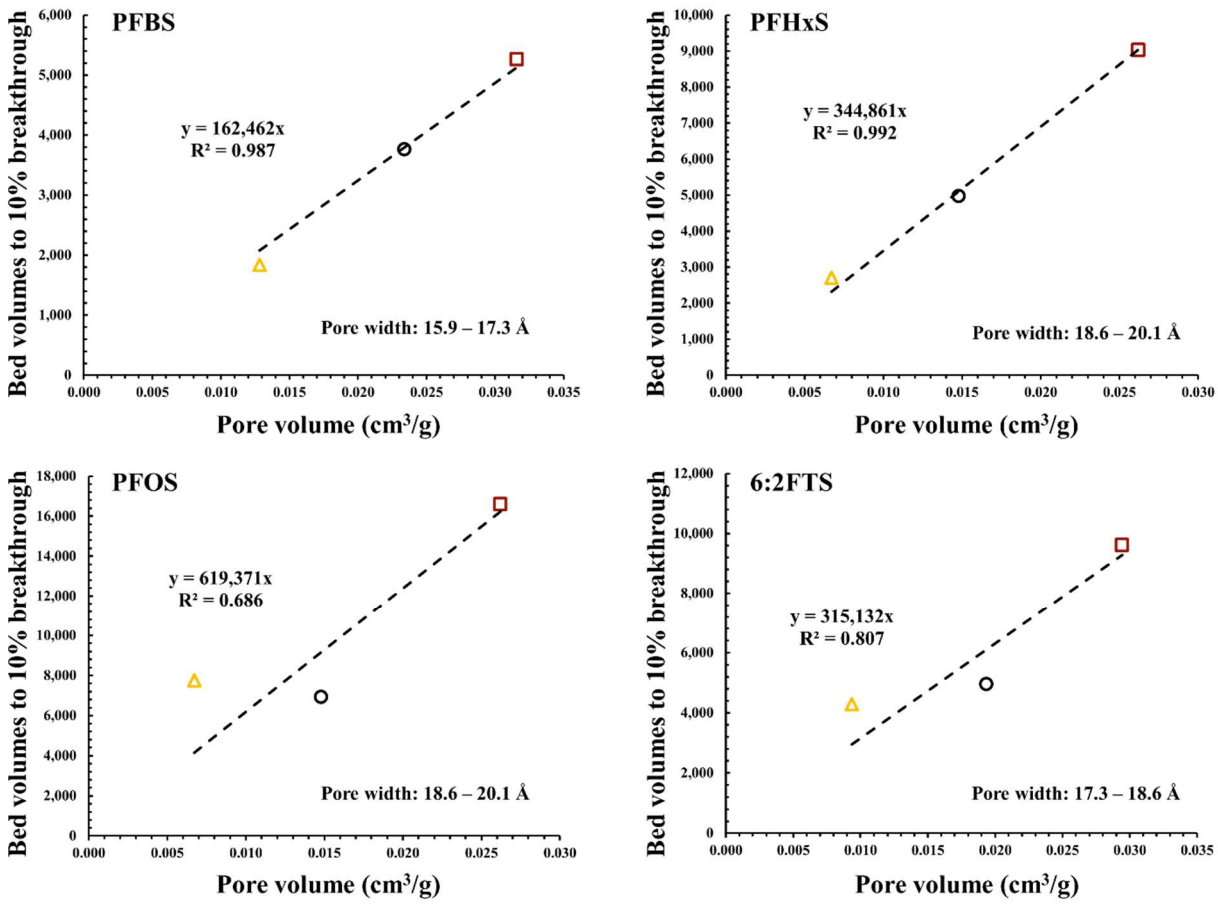

Figure C.26: Relationships between bed volumes to 10% breakthrough and pore volumes in the secondary micropore range in coagulated/settled surface water. Carbon A (black circle), Carbon B (red square), Carbon D (yellow triangle).

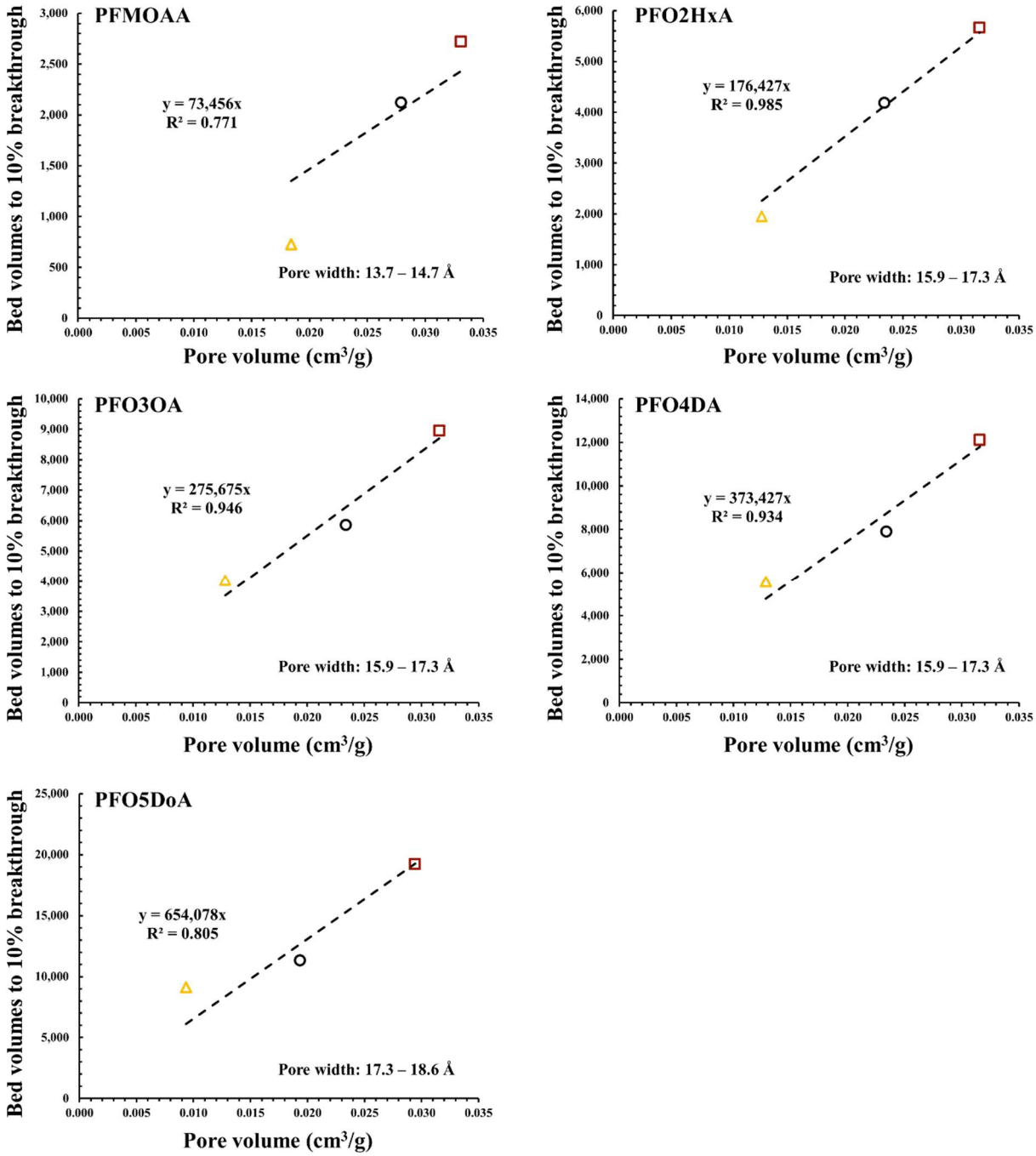

Figure C.27: Relationships between bed volumes to 10% breakthrough and pore volumes in the secondary micropore range in coagulated/settled surface water. Carbon A (black circle), Carbon B (red square), Carbon D (yellow triangle).

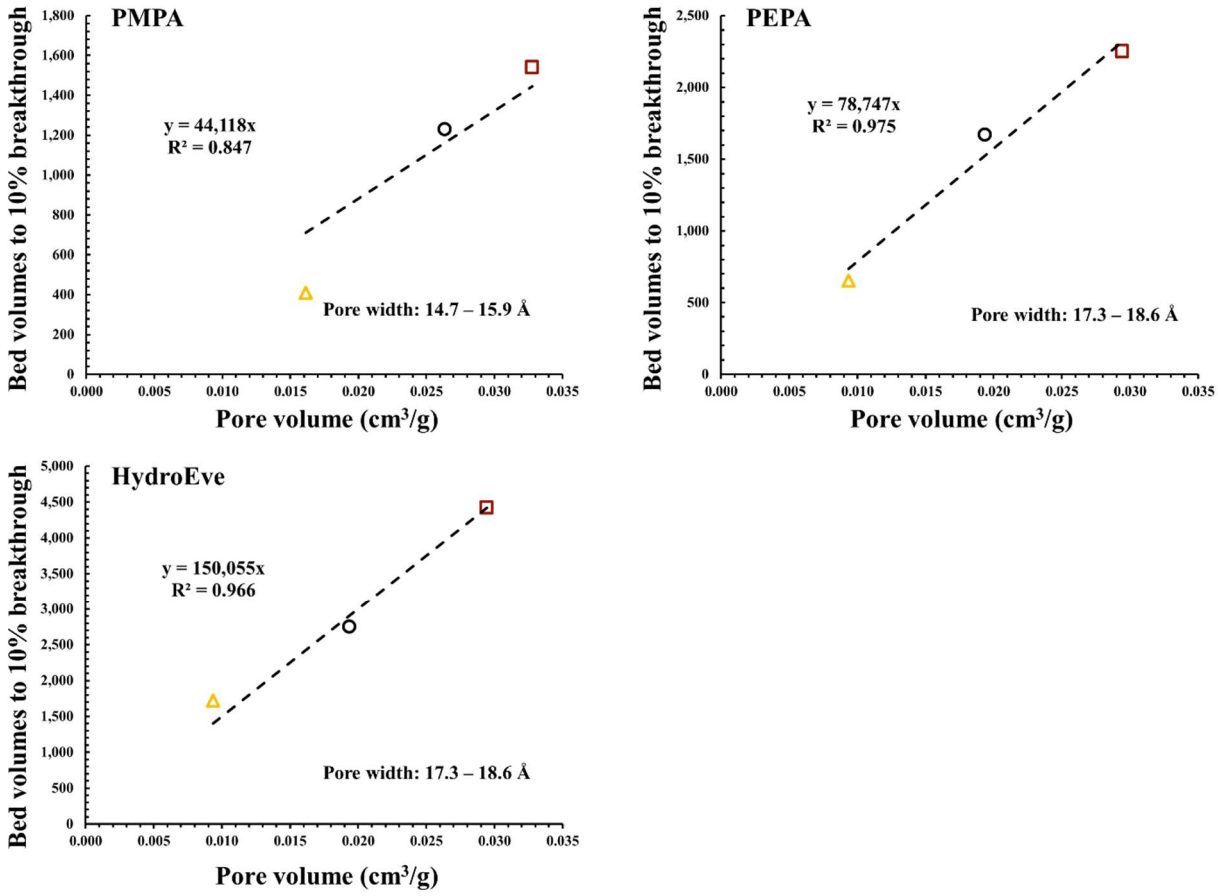

Figure C.28: Relationships between bed volumes to 10% breakthrough and pore volumes in the secondary micropore range in coagulated/settled surface water. Carbon A (black circle), Carbon B (red square), Carbon D (yellow triangle).

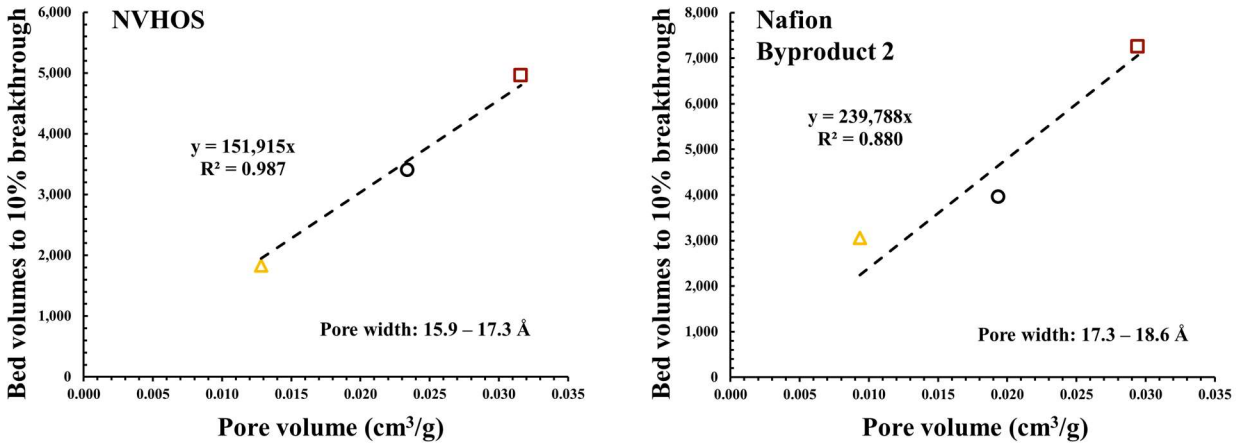

Figure C.29: Relationships between bed volumes to 10% breakthrough and pore volumes in the secondary micropore range in coagulated/settled surface water. Carbon A (black circle), Carbon B (red square), Carbon D (yellow triangle).